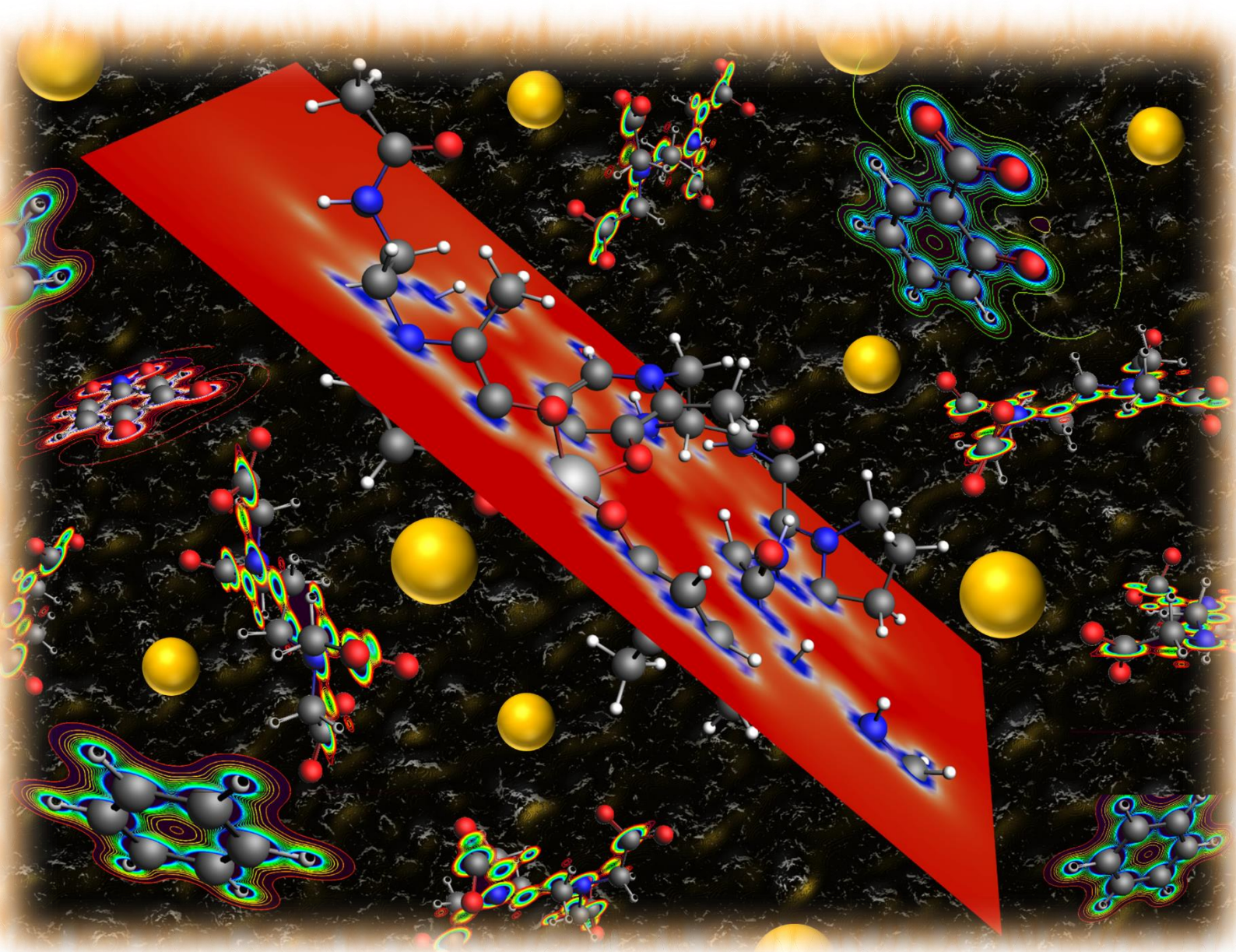# Computational approach to aluminum biochemistry and development of new chelation strategies

Supervisor: Prof. Xabier Lopez

Supervisor: Prof. Maria João Ramos

Gabriele Dalla Torre

2019

eman ta zabal zazu

Universidad del País Vasco   Euskal Herriko Unibertsitatea

U. PORTO

European Joint Doctorate on Theoretical Chemistry and Computational Modelling

(ITN-EJD-TCCM)

Organized by the Autonomous University of Madrid

Candidate: Gabriele Dalla Torre

Title of the dissertation

Computational approach to aluminum biochemistry and development of new chelation strategies

1. **Euskal Herriko Unibertsitatea** (University of the Basque Country and Donostia International Physics Center, Spain – 16 months).
   Supervisor: Prof. Xabier Lopez.

2. **SmartLigs® Bioinformatica S.A.** (Madrid, Spain – 4 months).
   Supervisor: Dr. Almudena Perona.

3. **Universidade do Porto** (University of Porto and UCIBIO, Portugal – 16 months).
   Supervisor: Prof. Maria João Ramos.

And in collaboration with external experimentalists from the University of Cagliari (Dr. Joanna I. Lachowicz).

"Well my soul checked out missing as I sat listening
To the hours and minutes tickin' away
Yeah just sittin' around waitin' for my life to begin
While it was all just slippin' away
I'm tired of waitin' for tomorrow to come
Or that train to come roarin' 'round the bend
I got a new suit of clothes a pretty red rose
And a woman I can call my friend

These are better days baby
Yeah there's better days shining through
These are better days baby
Better days with a girl like you

Well I took a piss at fortune's sweet kiss
It's like eatin' caviar and dirt
It's sad funny ending to find yourself pretending
A rich man in a poor man's shirt
Now my ass was draggin' when from a passin' gypsy wagon
Your heart like a diamond shone
Tonight I'm layin' in your arms carvin' lucky charms
Out of these hard luck bones

These are better days baby
These are better days it's true
These are better days
There's better days shining through

Now a life of leisure and a pirate's treasure
Don't make much for tragedy
But it's a sad man my friend who's livin' in his own skin
And can't stand the company
Every fool's got a reason for feelin' sorry for himself
And turning his heart to stone
Tonight this fool's halfway to heaven and just a mile outta hell
And I feel like I'm comin' home

These are better days baby
There's better days shining through
These are better days
Better days with a girl like you

These are better days baby
These are better days it's true
These are better days
Better days are shining through"

(B. Springsteen, Better Days)

Computational approach to aluminum biochemistry and development of new chelation strategies

Thesis dissertation by

Gabriele Dalla Torre

January 1, 2019

Schio

To my endless nights…

Acknowledgements

Too many people to thank, really too many. This should mean that a lot of people have crossed the long, windy road of my life.

Three years have gone too fast…

Beautiful people, funny jerks, great souls and lonely hearts.

May God know how, each of them, have improved, in some way, my knowledge, my strength, my faith and my happiness.

First of all, many thanks to Prof. Xabier Lopez, Prof.Maria Joao Ramos and Dr. Almudena Perona, my three supervisors, for givin' me all the instruments that I need to going on with my scientific career, and to realize my ambitions.

And, of course, for the huge degree of patience.

Many thanks to all the Theoretical people of Xabi's, Maria's and Almudena's group. A lot of guys, too many to remember all of them throughtout these years; I'm proud for having been working with you. Special mention goes to Joni Mujika, Elena Formoso (EHU), Eduardo Oliveria and Rui Neves (Uporto) and David (Smartligs); their help was priceless.

Thanks to Federica Amato, for shining on me like a blooming flower in the Badlands.

Thanks, obviously, to my parents, my family, my sister, my cousins and my relatives, because life can change and we are not stuck in vain.

And thanks to all the fuckers, as they taught me that I have one more reason to be a better person, to fly over the shadows, and, someday, the King of gloom will be forever doomed.

Finally, many thanks to all of you, for reading this manuscript.

May the Force be with you.

Abstract

Aluminum is the third most abundant element on Earth's crust, and the first metal. Nevertheless, its complex chemical features, mainly its low solubility, have prevented its utilization within the biological cycles of living organisms, leading to a not fully understood paradox from an evolutionary point of view[1].

In the last Century, the acidification of the environment due to the human intervention, has allowed Al(III) to become one of the main components of our daily lives. It has become so highly (bio)available that some authors state that we are currently living "The Aluminum Age"[2].

As a consequence of such massive human exposure to this non-essential metal ion, detrimental neurological effects have been reported, raising concerns about the potential toxic role of aluminum in the biological environment[3]. In particular, the link between the presence of Al(III) in neuronal tissues and the development of Alzheimer's Disease is a matter of debate and controversy, despite all the many efforts made in order to unveil the pathogenic effects of Al(III)[4,5].

In this rather controversial context, the quest for reliable chelating agents that can efficiently remove Al(III) from the biological environment has attracted much interest in the last years[6]. The goal of chelation therapy is the development of chelating agents with a high affinity and specificity for a given metal ion, lack of toxicity and strong competitiveness with respect to endogenous metal ions and chelators. However, due to the complex chemistry of aluminum, a suitable and specific Al(III) chelating agent has not yet been found[6].

Accordingly, we believe that a computational approach to aluminum biochemistry, by using state-of-the-art computational tools and in collaboration with experimental partners, would allow for a strong help towards a clearer understanding of the role and the behavior of Al(III) in the human organism.

In this sense, the present PhD project has covered three main areas: i) chelation therapy and development of new chelation strategies. ii) Understanding of the potential toxic role of aluminum in the biological environment, considering different bioligands. iii) Validation and calibration of the accuracy of theoretical methods (mainly DFT) with respect to available experimental data and other high level benchmarks, in order to improve the reliability of our computational approach. Moreover, the work was carried out in close collaboration with experimental partners from the University of Cagliari (Italy).

A wide range of methods have been used for that purpose, such as cluster-*continuum* approaches at the DFT level of theory, thermodynamics of metal-ligand complexes in solution, chemical bond analysis, QM/MM simulations. The availability and fine understanding of experimental data has allowed the setup of a reliable computational protocol suitable for the investigation of Low-Molecular-Mass (LMM) aluminum chelators. Additionally, other methodologies were used during the secondment at SmartLigs®, such as classic MD simulations, docking and MonteCarlo-based conformational sampling techniques.

All results achieved so far are contained in the publications list along with the scientific production (e.g. conferences, meetings etc.), and will be presented and discussed in this Thesis dissertation.

Contents

Chapter 2

METHODS..65

PART I: Chelation therapy and development of new chelation strategies

Chapter 3

Tuning the affinity of catechols and salicylic acids toward Al(III): characterization of Al-chelator interactions 85

Chapter 4

Design of new efficient chelators of aluminum based on Mimosine-containing peptides

PART II: Understanding the potential toxic roles of Al(III) in the biological environment

Chapter 5

Chapter 8

SCIENTIFIC IMPACT OF THE PROJECT 199

Chapter 9

CONCLUSIONS 207

APPENDIX A 215

APPENDIX B 241

INTRODUCTION

"My name is Joe Roberts I work for the state
I'm a sergeant out of Perrineville barracks number 8
I always done an honest job as honest as I could
I got a brother named Franky and Franky ain't no good"

(B. Springsteen, Highway Patrolman)

1.1 Living the "Aluminum Age"

1.1.1 What's wrong with aluminum ?

Aluminum is the third most abundant element on Earth's crust (8%) , after oxygen and silicon, and it is the most abundant metal[7]. Al(III) is locked into minerals, and in Nature it occurs only in combined forms: as an oxide in bauxite, the primary one, and in complex with aluminosilicates such as micas and feldspars[7-9]. Interestingly, the reaction of silicic acid $[Si(OH)_4]$ with aluminum hydroxide $[Al(OH)_3]$ to form hydroxyaluminosilicates (HAS) has been proposed to be critical for the non-selection of aluminum in biochemical evolution and, therefore, as a natural mechanism to combat the eco-toxicity of Al(III) including human exposure to this metal[8]. In other words, it is thought that the formation of HAS is a process, created by Nature, to reduce the biological availability of Al(III) and, therefore, to reduce its potential toxic effects in living organisms.

In contrast to its abundance in the crust, the ocean concentration of aluminum is below 1µg of Al/L; this low level may be the result of the accumulation of aluminum and silicon by diatoms[7].

However, with the advent of acid rain, metals like aluminum are able to escape from mineral deposits and dissolve in fresh waters. Accordingly, acid rain is the key responsible for metal ions release, leading to their accumulation in fresh water and, in turn, to their availability to living organisms[7].

Such an acidification of the environment, mainly due to the human intervention in the last Century that dramatically changed the environment, is therefore the main factor that led aluminum to become highly available and, most importantly, for the first time bioavailable.

Indeed, it has been proposed that the non-availability of biologically reactive aluminum species throughout the biochemical evolution is what today explains its lack of essentiality in all extant biota[2]. In addition, due to the improvements in the ability to separate aluminum metal from its ores on an industrial scale, Al(III) changed from being a largely decorative metal to the most widely used metal of the 21st Century[2]. It has been so widely used that Prof. Christopher Exley (Keele University, UK), probably the leading researcher on Al(III) biochemistry, states that we are currently living "The Aluminum Age" [2,10,11].

It follows that the ordinary exposure to this metal is the reason that transformed the geochemical cycle of aluminum into a biogeochemical cycle, raising concerns about the potential toxic effects that such an exogenous and non-essential metal ion can have on the human organism.

It is indeed true that aluminum finds its way into virtually every aspect of our everyday lives (Fig. 1.1): it is used in cans and cookware, aluminum foil, housing materials, components of electrical devices, airplanes, boats, cars and numerous hardware items[10].

In terms of bioavailability, nowadays aluminum is found in drinking water due to its action as a flocculant, is a common additive in various processed foods, is added to cosmetics of many types, and, increasingly, is used in pharmaceutical products. In particular, regarding the latter aspect, it is worth to emphasize that various aluminum salts are used as vaccine adjuvants[10]. This is particularly important at present, since such metal-based adjuvants raised concerns about the involvement of Al(III) towards the insurgence of autism[12-14].
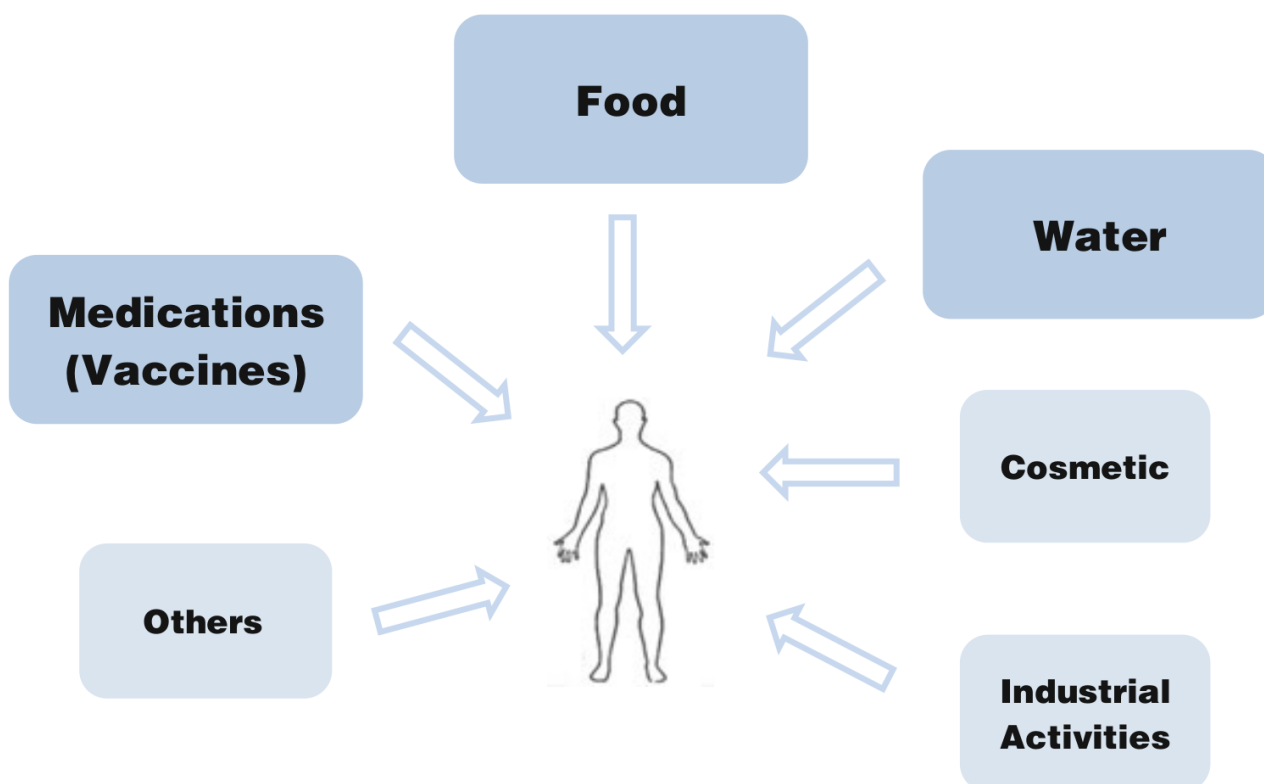
Fig.1.1. Sources of aluminum in our everyday lives. Taken from ref.[10].

In light of the above discussion, it is therefore surprising how such an abundant metal, from an evolutionary point of view, has not been employed in the biological cycles of living organisms. It is reasonable to argue that the complex chemistry and properties of the aluminum ion, mainly its low solubility at physiological (biological) conditions, have prevented its utilization within the biochemical pathways and molecular life of humans.

This "big" paradox has been unveiled and discussed in an elegant way by C. Exley in its opinion article *"Darwin, natural selection and the biological essentiality of aluminum and silicon"* [1].

According to Prof. Exley, *"the abundance of an element in the lithosphere only becomes a major driving force for its selection for biochemical purpose when abundance is commensurate with the availability of biologically reactive forms of the element. Selection acts upon the biological reactivity*

of an element through pressures such as reaction thermodynamics and reaction kinetics. The former are exemplified by equilibrium constants which define properties of reaction products such as solubility and complex stability whereas kinetic constraints influence how (bio)chemical equilibrium is approached and ultimately which biochemical pathways predominate" [1].

These arguments clearly explain why Aluminum has not evolved as an essential and widely employed element in the (bio)chemical environment: it is indeed mainly the low solubility of Al(III) that provokes its unfavorable thermodynamics in aqueous solution, as it will be largely investigated and discussed throughout the results of this thesis dissertation. As previously mentioned, the role of silicates, another non-essential element, could be a protective one against Al(III).

According to what it has been discussed up to this point, an automatic question would be:

"So, what's wrong with aluminum?".

In fact, this exogenous metal has been related to many toxic effects[10,15], and ultimately to an involvement towards the development of neurodegenerative diseases, in particular the Alzheimer's Disease[5], among others.

Before deepening this rather controversial topic, in the next section a survey on the *physico*-chemical properties of this metal ion, as well as its binding features, is presented.

1.1.2 The complex and unique (bio)chemistry of the aluminum ion and coordination principles

1.1.2.1 Hard and Soft Acids and Bases (HSAB) principle

Aluminum exists only as a trivalent ion in the biological environment of living organisms, and it is too reactive to be found in its elemental state in nature[16], as discussed in the previous section.

All metals and metal ions are Lewis acids (electron pair acceptors, i.e. electrophiles) that have incomplete valence electron shells. They complex with Lewis bases (electron pair donors, i.e. nucleophiles), which are small molecules or ions that have at least one electron pair that can be donated[16].

In coordination chemistry, a very useful concept to classify the properties of these metal-donor complexes is the Pearson's Hard and Soft Acids and Bases (HSAB) principle[17]. According to the HSAB classification, small metal atoms with high charge density, that are not easily polarizable, are defined as "hard" (Table 1.1). These metals have the tendency to form almost purely ionic bonds with hard bases, while bigger and more polarizable atoms, that therefore belong to the "soft" category, form mostly covalent bonds with complementary "soft" bases (Table 1.1).

Considering these main rules, it has been possible to make useful predictions, in terms of Lewis acids and bases, of metal complexes with various ligands[18]. However, it should be taken into account that

the HSAB principle is not universal and, moreover, it has been the subject of criticisms in recent years[19].

Acids

HARD	SOFT
H^+, Li^+, Na^+, K^+, Be^{2+}, Mg^{2+}, Ca^{2+}, Sr^{2+}, Ba^{2+}, Al^{3+}, Sc^{3+}, Ga^{3+}, In^{3+}, La^{3+}, Gd^{3+}, Lu^{3+}, Cr^{3+}, Co^{3+}, Fe^{3+}, As^{3+}, Si^{4+}, Ti^{4+}, Zr^{4+}, Hf^{4+}, Th^{4+}, U^{4+}, Pu^{4+}, Ce^{4+}	Cu^+, Ag^+, Au^+, Ti^+, Hg^+, Pd^{2+}, Cd^{2+}, Pt^{2+}, Hg^{2+}, Pt^{4+}, Te^{4+}, Br^+, I^+

Borderline

Fe^{2+}, Co^{2+}, Ni^{2+}, Cu^{2+}, Zn^{2+}, Pb^{2+}, Sn^{2+}, Sb^{3+}, Bi^{3+}, Rh^{3+}, Ir^{3+}

Bases

HARD	SOFT
H_2O, OH^-, F^-, PO_4^{3-}, SO_4^{2-}, Cl^-, CO_3^{2-}, CH_3COO^-, ClO_4^{-}, NO_3^{-}, NH_3, ROH, RO^-, R_2O, NH_3, RNH_2,	R_2S, RSH, RS^-, I^-, SCN^-, $S_2O_3^{2-}$, R_3P, R_3As, CO, $(RO)_3P$, CN^-, RNC, C_2H_4, H^-, R^-

Borderline

N^{3-}, Br^-, NO^{2-}, N_2, SO_3^{2-}

Table 1.1. Hard and soft acids and bases according to the HSAB principle. Borderline cases are molecules that show ambiguous behavior[17].

Al(III) is therefore a hard acid (and the hardest trivalent metal ion) because of its small ionic radius and high oxidation state. It possesses an effective ionic radius of 0.50 Å, which is smaller than other trivalent metals ions like Fe(III), which is a key feature in the field of chelation therapy[6].

Following the HSAB principle, aluminum has high affinity for hard anions (Table 1.1); among the hardest donors is the oxide (OH^-) anion[20]. Although OH^- and F^- are isoelectronic, the OH^- ion has much more affinity for Al(III) because of the partially covalent nature of the Al-O bond, while the Al-F bond is almost purely ionic[20]. The partial (and small) covalency of the Al-ligand coordinate bond is important since it plays an important role in the modulation of the aluminum-ligand binding affinity[21]. Considering the nature of the coordinate (dative) Al-O bond, such covalent character has been confirmed to be due to the high electron donation from the donor's lone pair to the formally empty 3s and 3p valence shell of aluminum[21]. However, in agreement with the HSAB principle, the Al-O bond is mainly electrostatic in nature (see chapter 3).

The high affinity for OH$^-$ molecules leads to the fact that, in solution, $[Al(OH)_4]^-$ is the most stable complex[7,22], as it will be discussed in the next section. Such a situation is coherent with the fact that, being hydrogen less electronegative than, for instance, carbon, an OH$^-$ oxygen is more basic (i.e. bears higher electron density) than a phenoxide (CO$^-$) or a superoxide (O$_2^-$) oxygen[23]. This higher basicity is, in turn, reflected by the higher covalent character of the Al-O bond[23].

However, it should be always taken into account that, despite the presence of this small but yet important covalent character, the Al-ligand bond is mainly ionic/electrostatic driven, a factor that shifts the preferential binding of Al(III) to negatively charged donors such as the carboxylate donors of protein siechains[24]. It is important to emphasize that the above discussion is mainly the fruit of some of the results achieved in this thesis dissertation, that will be presented and more deeply discussed in chapters 3-7.

As a result, negatively charged oxygen atoms are the main donors to aluminum, with phenolates, carbonyls, carboxylates, catecholates and (bio)phosphates being the main donor groups that can be found in the biological environment, and that are used in the design of therapeutic Al(III) chelating drugs[6,22,25].

The preferential binding of aluminum to different types of O-donors is, as discussed before, dictated by their basicity; the more basic the donor, the stronger the binding affinity with this hard metal ion[20]. An important consideration must be made at this point: indeed, the increase in basicity of oxygen donors is not only responsible for the enhancement of their affinity towards the aluminum ion, but also towards the proton. This is due to the fact that H$^+$ is also a hard acid according to the HSAB principle[20] (Table 1.1). Such a situation is reflected by the increase of the protonation constants of the O-donors, a situation that makes energetically more expensive for Al(III) to displace the proton(s) and bind to the coordination site of a given ligand[21]. Accordingly, the aluminum ion/proton competition is an aspect that must be seriously taken into account when evaluating the performance of Al(III) chelating agents. This aspect will be discussed in chapter 3.

On the other hand, amines and thiolates are not competitive aluminum binders, as they can barely compete with Al(III) hydrolytic species under physiological conditions. Similarly, the nitrogen bases of nucleic acids or nucleotides are not strong aluminum binders[22]. However, it is important to note that, if nitrogen donors are placed in a coordination site close to O-donors, then their binding ability may change considerably[22].

Clearly, the stronger binding affinity of oxygen atoms over amines and thiolates is due to the mainly electrostatic nature of the aluminum-ligand interactions, as discussed before, and aluminum shows preference towards negatively charged donors. This is highlighted by the fact that carbonyl groups,

such as those that can be found in the backbone of proteins, are not competitive Al(III) binders when compared to carboxylates that are found in the sidechains of peptides[24] (see chapter 5).

1.1.2.2 Aluminum chelation principles and binding features

Al(III) preferred coordination number is six, with a preference to form stable octahedral complexes with its ligands, although very stable tetrahedral $[Al(OH)_4]^-$ complexes can also be formed in solution depending on the pH (Fig. 1.2), as it will be discussed in the next section. At low pH values (lower than 5.0, Fig. 1.3), the octahedral $[Al(H_2O)_6]^{3+}$ complex has been proposed to be higly symmetric with a T_h point group symmetry, on the basis of both experimental and computational studies[26]. The average Al-O equilibrium bond length was found to be 1.90 Å in ref.[26], although this value can vary slightly considering different reference works. Interestingly, Hay and coworkers suggested that both Al 3p—O 2s and Al 3p—O 2p orbital contributions contribute to the stability of the octahedral $[Al(H_2O)_6]^{3+}$ complex[26].

Different ligands (ions, biomolecules, organic compounds) can interact with aluminum through different binding modes, i.e. different denticities, which is another important factor that modulates the strengths of the Al-ligand(s) affinity.

The term "chelator" comes from the Greek and refers to the claw of the crab; a chelator is a molecule that is able to form at least two or more coordinate bonds with a metal ion, where each functional group donates a pair of electrons. The term "denticity", that comes from the Latin and stays for tooth, is used to classify a chelator by the number of donor groups that coordinate a given metal.

In the case of Al(III) we can have bidentate, tridentate, tetradentate and hexadentate chelators (Fig.1.2). Pentadentate chelators are not common since they require the distortion of the octahedral or tretrahedral geometries, that are the most common point group symmetries of metals. However, in some special cases that involve chelators with many degrees of freedom such as Desferroxamine, intra-molecular forces (steric repulsions, H-bonds, etc.) may lead to pentadentate binding modes (Fig.1.2).

The denticity of a given chelator is important since it defines its binding strength towards the metal: therefore, considering the thermodynamic equilibria of the aquo aluminum ion in solution (in its octahedral state) with a given bidentate chelator (LIG$_{bid}$), we will have:

$$Al(H_2O)_6 + LIG_{bid} \rightleftharpoons [LIG_{bid} - Al(H_2O)_4] + 2H_2O \qquad \textbf{(1.1)}$$

$$Al(H_2O)_6 + 2 * LIG_{bid} \rightleftharpoons [2LIG_{bid} - Al(H_2O)_2] + 4H_2O \qquad \textbf{(1.2)}$$

$$Al(H_2O)_6 + 3 * LIG_{bid} \rightleftharpoons [3LIG_{bid} - Al] + 6H_2O \qquad \textbf{(1.3)}$$
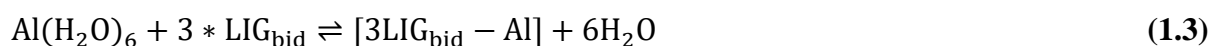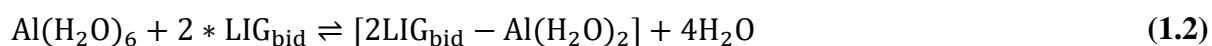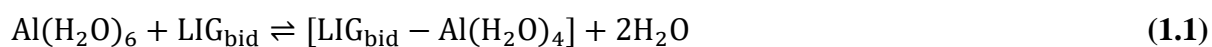
For bidentate ligands, three stoichiometric aluminum-chelator complexes are possible; it is important to take into account, however, that the formation of these complexes is pH dependent, and it is affected mainly by the number of tritratable groups present in the ligand. As discussed before, the protonation constants of the ligand's donor groups to aluminum (e.g. the competition between the metal ion and the proton for the ligand binding site) is a pivotal factor that determines the chelation performance of a given chelating agent. Such an aspect will be discussed more into detail in chapter 3.

Following the equilibria outlined previously for bidentate chelators, in the case of tridentate ligands (Fig. 1.2) we get:

$$Al(H_2O)_6 + LIG_{tri} \rightleftharpoons [LIG_{tri} - Al(H_2O)_3] + 3H_2O \qquad (1.4)$$

$$Al(H_2O)_6 + 2 * LIG_{tri} \rightleftharpoons [2LIG_{tri} - Al] + 6H_2O \qquad (1.5)$$

And, for hexadentate chelators:

$$Al(H_2O)_6 + LIG_{hexa} \rightleftharpoons [LIG_{bid} - Al] + 6H_2O \qquad (1.6)$$

octahedral
Al(H₂O)₆

tetrahedral
Al(OH)₄

bidentate
(Al-catechol)

tridentate
(Al-citrate)

tetradentate
(Al-phorphirin)

pentadentate
(Al-desferroxamine)
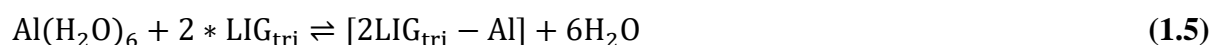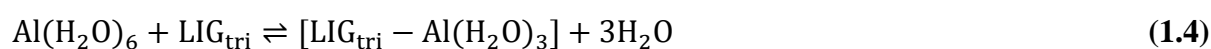
hexadentate
(Al-EDTA)
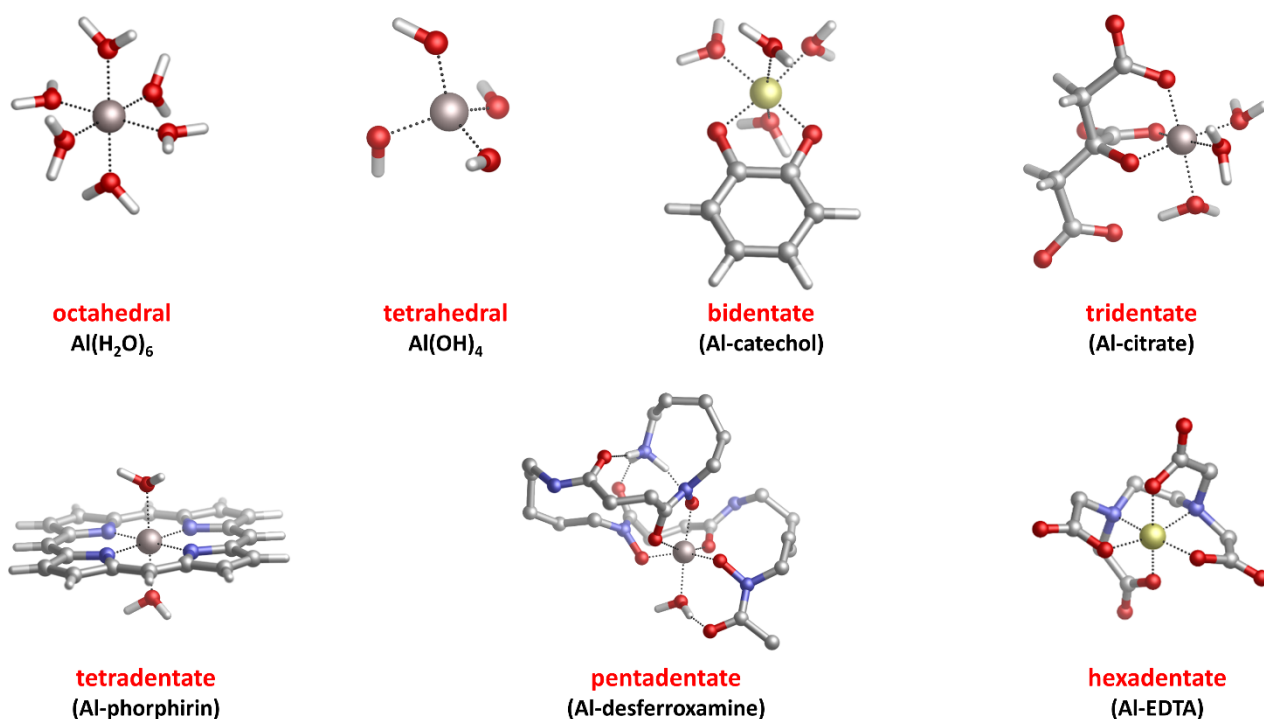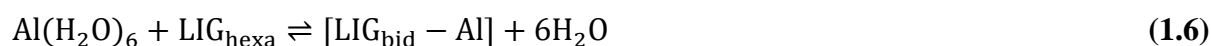
Fig 1.2. Main species of aluminum in solution and binding modes (denticities) of some common endogenous and exogenous Al(III) chelators. Geometries optimized at the B3LYP-D3(BJ)/6-31++(d,p) level of theory.

It is clear, from a thermodynamic point of view, that the binding affinity provided by hexadentate chelators is much stronger than bi- or tri-dentate chelating agents. Indeed, if we consider the metal fully coordinated by the ligand(s), bidentate chelators require three separate reaction steps to completely bind to aluminum, tridentate chelators two and hexadentate one. Accordingly, the total entropy required in the latter case to form the complex is smaller than those of the previous ones[27,28]. Such an aspect will be further discussed in section 1.2.2.1.

1.1.2.3 Aluminum speciation in solution

The solubility and speciation of the aluminum ion in aqueous solution are a central point to understand the behavior of this metal in the biological environment and, therefore, to investigate its interactions with endogenous and exogenous ligands.

Due to its complex chemical properties, Al(III) forms different hydrolytic species in solution according to the pH (Fig. 1.3)[7,22]. At acidic conditions (pH < 5), aluminum exists as an octahedral hexahydrated complex, $[Al(H_2O)_6]^{3+}$. As the solution becomes less acidic, the hexahydrated aluminum complex undergoes successive deprotonations leading to $[Al(OH)]^{2+}$, $[Al(OH)_2]^{+}$ and a soluble $[Al(OH)_3]$ complex, with a decreasing and variable number of water molecules[7]. This latter aspect implies that other different geometries than the octahedral one are possible in solution.

Neutral solutions give an $[Al(OH)_3]$ precipitate that re-dissolves, due to the formation of the tetrahedral $[Al(OH)_4]^{-}$ complex, the primary and most stable Al(III) species at pH > 6.2, which is the prevalent one at basic pH ranges (Fig. 1.3)[7,22].
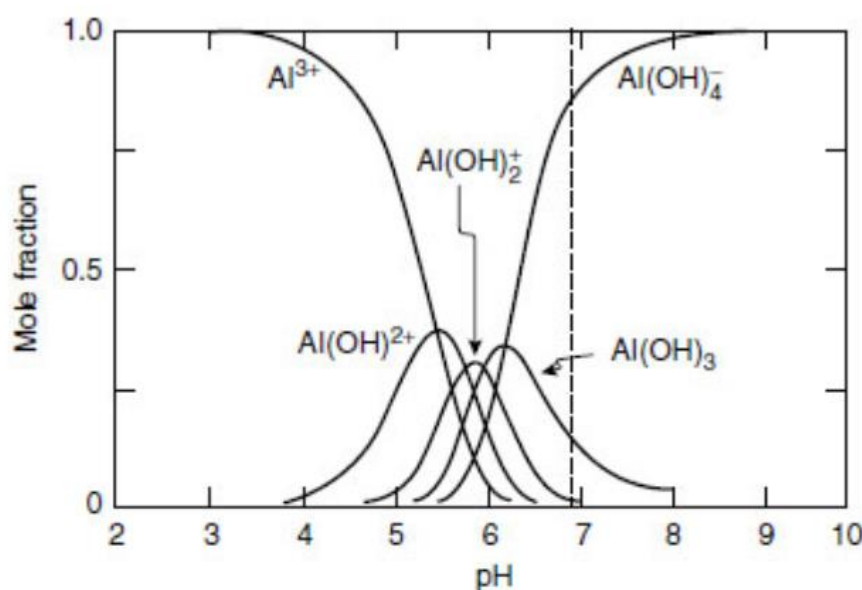
Fig 1.3. Speciation diagram of Al(III) in solution. Taken from ref.[29].

The four successive deprotonations from $[Al(H_2O)_6]^{3+}$ to give rise to $[Al(OH)_4]^-$ are confined within an unusually restrained pH range of less than 1 log unit, with pK_a values of 5.5, 5.8, 6.0 and 6.2[7]. This narrow span for Al(III) is explained by the cooperative nature of the successive deprotonations due to a concomitant decrease in the coordination number from 6 to 4 (Fig. 1.3). Interestingly, while Al(III) is 3 log units less acidic than Fe(III), $[Al(OH)_4]^-$ becomes the dominant species at almost 3 units lower pH than $[Fe(OH)_4]^-$ [7]. In the case of Al(III), only two species dominate over the entire pH range, the octahedral hexahydrate $[Al(H_2O)_6]^{3+}$ at acidic pH values and the tetrahedral $[Al(OH)_4]^-$ at basic pH values, while there is a mixture of different hydrolytic species and coordination numbers near physiological pH values (Fig. 1.3)[7].

In light of the above discussion, it is clear that the investigation of aluminum in solution is a very challenging task from an experimental point of view, but also for modelling the behavior of such metal in solution by means of theoretical approaches. In this latter case, it is important to emphasize that, although a reference complex (e.g. an aluminum hydrolytic species) has to be chosen, one should always also consider the other different Al(III) species present at a given pH. Different aluminum species may lead to different patterns of interactions and binding modes with ligands, providing different pictures and scenarios that can provoke the misinterpretation of results. Another challenging task and big source of errors concerns the proper evaluation of solvation effects in solution, especially when dealing with implicit solvation models[30]. A paradigmatic case in this sense is a work published in *Angew. Chem. Int. Ed.* where authors limited their investigations and speculations to a single $[Al(OH)(H_2O)_5]^{2+}$ complex, also without considering solvation effects[31]. As we demonstrated, the account for other aluminum species and for proper solvation models in the calculations changes considerably the nature of the results[24] (see chapter 3). The speciation of Al(III), along with its hybrid bonding nature with ligands, is a big limiting factor for the parameterization of specific Force Fields and semiempirical methods[32,33]. More details about the solutions and strategies that we adopted in our computational approach to aluminum biochemistry are discussed in the results section.

1.1.3 Is aluminum a (neuro)toxic element ? A (still) controversial topic

The potential toxic effects of Al(III) are a highly debated matter that still nowadays is not fully accepted. The first evidence of the influence of aluminum on the biochemical reactions that govern the homeostasis of our body dates back to the 70's.

In 1970, it was believed that the phosphorylation of glucose by the hexokinase enzyme in the presence of ATP required some kind of "activator" such as citrate at physiological pH. Later, in 1979, the so-called allosteric activity of citrate (and other activators) was found to be the consequence of contamination of laboratory supplies of ATP by aluminum[11]. Considering the strong affinity that ATP

has with respect to Al(III) compared to its usual co-factor Mg(II), it follows that when the Al-ATP complex replaces Mg-ATP as a source of phosphate, then the activity of hexokinase is significantly lowered[11]. Under the same conditions, but additionally in the presence of citrate (an extremely competitive Al(III) chelator in the biological environment[34-36]), the Al-ATP complex dissociates and the formation of Al-citrate complexes protects the enzyme-substrate complex from the inhibitory effect of Al-ATP[2].

In order to argue whether aluminum is toxic or not, first of all it is important to fully understand the human's exposure to this exogenous metal as well as its potential interference with biochemical pathways and molecular processes in the biological environment.

As mentioned in the beginning, we are all exposed to aluminum because of the human intervention in the last Century, that allowed Al(III) to become a major component of our daily lives. An interesting concept that provides a mean of the ways by which Al(III) is accumulated in our body is the "body burden" of aluminum introduced by Prof. Exley[2].

"The body burden of aluminum is defined as the sum of aluminum atoms associated with the body at any one moment in time. It includes aluminum on the surface of the skin, aluminum in hair and nails, aluminum associated with external secretions/excretions in the mouth, nose, ear, lung, stomach, small intestine, urinary and reproductive tracts and aluminum in the large intestine. It also includes Al(III) associated with all of the systemic compartments including endo/epithelia, blood, lymph, sweat, tears, humours, tissues, organs and bone"[2].

According to the picture outlined above and shown in Fig. 1.4, it is clear the aluminum ion has the potential to interact with many tissues and, therefore, different cellular types and cell components. However, in order for that to happen, obviously we must be in close contact with Al(III). Therefore, how are humans exposed to aluminum ?

It has been shown that in order to meet the annual global demand for this metal, approximately 11kg of aluminum has to be accumulated for every person from Earth. This aluminum is extracted by industry and finds its way in many aspects of our everyday life, as discussed in section 1.1.1; if we assume that, for instance, we are exposed to the 0.1% of this potential (e.g. 11kg/year), then it has been calculated that our everyday intake of aluminum is 30mg. On the same basis, our intake was 1mg in 1950 and would be 100mg per day in 2050[2].

The first significant contribution to the body burden of aluminum is the air that we breath (Fig. 1.4). Aluminum-based particulates of myriad sizes, shapes and compositions are components of aerosols, especially in industrialized centers of rapidly growing economies such as China. Exposure to aluminum by breathing can be increased in many ways, like industrial workplaces, smoking of cigarettes and cannabis[2].
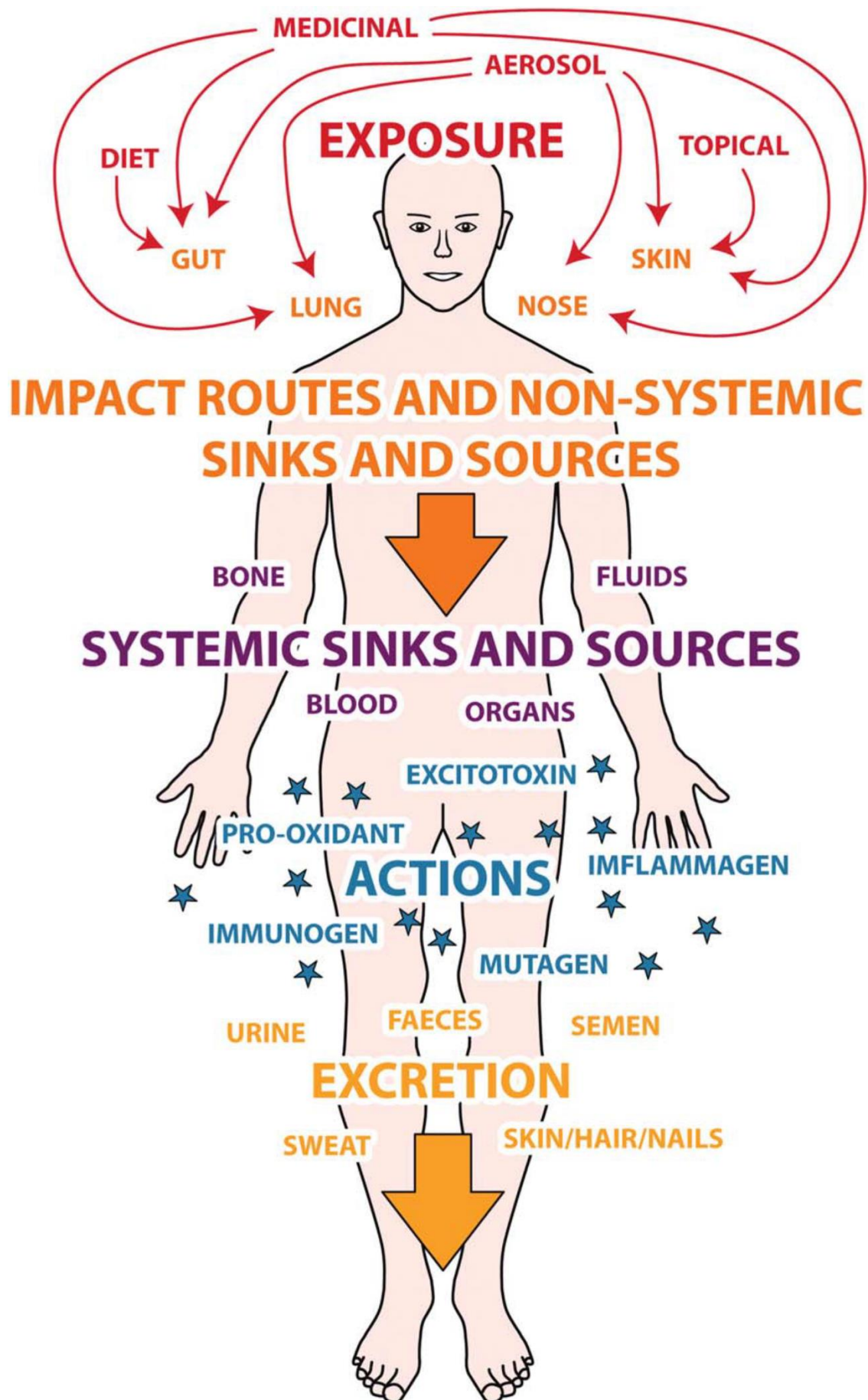
Fig. 1.4. The body burden of aluminum. Taken from ref.[2].

Diet is another significant contributor to the body burden of Al(III). Intake of aluminum from the diet has been measured to be between 1 to 20mg per day[2].

Topically applied cosmetics, hair, skin and hygiene products are often significant contributors of the daily intake of aluminum. This is especially true for antiperspirants, as their use involves the application of about 2g of aluminum every day[2].

Finally, it is important to mention that sources of aluminum intake come from intentional and unintentional component of many medicines. Intentional ones include antacid and buffered aspirin, as well as adjuvants that are added to vaccines and allergy treatments[2].

A more detailed picture (Fig. 1.5) about the systemic pathways and cellular components that are affected by the body burden of aluminum can be found in ref.[2] and is beyond the scope of this thesis dissertation.

However, it is important to take into account that upon absorption, in an open biological environment Al(III) can interact with a wide range of High Molecular Mass (HMM, e.g. transferrin) and Low Molecular Mass (LMM, e.g. citrate) endogenous ligands, as well as to easily cross cellular membranes and the blood-brain-barrier (Fig. 1.5). Obviously, this makes the understating of the possible mechanisms of toxicity of Al(III) a very challenging task.
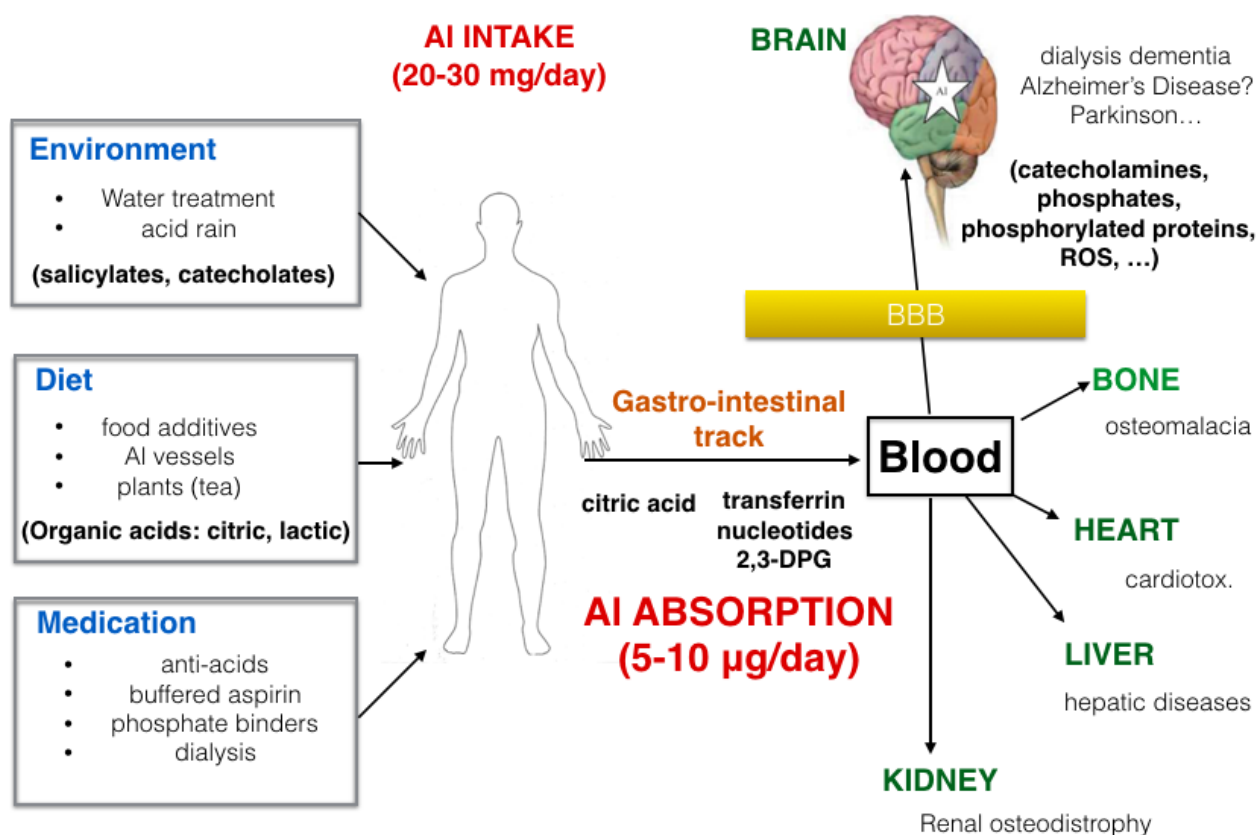
Fig.1.5. Schematic representation of sources of aluminum intake and its speciation in the biological environment.

In conclusion, in this section a general picture about the human's exposure to Al(III) and, moreover, its potential interferences with the biochemical environment of the human organism has been provided. In light of what it has discussed up to this point, can we state that aluminum is a potential health problem? Unfortunately, there is not a clear answer to this question. It depends on many factors, the most important of which is the concentration of aluminum that we are exposed to. It is undoubted that, as discussed in this section, in places where for environmental, workplace-based or atmospheric reasons there is a high exposure to this exogenous metal, then it is reasonable to argue that (long-term) toxic effects mediated by Al(III) may occur due to its accumulative power in the organism.

In this sense, I think that it is worth to mention the McIntyre Powder Project (http://www.mcintyrepowderproject.com/) by Janice Martell. The goal of this non-profit project is to gather information about the health issues (mainly neurological) caused by aluminum dusts to miners and other steelworkers of several regions of Canada. This project was started after Janice's father, one of these steelworkers, was diagnosed with Parkinson's Disease.

However, a central point to understand aluminum's toxicity is the concept of tolerance. It is well assessed that plants, in order to protect from the detrimental effects of Al(III), have evolved some mechanisms that induce tolerance to this non-essential metal[37]. In humans, it has measured that the tolerable weekly intake of Al(III) is 1mg aluminum/kg body weight[38]. Nevertheless, mechanisms and genes that may be involved in the biological tolerance of aluminum in humans are not known yet.

This is clearly pivotal in order to address the effective toxicity of this metal in "standard" daily lives, and, in that sense, to develop different and more specific therapeutic strategies than chelation therapy. A general view of the proposed molecular basis of aluminum toxicity, with special focus on tis role with respect to Alzheimer's Disease, will be provided in the next section.

1.1.4 The (neuro)toxicity of aluminum and its link to Alzheimer's Disease: an overview of the current status

1.1.4.1 Aluminum's interaction with the biological environment

Several potential detrimental effects have been attributed to the aluminum ion in the biological environment; these include interaction with Low Molecular Mass (LMM) molecules such as citrate[36,39], 2,3-diphosphoglycerate[22,40], Glucose-6-phosphate[41], nicotinamide adenine dinucleotide (NADH)[42,43], catecholamines[44], biophosphates (DNA, RNAs and in particular Adenosine-5-phosphates like ATP)[22,45] among others. Likewise, Al(III) can interact with High Molecular Mass (HMM) ligands such as transferrin[22,46,47], albumin[22] and Aβ-amyloid[48-50].

Moreover, the interference of aluminum with the biochemical processes of the cell has been related to the production of dangerous free radicals[51-53]; in particular, although Al(III) is a non-redox metal, it has been proposed that its pro-oxidant activity is mediated through its interference with the Fenton reaction[54-56] (see chapter 6).

The harmfulness of aluminum has been also related to patients with chronic renal failure and dialysis[14,36,57], dialysis encephalopathy[5,14,58], autism[12,13] and neurodegenerative diseases such as amyotrophic lateral sclerosis (ALS)[5,6], Gulf War Syndrome[5,6], and, above all, Alzheimer's Disease (AD)[4,5,48,49,59-61] and Parkinson's Disease (PD)[49,62-64].

Due to the enormous size of the topic, the following section will focus in detail on the role of Al(III) in the brain and on its link with neurodegenerative diseases, in particular AD.

1.1.4.2 Aluminum and neurodegenerative diseases: towards a link with Alzheimer's Disease

Although the potential toxic role of Al(III) has been presented and discussed in the previous setions, the mechanisms and the molecular basis by which this metal influences the physiological activities of the cell are still obscure. This is particularly true when we consider the effects of aluminum in the brain, where its competition with myriad of biomolecules and other endogenous metals, as well as its low concentration, make the speculation of its detrimental effects a hard matter, as outlined by Exley:

"The neurotoxicity of aluminum is well documented and widely accepted while the mechanisms through toxicity is brought about are much less completely understood"[49].

In Table 1.2 and Fig. 1.6, sites of the central nervous system (CNS) that are affected by the presence of aluminum according to the most recent literature are summarized. These adverse effects include crucial reactions for brain development such as the axonal transport, neurotransmitter synthesis (specially the catecholamines pathway, see chapter 7), synaptic transmission, phosphorylation or dephosphorylation of proteins (such as Tau), protein degradation, gene expression and infiammatory responses (Table 1.2). An excellent review that discusses these aspects in detail can be found in Ref.[5].

Effects of aluminum in the central nervous system (CNS)

Nucleus and gene expression	
Binding to DNA	• Binds to Histone-DNA complex and induces conformational changes of chromating. • Induces topological changes of DNA.
Altered gene expression	• Induces decreased expression of neurofilaments and tubulin.

	• Induces altered expression of genes of neurofilament, APP, and neuron specific enolase. • Induces decreased expression of transferrin receptor. • Induces altered expression of RNA polymerase I. • Induces downregulation of mitochondrial cytochrome c oxidase. • Induces altered expression of calbindin-D28k. • Induces decrease in the expression of nerve growth factor (NGF) and brain derived neurotrophic factor (BDNF). • Induces expression of pro-inflammatory genes and pro-apoptotic genes. • Induces elevated expression of APP. • Induces altered expression of oxidative stress marker genes (SOD1, glutathione reductase, etc.). • Induces decreased expression of neprilysin. • Induces altered expression of *β*-APP secretase (BACE1 and BACE2).
Cellular functions	
Energy metabolism	• Inhibits the activity of hexokinase. • Inhibits the activity of phosphofructokinase. • Inhibits the activity of glucose-6-phosphate dehydrogenase. • Causes mitochondrial dysfunction and depletion of ATP. • Decreases in activity and expression of TCA-cycle related enzymes (succinate dehydrogenase (SDH), alpha-ketoglutarate dehydrogenase (KGDH), isocitrate dehydrogenase-NAD$^+$ (IDH), fumarase (FUM), aconitase (ACN), and cytochrome c oxidase (Cyt C Ox)).
Phosphorylation and dephosphorylation	• Inhibits the activity of protein phosphatase. • Increases the activity of protein kinase C and cytoskeleton proteins. • Accelerates phosphorylation and accumulation of neurofilament. • Enhances Ca_2^+/Calmodulin dependent protein kinase activity. • Accelerates phosphorylation of MAP 2 and neurofilament. • Inhibits dephosphorylation of tau. • Induces nonenzymatic phosphorylation of tau.

Abnormal accumulation of proteins	• Causes the conformational change and the accumulation of neurofilament and MAP1A, MAP1B. • Accelerates the phosphorylation of tau and its accumulation. • Causes the accumulation of tau protein in neuroblastoma cells or in primary cultured neurons. • Causes the accumulation of tau protein in experimental animals. • Causes neurofibrillary degeneration *in vivo*. • Causes the accumulation of Aβ-amyloid in cultured neurons or in neuroblastoma cells. • Causes the accumulation of Aβ-amyloid *in vivo*.
Neurotransmitter release	• Inhibits glutamate release. • Impairs synaptic transmission. • Inactivates glutamate dehydrogenase. • Inhibits NMDA-type glutamate receptor. • Inhibits choline acetyl transferase and tyrosine hydroxyl11ase, glutamate decarboxylase. • Influences acetyl-CoA and inhibits acetylcholine release. • Activates monoamine oxidase. • Inhibits dopamine beta-hydroxylase. • Inhibits uptake of serotonin and noradrenalin in synaptosomes.
Channel inhibition	• Influences the activities of Na^+ channels and K^+ channels. • Enhances the voltage-activated Na^+ channels. • Inhibits the voltage-gated calcium channel. • Inhibits the IP_3-mediated Ca^{2+} release.
Others	• Influences GTP binding proteins as aluminum fluoride. • Inhibits GAP junction. • Inhibits axonal transports. • Binds to calmodulin and inhibition of calmodulin-binding enzymes. • Induces inflammatory responses.
Membrane lipids	
Peroxidation	• Accelerates iron-induced membrane lipid peroxidation.

	• Enhances lipid peroxidation in liposomes. • Induces peroxidation of myelin lipids *in vivo*. • Increases peroxidation products (malondialdehyde).
Membrane properties	• Causes the change the lipid/phospholipids profiles of myelin *in vivo*. • Induces the change in membrane physical properties (surface potential, lipid fluidity, and lipid arrangement). • Induces the change of membrane fluidity.
Higher properties	
Cell death	• Causes the apoptotic neuronal death. • Causes the apoptosis of astrocytes. • Causes the death of motor neuron.
Behavior, learning and memory, others	• Inhibits long term potentiation (LTP). • Causes learning disorder or memory deficit in experimental animals. • Influences electrical activity in hippocampus and inhibits spatial learning memory deficit in aging rats. • Causes memory deficit in AD model mice. • Causes encephalopathy in dialysis patients. • Causes encephalopathy in patients with renal failure.

Table 1.2. Effects of aluminum in the central nervous system (CNS). Edited from ref.[5] and references herein.

It is clear that Al(III) has the potential to affect the normal biochemistry of neuronal cells at many different levels; accordingly, what is the controversial role of aluminum in the pathogenesis of Alzheimer's Disease (AD) ? What are the evidences in this sense and (if any) the molecular basis that lead to the neurodegenerative phenotype ?

AD is a severe type of senile dementia first reported in 1906[5]. The pathological hallmarks are the deposition of extracellular senile plagues, intracellular neurofibrillary tangles (NFTs) and the selective loss of synapses and neurons in the hippocampal and cerebral cortical regions[5].

Intracellular NFTs are mainly composed of the phosphorylated tau protein. In a pioneering study, Hollender *et al.*, investigated the structural features of an octapeptide NFT analogue (GEGEGSGG) and its phosphorylated serin (ser(P)) derivative, both in presence/absence of Al(III)[65].
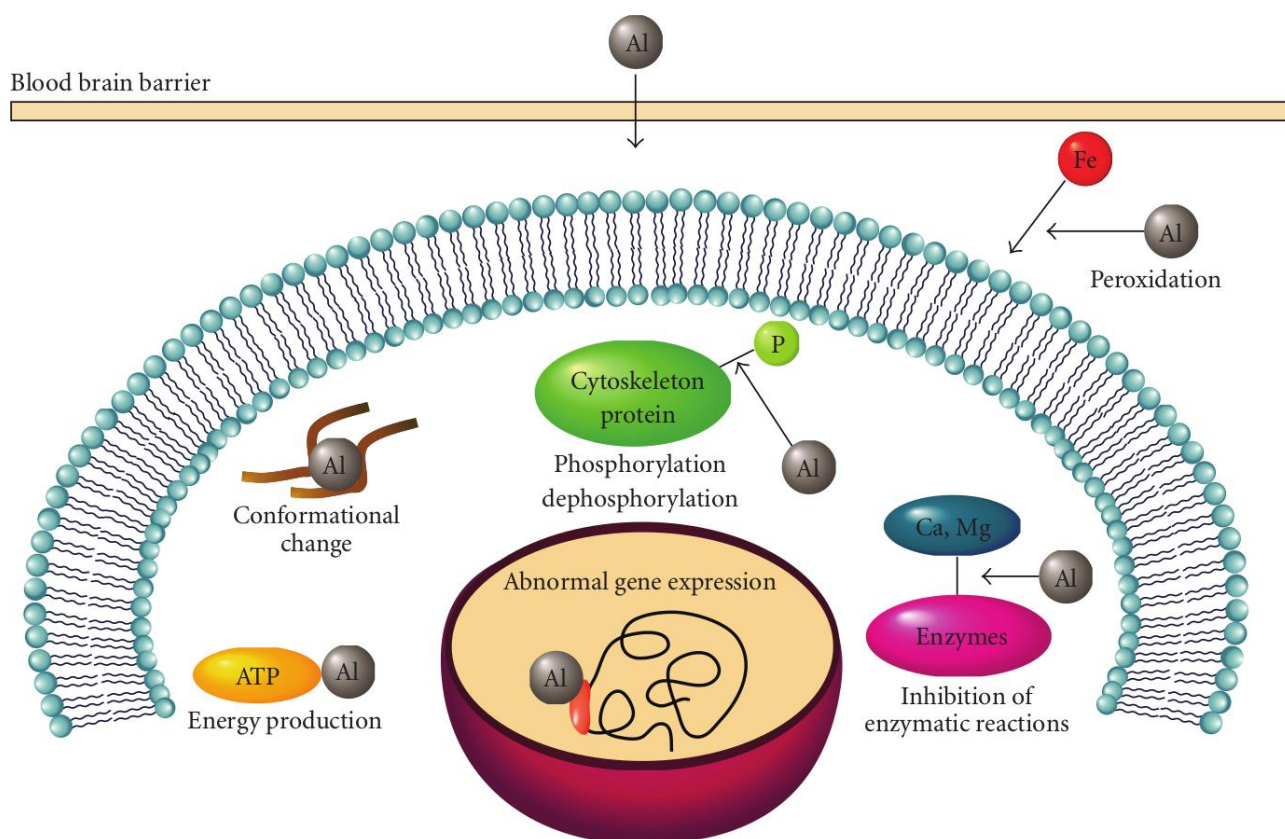
Fig. 1.6. Major biological effects of Al(III) in the central nervous system (CNS). Taken from ref.[5].

Their results revealed that both phosphorylated and dephosphorylated octapeptide is able to bind aluminum; however, NMR chemical shifts pointed to a significant change in the Al-binding pattern upon phosphorylation[65].

Further computational studies, were able to unveil the effect of phosphorylation to this NFTs analogue: the addition of phosphates has been proposed to (i) change the binding pattern to Al(III) shifting the preferential site from C-terminus to ser6(P). (ii) Increase its binding affinity by 15 kcal/mol, a fact mainly due to the increase in the overall negative charge upon phosphorylation; and (iii) cause important changes in the secondary structure of the polypeptide chain, which may be a contributing factor to the aggregation process of NFTs in Alzheimer's Disease[66].

Extracellular senile plagues contain a large amount of Aβ-amyloid protein[67]. The hypothesis that Al(III) is an environmental contributor of the pathogenesis of AD, the "aluminum hypothesis", was proposed in 1960s based on various neurotoxicological, analytical and epidemiological evidences[5]. In a seminal study, Exley *et al.* demonstrated the affinity of aluminum for Aβ-amyloid$_{(1-40)}$, and highlighted the partial loss of α-helical conformation of the oligopeptide upon aluminum binding, leading to a β–sheets rich structure, typical of the amyloid aggregates[68]. Moreover, very recent studies with state-of-the-art experimental techniques demonstrated the presence of high levels of aluminum

in brain tissues of patients diagnosed with familial AD[69,70], and that this non-essential metal might be a strong contributor to the development of AD[4].

However, in spite of these findings, the aluminum hypothesis has been the subject of much debate and criticism for several decades, and still it is.

In order to try to explain and clarify the link between Al(III) and AD at the molecular level, many hypothesis have been made:

I. A first hypothesis proposes that aluminum may lead to conformational changes in the Aβ peptide from an α-helices based structure to a β-sheets rich one, as mentioned before[68], also promoting their incorporation into cell membranes as calcium-permeable channels and provoking the increase of intracellular calcium levels and cell death[6,68].

II. In the second hypothesis, the idea is that Al(III) may interact with the acidic groups of Aβ-amyloid promoting its aggregates and accelerating the formation of amyloid fibrils[6,71].

III. A third possibility states that aluminum facilitates iron-mediated oxidative damage in neurons, caused by co-deposition of Aβ peptides with Al(III) and Fe(III) [6,72].

IV. The fourth hypothesis, that has been called the "amyloid cascade hypothesis" [5], shares characters from the previous hypothesis and tries to outline a multistep complex picture. It relies on the fact that the metal-induced conformational changes of Aβ-amyloid, and its consequent neurotoxicity, play a central role in the development of AD. Al(III) as well as other endogenous metals such as Fe(III), Zn(II) and Cu(II), influence, in different manners and at different stages, the oligomerization and conformational changes of Aβ-amyloid thus acting as bridging factors with respect to negatively charged oligopeptides side chains[5]. A more detailed discussion on this aspect is provided in the next section.

1.1.4.3 The amyloid cascade hypothesis

Aβ-amyloid (AβP) is a small peptide consisting in 39-42 aminoacids, secreted by cleavage of the amyloid precursor protein (APP), a membrane protein whose primary function is still unknown. The N-terminus of APP is cleaved by the β-site APP cleaving enzyme 1 (BACE 1) while its intramembrane C-terminus is cleaved by γ-secretase[5].

The resulting AβP is a hydrophobic peptide with an intrinsic tendency to self-assemble and form stable oligomers in aqueous solution. In its monomeric form, AβP has a random coil structure, while

the oligomeric form is mainly composed of by β-sheet structures and form insoluble aggregates, known as amyloid fibrils[5].

As previously mentioned, it has been proposed that aluminum can bind to the negatively charged side chains of AβP. Other metals share the binding site, although their stability constants (i.e. binding affinities) are different. Al(III) is known to bind and affect several metal binding proteins, as well as to influence the homeostasis of other biologically important metals; therefore, the interplay of aluminum with other endogenous metals should be considered a possible explanation for the implications of various trace elements in the pathogenesis of AD[5].

Figure 1.7 summarizes the hypothesized synergic interactions between aluminum and other metals towards the formation and stabilization of detrimental amyloid aggregates.

Aluminum, as an hard Lewis acid, shares some similar characteristic to the trivalent Fe(III) ion, and therefore is prone to ligate to iron regulatory proteins such as transferrin or the iron regulating protein (IRP). The iron responsive element/iron regulatory protein network (IRE/IRP) regulates the production of iron binding proteins (transferring, ferritin) which prevent the formation of free Fe(II) ions that are involved in dangerous free radicals production[5] (Fig. 1.7).

In iron-deficient conditions, IRP binds to IRE and regulates the expression of genes that contain iron responsive elements in their mRNA such as transferrin or ferritin. As the concentration of Fe(II) increases, iron binds to IRP and the expression of transferrin is downregulated while that of ferritin is upregulated leading to a decrease in the amount of free Fe(II)[5].

Al(III) can also bind to IRP and therefore influences the expression of iron binding proteins that contain IREs in their mRNA, causing high concentrations of iron in the cell (Fig. 1.7)[5].

In this way aluminum affects iron homeostasis and the expression of genes regulated by its homeostasis. The crucial point is that APP-associated mRNA contains an IRE as well as ferritin, and its expression is regulated by iron. The consequence is that aluminum causes elevated expression of APP[5].

On the other hand, it has been found that Zn(II) inhibits the ferroxidase activity of APP; moreover, APP contains copper/zinc binding sites in its N-terminal and in the AβP domain and therefore it may be involved in the homeostasis of these metals[5].

An abnormal expression of APP could lead to an increased production of AβP and enhance its accumulation. AβP is usually degraded by proteases like neprilysin after a shor period. Al(III) has been shown to downregulate neprilysin, which in turn implies increased accumulation of AβP[5]. Other evidences point to a promotion of the oligomerization of AβP in presence of trace metals like Al(III), Zn(II) and Fe(III), to its resistance to proteases and its accumulation in brain.
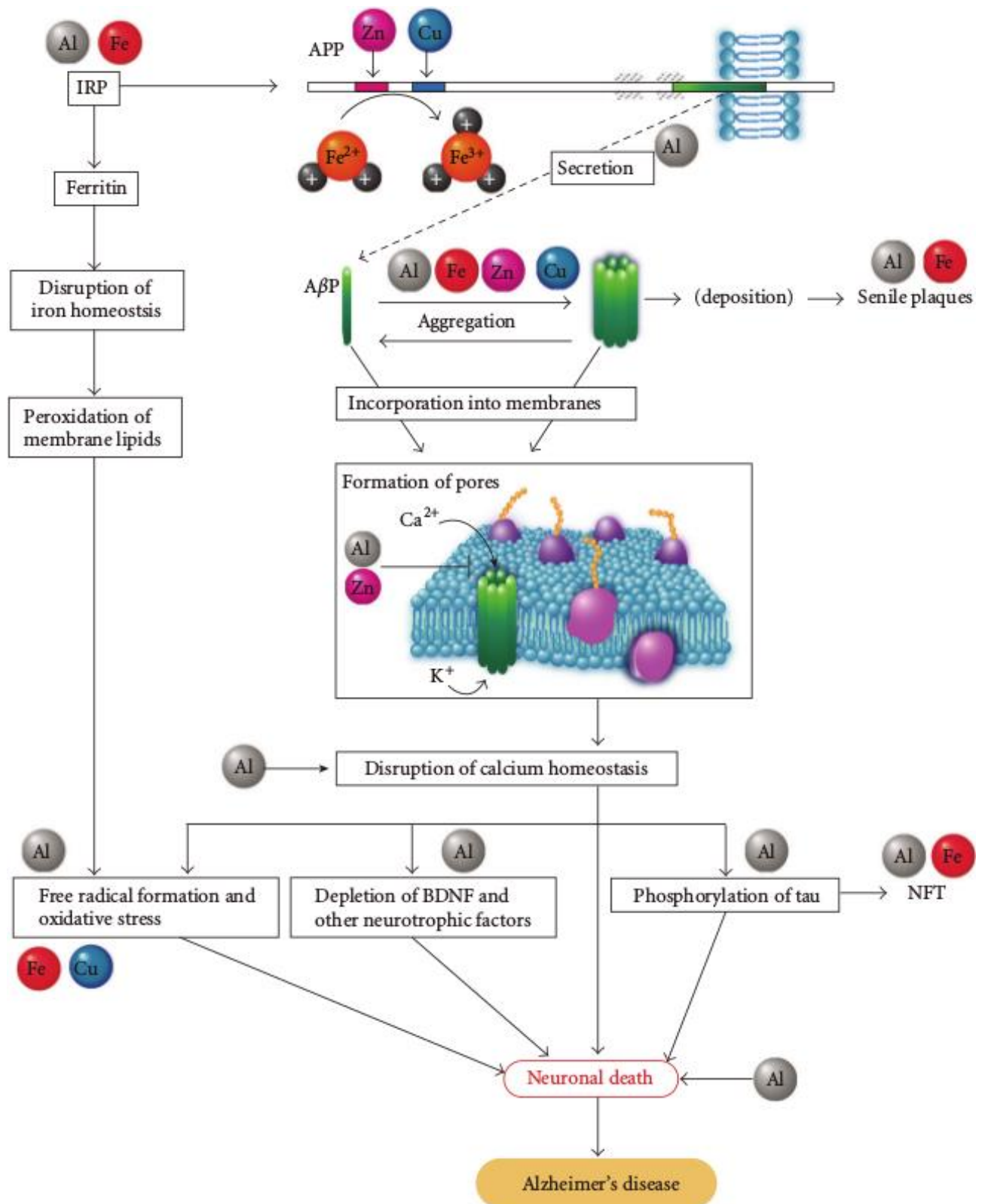
Fig. 1.7. Schematic representation of the amyloid cascade hypothesis. Taken from ref.[5].

The newly formed AβP oligomers could be incorporated into cell membranes, resulting in the formation of ion channels. A subsequent influx of calcium through these amyloid-based channels

would lead to the phosphorylation of tau proteins, depletion of neurotrophic factors and the formation of free radicals, whose final outcome would be neuronal death (Fig. 1.7)[5].

It is worth to mention that, in light of the above discussion, the use of chelation therapy as a potential cure for the attenuation of the severe phenotypes caused by AD has shown very promising results[73], which is another evidence towards the involvement of trace metals, and aluminum among them, in the pathogenesis of neurodegenerative diseases.

As previously mentioned, the exact molecular basis of the binding of Al(III) to Aβ-amyloid are not well understood. However, a recent computational study carried out in our group by means of a multi-level approach ranging from Quantum Mechanical cluster models to full size QM/MM hybrid simulations helped in elucidating, for the first time, a possible 3D structure of Al(III)-AβP$_{(1-42)}$ (Fig. 1.8)[74].
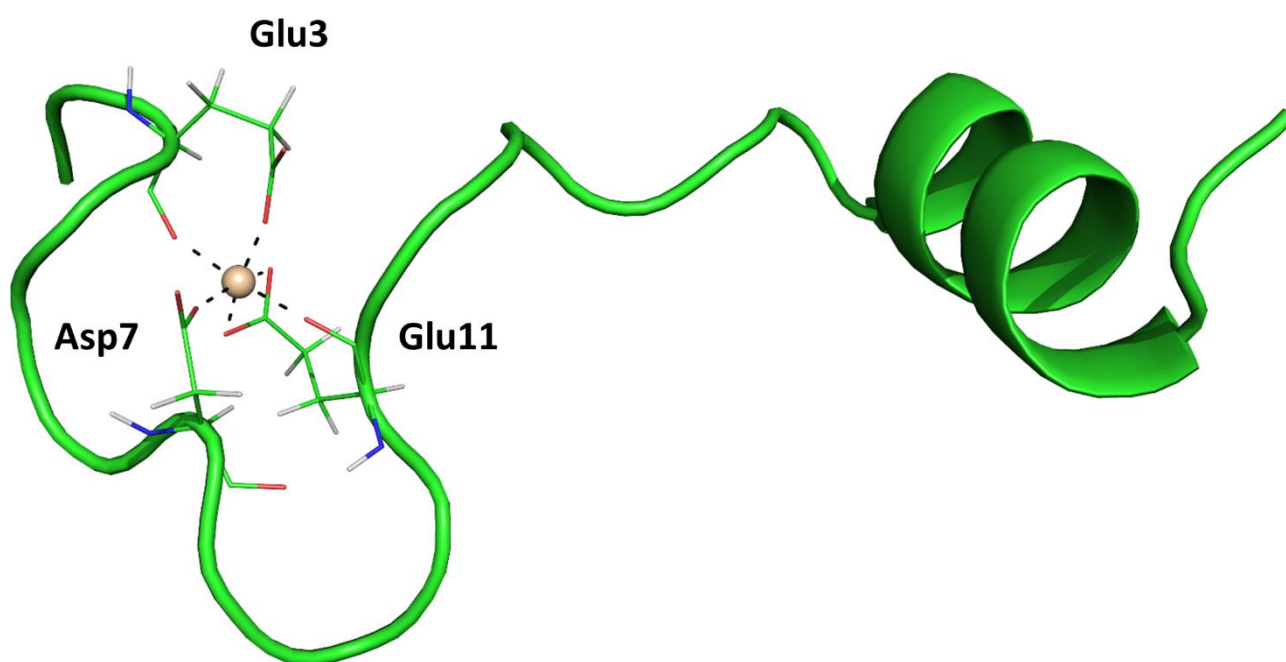
Fig. 1.8. Proposed structure for the most stable 1:1 Al(III)- β-amyloid complex. Created with data from ref.[74].

By translating the pre-organization concept of host-guest interaction for the binding of metals to peptides, this study proposes that the most stable structures are formed by the interaction of aluminum with the negatively charged carboxylate groups of Glu3, Asp7 and Glu11; some peptide bond carbonyl oxigens may fill the coordination sphere of Al(III) through dative bonding (Fig. 1.8)[74].

The calculated interaction energy (ΔE) of the most stable Al-AβP complex was found to be -172.9 kcal/mol at the PBE/def2-SV(P) - COSMO level of theory. Comparing the relative binding affinity with those of other bioligands previously calculated in other works, it has been found that the stability

of the complex is comparable to those of citrate (the strongest endogenous Al(III) chelator)[39]. These findings are coherent with hypothesis that monomeric β-amyloid has high affinity for this metal and, accordingly, it might be a primary aluminum chelator in the brain.

Such a study aimed to help to unveil a possible structure for the aluminum-amyloid complex in absence of an experimental X-ray template; the aforementioned results may be a starting point towards the understanding of the molecular basis of the role of aluminum in the aggregation process of amyloid fibrils.

1.2 Chelation therapy

1.2.1 The goal of chelation therapy

Chelation therapy can be defined as the use of a chelating agent in order to remove an undesired metal ion and/or the attenuation of its toxicity by transforming it into less toxic compounds.

Metal-induced toxicity can be classified according to the source and the effect:

1. *__Acute ingestion__* of a toxic metal, that can be accidental (children) or voluntary or self-induced (suicidal/homicidal purposes).

2. *__Chronic intoxication__*, that may have environmental, occupational or iatrogenic causes.

3. *__Metal overload__* due to genetic diseases (e.g. Wilson's Disease[75]).

It is clear that, as thoroughly discussed in the previous sections, Al(III) mainly relates to point 2, as the environmental and occupational features of the "Aluminum Age" are supposed to lead to chronic accumulation of this metal with long-term effects that may be related to the insurgence of neurodegenerative diseases.

One of the main challenges of chelation therapy, that will be discussed in section 1.2.4, is the small degree (or, in some cases, lack) of specificity, i.e. the distinction between different essential and toxic metal ions.

1.2.1.1 Essential and non-essential metal ions

Essential elements are chemical compounds that are fundamental for the biochemical processes of living cells; mammalians require 30 essential elements, that can be classified as essential, inert and toxic[18]. Among these elements, eukaryote cells require 17 metals. Much of these metals paly a dual role in the organism, according to their concentration: toxic compounds can be tolerated in low doses, while essential elements can be toxic at thigh concentrations, as showed in the Bertrand diagram of Fig. 1.9.

Essential metals include copper, which is a cofactor of many oxidative enzymes such as the Dopamine-β-hydroxylase involved in the catecholamine biosynthesis pathway[64,76,77] (see chapter 7). Iron is involved in hundreds of enzymatic reactions (such as the Fenton reaction[54], chapter 6) and is the most important component of hemoglobin, the oxygen carrier in red blood cells. Zinc is a component of more than three hundred of proteins[18]. Zinc deficiency, which is often encountered in third world countries, can lead to dwarfism, and adolescent nutritional-associated disorder[18].
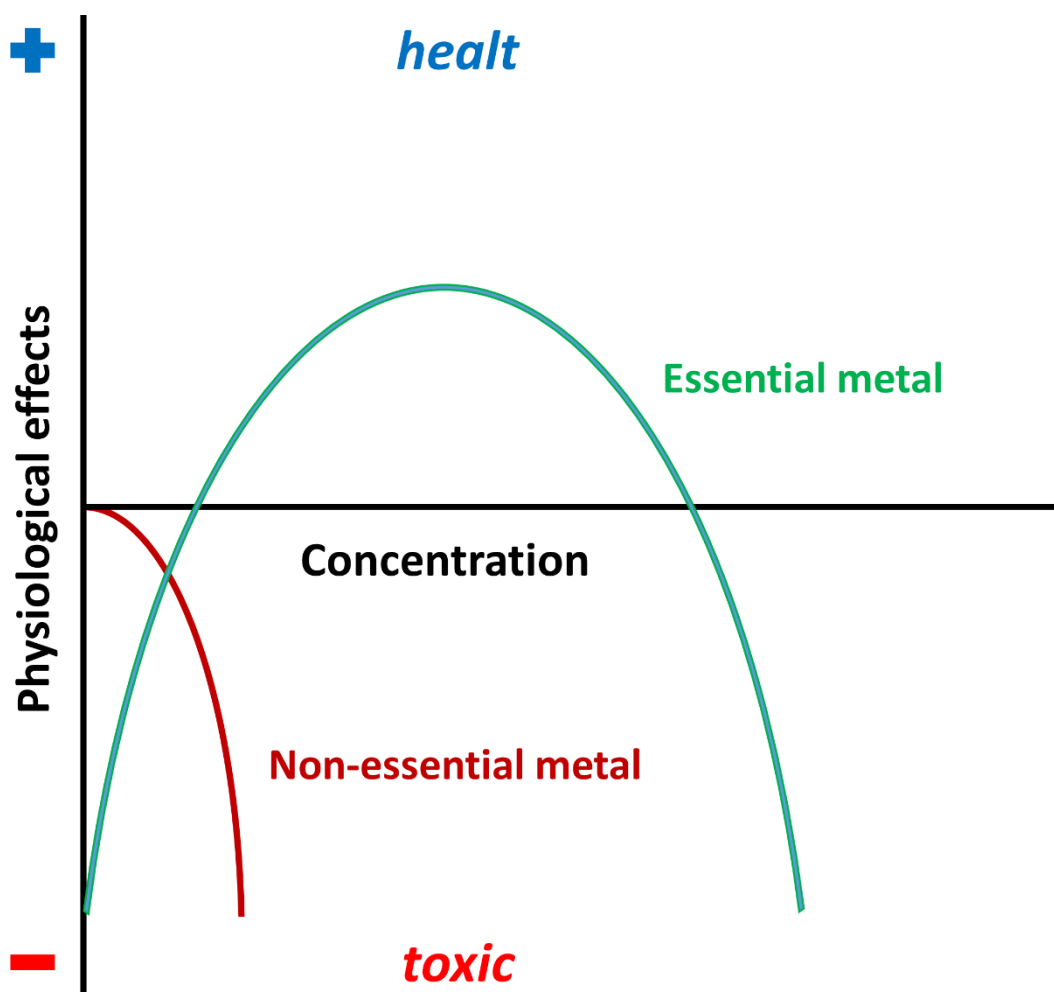
Fig. 1.9. Bertrand diagram showing essential and non-essential (toxic) metal ions.

Cobalt is an essential cofactor of vitamin B12, which is involved in DNA regulation; manganese is a cofactor of many enzymatic reactions involving phosphorylation, cholesterol and fatty acids synthesis. Selenium is essential for several anti-oxidant enzymes; it is interesting to note that, contrary to animals, plants do not require selenium to survive, however they can adsorb it and this is the reason of selenium poisoning that may occur upon eating plants growing in selenium rich soils[18].

Molybdenum is an essential cofactor for xanthine oxidase and aldehyde oxidase; it is also essential to plant as it is involved in the regulation of nitrogen metabolism through bacteria[18].

Fundamental and clear knowledge of the essential metal ions is mandatory since aluminum, a non-essential element, can influence and interfere with the concentrations and biochemical pathways of many of these essential metals in several different ways that are still not properly understood.

From an experimental point of view, the behavior of a metal at physiological conditions mainly depends on its speciation, as discussed in section 1.1.2.3. In this sense, different species that are formed, as well as the thermodynamic equilibria in solution and their stability constants, allow to determine their soluble/insoluble species, complexes with endogenous/exogenous chelators and their concentrations. In this sense, the thermodynamic approach is a very reliable choice in analytical chemistry for the study of ligands that interact with metal ions like aluminum[78-80].

In particular, such an approach has been found to be very reliable for the study of ligands that may be used as chelating agents for metal intoxication[6,25,28]. In the next section an overview on the properties of these chelators is provided.

The concepts of "chelator" and "denticity" were introduced in section 1.1.2.3, explaining the possible binding modes with respect to aluminum (Fig. 1.2).

1.2.2 Al(III)-based chelating agents

Chelating agents (chelators) are organic or inorganic compounds able to bind metal ions and form complex ring-like structures called "chelates". As introduced in section 1.1.2.3, they can have different binding modes (denticity, Fig. 1.2) which influence the strength and the stoichiometries of the formed complex according to the pH considered.

In light of what it was discussed in section 1.1.2 in the case of aluminum, the main determinants that influence the Al-chelator binding affinity can be summarized as follows, ordered by their relative effect on the stability:

i) ***Aluminum/proton competition for the ligand's binding site:*** since both Al(III) and H$^+$ are hard Lewis acids, the higher the pK_a of the donor atoms of the chelator, the higher the

affinity for the proton and, therefore, the higher the energy required for Al(III) to displace the proton and bind the ligand.

ii)   ***Competition with aluminum hydroxide:*** $[Al(OH)_4]^-$ is the most stable aluminum species in solution at physiological and basic pH range; therefore, in order to bind Al(III), a given chelator must form complexes that are thermodynamically more stable than aluminum hydroxide formation.

iii)   ***Steric effects (geometrical distortions):*** Al(III) first coordination shell can accept up to six donor atoms, with octahedral and tetrahedral geometries being the preferred ones. When steric hindrances take place within the Al-chelator complex due to intramolecular H-bonds (Desferroxamine in Fig. 1.2) or substituents close one another (6-methylsalicylic acid in Ref.[81]) then the final complex may contain distorted geometries that lower the overall complex stability.

iv)   ***Denticity and stoichiometry:*** different pH values lead to different stoichiometric Al-ligand complexes depending on the denticity of the chelator; due to the chelate effect (explained in the next section), ligand's denticity usually follows the affinity trend monodentate < bidentate < tridentate < tetradentate < pentadentate < hexadentate.

v)   ***Charge of the donor atoms:*** as previously discussed, Al(III) prefers to bind to negatively charged donors, although it can also bind to neutral ligands (H_2O, amines) *via* their lone pairs because of the dative nature of most of the Al-ligand interactions. The charge of the donors is so important that may overcome the denticity of the chelator.

vi)   ***Basicity of the donor atoms:*** when donor atoms bear the same charge, then the determinant for the stability of the Al-ligand complex shifts to their basicity; the higher their Lewis basicity, the higher their affinity for Al(III).

vii)   ***Kinetic factors and relative concentrations:*** finally, other important factors to be considered in an open biological environment are the competition with endogenous aluminum chaltors (e.g. citrate), the relative Al(III)/ligand concentrations in a given site and the kinetics or their reaction[1,82,83] . These latter factors are far beyond the scope of this dissertation (and an extremely challenging task in computational modelling based on

cluster-continuum approaches); this thesis work will mainly focus on the thermodynamics of the Al-ligand interactions.

Therefore, an effective and potentially therapeutic aluminum chelating agent must meet the requirements summarized above in order to be able to form competitive complexes.

In addition, an "ideal" and clinically relevant chelating agent should possess the following features[6,28]:

- Low toxicity of both the chelating agent and the formed complex.
- Fast elimination of the metal-chelator complex.
- High selectivity toward the aluminum ion (extremely challenging).
- Biochemical metabolism of the chelating agent once entered in the body.
- Fast kinetic and exchange with endogenous ligands.
- Favorable intestinal adsorption.

Most of these biomedical factors belong to medicinal chemistry and are not the subject of this thesis dissertation.

1.2.2.1 The chelate effect

The "chelate effect" relies on entropic parameters. Considering the thermodynamic relationship between Gibbs free energy and stability constants[79,80] (logβ, discussed in section 1.2.3.1):

$$\Delta G = RT ln\beta \qquad\qquad (1.7)$$

$$\Delta G = \Delta H - T\Delta S \qquad\qquad (1.8)$$

Where ΔG is the Gibbs free energy, R is the gas constant (1.987 cal mol^{-1} K^{-1}) and T is the temperature. Accordingly, β increases as ΔG becomes more negative (due to more negative ΔH or more positive ΔS).

As a very simple case, consider the reaction equilibria of eq. 1.9 and 1.10 as well as their thermodynamic data reported in table 1.3 (taken from Ref.[18]):

$$Cd_{aq}^{2+} + 4 * CH_3NH_2 \rightleftharpoons [Cd(CH_3NH_2)_4]_{aq}^{2+} \qquad log\beta=6.5 \qquad (1.9)$$

$$Cd_{aq}^{2+} + 2 * NH_2CH_2NH_{2\,(aq)} \rightleftharpoons [Cd(NH_2CH_2NH_2)_2]_{aq}^{2+} \qquad log\beta=10.6 \qquad (1.10)$$
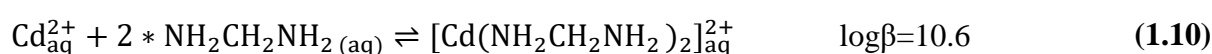
Ligand	ΔH (kJ mol^{-1})	ΔS (J mol^{-1} deg^{-1})	$-T\Delta S$ (kJ mol^{-1})	ΔG (kJ mol^{-1})
4(CH$_3$NH$_2$)	-57.3	-67.3	20.1	-37.2
2(NH$_2$CH$_2$NH$_2$)	-56.5	14.1	-4.2	-60.7

Table 1.3. Thermodynamic data of a purely entropic chelate effect.

In this example, Cd(II), whose coordination shell has a tetrahedral geometry, coordinates four methylamines (eq. 1.9) and two ethylenediamines (eq 1.10).

As shown in Table 1.3, the enthalpies of the two reactions are similar, therefore the difference in stability constants can be attributed solely to the difference in entropy. The main cause for the large increase in entropy is probably the net increase in the number of unbound water molecules.

Thus, although four CH$_3$NH$_2$ displace four H$_2$O from cadmium with no net change in the number of indipendent molecules, it takes only two ethylenediamines to displace four waters.

In summary, the chelate effect, that is, the increase in the metal-chelator complex stability through different denticities is (usually) an entropic-driven process.

However, it is worth to emphasize one more time that other determinants (discussed in the previous section) concur in the modulation of the stability of a given complex. All of these components lead to an overall complex picture whose clear understanding is of paramount importance towards the development of new and powerful Al(III) chelating agents.

1.2.2.2 Al(III) chelating agents: the current status

Since the trivalent aluminum ion shares many properties with the trivalent iron ion, in particular they are both hard Lewis acids, the Al(III)-based chelation therapy is irreversibly coupled with Fe(III)-based chelation therapy. Indeed, all chelating agents developed so far for the treatment of iron overload disorders are also employed in aluminum-related toxicity such as dialysis dementia [84,85].

The reason is that all chelators that show high affinity for Al(III) also retain high (and in almost all cases higher) affinity for the trivalent iron ion, due to the main ionic nature of the metal-chelator interactions. This lack of specificity is an important problem that has not been solved yet and will be discussed more in detail in section 1.2.4.

Currently, there are two main commercial chelating agents that have been approved by the U.S. Food and Drug Administration (FDA) for the treatment of iron- and aluminum-related pathologies: deferiprone (Ferriprox®) and deferoxamine (Desferal®), presented in Fig. 1.10.

Deferiprone (1,2-dimethyl-3-hydroxy-4-pyridinone, Fig. 1.11) has been approved and introduced into clinical practice since 2000[27,86]. It is a bidentate chelating agents, and, most importantly, it is orally active, in contrast to other chelators such as deferoxamine that need to be administred by subcutaneous injection[87]. It binds the metal through the negatively charged phenoxide, after deprotonation, and the carbonyl oxygen (Fig. 1.11). The phenoxide group bears a relatively small pK_a value of 9.8[86], which allows the metal to have a good competition with respect to the proton; on the other hand, the metal binds through dative bonding to the lone pairs of the carbonyl. The presence of both a single proton competition (opposed to a dual proton competition as in the case of catechols, explained later on in this section) and the methyl in position 3 (electron donating group, see chapter 3) result in a good chelating performance for this chelator expressed by the value of pAl (see section 1.2.3.2) of 15.8[86].

The main drawbacks of this widely studied Al(III) chelating agent are its poorer performance when compared with other hexadentate cheators such as deferoxamine, due to the chelate effect explained before, its lack of specificity for aluminum[6] and the presence of some undesired side effects during the therapy[87].
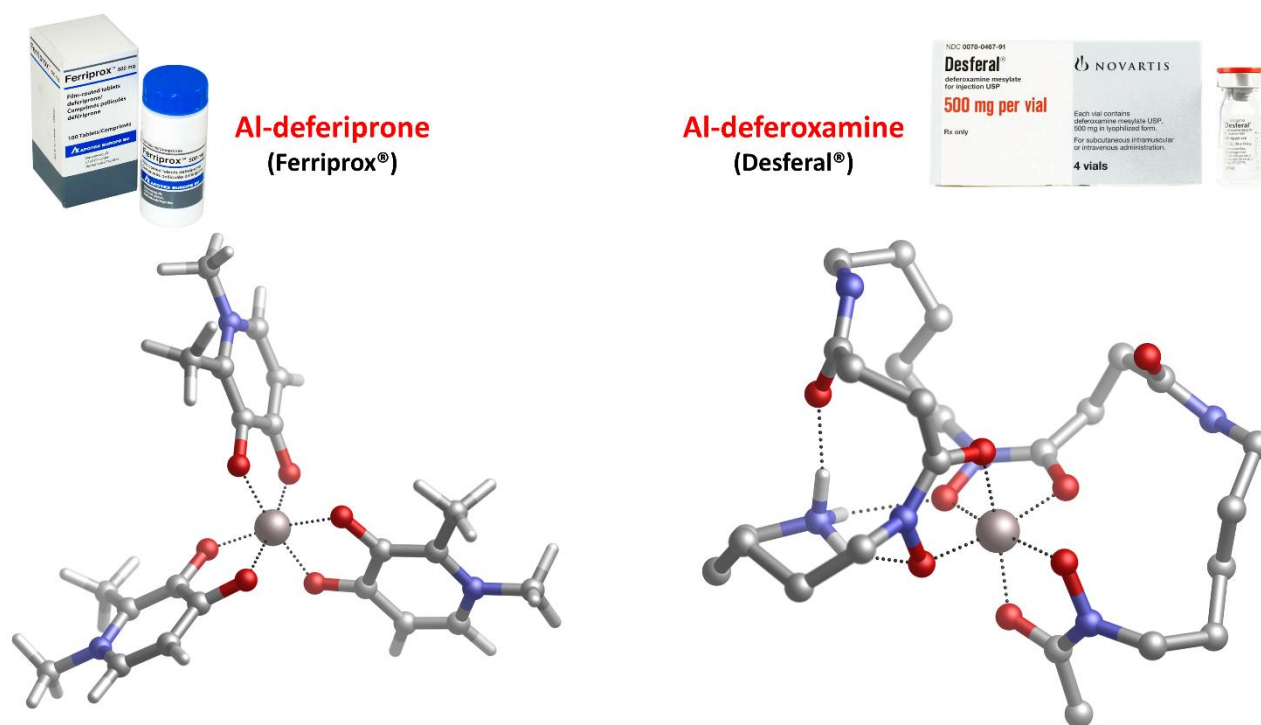
Fig. 1.10. Commercially available aluminum chelating agents: deferiprone (bidentate chelator) and deferoxamine (hexadentate chelator). Geometries optimized at the B3LYP-D3(BJ)/6-31++G(d,p) – IEFPCM level of theory.

Deferoxamine (DFO, DFB, Fig. 1.10 and 1.11) is a naturally occurring hidroxamate-based siderophore, used as a metal sequestering agent[88]. The linear tri-hidroxamic acid is composed by alternating 1,5-diaminopentane and succinic acid residues (Fig. 1.11); DFO is used by microorganisms for the solubilization and transport of iron, properties that make this compound to be an excellent chelating agent[88]. Although all three hydroxamate coordinating groups are protonated at physiological pH, the proton/metal competition is highly favoured by the chelate effect, which leads to extremely stable Al-DFO complexes, with a pAl value of 19.4[89].

However, there are some limitations in the use of this chelating agent in aluminum therapy; the first shortcoming is that DFO is not orally active, which means that it must be administrated by invasive intravenous injections. Moreover, like in the case of deferiprone, long-term treatments with deforaximine have been related to the production of undesired and potentially dangerous toxic effects[16]. Again, the high affinity of DFO for iron is clearly another big limitation in the use of this compound for the treatment of chronic Al(III) intoxications.

In light of the points discussed above, the quest for efficient, non-toxic and specific aluminum chelating agents has been the subject of several and important efforts in recent years[6,16,25,90-93]. A summary of the main and more promising building blocks that are commonly employed in the design of chelators with this aim is provided below and in Fig. 1.11.

Catechol and salicylic acid are the two building blocks that, potentially, show the highest affinity for aluminum[20,94]. The reason relies on the fact that two phenoxide groups of catechol are among the hardest Lewis bases[20], therefore are able to form strong dative bonds thanks to their high electron density. The big shortcoming for their use, as single compounds in chelation therapy, comes from the high pK_a values of the two phenoxide that make the metal/proton competition at physiological pH highly unfavorable (Fig. 1.11). Such an aspect is thoroughly explained in chapter 3. On the other hand, catechol-based moieties have been extensively used to design several hexadentate chelating agents whose chelate effect, in principle, would overcome the negative competition related to the deprotonation of the oxygen donors by aluminum[89]. This strategy is successfully employed in Nature in the case of the tris-catechol based siderophore Enterobactin.[95]

Salicylic acid (Fig. 1.11) allows for a better performance regarding the metal/proton competition because of the low pK_a of the carboxylate group[94]. However, the latter is a weaker Lewis base than phenoxide due to its intrinsic resonance and, therefore, leads to lower affinity towards Al(III) than catechol[20]. This compound is also widely analyzed in chapter 3.

Hydroxy-pyridin-carboxylic acids (HPCs, Fig. 1.11) are among the most promising aluminum chelating agents[25,92,96]. They retain the advantage of the small pK_a value of the carboxylic group at

physiological pH; moreover, the electronegativity of the nitrogen placed in the ring lowers the pK_a of the phenolate by decreasing its electron density, allowing for an improved metal/proton competition.

| Catechol | Salicylic acid | HPC | HPC |

| Kojic acid | Deferiprone | EDTA |

Deferoxamine
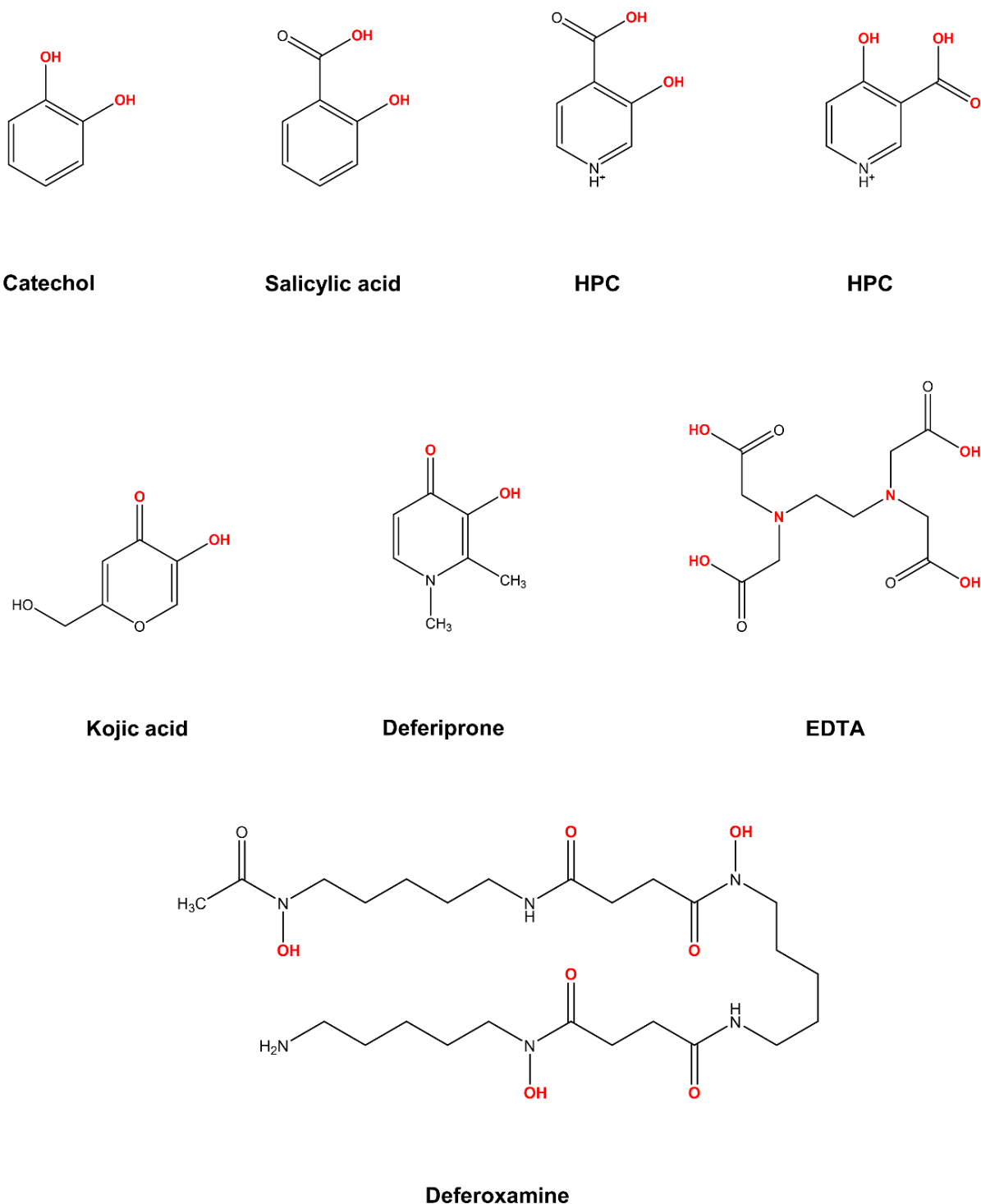
Fig. 1.11. Main bidentate and hexadentate Al(III) chelating agents commonly used as building blocks in chelation therapy. In red, donor atoms that form the coordination site for aluminum. HPC=Hhydroxypyridincarboxylic acid. EDTA=ethylenediaminetetraacetic acid.

On the other hand, the reduction of electron density in the two oxygen donors makes them poorer Lewis bases, leading to less competitive metal-ligand complex stabilities than those of salicylic acid and catechol. A promising strategy to improve their stability may be the tuning of the pyridinic ring by the addition of electron donating groups such as the methyl, as experimentally assessed by Di Marco's group[25]. Hydroxypyridinones (HPOs) is a highly related family that includes the commercial drug deferiprone previously described; they differ from HPCs by the fact that they contain a carbonyl instead of the carboxylate, and they share very similar properties to HPCs . Due to their promising features, both HPCs- and HPOs-based building block have been extensively used to design a wide range of polydentate chelating agents[90,91,96-99].

Hydroxypyrones are kojic acid derivatives (Fig. 1.11) that differ from HPOs by an oxygen in the ring in place of the nitrogen. The stronger electronegativity of the oxygen has the positive effect of further lowering the pK_a value of the phenolic oxygen but, at the same time, the negative one of further decreasing the electron density from the oxygen donors, thus leading to even less stable aluminum-chelator complexes. Despite these shortcomings, the polyfunctional heterocyclic ring allows for an extensive tuning of the properties of these compounds as well as the synthesis of many improved derivatives with higher denticities[100-102]. The main developments in this sense have been made by Crisponi's group[25].

The current status of the cutting edge research on aluminum's chelating agents is based on the building blocks discussed above and depicted in figure 1.11. They conjugate the affinity towards Al(III) in terms of Lewis basicity with metal/proton competition for the binding site in different extents, with the aim of identifying the "ideal" and most suitable solution. It is important to highlight that, experimentally, metal-ligand binding affinity and metal/proton competition for a given ligand are measured by two important parameters, stability constants and pM, respectively. They will be discussed in the next section.

Finally, it is also worth to mention that, for hexadentate chelators, a pre-organization hypothesis has shown to be very promising towards the design of new and efficient sequestering agents[80]. This hypothesis was firstly demonstrated for the conformational properties of the natural and powerful siderophore Enterobactin[95] (Fig. 1.12). It has been shown that, in this highly flexible ligand that contains many degrees of freedom, multiple intra-molecular H-bonds networks are responsible for the stabilization of a pre-organized structure where the ligand's chelation groups are placed in such a way that are ready to bind the metal[95,103,104]. In other words, the entropy needed to deform the ligand in order for it to adopt a conformation suitable to chelate the metal ion is minimal due to the presence of a pre-organized structure stabilized by intra-molecular H-bonds and other interactions (Fig. 1.12).
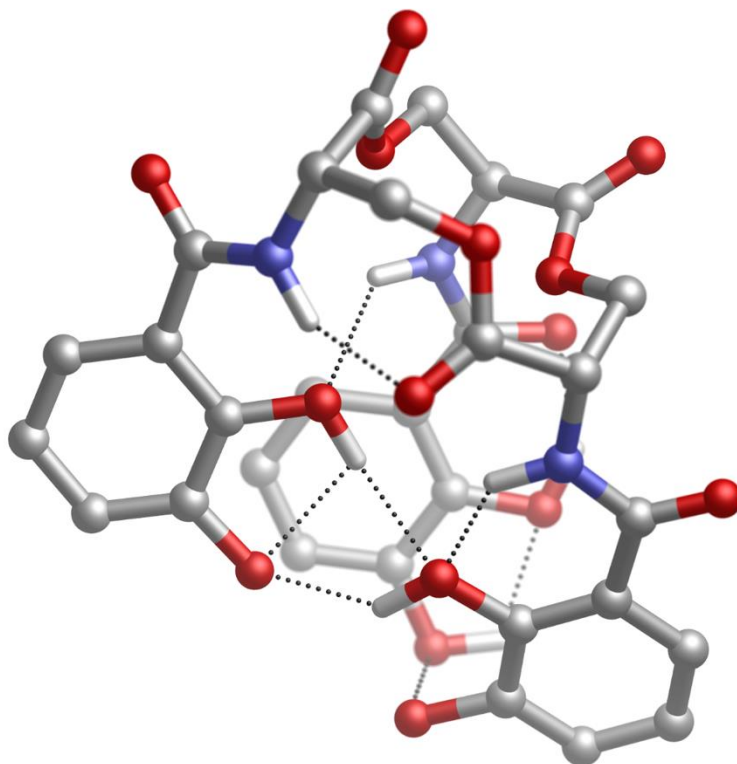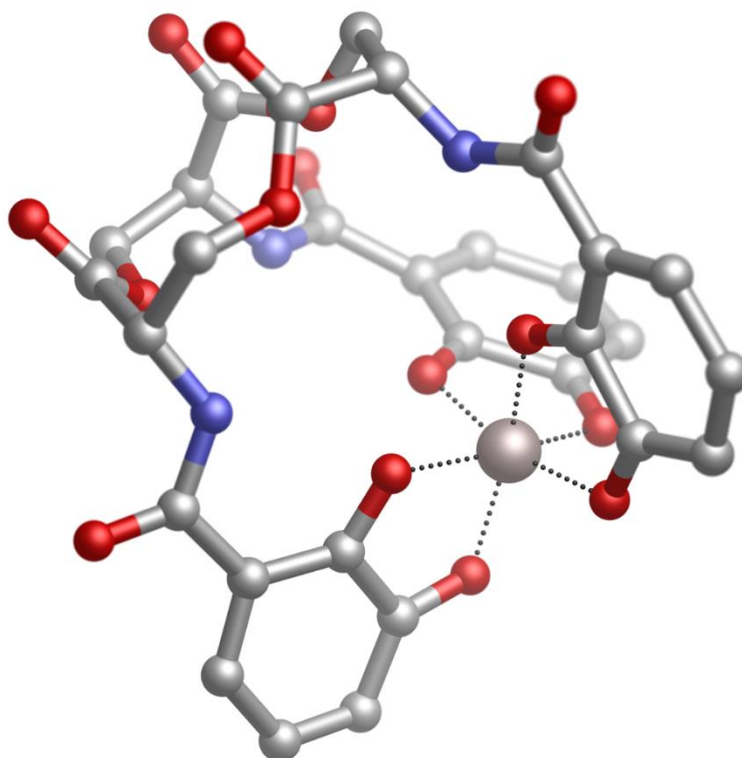
Figure 1.12. **(A)** Pre-organized structure of free Enterobactin in solution. Intramolecular interactions and significant hydrogen atoms are highlighted. **(B)** Aluminum-bound Enterobactin. Geometries obtained by means of conformational analyses followed by DFT optimization with implicit solvation models.
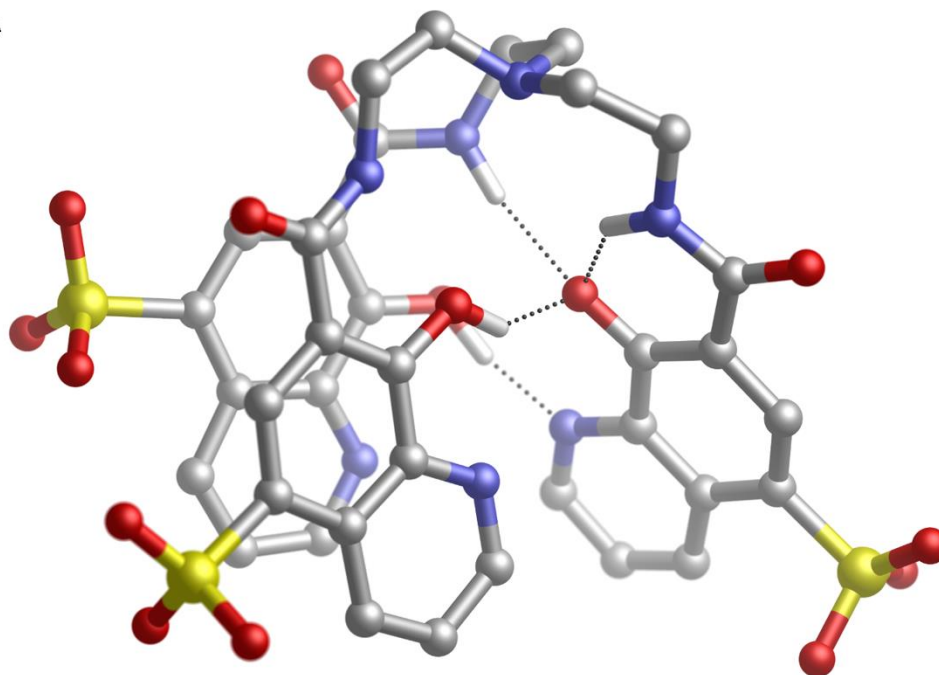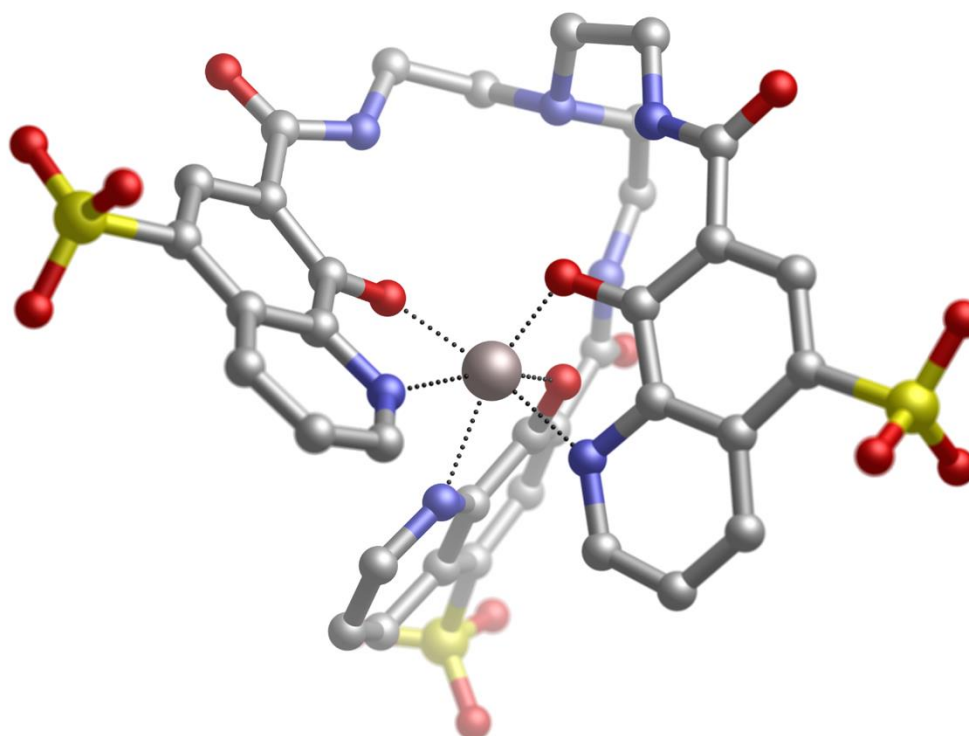
Figure 1.13. **(A)** Pre-organized structure of free O-TRENSOX in solution. Intramolecular interactions and significant hydrogen atoms are highlighted. **(B)** Aluminum-bound O-TRENSOX. Geometries obtained by means of conformational analyses followed by DFT optimization with implicit solvation models.

The same hypothesis has been invoked to explain the high affinity for Al(III) (pAl=20.0) showed by the synthetic chelator O-Trensox (Fig. 1.13)[89,105,106].

1.2.3 Experimental criteria to evaluate the performance of a given chelator in solution

1.2.3.1 Stability (formation) constants

From an experimental pont of view, the thermodynamics of aluminum-ligand affinity is measured by means of stability constants. These experimental parameters are a measure of the strength of the interaction between a metal and a ligand that form a given complex. In fact, the formation of a complex between a metal M and a ligand L in aqueous solution is usually a substitution reaction[107]:

$$[M(H_2O)_n] + L \rightleftharpoons [M(H_2O)_{n-1}L] + H_2O \tag{1.11}$$
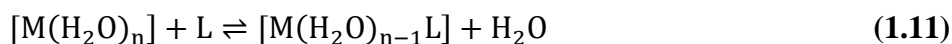
where n is the number of water molecules that surround the ligand. Notice that, for convenience, eq. 1.11 considers an hypothetical monodentate ligand.

Although equilibrium constants can be very useful in predicting the direction of a given reaction and the thermodynamic stability, it is important to bear in mind that they don't provide any information concerning the rate of the reaction. Indeed, we can find that a given metal-chelator formation equilibrium is very favorable, but the rate of the reaction is slow, so the ligand is not useful in practical terms[107]. This latter information rely on kinetics; however, since this thesis dissertation is focused on the thermodynamics of metal-ligand complexes in solution, as previously emphasized, the evaluation of kinetic effects either from a theoretical or experimental point of view is beyond the scope of the present work.

There are three main formation constants that are commonly used in literature: stepwise, cumulative and conditional stability constants.

Considering the reaction equilibrium outlined in eq. 1.11, the equilibrium constant K is given by:

$$K = \frac{[M(H_2O)_{n-1}L][H_2O]}{[M(H_2O)_n][L]} \tag{1.12}$$

We can greatly simplify this expression considering that the number of water molecules surrounding the metal ion are constant, since in excess of water (e.g. in solution), the concentration of water is constant. Accordingly, we get:

$$K = \frac{[ML]}{[M][L]} \tag{1.13}$$

Stepwise stability constants refer to the formation of metal-ligand complexes one step at a time. Considering the formation equilibria of a complex ML_2 formed by one metal M and two ligands L, we get:

$$M + L \rightleftharpoons ML \qquad\qquad K_1 = \frac{[ML]}{[M][L]} \qquad\qquad (1.14)$$

$$ML + L \rightleftharpoons ML_2 \qquad\qquad K_2 = \frac{[ML_2]}{[ML][L]} \qquad\qquad (1.15)$$
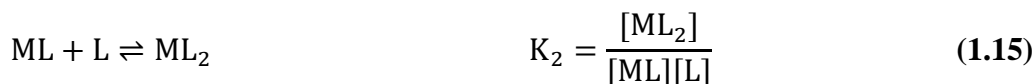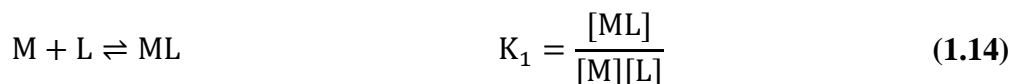
Cumulative stability constants are designed by the symbol β and are the product of all stepwise constants of a given reaction:

$$\beta = K_1 K_2 \qquad\qquad (1.16)$$

$$M + 2L \rightleftharpoons ML_2 \qquad\qquad \beta = \frac{[ML_2]}{[M][L]^2} \qquad\qquad (1.17)$$
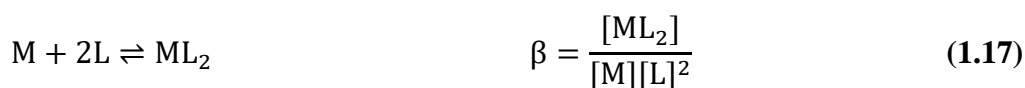
In literature, cumulative stability constants are usually reported as a logarithmic function (logβ), and this is the usual parameter employed to report and compare the strength of the interaction between a metal and a ligand[78].

It is important to highlight that the calculation of logβ considers the ligand's coordination site in its unprotonated form; in this way, the metal/proton competition for a given coordination site is not taken into account. This can lead to a misinterpretation of results when, for instance, the energetic penalty to deprotonate a coordinating group is high (e.g. the functional group bears high $pK_a(s)$).

In order to try to overcome this issue and provide more realistic formation equilibria, conditional stability constants have been introduced; these latter parameters weight the overall formation constant of a given reaction according to the $pK_a(s)$ of the coordination site of the chelator.

Considering the ML_2 complex of the previous example, the conditional stability constant β' derived from stability constant β of eq. 1.17 is expressed as[94]:

$$\beta' = \beta \times [1 + K_{HL} \times [H] \times (1 + K_{H2L} \times [H])]^2 \qquad\qquad (1.18)$$

Where K_{HL} and K_{H2L} are the protonation constants of the ligand. It follows that, when the protonation and the stability constants decrease by the same order of magnitude, the conditional stability constant increases, since the protonation constants are raised to the second power in eq. 1.18[94].

Although the use of conditional stability constants provide a more reliable picture when comparing the chelation properties of different ligands towards a given metal ion, they still retain a big shortcoming: they cannot be used to compare ligands bearing different denticities[78].

As mentioned before, stability constants rely on the thermodynamics of formation of metal-ligand complexes. Therefore, the formation of the 1:3 Aluminum-deferiprone complex (Fig. 1.10) requires three reaction steps to fill the coordination sphere of Al(III) , being deferiprone a bidentante chelator (Fig. 1.10). On the hand, the formation of the 1:1 aluminum-deferoxamine complex (Fig. 1.10) requires only one reaction step to fill the six coordination sites of the metal; indeed, deferoxamine is a hexadentate chelator. Accordingly, the cumulative stability constant of a given 1:3 complex is thermodynamically different from that of a given 1:1 complex; this is mainly due to the different entropic contributions needed for the ligands to bind to aluminum, as explained in section 1.2.2.1 regarding the chelate effect. This becomes a big issue when one needs to evaluate the performance of different chelators displaying different binding modes (Fig.1.2).

In order to overcome this problem, the pM parameter has been introduced, and will be explained in the next section.

Finally, an important remark should be reported. In principle, experimental stability constants can be derived by using first principle methods such as DFT, as it can be calculated as a Gibbs free energy change associated to the metal-ligand complexation[108]. The thermodynamic relationship between the stability constant β and the Gibbs free energy is:

$$\Delta G = -RTln\beta \qquad\qquad (1.19)$$

However, in practice, the error associated to the absolute values of ΔG calculated at the DFT level (or other first principle methods) is usually huge[108]. This is mainly due to the fact that experimental values are taken in solution, and the use of approximate *continuum* solvation models severely under/overestimate theoretical solvation energies, especially when dealing with charged compounds[108].

For this reason, when comparing experimental data with theoretical results, it is much more convenient to rely on relative trends between the theoretically calculated Gibbs free energies (ΔG^{Theo}) and experimental stability constants, usually reported in a logarithmic scale (logβ^{exp}). In this way, when the thermodynamics of complexation energies of given metal-ligand complexes are properly calculated at the DFT level, relative stability trends between ΔG^{Theo} and logβ^{exp} can be very similar. This is the strategy that has been adopted in this thesis work and that will be explained and discussed in the various results chapters..

1.2.3.2 The pM parameter

In order to try to overcome the limitations intrinsic of the use of formation constants as a measure of the chelation performance towards a given metal, the pM criterion has been introduced[109]. This parameter is defined as -log[M_F] usually taken at [M_T] = 1x10^6 M and [L_T] = 1x10^5 M at pH 7.4, where [M_F] is the concentration of free metal in solution (in this case Al(III)), and [M_T] and [L_T] are the total concentration of the metal and the ligand, respectively[78].

In other words, pAl measures the concentration of free Al(III) in solution upon addition of a given chelating agent. The higher the pAl value, the lower the concentration of free aluminum and, therefore, the better the chelation performance of the ligand. Conversely, the lower the value of pAl, the lower the affinity of Al(III) for a given chelator. A list of pAl values for some common aluminum chelators is provided in table 1.4.

Ligand	pAl
Hydroxide (Fig. 1.2)	12.1[7]
Catechol (Fig. 1.11)	10.1[94]
Salicylic acid (Fig. 1.11)	8.2[94]
Kojic Acid (Fig. 1.11)	9.1[110]
Deferiprone (Fig. 1.11)	15.4[111]
Deferoxamine (Fig. 1.11)	20.8[7]
EDTA (Fig. 1.11)	16.4[7]
Citric acid (Fig. 7.1)	14.4[7]
Dopamine (Fig. 7.1)	10.8[*]

Table 1.4. pAl values for some common Al(III) endogenous and exogenous ligands. [*]Chapter 7.

The advantages in the use of this metal affinity criterion are that pAl does not depend on the stoichiometry of ligand-metal complexes, since it directly considers all species that are formed in solution at physiological pH. This is extremely useful as it allows for an immediate and direct comparison of the chelation performance of chemically different chelating agents towards aluminum. Moreover, pAl clearly takes into account the aluminum ion/ proton competition for the binding of a given ligand, providing in this way a very reliable information concerning chelation affinity[78].

In this sense, the pM parameter is the most widely used criterion in literature to compare newly developed chelating agents for a given metal ion.

However, since it provides only a general information about the performance of a ligand (e.g. it includes contributions from different chemical properties), then more specific and detailed information about the chelation properties of the ligand must be evaluated, such as stability constants, protonation constants, number and types of complexes that can be formed, influence of the pH etc. An overview about the predominant parameters employed in coordination chemistry can be found in ref.[78].

A question that comes to mind is: "What is the relationship between pM and logβ ?".

In principle, they are in linear correlation, since the higher the stability constant (e.g. the strength of a given metal-ligand complex), the lower the amount of free metal in solution and, therefore, the higher the pM value.

However, this is not always true. The reason relies on the fact that, as previously discussed, logβ does not take into account the effect of protonation constants at the ligand's binding site. Accordingly, when there is a significant modulation of their pK_a values like, for instance, upon addition of electron donating/withdrawing groups (EDGs and EWGs, respectively), then a small effect towards stability constants might be overcame by a higher effect towards pM. As a result, an inverted trend between the two metal affinity parameters is found[21]. A paradigmatic case in this sense is presented in chapter 3 of the results section, where we investigated the effects of different substituents (EDGs, CH_3 and OCH_3, EWGs, NO_2 and CF_3) towards the modulation of the molecular properties of two families of Al(III) chelating agents (catechol and salicylic acid)[21].

It follows that, for a proper characterization of a new ligand, different sources of information need to be investigated, and there not exists a single and universal parameter that can be unequivocally used to evaluate the reliability of a given chelator.

Finally, it is important to mention that, again, it is very challenging to predict (at least in terms of trends) of the pM parameter from a theoretical point of view. The efforts and strategies that we adopted in order to compare theoretical results with respect to experimental pAl values are presented and discussed throughout the results section.

The development of a suitable theoretical protocol that would be able to unequivocally predict experimental pAl trends is currently work in progress and will not be included in the current thesis dissertation.

1.2.4 The dark side of Al(III) chelation therapy: challenges and perspectives

So far, an overview on the properties that the ideal Al(III) chelating agent should possess have been provided, along with the current status on the most promising chelating agents and a focus on the main experimental criteria used to measure their chelation performance.

Nevertheless, despite many efforts have been made in order to identify a suitable aluminum chelator to be used in Al(III) chelation therapy, one major shortcoming is still present: the lack of specificity. Indeed, as mentioned in the previous sections, Al(III) chelation therapy is indissolubly coupled to Fe(III) chelation therapy, since all chelators that show affinity for aluminum, show affinity for iron as well.

This is due to the fact that, as discussed before, the Al-ligand interactions are mainly of electrostatic nature. Therefore, a negatively charged ligand's binding site will not show particular specificity towards trivalent metal ions bearing the same charge. This is witnessed by the clinical use of deferiprone and deferoxamine (Fig. 1.10 and Fig. 1.11) in both aluminum- and iron-based overload diseases[6,28]. However, considering that the amount of the exogenous aluminum ion in the body is much smaller than the amount of the endogenous ferric ion, short time therapies with deferiprone will be able to sequester all Al(III) and will non severely affect the homeostasis of iron[6,112].

An interesting point concerns the higher affinity shown by all ligands tested so far with respect to Fe(III) compared with Al(III). Crisponi *et al.* compared the stability constants of a wide range of 1:1 aluminum- and iron-chelator complexes reported in literature, finding a remarkably good correlation (R= 0.988) with a $loK_{Fe}/logK_{Al}$ ratio of 1.21[6]. Interestingly, this ratio resembles the electronegativity ratio of Fe(III) and Al(III), 1.96/1.61=1.22[6].

A possible explanation for the higher iron affinity over aluminum is given by Albrecht-Gary and Crumbliss[113], who state: *"... a consequence of the different charge/radius ratios for Fe(III) and Al(III) is the fact that the free energy of formation of the hydrated metal ion ($\Delta G°_f [M^{3+}_{aq}]$) is less negative for Fe^{3+}_{aq} (−10.6 kJ mol^{-1}) than for Al^{3+}_{aq} (−486 kJ mol^{-1}). Since a stability constant for complex formation between the aquated metal ion and the metal complex, the more strongly aquated Al^{3+} ion will not be as likely to have as great a $\Delta G°$ between the hexaaquo ion and the complex as will Fe^{3+}".* In other words, according to this hypothesis, the hydrated aluminum ion in solution is more stable than the hydrated iron ion, and, therefore, is less prone to leave water molecules and to bind to a new ligand than iron does. Notice, however, that the presence of hydroxide species is not taken into account.

Accordingly, it seems that, in principle, it is not possible to target ligands selectivity towards aluminum due to its intrinsic *physico*-chemical properties in solution.

Crisponi *et al.*, in a different paper, proposed two possible strategies to shift ligands selectivity towards aluminum[79]:

i) Insertion of proper substituents such as EDGs and EWGs in the ligand's scaffold; this can be of paramount importance in altering the chelation properties of the coordination site.

The fine modulation of the *physico*-chemical properties of the ligand might result in a change of its selectivity between Al(III) and Fe(III).

ii)   Pre-organization of the ligand; due to the smaller ionic radius of Al(III) compared to Fe(III), the design of proper ligands forming four- five- or six-membered rings may lead to a significant change in metal selectivity. Additionally, the design of ligands able to discriminate metal ions by the ionic radius might be a potentially reliable strategy.

The lack of aluminum selectivity of most chelators is not only a problem with respect to trivalent metal ions. There are many essential metal ions needed by the human metabolism, as discussed in section 1.2.1.1. Some chelators can have such a strong chelation performance that retain significant affinity not only for trivalent metal ions, but for divalent ones as well.

This is specifically the case of ethylenediaminetetraacetic acid (EDTA, Fig. 1.2 and 1.11). Although this chelator has been proposed as a potential therapeutic cure against aluminum-induced neurodegeneration[114], its use in Al(III) chelation therapy is still very controversial. Indeed, it has been shown that EDTA can alter and imbalance the homeostasis of essential metal ions[112]. In particular, EDTA was found to form stable complexes with Mg(II), Zn(II) and, most importantly, Ca(II). This chelating agent can severely perturb the homeostasis of calcium leading to detrimental effects when assumed at high concentrations, and ultimately to death[112].

The potentially undesired toxicity related to the chelation properties of a given chelator towards essential metal ions is a subject that must be carefully taken into account, and that is not always easy to be overcame.

In this sense, the understanding of the determinants behind metal selectivity is a topic that needs to be improved with the aim of finding new and efficient aluminum chelating agents, and computational approaches might provide a fundamental help in that sense.

1.3 A computational approach to aluminum biochemistry

1.3.1 Thermodynamics of Al-ligand complexes in aqueous solution

Challenges in the investigation of the potential toxic role of Al(III) in the biological environment, as well as in the design of efficient aluminum chelating agents, have been highlighted through the previous sections. In light of that, modern molecular modelling approaches, when properly applied,

might be a valuable source of insights helping to elucidate binding mechanisms and/or rationalizing experimental procedures.

In particular, the computational approach towards the characterization and evaluation of the thermodynamics of Al-ligand complexes in solution was introduced, for the first time, some years ago by Prof. Xabier Lopez's group at the University of the Basque country. The purpose is the understating of the properties of the aluminum ion in the biological environment with respect to different low- and high-molecular mass bioligands (Fig. 1.14 and 1.15).

A wide range of computational tools have been used for that purpose, ranging from classical MD simulations, hybrid QM/MM simulations, chemical bond analysis using the Bader's Quantum Theory of Atoms in Molecules (QTAIM) and Natural Bond Orbital (NBO) theory, high level CASSCF and
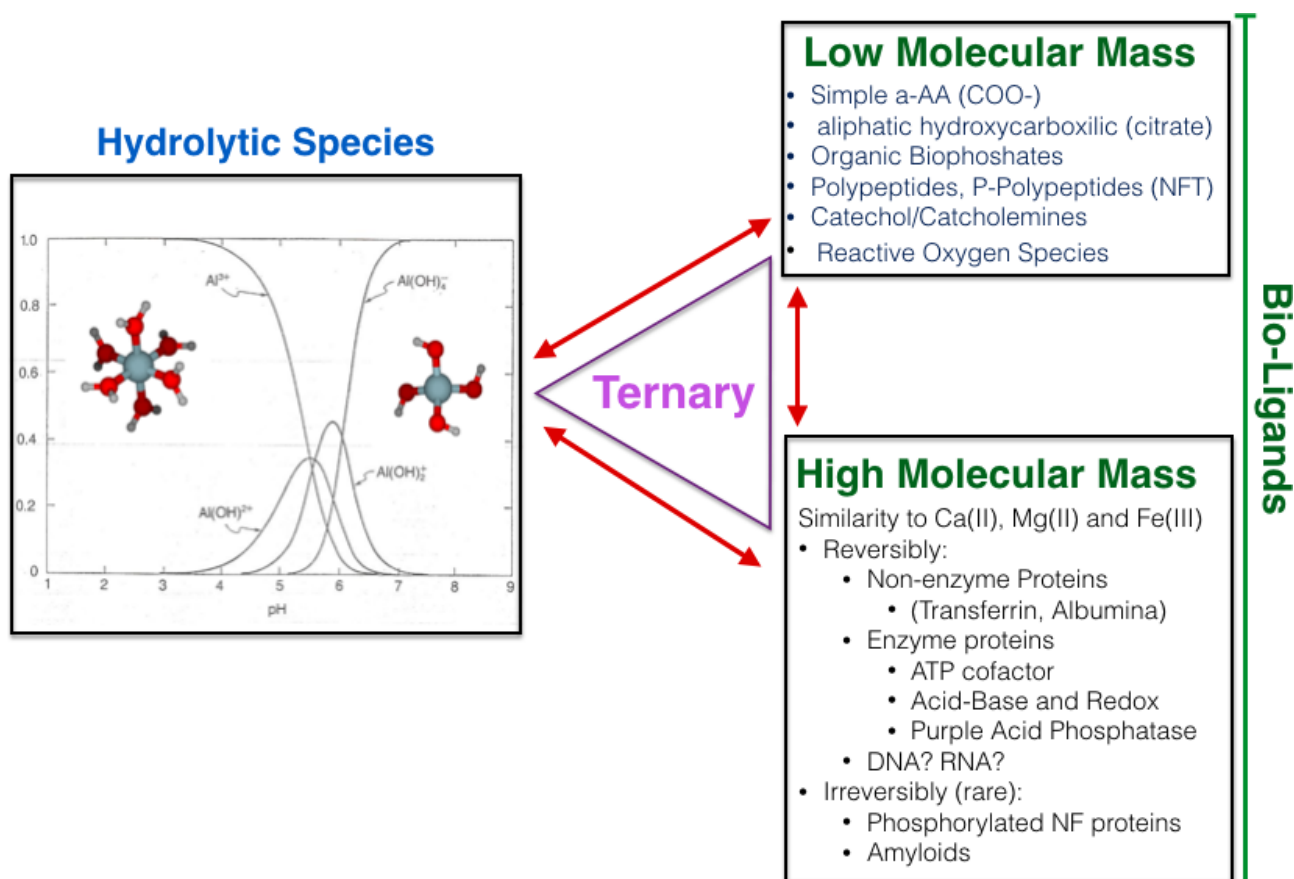
Fig. 1.14. Main topics covered in Xabier Lopez's group.

CASSPT approaches, and others (Fig. 1.15). The main sources of information rely on the evaluation of the thermodynamics of binding energies in aqueous solution, obtained by means of a cluster-*continuum* approach[115].

Such an approach, has allowed to unveil several properties and binding features of the interaction of Al(III) with several different bioligands, providing a clear understanding and rationalization of the available experimental data and, moreover, providing an answer to some unknown issues such as the role of neurofibrillary tangles (NFTs)[66], hydroxyaluminosilicates (HAS)[8] and a possible structure for the 1:1 Al-Aβ_{1-42} complex[74].

1.3.2 Aim of the thesis

In light of what it has discussed up to this point, the goal of the present thesis project is to carry on with the computational approach to aluminum biochemistry, with the aim of increasing the knowledge in this rather controversial field. For such a purpose, different theoretical methods have been used, which will be presented and discussed throughout the results sections, where the main computational protocol (Fig. 1.16) was adapted and fixed according to the specific systems and properties under investigation.
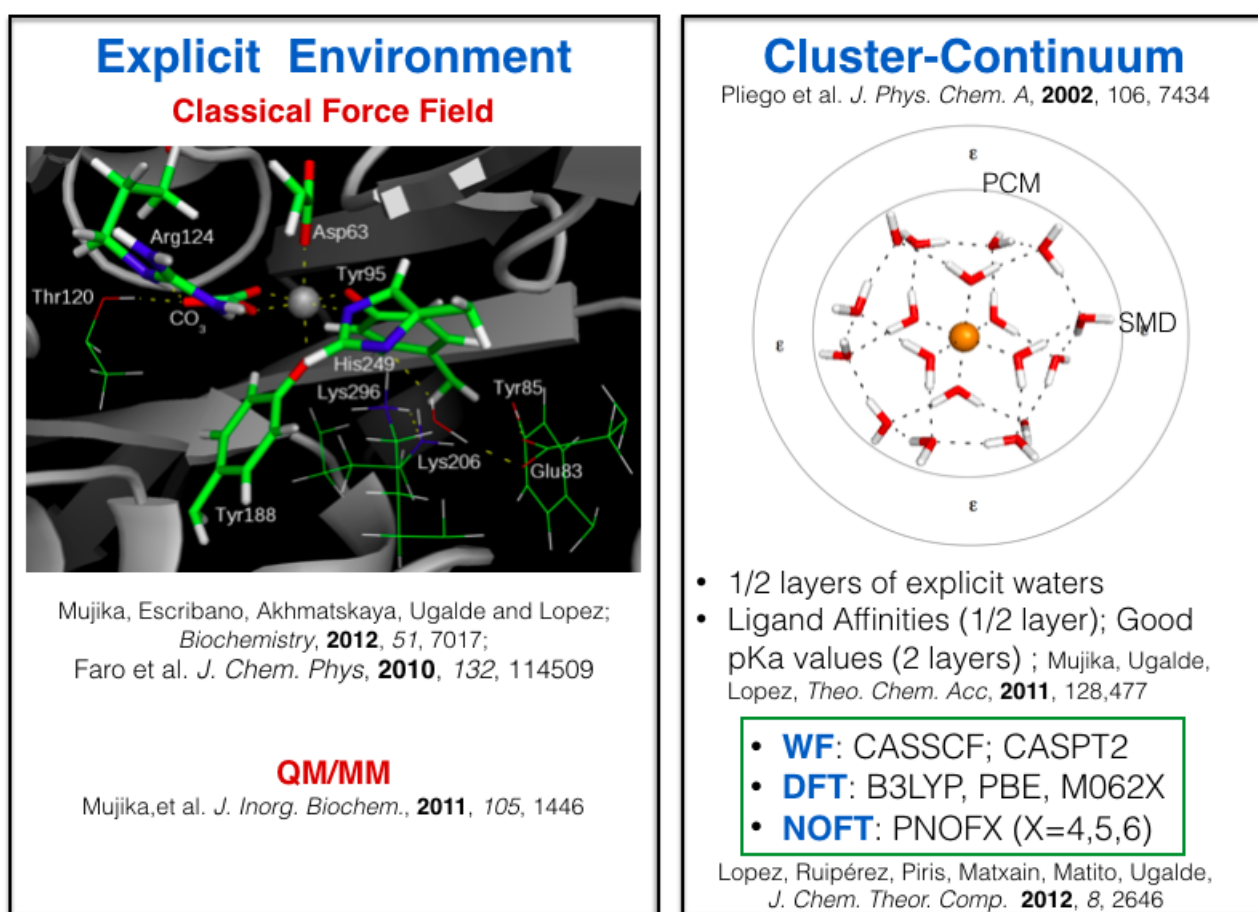
Fig. 1.15. Detailed schematic representation of the research lines and methodologies developed in Xabier Lopez's group.

More into details, this Ph.D. project has covered three main areas:

1. ***Chelation therapy and development of new chelation strategies.***

   In this rather new research topic, not covered before in Xabier Lopez's group, the aim is to develop a computational protocol that would be able to fully characterize Al(III)-based chelating agents, and therefore help towards the design of new and efficient compounds that might be used in aluminum chelation therapy. The fine understanding of experimental data (e.g. stability constants and pAl), as well as the modulation of their trends upon addition of chemically different substituents, is a central part of the work, that allowed for a strong validation of the computational protocol. Moreover, in collaboration with experimentalists from the University of Cagliari, we have designed and characterized a novel family of peptide-based Al(III) chelating agents.

   Results obtained in this topic led to two publications (chapter 3 and chapter 4 of the results section).

2. ***Understanding the potential toxic role of Al(III) in the biological environment.***

   This is the main research area of Xabier Lopez's group, that has been active since early 2000. Departing from the knowledge obtained from previous works published in the group, as well as using knowledge gained from the previous research topic (chelation therapy), the molecular basis of the potential mechanisms of toxicity of aluminum with respect to different endogenous ligands in aqueous solution (model peptides, citric acid, neurotransmitters) were investigated. Biological implications of the results in light of an open biological environment are discussed using previous reports in literature; additionally, new hypotheses and speculations have been made, that will be the substrate for future works in this area.

   Results are presented in chapters 5, 6 and 7 of the results section.

3. ***Calibration of the computational protocol and benchmarking of approximate theoretical methods.***

   The third and very important research area concerns the thorough evaluation of the accuracy of the theoretical methodologies utilized in the present thesis work. Investigations in this sense include the validation of the computational protocol with respect to experimental stability constants and experimental pAl values, as well as the adaptation of the computational protocol according to the different systems under investigation (chapters 3-7). Moreover, an independent work has been made in order to benchmark approximate exchange-correlation

functionals and semiempirical methods with respect to high level CCSD(T)/CBS reference energies. The purpose is to benchmark binding energies of seven different 1:1 metal-chelator complexes in aqueous solution so that to highlight what are the functionals and corrections (e.g. dispersion, range-separation) that may improve the accuracy of the thermodynamics and geometries of our metal-ligand complexes. We took advantage of the extensive experience of Prof. Maria João Ramos's group in that field[116-118].

This latter work is currently work in progress, and some preliminary results will be discussed in the concluding remarks of this thesis dissertation.
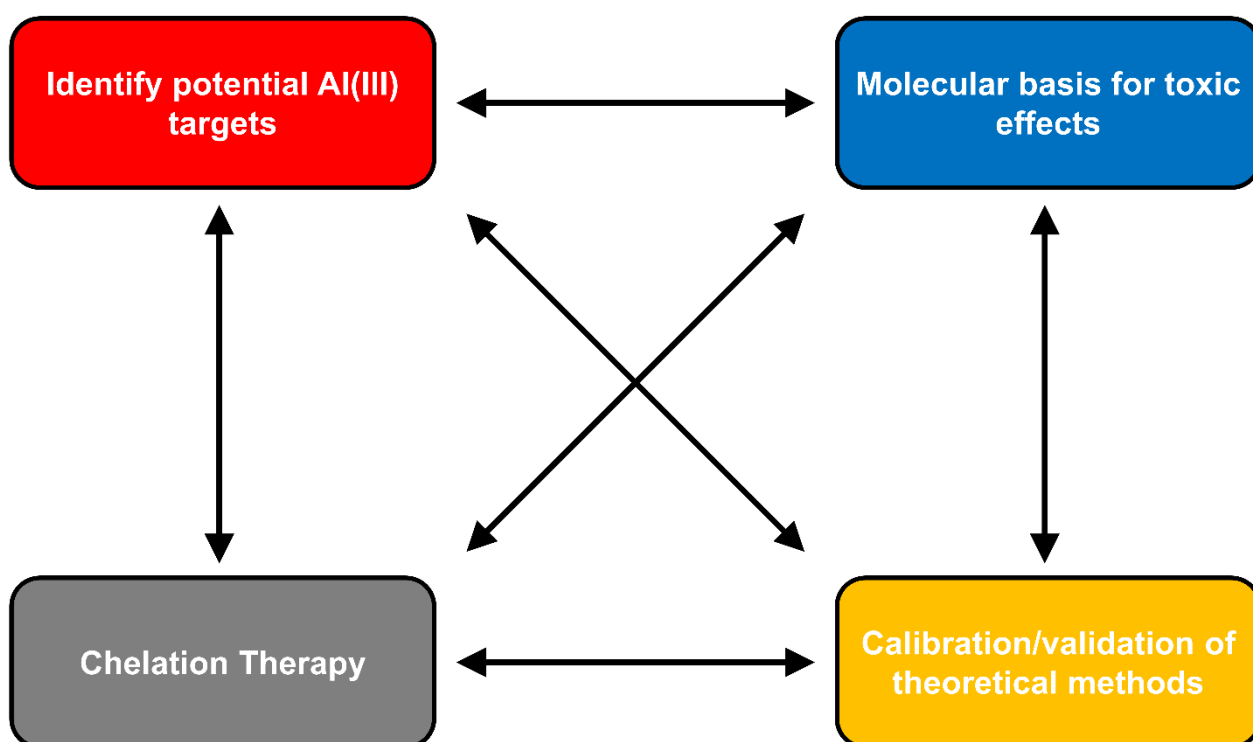
Fig. 1.16. Schematic representation of the topic covered in the present thesis dissertation.

METHODS

"Every day here you come walking
I hold my tongue, I don't do much talking
You say you're happy and you're doin' fine well go ahead, baby, I got plenty of time
Sad eyes never lie
Sad eyes never lie"

(B. Springsteen, Sad Eyes)

2.1 Potential energy surfaces

The Potential Energy Surface (PES) associated to a given reacting system is a hypersurface defined by the potential energy of all the atoms over all possible atomic arrangements[119].

A useful way to describe the PES of a system is to consider its internal or geometric coordinates (e.g. bond distances, angles and torsions); in this way, the PES has $3N - 6$ degrees of freedom, where N is the number of atoms of the system ($N \geq 3$).

Let us imagine to have a three atoms system. The choice of the first atom involves no degrees of geometric freedom as the first atom defines the origin. The position of the second atom is specified by its distance from the first atom; therefore, a two atoms system contains a single degree of freedom. The third atom can be specified by either its distances to each the two preceding atoms or by a distance from one and an angle between the two bonds formed by the three atoms. It follows that a three atoms system contains a total of 3 degrees of freedom; each additional atom requires the specification of three geometric coordinates to describe its position.

Usually, the PES is investigated within the Born-Oppenheimer approximation[120], which enables to separate the motion of electrons and nuclei so that to consider electrons at fixed nuclear positions, because of their much smaller mass and much higher velocity compared to nuclei (10^7cm/s and 10^5 cm/s respectively, at 300 K).

It is important to bear in mind that the shape PES depends, to a certain extent, on the method utilized to calculate its potential energy. Accordingly, the PES of a system calculated by means of molecular mechanics (force fields) methods can be very different from those calculated by means of *ab initio* methods, due to the lack of electrons in the former. The choice of the most suitable method for the study of a given a given system is a critical step in each Molecular Modelling investigation; ideally, the "calculated" PES should be parallel to the "real" PES, which means that the chosen method is able to describe the shape and features of the real system.

Usually, one is not interested in the calculation of the whole PES, but rather in the identification of the most interesting and most informative points of the PES. These include local minima, which correspond to optimal molecular structures (e.g. points where all second derivatives are zero), the global minimum, which is the lowest energy (most stable) structure and saddle points, characterized by having no slope in any direction, downward curvature for a single coordinate and upward direction for all the other coordinates. Saddle points are the lowest energetic barriers on paths connecting minima, so they have been related to the chemical concept of transition state[119].

When a given system contains many degrees of freedom, it can be very challenging to identify all the local minima and/or the global minimum of its PES, because of the huge number of possible

conformations. For such a purpose, a wide range of conformational sampling techniques suitable for different problems/systems have been developed so far, including molecular dynamics-based ones. Some interesting review in that sense can be found in ref.[119,121-124].

In the present PhD dissertation, we mainly focus on ground state local minima of the systems under investigation by using Densify Functional Theory-based methods. However, as discussed above, when the system under investigation is very flexible, we have used QM/MM approaches in order to properly sample the conformational space of the ligand and identify the most relevant conformations.

2.2 Density Functional Theory (DFT)

Density Functional Theory (DFT) is one of the most popular approaches that provides, in principle, an exact approach to the problem of electronic structure theory[125].

As demonstrated by Hohenber and Kohn, within the Born-Oppenheimer approximation the electronic energy $E_e[\rho(r)]$ can be written as a functional of the electron density (ρ) [125]:

$$\rho(r) = \sum |\Psi(r)|^2 \tag{2.1}$$

$$E_e[\rho(r)] = T[\rho(r)] + V_{en}[\rho(r)] + J[\rho(r)] + Q[\rho(r)] \tag{2.2}$$

where $T[\rho(r)]$ is the kinetic energy of the electrons, $V_{en}[\rho(r)]$ is the nuclear-electron attraction, energy, $J[\rho(r)]$ is the Coulomb electron-electron repulsion energy and $Q[\rho(r)]$ is the electron-electron interaction energy[126].

The second and third terms of equation (2.1) are known and can be computed according to equations (2.3) and (2.4), respectively:

$$V_{en}[\rho(r)] = -\sum_{A=1}^{M} \int \frac{Z_A}{|r - R_A|} \rho(r) dr \tag{2.3}$$

$$J[\rho(r)] = \frac{1}{2} \iint \frac{\rho(r_1)\rho(r_2)}{r_{12}} dr_1 dr_2 \tag{2.4}$$

The goal of DFT is to develop accurate approximation for $T[\rho(r)]$ and $Q[\rho(r)]$. Since the kinetic energy contribution is the largest unknown term, the corresponding kinetic energy functional must be approximated or, ideally, its exact nature must be identified.

The simplest approximation to $T[\rho(r)]$ is the Thomas-Fermi model, which is exact for an infinite uniform electron gas (UEG)[127]:

$$T[\rho(r)] = \frac{3}{10}(3\pi^2)^{2/3} \int \rho(r)^{5/3} dr \tag{2.5}$$

However, such an approximation is only applicable to systems with nearly uniform densities like some alloys and semiconductors and cannot properly describe chemical bonds[126].

Accordingly, designing accurate kinetic energy functionals for molecular applications is a difficult task that has yet to be satisfactorily accomplished.

In this sense, the kinetic energy problem has been greatly improved by Kohn and Sham equations (KS)[128]. They demonstrated that the kinetic energy could be accurately approximated by a single Slater determinant (of orbitals $\{\phi_i\}$) describing a fictious system of non-interacting electrons that has the same density as the exact electronic wave function.

The KS non-interacting kinetic energy $T_s[\{\phi_i\}]$ can be written as:

$$T_s[\{\phi_i\}] = -\frac{1}{2}\sum_{i=1}^{n} \int \phi_i^*(r)\,\nabla^2\phi_i(r)dr \tag{2.6}$$

Considering that the non-interacting kinetic energy is not equal to $T[\rho(r)]$, the difference between these two terms is combined with $Q[\rho(r)]$ tp define the exchange-correlation energy, $E_{xc}[\rho(r)]$ [126]:

$$E_{xc}[\rho(r)] = T[\rho(r)] - T_s[\{\phi_i\}] + Q[\rho(r)] \tag{2.7}$$

The only unknown term in KS-DFT is the exchange-correlation functional (eq. 2.6), which is often represented as a sum of an exchange functional, $E_x[\rho(r)]$, and a correlation functional, $E_c[\rho(r)]$.

Like DFT, KS-DFT is in principle exact; however, the quest for the exact exchange-correlation term, and therefore for the "universal" DFT functional that can be applied for any molecular system, is still far from being accomplished[129].

In the past thirty years hundreds of non-empirical and semi-empirical DFT functionals have been developed, mixing in many different flavors as the main ingredients of KS-DFT, as well as *ab initio* ones such as Hartree-Fock (HF) and Möller-Plesset second order perturbation theory (MP2), in order to try to reach the chemical accuracy[126,129]. As a result, many different types of functionals containing different functional forms are nowadays available. In this sense, a useful concept to provide a classification and a hierarchy is represented by Perdew's Jacob's Ladder[130] (Fig. 2.1).

In this metaphorical representation, the Jacob's Ladder is composed of five rungs corresponding to increasingly sophisticated models for the unknown exchange-correlation functional. The ladder has its foundation on the "Hartree World", where the exchange-correlation energy (eq. 2.7) is zero and electron-electron interaction is provided solely by classical electrostatic, $J[\rho(r)]$. Moving up the ladder introduces additional ingredients into the functional form, culminating in the "Heaven" of chemical accuracy (e.g. ≤ 1 kcal/mol). Since each rung contains new physical content that is missing in lower rungs, improved accuracy should be attainable at each higher level[126].

The majority of the most popular DFT functionals fall within rung 4 of the Jacob's Ladder (Fig. 2.1), which belongs to the hybrid and meta-hybrid General Gradient Approximation (GGA). The reason relies on the fact that such approximations were found to provide reasonable accurate results for many systems, compared to the previous rungs, at a very affordable computational cost compared to rung 5^{126}.

Nevertheless, in rung 5 there still remain some important inaccuracies in the functionals developed so far; the most important ones, that were the subject of intensive work in the past fifteen years to try to solve the issue are[126]:

1. Self-interaction error (SIE), that led to the development of range-separation corrections briefly presented in section 2.2.2.

2. Long range dynamic correlation (London dispersion forces), that are pivotal especially for biological systems, which is discussed in section 2.2.3.

3. Strong correlation; this issue has not yet been properly investigated or solved.

Several correction scheme have been proposed and implemented over the past years to solve, or at least to attenuate, point I and II, which allowed for a great improvement in the performance of hybrid-GGA functionals. However, one has bear in mind that there not exist (yet) the "universal" DFT functional; therefore, one should always consider the question "which functional should I use ?". To find the answer, insights from the literature about the properties of specific system under investigation, the comparison/validation with respect to available experimental data and/or benchmarking of different functionals with respect to high level reference calculations (such as the CCSD(T)/CBS level of theory, considered the "golden standard") are the most straightforward strategies that one should always pursue prior to any molecular modelling job.

A survey on all the DFT exchange-correlation approximations (Fig. 2.1) is far beyond the scope of this thesis dissertation (two excellent reviews can be found in refs.[126,129]).
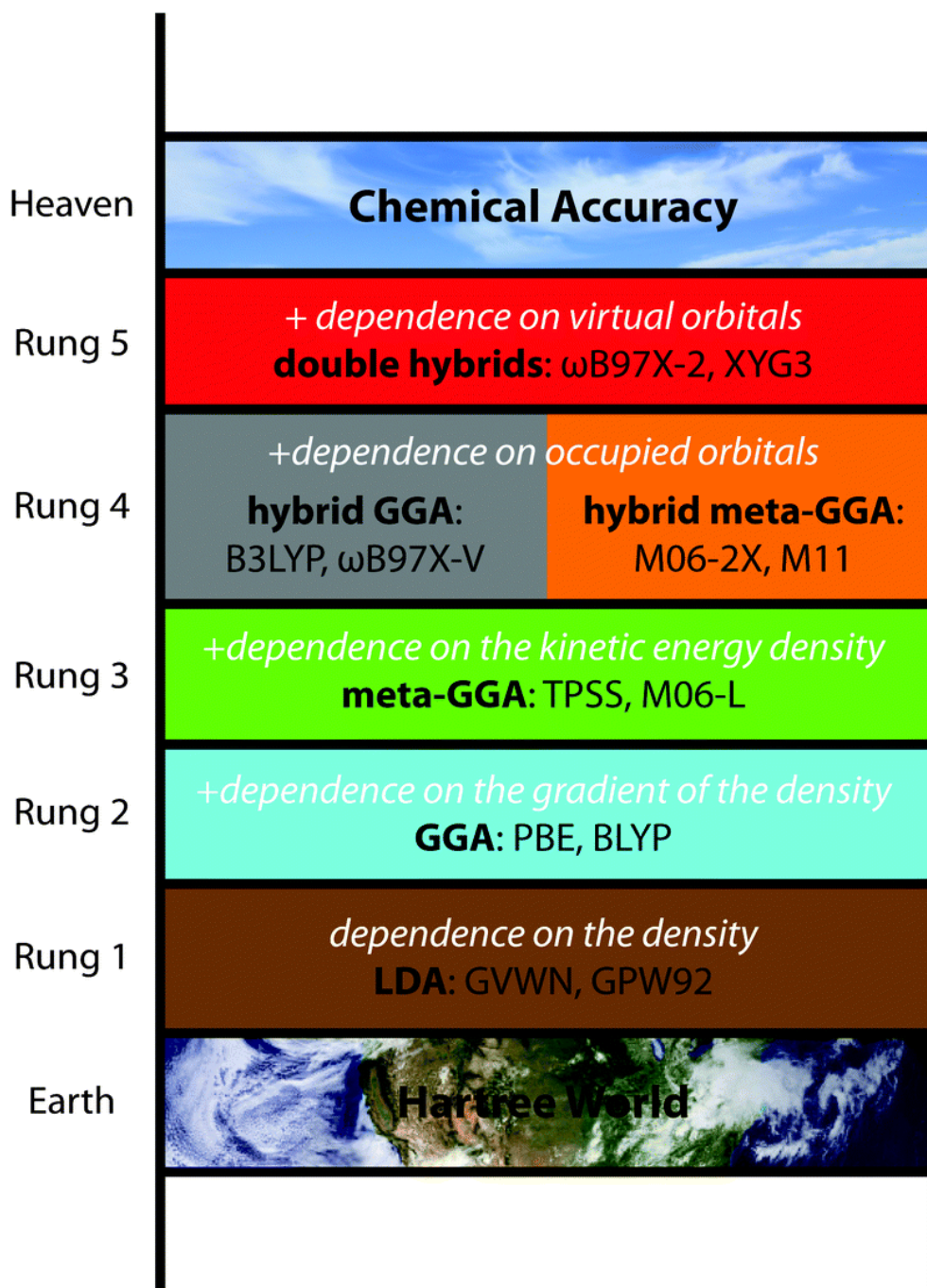
Fig. 2.1. Perdew's metaphorical Jacob's Ladder of DFT hierarchy. Taken from ref.[131].

The majority of the work has been carried out employing the hybrid-GGA B3LYP functional in conjunction with Grimme's D3(BJ) dispersion scheme (see next sections) and will be presented in the next section.

The reason of that choice relies on the very good performance of the B3LYP-D3(BJ) corrected functional for metal-containing systems and non-covalent interactions, which will be discussed in more detail in each chapter of the results section, along with comparison with experimental data.

Moreover, it is worth to mention that these speculations were confirmed by our benchmark of different correlation-exchange functionals in the calculation of metal-ligand binding energies, compared to CCSD(T)/CBS reference data. The B3LYP-D3(BJ) functional was found to be one of the best performers (briefly discussed in the concluding remarks of this thesis dissertation).

2.2.1 B3LYP

The popular, and yet mystical, B3LYP functional is a hybrid (or global-hybrid) GGAs family (rung 4, Fig. 2.1). The idea behind the creation of hybrid-GGAs was an attempt to attenuate the self-interaction error (electrons interacting with themselves) of most exchange-correlation functionals.

The simplest way to demonstrate SIE is to consider the Hartree-Fock (HF) description of the hydrogen atom. Since the hydrogen atom contains only one electron, the electron-electron interaction energy should be exactly zero. At the complete basis set limit (CBS), the HF energy for the hydrogen atom is -0.5 Hartrees, which comes from summing the kinetic (0.5 Hartrees), nuclear-electron attraction (-1.0 Hartrees), Coulomb (0.3125 Hartrees) and exchange (-0.3125 Hartrees) energy contributions. Accordingly, the classical and non-classical electron-electron contributions cancel each other exactly, making HF one-electron SIE free[126].

In KS-DFT, since the exact exchange term is replaced by approximate exchange correlation terms, most of functionals are not one-electron SIE free (e.g. $J[\rho(r)] + E_{xc}[\rho(r)] \neq 0$) for the hydrogen atom[126].

A strategy to overcome, or at least to attenuate such issue came from the idea of replacing the local exchange functional with the exact exchange functional (Hartree-Fock), while employing a local correlation functional that gives exactly zero correlation energy for any one-electron system. Despite the many efforts done to combine exact and different DFT functionals, the overall performance did not show significant improvements until early 1990 when Becke introduced the idea of mixing only a global fraction of exact exchange with the exchange-correlation functional[132,133].

Such an approach gave rise to rung 4 of the Ladder, the family of hybrid-GGas exchange correlation functionals. Becke's B3LYP functional has been one of the most popular ones with broad

applicability; taking advantage of the adiabatic connection theory[134-137], the B3LYP functional can be written in the form:

$$E_{xc}^{B3LYP} = (1 - a)E_x^{LDA} + aE_x^{HF} + bE_x^{B88} + (1 - c)E_c^{LDA} + cE_c^{LYP} \qquad \textbf{(2.8)}$$

Where E_x^{LDA} and E_c^{LDA} are the Local Density Approximation (LDA, rung 1 of Fig. 2.1) exchange and correlation VWN functionals[138], respectively. E_x^{B88} is Becke's B88 exchange functional[139], E_c^{LYP} is the Lee-Yang-Parr correlation functional[140]. Finally, *a, b* and *c* are three empirical parameters (0.20, 0.72 and 0.81, respectively).

Therefore, considering eq. (2.8), B3LYP contains 20% of exact (HF) exchange energy. This percentage differs in other hybrid-GGAs, as it is optimized according to the functional form and eventual empirical parameters.

This venerable functional has been found to be rather versatile, as its broad use in the calculation of different properties such as barrier heights, kinetics, heats of formation, non-covalent interactions showed acceptable performances, although it does not excel in any of these properties[126,129]. However, the addition of some correcting terms such as dispersion and range separation corrections greatly improved the performance of the B3LYP functional compared to other popular functionals, as emphasized by Stefan Grimme[141]:

"Of particular note is that the B3LYP-D3 method provided the best geometries, suggesting that this much (and justly) maligned functional can be significantly improved with just the simple D3 fix".

As introduced in the previous section, these two corrections represent a huge improvement in the accuracy of approximate exchange/correlation functionals, and will be briefly presented in the next sections.

2.2.2 Range-separated DFT

In order to try to alleviate the problem of self-interaction errors in global hybrid functionals, the range separation approach has been proposed. The basic idea is that the interelectronic Coulomb operator can be split in a short range (SR) part and long range (LR) part.

This effort is usually achieved by using an operator such as[129]:

$$\frac{1}{r_{12}} = \frac{erfc(\omega r_{12})}{r_{12}(SR)} + \frac{erf(\omega r_{12})}{r_{12}(LR)} \qquad \textbf{(2.9)}$$

Where r_{12} is the interelectronic distance. The Coulomb operator of the short-range component (SR) is attenuated by the complementary error function erfc(ωr_{12}), while the long-range component is attenuated by the error function erf(ωr_{12}). The error function is used since it allows a simple calculation of integrals[129].

The most popular kind of range-separated hybrid functionals is called long-range corrected (LC) functionals, using the popular LC scheme developed by Hirao and co-workers[142]. They use 100% of HF exchange in the LR limit and a smaller value, usually between 0% and 50%, in the SR limit. Notice that the Hartree-Fock theory is SIE-free, therefore the use of 100% HF exchange in the LR limit ensures a strong attenuation of the self-interaction error.

Another closely related range-separation strategy is those employed in the CAM-B3LYP functional, which has 19% non-local exchange in the SR limit and 65% in the LR limit[143].

An alternative (and opposite) approach to LC is represented by the so-called screened-exchange hybrid functionals, such as the HSE-based family of functionals[144,145] and Truhlar's N12-SX[146] and MN12-SX[146]. This approach uses a finite amount of HF exchange at SR, but none in the LR limit, in order to cut the computational cost of non-local exchange integrals for extended systems, while, at the same time, (in principle) retaining the good performance features of global hybrid functionals for most chemical properties[129].

2.2.3 London dispersion corrections

London dispersion forces (interactions) are the attractive part of a van der Walls (vdW)-type interaction potential between atoms or molecules that are not directly (covalent or ionic) bonded each other[147]. According to a more precise definition, London dispersion interactions result from relatively long-ranged electron correlation effects in any many-electron system that neither requires "polarity" nor wave function (WF) overlap[147].

In 1930, from the simplest perturbation theory, Eisenschitz and London have derived the famous asymptotic formula for the dispersion energy between two atoms A and B at large distance R[148]:

$$E_{disp}^{AB} \approx \frac{3}{2} \frac{I_A I_B}{I_A + I_B} \alpha_A^0 \alpha_B^0 R^{-6} = C_{6,approx}^{AB} R^{-6} \qquad (2.10)$$

Where α^0 is the static dipole polarizability and I is the atomic ionization potential. The atomic constants can be condensed to the pair-specific C_6 dispersion coefficient, which determines the strength of the interaction. Note that E_{disp} is attractive for any distance and hence stabilizes molecules with respect to their constituting atoms, condensed phases over the (diluted) gas phase[147].

Since London dispersion forces are a component of vdW interactions, of course they are most important when aiming to describe noncovalent interactions; in particular, they are fundamental when characterizing biological systems.

Mean-field electronic structure methods such as Hartree-Fock, Kohn-Sham DFT and semiempirical ones are not able to describe long-range electronic effects and, therefore, are not able to account for London dispersion forces[147].

For this reason, different DFT and semiempirical correction schemes have been proposed during the last years, with the aim of improving the description of dispersion energies. Among the DFT schemes, the most popular ones were mainly (but not only) developed by three different groups:

1. G. DiLabio's group; they designed dispersion-correcting potentials for global nd range-separated hybrid functionals. They are known in literature as "DCP" corrections[149-151].

2. Vydrov and Van Voorhis's group; they developed some nonlocal vdW-based functionals that model the contribution of the dispersion energy arising from the fluctuations of electron density fluctuations in distant regions of a system by explicitly accounting for the interaction of those distant parts. Such kind of correction is termed in literature "DFT-NL" and the latest development in such regard is known as "VV10"[152].

3. S. Grimme's group; S. Grimme developed a so-called atom-pairwise approach which consists in the addition of the semiclassical treatment of dispersion energy evaluated between atom pairs to the electronic energy of the DFT functional. This is achieved by simple empirical fitting of such semiclassical dispersion energy (parameterized for many different systems). The latest improvement in that sense is known in literature as "D3"[147,153,154].

Interestingly, it has been found that, in general, all of these different approaches improve the performance of DFT methods towards non-covalent interactions[155], as well as towards many other properties[156,157]. Moreover, they have been also found to improve geometries[141].

It is important to mention that, however, these different approaches to account for London dispersion forces improve the accuracy of KS-DFT functionals by very similar degrees[158]. Accordingly, there is not a given correction approach that prevails over the others.

Nevertheless, the Grimme's approach has become the most widely used and widely implemented one in most computational chemistry packages. The reason, very simple, relies on the fact that, being the

D3 method an empirical fitting, it does not lead to any significant increase in the computational cost of a given calculation when applied. This is, clearly, a huge advantage in routine calculations.

For such a reason, it is often discussed that, nowadays, dispersion corrections such as the D3 one should be used by default in *Quantum* chemistry independently from the real need of using it.

The popular atom-pairwise D3 method developed by S. Grimme to correct the lack of dispersion energy in most density functionals is given by[147,159]:

$$E_{disp}^{DFT-D3} = -\sum_{AB} \sum_{n=6,8,10,\dots} = s_n \frac{C_n^{AB}}{R_{AB}^n} f_{damp}(R_{AB}) \tag{2.11}$$

Where, the sum is over all atom pairs of the system, C_n^{AB} denotes the averaged (isotropic) nth-order dispersion coefficient, (orders n=6,8,10,…) for atom pair AB, and R_{AB} is their internuclear distance. Global (functional-dependent) scaling factors s_n are typically used to adjust the correction to the repulsive behavior of the chosen density functional[159].

However, it has been found that C_n^{AB} alone is not able to describe medium- and short-range dispersion, but only long-range effects (Fig. 2.2)[159].

Accordingly, in order to overcome that limitation and provide the asymptotically correct behavior of dispersion energy (depicted in Fig. 2.2), several damping functions (f_{damp}) have been provided; the most widely used one (along with the D3 methods) is based on the scheme proposed by Becke and Johnson[160]:

$$f_{damp}^{(n)}(R) = \frac{R^n}{R^n + (a_1 R_0 + a_2)^n} \tag{2.12}$$

Where the density functional specific parameters a_1 and a_2 and the radii $R_0 = \sqrt{C_8^{AB}/C_6^{AB}}$ are introduced[147].The overall dispersion correction (eq. 2.11 and 2.12) are known in literature with the suffix "D3(BJ)", and specific parameters were developed for several density functionals[153,154].

It is important to highlight that the introduction of the D3(BJ) scheme has allowed for a huge improvement of the accuracy of most DFT functionals specially in the case of non-covalent interactions[155,156] and metal-containing systems[141]. Therefore, in this sense, the D3(BJ) scheme outperforms the D3 one and it is the recommended one when dealing with interactiong systems.

Finally, it should be mentioned that dispersion corrections, as well as hydrogen bond corrections, were developed for semiempirical methods, mainly thanks to the work of Hobza and co-workers[161-164]. Like in the case of DFT-based corrections, methods that ensure the proper treatment of dispersion

energy in PM6 and PM7 semiempirical methods significantly increased their accuracy in many systems[161].
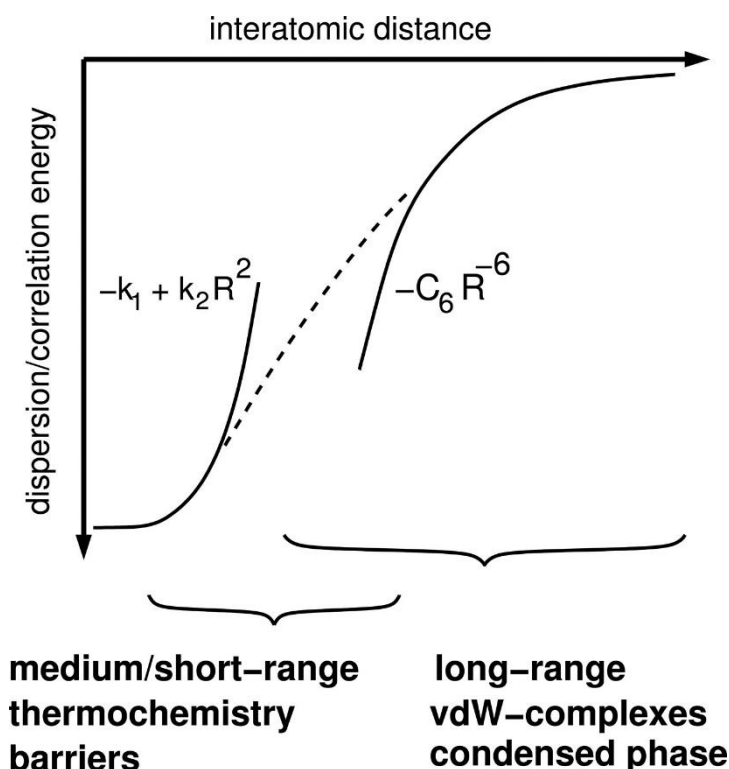
Fig. 2.2. Qualitative behavior of dispersion energy at short-, medium- and long-range distances (R). k_1, k_2 and C_6 are system specific constants. Taken from ref.[147].

Most of the calculations presented in the results section were performed using the D3(BJ) dispersion correction applied to the B3LYP functional, as mentioned before. Comparison with other dispersion-corrected functionals (also including different dispersion schemes) is also provided.

2.3 Basis sets

The Schrödinger equation[165] can only be analytically solved for hydrogen-like atoms, that is, for mononuclear systems. In other cases, the Schrödinger equation needs to be solved in an approximated way; in this sense, a useful strategy is to use a set of basis functions to construct the corresponding wave function (ψ). Indeed, the wave function is formed by a set of molecular orbitals, that result from the combination of these basis functions. This is usually achieved by using the convenient Linear Combination of Atomic Orbitals (LCAO) approach, firstly reported by Lennard-Jones in 1929[166]:

$$\phi_i = c_{1i}\chi_1 + c_{2i}\chi_2 + c_{3i}\chi_3 + \cdots + c_{ni}\chi_n = \sum_r c_{ri}\chi_r \qquad \textbf{(2.13)}$$

Where ϕ_i is a molecular orbital represented as a sum of n atomic orbitals χ_r, each multiplied by a corresponding coefficient c_{ri}, and r (numbered 1 to n) indicates which atom orbital is combined in the term.

Basis functions are typically hydrogen-like orbitals that consists of a radial $R_{n,l}$ and spherical harmonic angular part $Y_{l,m}$:

$$\phi(\boldsymbol{r}; \alpha, R) = R_{n,l}Y_{l,m} \qquad \textbf{(2.14)}$$

Where the radial part, $R_{n,l}$, is of Slater type.

Slater Type Orbitals (STO)[167] are defined as:

$$\phi^{STO}(\boldsymbol{r}; \alpha, R) = Ar^l e^{-\alpha(r-R)} \qquad \textbf{(2.15)}$$

Where r is the electron position, R refers to the position of the nucleus, α is a charge dependent constant, l an integer number accounting for the angular momentum and A is the normalization constant so that $\int |\phi^{STO}|^2 dr = 1$.

Slater type orbitals are functions that describe well the exponential behavior of electrons' orbitals. However, three and four-center two electron orbitals involving STO cannot be easily solved analytically. For this reason, a more convenient approximation is given by Gaussian Type Orbitals (GTO)[168]. GTO are easier to integrate, and, accordingly, are less computationally demanding:

$$\phi^{GTO}(\boldsymbol{r}; \alpha, R) = Ar^l e^{-\alpha(r-R)^2} \qquad \textbf{(2.16)}$$

The main problem with GTO is represented by the fact that they are not able to represent the cusp of STO near the nucleus, and decay too rapidly far from the nucleus. In order to try to alleviate these significant shortcomings, the solution is to represent STO as a linear combination of many GTO:

$$\phi^{STO} \approx \sum_{i=1}^{L} c_{i\mu}\phi^{GTO} \qquad \textbf{(2.17)}$$

In the present thesis work, both STO and GTO have been used.

2.3.1 Basis Sets Superposition Errors (BSSE)

The BSSE is a significant problem that arises in dimers. Such an issue is a consequence of a sharing of basis sets coming from each monomer that form a complex. Originally introduced by Liu and McLean in 1973[169], it was firstly reported by Kestner in 1969[170].

From a conceptual point of view, BSSE can be explained as having a dimer AB, formed by monomer A and monomer B. When forming the complex AB, each monomer is further stabilized because A donates extra basis functions to B, and B donates extra basis functions to A. Such a phenomenon cannot occur in separate monomers and, therefore, the dimer is overstabilized. In other words, it is an artificial shortening of intermolecular distances with a concomitant artificial strengthening of intermolecular interactions[171].

A popular strategy to overcome that issue is represented by the counterpoise corrections to the BSSE[172,173]. This is achieved by including the neighbor monomer's orbitals in order to have the same basis set as in the dimer. However, such an approach has serious issues when dealing with open shell systems and solvation treatments.

Several cases have been critically discussed by Alvarez-Idaboy and Galano[174]; it was concluded that the best solution is to not take into account counterpoise corrections and to try to use as much as large basis sets as possible, so that to attenuate the BSSE problem.

Extensive triple-ζ Pople's basis sets[175] (6-311++G(3df,2p)) were mostly used in the result section of this thesis work, when dealing with GTO functions. When STO are needed, we have employed very large quadruple-ζ even-tempered basis sets[176].

2.4 Solvation

Biochemical processes arising in an open biological environment take place mainly in water, unless some special cases such as the catalytic pockets of enzymes that can be solvent-free. Therefore, in order to properly investigate the behavior of aluminum with respect to common bioligands, it is important to mimic the behavior of the solvent. Implicit solvation models are often used in *Quantum* chemistry as they allow computationally affordable treatments of solvation effects, rather than explicitly consider solvent molecules[177].

From a conceptual point of view, solvated molecules can be viewed as a process in which first a cavity has to be created in the solvent in order to place the solute (molecule). Then, the cavity becomes polarized because of the electric field created by the solvent. The polarization of the cavity generates an electric field at the solvent molecules. It is this last effect that can be modelled as a perturbation operator which is added to the Hamiltonian of the solute in gas phase.

The solute is embedded in a polarizable continuum of dielectric ε. The first step is to create a cavity in order to accommodate the solute; the free energy variation in this step is called the "cavitation energy". When the molecule with the gas phase geometry and electronic structure is placed within the cavity, the electric field created by the molecule polarizes the continuum and an electrostatic potential arises in the cavity. Such electrostatic potential is called "reaction potential" and interacts with the molecule generating a total free energy change.

This latter change in free energy arises from the solute-solvent, solvent-solvent and internal solute electrostatic interactions; such energy is called "electrostatic" contribution. Finally, the solute-solvent dispersion energy gives rise to the "dispersion" term.

Accordingly, the solvation free energy ΔG_{solv}, that is, the change in free energy needed to transfer a molecule from the gas phase to the solvation, is given by:

$$\Delta G_{solv} = \Delta G_{cav} + \Delta G_{elec} + \Delta G_{disp} \tag{2.18}$$

When the solvent is treated as a continuum, as discussed above, the Laplacian of the reaction potential, $\phi(r)$, is related to the free charge density, $\rho(r)$, by the Poisson's equation:

$$\nabla\varepsilon(r)[\nabla\phi(r)] = -4\pi\rho(r) \tag{2.19}$$

Where ε is the homogenous dielectric constant.

The polarizable continuum model (PCM)[177] solves the electrostatic problem by introducing a charge distribution spread over the cavity surface[178,179]. The volume of the cavity is obtained by adding up van der Waals spheres of solute's atoms. The surfaces of these resulting volumes are rather irregular and, in general, no analytic function can fit them.

For that reason, ΔG_{elec} is calculated numerically. The cavity surface is divided into a large number of small surface elements, and a point charge is associated to each surface element.

The reaction potential is added to the solute Hamiltonian and solved iteratively by means of the SCF procedure:

$$\hat{H} = \hat{H}_0 + \phi(r) \tag{2.20}$$

After each SFC cycle new values of the surface changes are calculated from the current wave function to update the reaction potential; this is then used in the next iteration until the solute wave function and the surface changes are self-consistent.

The dispersion and cavitation components are usually considered proportional to the surface defined by the van der Waals spheres and the solvent accessible surface is used to calculate dispersion contribution.

PART I

Chelation therapy and development of new chelation strategies

"Some girls they want a handsome Dan
Or some good-lookin' Joe, on their arm
Some girls like a sweet-talkin' Romeo
Well 'round here baby
I learned you get what you can get
So if you're rough enough for love
Honey I'm tougher than the rest"

(B. Springsteen, Tougher than the Rest)

Tuning the affinity of catechols and salicylic acids toward Al(III): characterization of Al-chelator interactions

Gabriele Dalla Torre, Jon I. Mujika, Elena Formoso, Eduard Matito, Maria J. Ramos and Xabier Lopez, *Dalton Trans.*, **2018**, *47*, 9592-9607.

Dalton Transactions
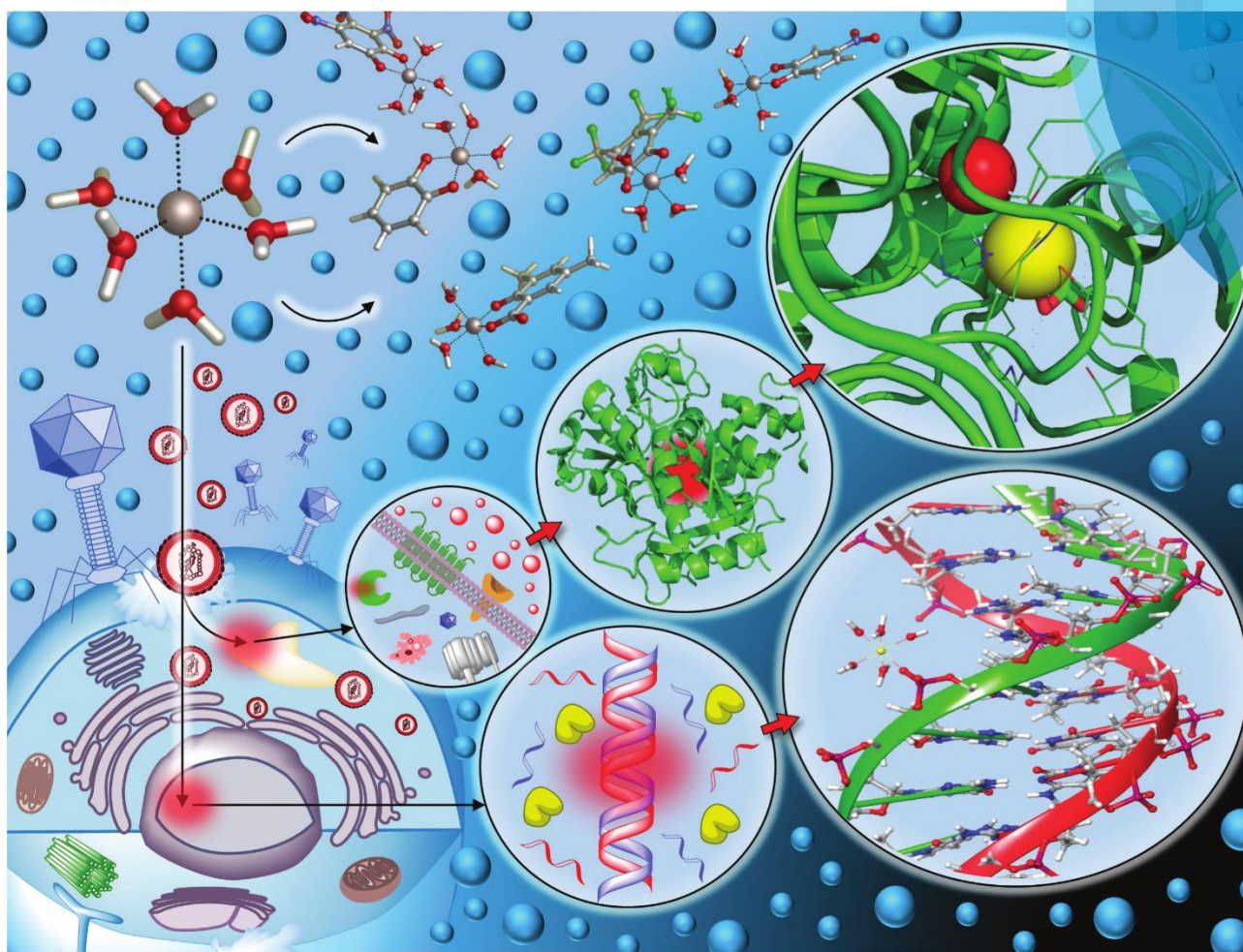
ROYAL SOCIETY
OF CHEMISTRY

Tuning the affinity of catechols and salicylic acids towards Al(III): characterization of Al-chelator interactions.

3.1 Introduction

Aluminum is the third most abundant element in the Earth's crust, following oxygen and silicon. However, complex but effective geochemistry has prevented its solubilization[8,180], allowing biological systems to evolve in the absence of this abundant metal. Nonetheless, in the last century, human intervention has made aluminum bioavailable in a myriad different ways, and as a consequence, important trace amounts of this element are found in the human body. The introduction of a nonessential element into biological cycles has raised justified concerns about its biological effects and potential toxicity[7,10,181], and the scientific literature on the adverse health effects of aluminum is extensive[182]. Although the exact mechanisms of aluminum toxicity are not well understood at the atomic level, there is increasing evidence that aluminum promotes oxidative stress[52,56,183], inhibits the normal function of several enzymes (such as hexokinase[184], glutamate dehydrogenase[185-187], etc.), interferes with several key cell metabolism cycles[188-190], and alters the structure and chemistry of important metabolites[186] and cofactors[42]. Aluminum is also considered a neurotoxic element[191]. Early studies supported this hypothesis, linking aluminum and the formation of neurofibrillary tangles (NFT)[192]. In fact, both experimental and theoretical studies have underlined the ability of aluminum to bind to phosphorylated peptides[66,193] and to promote hyperphosphorylation of normal neurofilaments[194]. In addition, the ability of aluminum to contribute to Aβ-amyloid aggregation has been recently demonstrated[49,50], and growing evidence is linking aluminum to be a decisive contributing factor in Alzheimer's disease[3,59,61].

In this controversial context, the quest for chelating agents that could make an effective treatment for aluminum-related disorders has attracted considerable interest[6,16,22,25,112]. In particular, catechols and salicylic acids have emerged as very promising building blocks for the design of effective alumninum chelators, because they constitute two of the strongest bidentate aluminum binding species[20]. The reason for that relies on the fact that Al(III) is a hard Lewis acid (and the hardest trivalent metal), and therefore it prefers to coordinate to hard Lewis bases such as phenoxide and carboxylate[20]. Moreover, the interaction of aluminum with such functional groups is supposed to be mainly of electrostatic nature[16]. Due to this inherent affinity, it is not surprising that the biochemistry of important neurotransmitters like catecholamines is highly affected by the presence of aluminum[195-197]. It has

been shown that aluminum affects the signaling process mediated by these neurotransmitters[198], it alters their content in animal models[195], and it interferes with enzymatic activities that involve these neurotransmitters[64,76]. Because of their strong binding affinity, both catechols and salicylic acids have been extensively studied[6,16,94,199] in the framework of aluminum chelation therapy with the aim of finding improved and aluminum-specific chelators by tuning their chemical environment with different substituents. The efficiency of low molecular mass aluminum-chelator complexes has been studied by means of several experimental techniques, such as potentiometric titrations, UV/Vis. spectra, ^{1}H NMR and ESI-MS[94,102,199-201]. Nevertheless, the effects mediated by the inclusion of different substituents in the molecule and how they may modulate the binding affinity toward aluminum are still not well understood[199,201]. In this sense, the understanding of the effect of electron withdrawing (EWGs) and electron donating groups (EDGs), the role played by aromaticity in these chelators, the rationalization of complex stability, and the specific nature of the Al-O bonds is of paramount importance to guide the quest for improved aluminum chelating agents. However, often this relevant information can not be deduced directly from experimental procedures alone.

The use of *state-of-the-art* theoretical methods can provide valuable insights on the properties of these systems, as demonstrated elsewhere[108,202,203]. In the present work, we present a comprehensive computational protocol to investigate the behavior of different chelating agents interacting with Al(III). Validation with respect to available experimental data is also performed. Then, the validated protocol is applied to the characterization of the substituent effects and the bonding nature of various aluminum-chelator complexes, as well as their aromatic-related properties, in order to provide a thorough rationalization of the behavior of these chelators. We have considered two main families of chelating agents, salicylic acids and catechols, bearing electron donating groups (EDGs, methyl and methoxy) and electron withdrawing groups (EWGs, nitro and trifluoromethyl) placed at different positions along the aromatic ring and in different quantities (see Fig. 3.1 and Table 3.2). These substituents were chosen since they exert opposite effects through different mechanisms of actions (resonance and/or induction). Our results demonstrate that although the Al-O bond is mainly of ionic nature, as it corresponds to a hard metal ion, the trend in the stability for these complexes is mainly determined by covalent dative interactions. We also analyze how Al(III)/proton competition modulate the properties of these chelators.

3.2 Methodology

The computational protocol that we developed for the investigation of different Al(III)-chelator complexes is outlined in Fig. 3.2 and presented in the following sections. For the sake of simplicity,

Catechol family

catechol

4-nitrocatechol

4,6-dinitrocatechol

4,5,6-trinitrocatechol

4-trifluoromethylcatechol

4,6-trifluoromethylcatechol

4,5,6-trifluoromethylcatechol

4-methylcatechol

4,6-dimethylcatechol

3,4,5,6-tetramethylcatechol

4-methoxycatechol

Salicylic acid family

Salicylic acid

3-nitrosalicylic acid

5-nitrosalicylic acid

3,5-dinitrosalicylic acid

3,4,5-trinitrosalicylic acid

5-trifluoromethylsalicylic acid

3,5-trifluoromethylsalicylic acid

3,4,5-trifluoromethylsalicylic acid

3-methylsalicylic acid

4-methylsalicylic acid

5-methylsalicylic acid

6-methylsalicylic acid

3,5-dimethylsalicylic acid

4,6-dimethylsalicylic acid

3,4,5-trimethylsalicylic acid

3,5-dimethoxysalicylic acid

Functional group	Inductive	Resonance	Overall
Methyl ($-CH_3$)	ED	-	EDG
Methoxy ($-OCH_3$)	EW	ED	EDG
Nitro ($-NO_2$)	EW	EW	EWG
Trifluoromethyl ($-CF_3$)	EW	-	EWG

Fig. 3.1. Summary of the two families of chelators with the four differents substituents considered in this work: methyl and methoxy (EDGs), nitro and trifluoromethyl (EWGs). The different mechanisms of action of the substituents are also summarized.
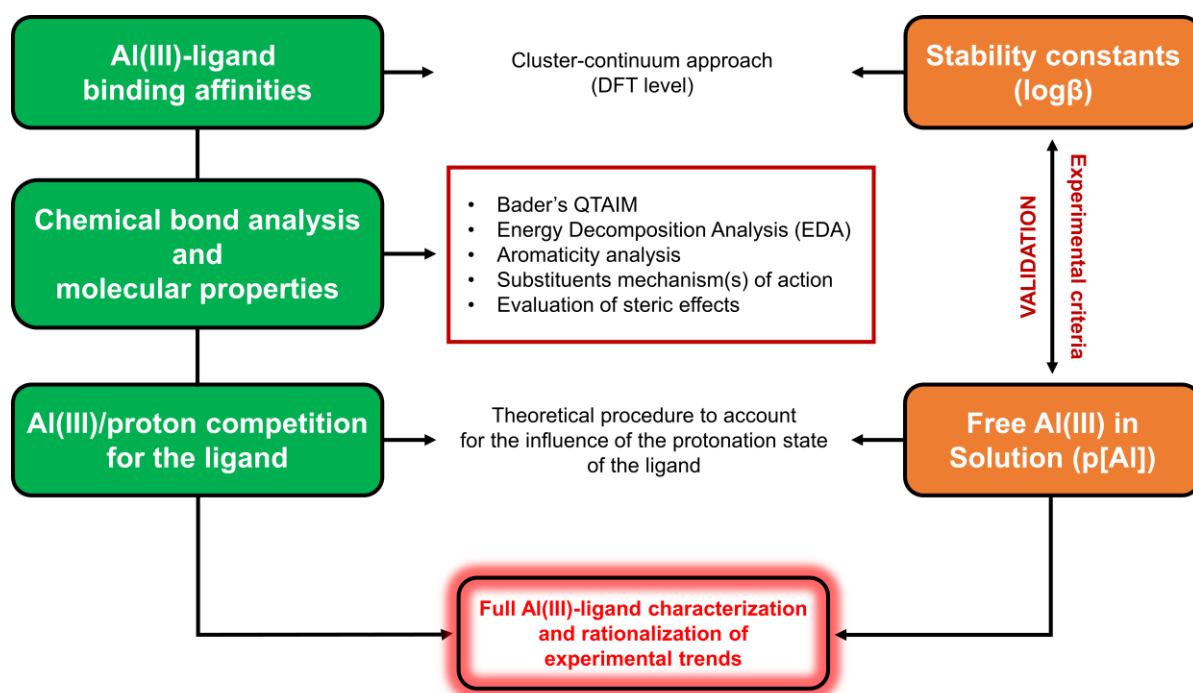
Fig. 3.2. Schematic representation of the computational protocol developed in this work.

we provide only a schematic overview of the whole protocol; therefore, for the full theory and technical details of each methodology we redirect the reader to the specific computational details section of Appendix A.

3.2.1 Definition of binding affinities: cluster-continuum approach

In order to investigate the thermodynamics of all Al(III)-chelator complexes in aqueous solution, we utilized the so-called cluster-continuum approach[115,204,205], with the first-coordination shell of aluminum surrounded by explicit water molecules in a octahedral fashion and a second solvation shell treated with a continuum dieletric model (see Fig. 3.4). Optimization and single point calculations were performed at the B3LYP-D3(BJ)/6-311++G(3df,2p)//B3LYP-D3(BJ)/6-31++G(d,p) using the integral equation formalism variant (IEFPCM) solvation model[177]. Such a choice was made since it has been shown that the introduction of dispersion corrections on both geometry and single point energy calculations improve the overall results[206]. In general, the addition of methods that properly take into account dispersion energies in DFT has been proven to improve the precision of computed non-covalent interactions[141,155].

For results with different Density Functionals and the MP2 methods and their evaluation versus experimental stability constants see Appendix A.

We characterized bidentate Al-Lig complexes with 1:1, 1:2 and the 1:3 stechiometry following the

ligand substitution reaction shown in eq. 3.1:

$$Al(H_2O)_6]^{3+}_{(aq.,1M)} + L^{-q}_{r(aq.1M)} \rightleftarrows Al(H_2O)_{6-m}L_r]^{3-q}_{(aq,1M)} + mH_2O_{(aq,1M)} \tag{3.1}$$
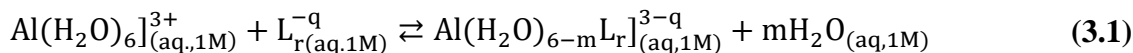
where q is the net charge of the ligand L, r the number of ligands and m depends on the stoichiometry of the complex, such as $m=2$, $m=4$ and $m=6$ for 1:1, 1:2 and 1:3 complexes, respectively. Notice that we consider the ligand in its unprotonated form, which is the state considered when evaluating experimental $log(\beta)$ (see section 3.3).

The enthalpy in solution corresponding to the binding of the ligand to Al(III) is therefore calculated as:

$$\Delta H^{comp}_{aq} = H_{aq}Al(H_2O)_{6-m}L_r + mH_{aq}(H_2O) - H_{aq}[Al(H_2O)_6] - H_{aq}(L)_r \\ + \Delta nRTln(24.46) \tag{3.2}$$

Since the enthalpies are determined using an ideal gas at 1 atm as the standard state, the last term in eq. 3.2 corresponds to the volume change due to the transformation from 1 atm to 1 M in solution, where Δn refers to the change in the number of species in the reaction[207]. In a similar way, the free energy of the complexes is determined as:

$$\Delta G^{comp}_{aq} = G_{aq}Al(H_2O)_{6-m}L_r + mG_{aq}(H_2O) - G_{aq}[Al(H_2O)_6] - G_{aq}(L)_r \\ + \Delta nRTln(24.46) + mRTln(55.34) \tag{3.3}$$

where the last term is the entropic factor that accounts for the concentration of 55.34 M of water in liquid water[207].

The validation of binding energies with respect to experimental stability constants (i.e. $log\beta$) is thoroughly discussed in section 3.3.

3.2.2 Chemical bond analysis and evaluation of molecular properties

At the second stage, to provide a quantitative and qualitative characterization of the interactions arising in these Al(III)-chelator complexes, as well as to unveil the effect of different substituents (EDGs and EWGs) toward complex stability, we have employed several *state-of-the-art* computational techniques summarized as follows:

- **Quantum Theory Of Atoms In Molecules (QTAIM):** the Bader's theory[208] allows to classify the nature of a given bond according to the carachteristics of its Bond Critical Point

(BCP), such as the electron density at the BCP $\rho(r_{BCP})$, the Laplacian of the electron density $\nabla^2(r_{BCP})$ and the total energy density $H(r_{BCP})$. Delocalization Indices $(D.I._{AB})$ provide a mean of the average number of electron pairs shared between two atoms A and B.

- **Energy Decomposition Analysis (EDA):** the EDA scheme by Morokuma[209] and Ziegler and Rauk[210] decomposes the total interaction energy (ΔE_{int}) between two molecules into three main components, that is, an electrostatic interaction term (ΔE_{elstat}), an orbital interaction term (ΔE_{oi}) and a Pauli repulsion term (ΔE_{Pauli}). Therefore, the EDA scheme allows to measure and quantify the electrostatic and covalent effects that may arise in a given complex.

- **Aromaticity analysis:** the analysis of the aromaticity of a molecule according to the I_{ring}[211] and MCI[212] aromatic descriptors is useful to compare the overall aromatic character of a given ligand with respect to a refence (i.e. benenze for an aromatic compound, ciclohexane for a non aromatic one); moreover, it is possible to analyze the effects that the addition of substituents of different nature may have on the aromatic-based properties (like resonance) of the ligand, so that to provide a rationale for their mechanism of action.

- **Evaluation of possible steric effects**: steric hindrances may take place between two or more functional groups placed close one another; accordingly, it is important to evaluate the change in stability due to repulsive phenomena upon addition of bulky functional groups.

3.2.3 Aluminum ion and proton competition

Finally, we developed a strategy to account for the influence of the protonation constants of a given ligand toward the stability of the complex with Al(III), and, therefore, for the competition between Al(III) and the proton for the ligand. The latter aspect is particularly important upon addition of substituents because different functional groups lead to different effects against ligand's pK_a, modulating the overall basicity/acidity of the chelator[94,199,213]. The whole strategy is presented and discussed in the aluminum ion/proton competition section; its evaluation and validation with respect to the experimental pAl criteria is also provided.

3.3 Results and discussion

3.3.1 Validation of binding affinities

Experimentally, chelation affinity is usually measured by using two different criteria: pM and $log\beta$ (cumulative stability constant)[27]. pM is defined as the negative logarithm of the concentration of the free metal in solution, calculated for total [ligand] = 10^{-5} M and total [metal] = 10^{-6} M at pH 7.4, usually calculated from data at 25°C and 0.1 M ionic strength[28]. This criteria is usually useful when comparing different chelators, as pM takes into account the effects of ligand protonation and denticity, so that it can provide a general and qualitative insight about the chelation properties of the molecule in solution[27,28,78]. On the other hand, stability constants $log\beta_{abc}$ can be expressed as $aM + bL + cH \rightleftarrows M_a + L_b + H_c$, where M is the metal, L is the ligand (in its unprotonated form) and H stands for a given protonation state. In other words, this is a measure of the strength of the interaction between the metal and the ligand that form the complex.

In order to validate our approach, theoretical binding energies of 1:1, 1:2 and 1:3 complexes were evaluated with respect to the available experimental $log\beta$ and pAl values taken from ref.[94]. At this stage, those complexes with available experimental data were included, namely: catechol, 4-nitrocatechol, salicylic acid, 3-nitrosalycilic acid, 5-nitrosalycilic acid and 3,5-dinitrosalycilic acid. Optimized geometries are shown in Fig. 3.4, and the ΔG_{aq}^{comp} and ΔH_{aq}^{comp} values reported in Table 3.1 along with experimental data.

As we can see in Fig. 3.3, our theoretical protocol is able to describe the relative affinity for this set of molecules. Indeed, theoretical ΔG_{aq}^{comp} shows the same trends as the experimental $log\beta$ for all stechiometries, with a total correlation coefficient of 0.9692. On the other hand, If we analyze the trends observed for pAl (Table 3.1), we can see that these trends are not the same order as for $log\beta$ and ΔG_{aq}^{comp}. Notice that pAl does not depend on the stochiometry (Table 3.1), so it is often used as an indirect ligand affinity indicator[78]. However, the observed discrepancies between pAl and $log\beta$ are due to the fact that, as previously mentioned, pAl depends not only on the stability of the complexes, but also on other factors like metal/proton competition, the number of different Al(III)-chelator species present at pH 7.4 and the denticity of the chelator[27,78]. This remarks the limits of using pM alone, as a unique measure of complex stability. A more detailed discussion about pAl is provided in the aluminum ion/proton competition section.

Optimized geometries for 1:1, 1:2 and 1:3 complexes can be found in Fig. 3.4. In all complexes the ligands interact bidentately with aluminum. Since Al(III) is always hexacoordinated, the remaining coordination sites are filled with water molecules. In 1:1 and 1:2 complexes, aluminum is always

placed coplanar to the aromatic rings.

In 1:2 complexes, the two ligands are not fully coplanar as they are slightly tilted one another (deviation dihedrals in the 8.0-11.0 degrees range, (Fig. 3.4). In the case of 1:3 complexes, whereas catechol family still retain the coplanarity (Fig. 3.4) of aluminum with respect to the aromatic rings, salicylic acid complexes show slight distortions, due to $\pi - \pi$ stacking interactions that arise between the adjacent aromatic rings.

Stoichiometry		Ligand	Theoretical		Experimental	
			ΔH_{aq}^{comp}	ΔG_{aq}^{comp}	$log\beta$	pAl
1:1 Complexes	Cathecolates	Cathecolate	-88.4	-91.4	16.3	10.1
		4-nitrocatecholate	-71.6	-75.8	13.3	14.2
	Salicylates	Salicylicate	-76.9	-78.7	13.3	8.2
		3-nitrosalicylicate	-64.2	-66.7	9.5	8.7
		5-nitrosalicylicate	-63.3	-65.4	9.3	8.4
		3,5-dinitrosalicylicate	-55.0	57.1	6.9	9.1
1:2 Complexes	Cathecolates	Cathecolate	-151.8	-157.7	31.7	10.1
		4-nitrocatecholate	-124.0	-130.8	24.8	14.2
	Salicylates	Salicylicate	-130.8	-136.9	24.2	8.2
		3-nitrosalicylicate	-110.6	-114.6	17.7	8.7
		5-nitrosalicylicate	-109.2	-114.2	17.7	8.4
		3,5-dinitrosalicylicate	-95.4	-101.0	13.3	9.1
1:3 Complexes	Cathecolates	Cathecolate	-183.1	-191.7	41.1	10.1
		4-nitrocatecholate	-154.8	-164.6	33.7	14.2
	Salicylates	Salicylicate	-160.6	-167.5	32.1	8.2
		3-nitrosalicylicate	-139.8	-145.8	23.7	8.7
		5-nitrosalicylicate	-137.8	-141.7	23.7	8.4
		3,5-dinitrosalicylicate	-125.8	-127.9	18.5	9.1
Total correlation coefficients					0.9692	0.1235

Table 3.1. Binding enthalpies (ΔH_{aq}^{comp}) and free energies (ΔG_{aq}^{comp}) in kcal/mol calculated for 1:1, 1:2 and

1:3 Al-ligand complexes with available experimental logβ and pAl data, taken from ref.[94].

Finally, we would like to point out that we repeated our calculations with other dispersion corrected DFT functionals, as well as at the MP2 level of theory (Appendix A), finding a good agreement between all different methods and B3LYP-D3(BJ) binding energies, which further validates our approach.
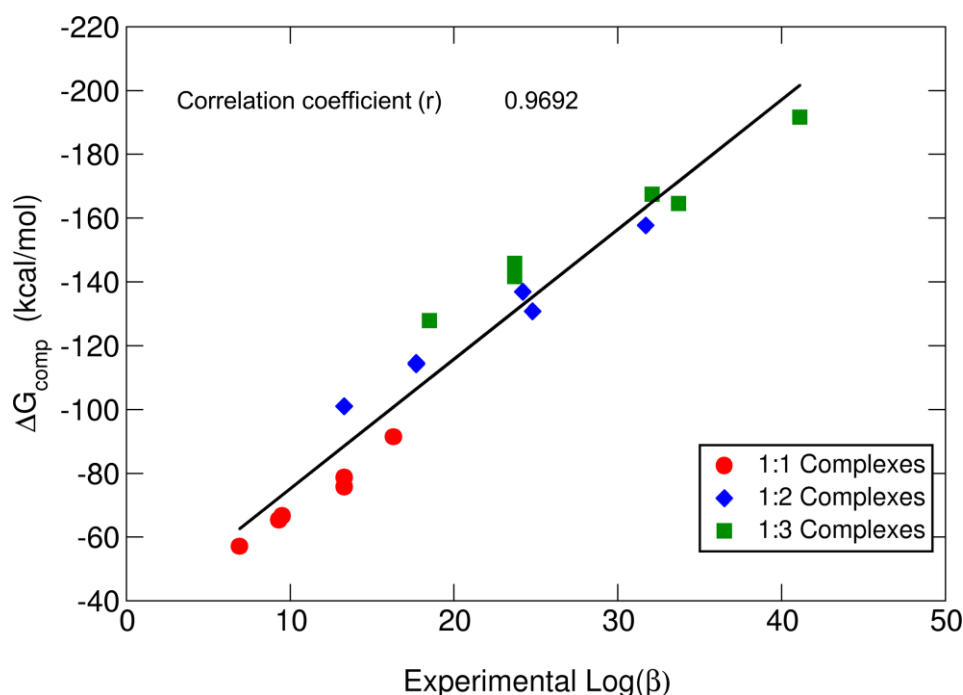
Fig. 3.3. B3LYP-D3(BJ) binding energies (ΔG_{aq}^{comp}) versus experimental stability constants (logβ)[94].

3.3.2 Modulation of the binding affinities by electron donating and withdrawing groups

Once validated our theoretical binding energies with respect to available stability constants, and taking into account that the relative affinities are not affected by the different stoichiometries, we focus in 1:1 complexes and enlarge our dataset of possible chelators by considering the four types of substituents presented in Fig. 3.1 (bottom table): methyl and methoxy (EDGs), and nitro and trifluoromethyl (EWGs). These substituents were placed at different positions of the catecholate/salicylate rings, and in different quantities. In this way, a total of 27 complexes were considered (1:1 complexes of Fig. 3.4 and 3.5). Results can be found in Table 3.2.

Our results show that the inclusion of methyl and methoxy groups leads to larger binding energies when compared with the unsubstituted compounds of both families, whereas the inclusion of nitro and trifluoromethyl groups leads to lower affinities. The destabilizing effect of the inclusion of a nitro
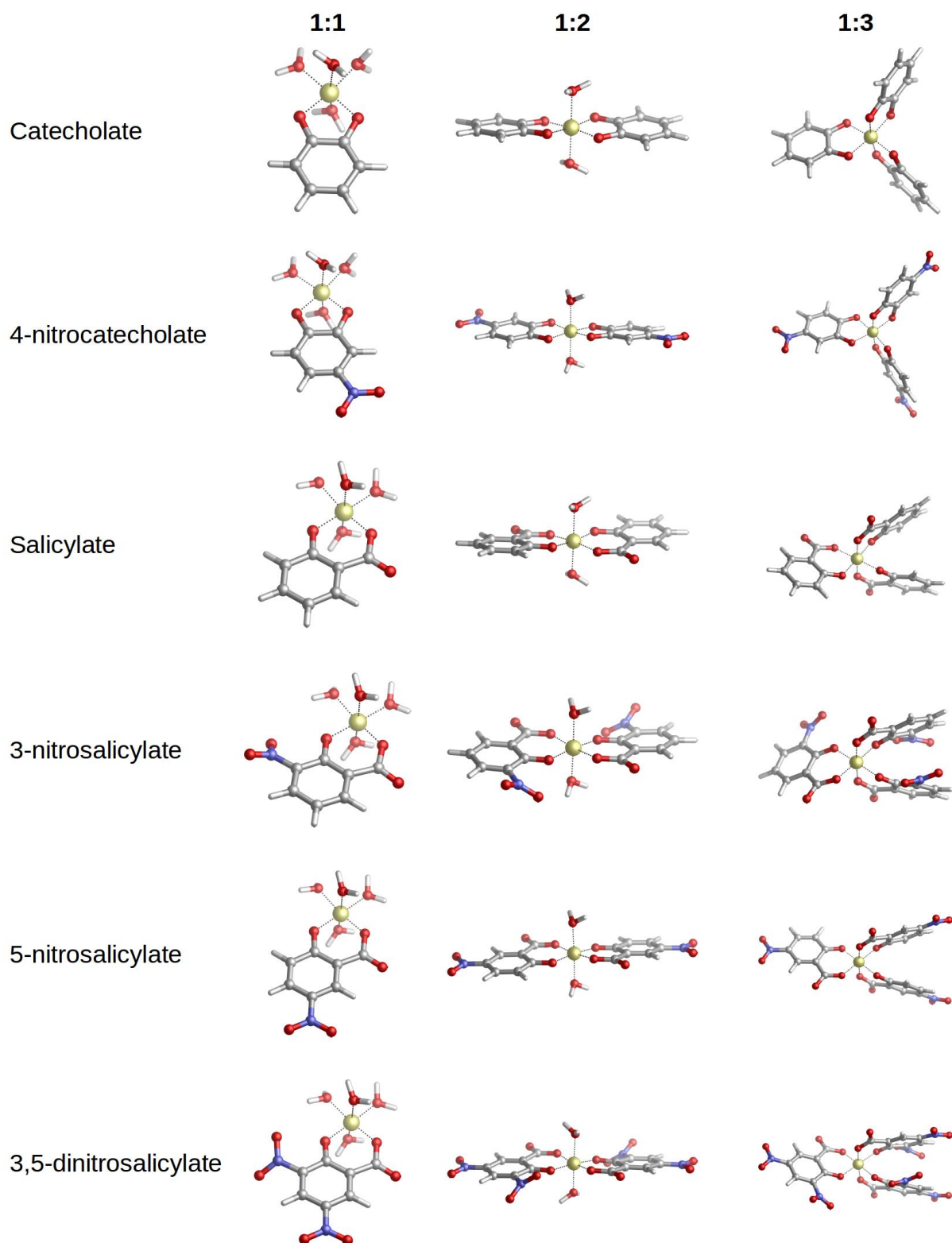
Fig. 3.4. Optimized geometries of 1:1, 1:2 and 1:3 Al(III)-chelator complexes used to validate the theoretical protocol: catechol, 4-nitrocatechol, salicylic acid, 3-nitrosalicylic acid, 5-nitrosalicylic acid, 3,5-dinitrosalicylic acid.

Ligand	ΔH_{aq}^{comp}	ΔG_{aq}^{comp}
Catecholates		
Catecholate	-88.4	-91.4
Electron Withdrawing Groups		
4-nitrocatecholate	-71.6	-75.8
4,6-dinitrocatecholate	-62.0	-65.9
4,5,6-trinitrocatecholate	-52.8	-56.4
4-trifluoromethylcatecholate	-81.4	-87.1
4,6-trifluoromethilcatecholate	-75.5	-78.6
4,5,6-trifluoromethylcatecholate	-70.1	-74.0
Electron Donating Groups		
4-methylcatecholate	-89.5	-93.3
4,6-dimethylcatecholate	-91.6	-95.4
3,4,5,6-tetramethylcatecholate	-97.2	-101.2
4-methoxycatecholate	-89.6	-92.8
Salicytates		
Salicylicate	-76.9	-78.7
Electron Withdrawing Groups		
3-nitrosalicylicate	-64.2	-66.7
5-nitrosalicylicate	-63.3	-65.4
3,5-dinitrosalicylicate	-57.1	-55.0
3,4,5-trinitrosalicylicate	-50.5	-52.4
5-trifluoromethylsalicylicate	-70.3	-75.3
3,5-trifluoromethylsalicylicate	-65.5	-67.6
3,4,5-trifluoromethylsalicylicate	-61.8	-64.2
Electron Donating Groups		
3-methylsalicylicate	-79.2	-82.5
4-methylsalicylicate	-79.3	-82.3
5-methylsalicylicate	-79.3	-82.9
6-methylsalicylicate	-74.9	-77.2
3,5-dimethylsalicylicate	-80.7	-83.6

4,6-dimethylsalicylicate	-76.4	-79.4
3,4,5-trimethylsalicilicate	-82.0	-85.3
3,5-dimethoxysalicylicate	-79.5	-82.3

Table 3.2. Binding enthalpies (ΔH_{aq}^{comp}) and free energies (ΔG_{aq}^{comp}) in kcal/mol computed for 1:1 complexes (compounds are shown in Fig. 3.1) considering the whole dataset of compounds bearing different substituents.

group is larger than the destabilizing effect of a trifluoromethyl group and, moreover, larger than the stabilizing effect of the inclusion of both methyl/methoxy groups.

This can be qualitatively explained in terms of inductive and resonance effects (see Fig. 3.1): nitro is an EWG by both inductive and resonance effects, whereas trifluoromethyl is an EWG only by induction. Moreover, methoxy shows contrary effects that partially compensate, i.e. an electron withdrawing effect by induction and a donating one by resonance. Finally, methyl is electron donating only by inductive effect. As we will see in the aromaticity section, resonance effects dominate over inductive effects and methoxy has an overall electron donating behavior. Our results are consistent with the hypothesis by Nurchi et al.[94] in that the decrease in the stability constants caused by the nitro substituent was due to a mixture of inductive/resonance effects. On the other hand, in a more recent paper, Nurchi et al.[199] also pointed to the increase in stability of complexes formed by methoxysalicylic acids and aluminum, although the origin of the enhancement of ligand affinity by methoxy substituents was not deeply analyzed. Another interesting feature that can be observed from our calculated binding affinities, is the additive character of the substituents effects: the higher the number of the substituents, the stronger their modulation of binding affinities. On the other hand, the specific position of the substituent in the aromatic ring does not lead to significant differences in the stability of both families of chelators (Table 3.2). These latter findings are in agreement with those reported in the literature, considering stability constants of differently substituted (EWGs or EDGs) salicylic acids[94,199].

In order to rationalize the opposite behavior of the two different classes of substituents and to obtain a more detailed picture about the change in the electronic structure of these complexes, we proceeded to characterize the nature of the Al-O interactions by means of the QTAIM theory and Energy Decomposition Analysis (EDA).

3.3.3 Chemical bond analysis of Al-chelator interactions

3.3.3.1 QTAIM analysis suggests a mainly ionic interaction but with a sizeable covalent degree

Results of QTAIM topological analyses of the Al-O bond critical points (BCPs) for all 1:1 complexes

are shown in Appendix A. The values of the electron density at all Al-O bond critical points, $\rho(r_{BCP})$, are rather small; such a situation has been reported in literature as a typical feature for metal-containing systems[214-216]. Interestingly, there is very good correlation between $\rho(r_{BCP})$ and binding affinities (ΔG_{aq}^{comp}): the higher the value of $\rho(r_{BCP})$, the stronger the affinity (see Appendix A).
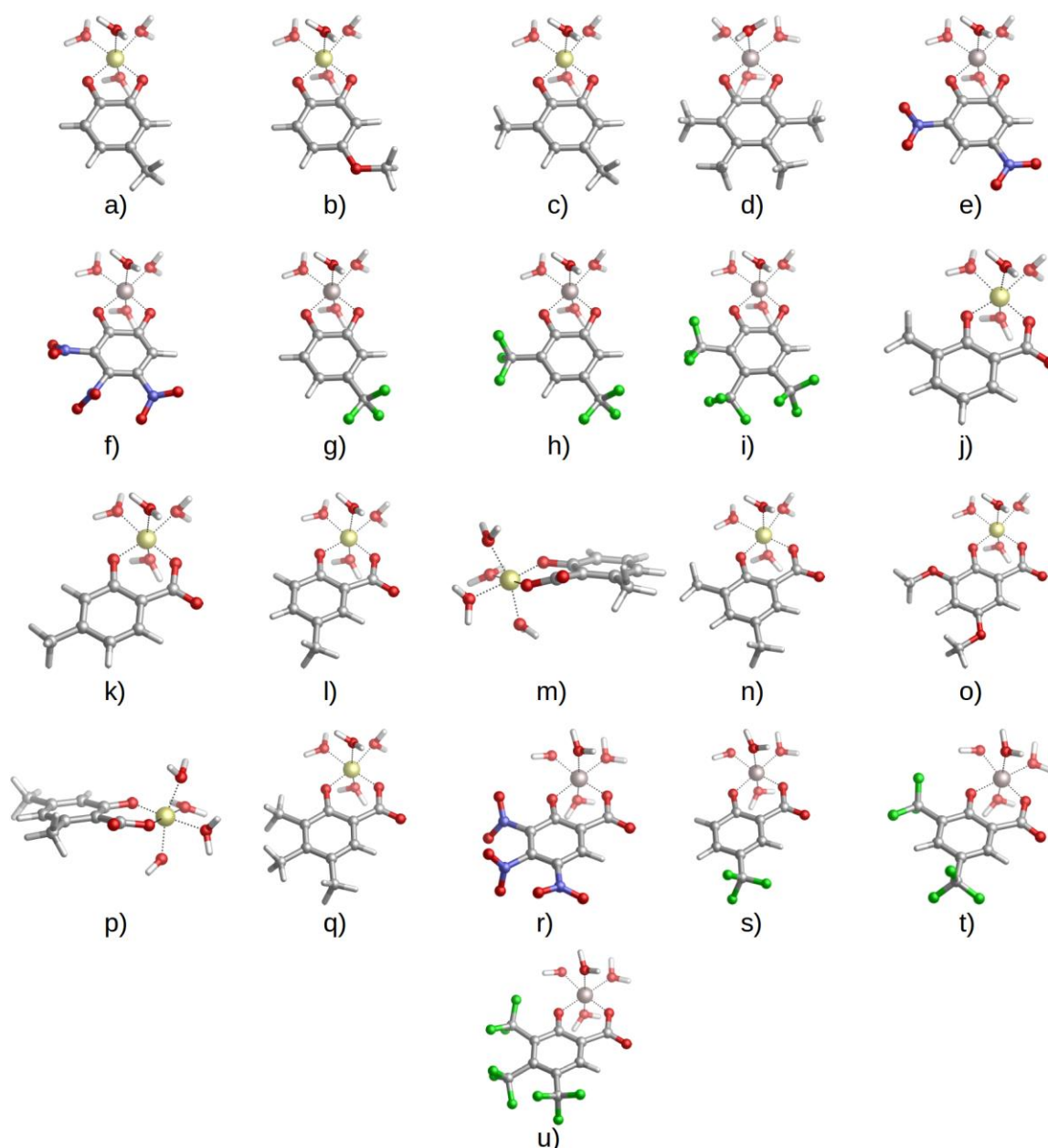
Fig. 3.5. Optimized geometries of 1:1 complexes between aluminum and catecholates or salicylates bearing the four different substituents: a) 4-methylcatecholate, b) 4-methoxycatecholate, c) 4,6-dimethylcatecholate, d) 3,4,5,6-tetramethylcatecholate, e) 4,6-dinitrocatecholate, f) 4,5,6-trinitrocatecholate, g) 4-trifluoromethylcatecholate, h) 4,6-trifluoromethylcatecholate, i) 4,5,6-trifluoromethylcatecholate, j) 3-methylsalicylate, k) 4-methylsalicylate, l) 5-methylsalicylate, m) 6-methylsalicylate, n) 3,5-dimethylsalicylate,

o) 3.5-dimethoxysalicylate, p) 4,6-dimethylsalicylate, q) 3,4,5-trimethylsalicylate, r) 3,4,5-trinitrosalicylate, s) 5-trifluoromethylsalicylate, t) 3,5-trifluoromethylsalicylate, u) 3,4,5-trifluoromethylsalicyate.

In addition, we find positive values of $\nabla^2(r_{BCP})$, and small but negative values of the energy densities at the bond critical points $H(r_{BCP})$, consistently for all Al-O BCPs. Positive values of $\nabla^2\rho(r_{BCP})$ and $H(r_{BCP})$ are indicative of closed-shell interactions (i.e. ionic or electrostatic bonds), while negative values for both quantities indicate the presence of shared (covalent) interactions. The mixed situation present in our results, previously reported for bonds involving metals[214], suggests that, although the Al-O bonds are mainly of ionic nature, there is also a small degree of covalency that could play a significant role. It is worth to emphasize that also both the Laplacians and the energy densities at all Al-O BCP show a strong correlation with binding energies (see Appendix A). To further investigate these findings, we decided to calculate the delocalization indices (D.I.) for all the Al-O bonds. These indices are quantities integrated in the whole volumes of the respective atom basins, and therefore they give a more global and reliable picture of a bond interaction than the analysis based on the properties of a single point in space like the bond critical point.

3.3.3.2 Delocalization Indices show a strong correlation versus binding affinities

D.I. for all Al-O bonds are shown in Appendix A, along with the Localization Indices of aluminum. In Fig. 3.6, we represent ΔH_{aq}^{comp} versus the sum of the two Al-O delocalization indices for each complex (D.I.$_{Al-O}$). The differences in Al-O bond delocalization indices among the various complexes are small. Nevertheless, there is a clear correlation between the values of these delocalization indices and the binding affinities (see Fig. 3.6), finding a remarkable linear correlation between ΔH_{aq}^{comp} and D.I.$_{Al-O}$, with a value of the correlation coefficient (r) of 0.9854 for salicylates (16 compounds), 0.9926 for catecholates (11 compounds), and 0.9884 for the whole dataset of 27 compounds. Since D.I. are a measure of the number of electron pairs shared between two atoms, they have been related to the covalent character of a given bond[217]. Our results point to a clear modulation of the D.I.$_{Al-O}$ by the opposite effect of EDGs and EWGs, confirming our previous findings of a small but important degree of covalency in these mainly electrostatic interactions.

The overall picture provides a clear rationalization of the effect of substituents: EDGs donate electron density to the aromatic ring, which in turn increase the covalency of the Al-O bonds, as it can be seen by larger values of D.I.$_{Al-O}$, higher $\rho(r_{BCP})$ and more negative $H(r_{BCP})$ of the Al-O bonds (Fig. 3.6, Appendix A). On the other hand, EWGs take electron density away from the aromatic ring, leading to weaker Al-O interactions with lower D.I.$_{Al-O}$ values, lower $\rho(r_{BCP})$ and less negative $H(r_{BCP})$. In summary, QTAIM topological analysis and D.I. suggest that there is a degree of covalency in the Al-

O interactions, modulated by the effect of substituents, which correlates with both theoretical (ΔG_{aq}^{comp}, ΔH_{aq}^{comp}) and experimental (*logβ*, when available) binding affinities. It is also important to note that values of aluminum Localization Indices (average number of electrons localized on a given atom) are stable among different compounds, suggesting that no charge transfer takes place in these aluminum-chelator complexes.
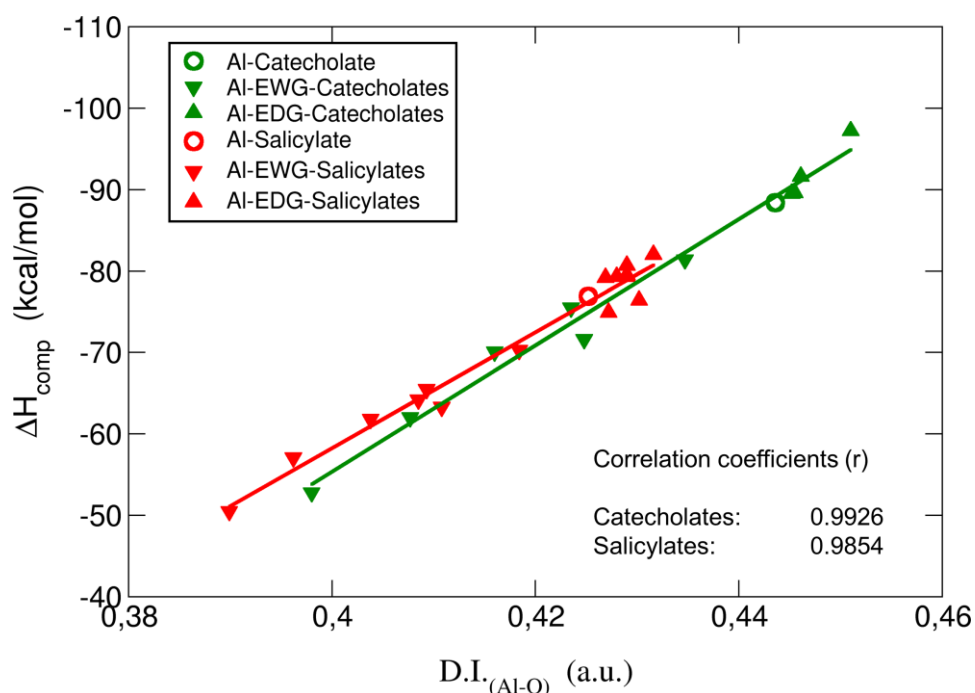
Fig. 3.6. Binding enthalpies ΔH_{aq}^{comp} in kcal/mol versus the sum of the two Al-O delocalization indices (D.I.$_{Al-O}$) in a.u. for all complexes.

Finally, we would also like to highlight the effect that substituents have in the modulation of atomic charges at the oxygen atoms coordinated to aluminum. In general, methyl and methoxy groups tend to increase the negative charges at those oxygen atoms, whereas the presence of nitro and trifluoromethyl groups lead to lower negative charges in both families (see Appendix A). Quite interestingly, high electron delocalizations from the lone pairs of the two oxygen atoms to the 3s and 3p orbitals of aluminum was assessed by means of the Natural Bond Orbital approach. According to these latter findings, we can rationalize such small covalent character as a dative interaction between the two oxygen donors and the formally empty orbitals of the metal.

To further investigate the relative contributions of the electrostatic and covalent components of these Al-O bonds, we performed the energy decomposition analysis (EDA) of all compounds.

3.3.3.3 Energy decomposition analysis confirms a mainly ionic bond with a significant covalent character that modulates the binding affinity

In Appendix A, we can find the values of the Energy Decomposition Analysis terms calculated at the B3LYPD3(BJ)/ET-QZ3P-1DIFFUSE level of theory in gas phase. In Fig. 3.7, we represent the values of binding enthalpies versus the total EDA interaction energies (ΔE_{int}), and its electrostatic (ΔE_{elstat}) and orbital interaction (ΔE_{oi}) components. First, we have to remark that there is a good linear correlation (r= 0.9727, salicylates and r= 0.9841, catecholates) between the total interaction energies calculated with EDA and ΔH_{aq}^{comp}, remarking the adequacy of using the EDA analysis to understand the origin of the different affinities of the chelators towards aluminum. The decomposition of interaction energies into electrostatic and orbital interaction (which accounts for the covalent character) terms points to mainly electrostatic interactions, and, in agreement with the previous QTAIM analysis, there is a sizable contribution from orbital interaction terms (between 27-37%). In general, the percentage of covalency is higher for catecholates than for salicylates (Fig. 3.7 and Appendix A), and EWGs tend to decrease the degree of covalency of these interactions, whereas EDGs increase it. However, it is important to take into account that such calculations were performed in gas phase, so environmental effects (i.e. implicit solvent) are expected to alter the degree of the covalent character. Interestingly, although ΔE_{elstat} is significantly larger than ΔE_{oi} in all compounds, it is only the latter that correlates with the binding enthalpies (See Fig. 3.7). The linear regression of ΔH_{aq}^{comp} versus ΔE_{oi} shows a correlation coefficient of 0.8964 for salycilates (16 compounds) and 0.9366 for catecholates (11 compounds), and 0.9185 if we consider the whole dataset of 27 compounds. Conversely, there is no correlation between ΔH_{aq}^{comp} and ΔE_{elstat}, and even though salicylates have on average larger electrostatic interaction energy than catecholates, they have lower affinity for aluminum. The other two terms of the EDA, ΔE_{Pauli} and ΔE_{disp} (Appendix A), don't show significant variations and therefore don't have a direct influence on the overall behavior of these compounds.

In summary, in agreement with QTAIM analysis, the tuning of the covalency of the Al-O bonds by the different EWG/EDG substituents modulates the differential affinities towards aluminum shown by these chelators. In this sense, the introduction of nitro and trifluoromethyl groups in the catecholate and salicylate rings leads to smaller absolute values of ΔE_{oi}, and this decrease is significantly larger for the former than for the latter. On the other hand, methyl and methoxy substituents lead to larger orbital interactions.

3.3.4 The role of aromaticity

The aromatic character of the ligands could be important to transmit the substituent effects. As it can

be seen in Fig. 3.1, the four substituents provide different effects: nitro is EWG by both inductive and
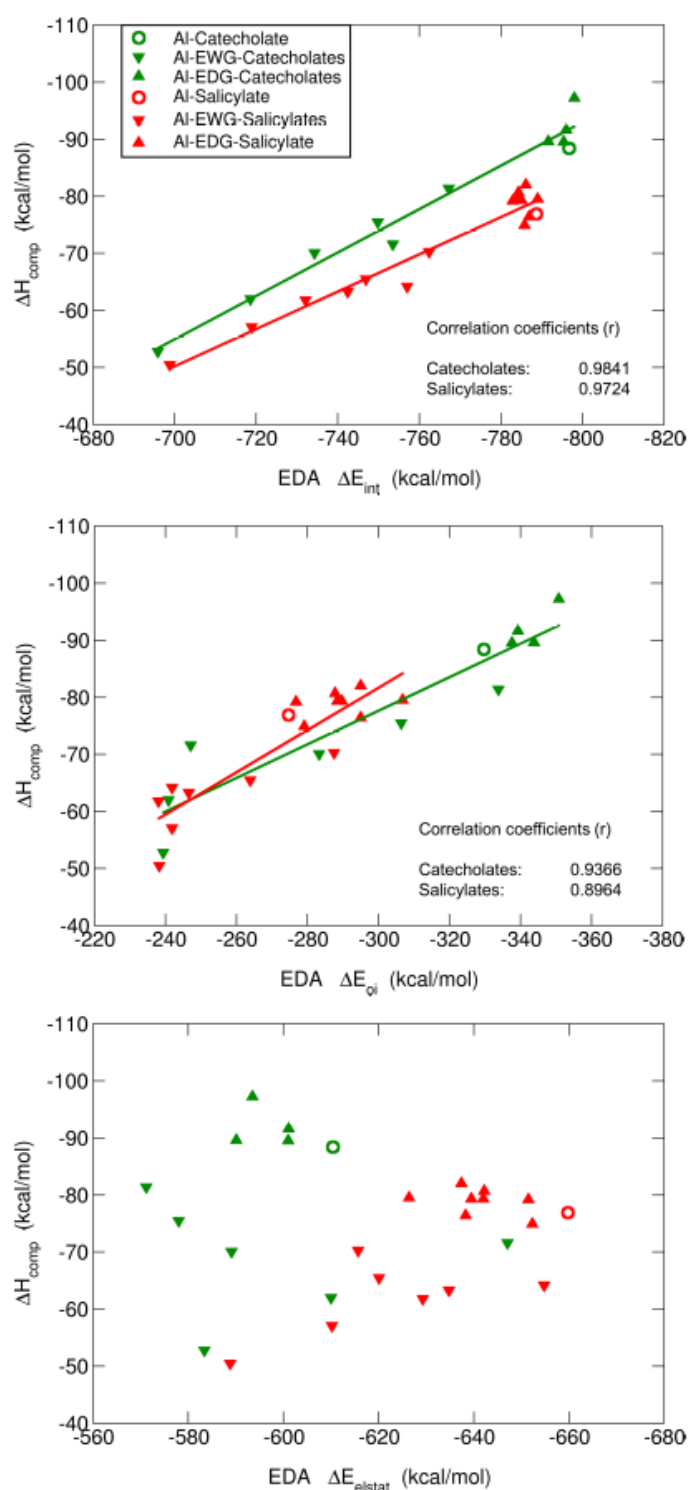
Fig. 3.7. Representation of the binding enthalpies (ΔH_{aq}^{comp}) versus three components of the Energy Decomposition Analysis: i) Total interaction energies (top diagram), ii) Orbital interaction term (middle diagram) and iii) Electrostatic energy term (bottom diagram) for all the 11 aluminum-catecholate and 16

resonance effects, trifluoromethyl is EWG only by inductive effect, methoxy shows opposite effects

that partially compensate, (electron withdrawing by induction and electron donating by resonance), and finally methyl is EDG only by inductive effect. Therefore, we chose to investigate how the aromaticity of the ligands changes upon aluminum binding and introduction of substituents. We investigate the aromatic character of all complexes according to the I_{ring} and MCI aromatic descriptors[218] (Appendix A). Both give similar trends and we will focus our discussion on I_{ring} indices. Benzene is used as reference for an aromatic compound, while cyclohexane for a non-aromatic one. As expected, both catechol and salicylic acid show lower aromatic characters than the pure benzene ring. Upon deprotonation, both catecholate and salicylate display a sizable reduction of the aromatic character to 0.0235 and 0.0306 a.u., respectively. Notice, however, that upon aluminum binding the values are restored to 0.0345 and 0.0351 a.u.. Thus, in terms of aromaticity, the interaction with aluminum recovers the values obtained for the original protonated catechol and salicylic acid. For the rest of the discussion, we will focus on Al-bound complexes, taking as reference the corresponding unsubstituted Al-catecholate/salicylate complex.

In both families of chelators, the addition of substituents, independently from the electron donating/withdrawing nature, decreases the aromatic character of the complexes. Moreover, such decrease in aromaticity follows a clear trend depending on the number of substituents that are added, so that the higher the number of substituents, the lower the aromatic character of the corresponding complex. Interestingly, substituents with a mechanism of action mediated by resonance (nitro and methoxy), show a larger decrease of aromaticity than those that work through inductive effects (methyl and trifluoromethyl). The lowest aromatic character is observed for tri-nitro-substitued compounds (4,5,6-trinitrocatecholate and 3,4,5-trinitrosalicylate), with values of 0.0207 and 0.0249 a.u. respectively. Regarding the electron-donating substituents, methoxy leads to lower aromaticity indices than methyl, because in aromatic molecules resonance effects dominate over inductive effects and methoxy has an overall electron donating behavior.

One may ask, as partially hypothesized by Dean et al. for similar pyridine-based aluminum chelators[200], whether the aromatic character of a chelating agent is one of the main factors contributing to the different stability of the Al-chelator complexes. Clearly, our calculations points to a negative answer. Both EWGs and EDGs decrease the aromatic character of the compounds, but in the latter case there is an increase in the affinity towards aluminum. Thus, aromaticity does not play a direct role in the stabilization of these aluminum-chelator complexes.

Nevertheless, the role of aromaticity is critical to modulate the mechanism of action of the substituents through resonance. In order to analyze this aspect, we calculated the binding energies of a series of non-aromatic 4-R-1,2-dihydroxy-ciclohexanes (See Fig. 3.8), and evaluated the changes in the binding affinities towards aluminum caused by the introduction of the four substituents listed

in Fig. 3.1. Results are summarized in Fig. 3.8, where we depict the relative binding energies $\Delta\Delta G_{aq}^{comp}$ of each complex with respect to the unsubstituted chelator in each case. We can see important differences in $\Delta\Delta G_{aq}^{comp}$ between aromatic and non-aromatic compounds; whereas in the case of non-aromatic chelators the range of $\Delta\Delta G_{aq}^{comp}$ expands from -0.6 kcal/mol to 6.4 kcal/mol, in the case of the aromatic catecholates $\Delta\Delta G_{aq}^{comp}$ expands to a much larger range, from -1.9 kcal/mol to 15.7 kcal/mol. This is indicative of a larger sensitivity of aromatic chelators towards substituent effects. Notice for instance, the large increase in the relative binding energies when considering the nitro group, 6.4 kcal/mol (non-aromatic chelator) versus 15.7 kcal/mol (aromatic chelator); clearly, this difference demonstrates that when the resonance transmission mechanism of the substituent is absent, the nitro group loses some of its electron-withdrawing character, partially maintained by the inductive-based one. Methoxy is a very significant case: while in the case of the aromatic chelator OCH_3 leads to stabilizing effects (-1.4 kcal/mol), in the case of the non-aromatic compound leads to a destabilizing effect (0.8 kcal/mol). This is due to the fact that OCH_3 acts as a EDGs by resonance, but as a EWGs by inductive effect. Accordingly, when resonance is absent like in 4-methoxy-1,2-dihydroxy-ciclohexane, the inductive-based electron withdrawing mechanism is the only one working.

In summary, although the introduction of electron donating/withdrawing substituents in both catecholate and salicylate families of chelators reduce the aromaticity of the compounds, the complexes still retain enough aromatic character to permit the transmission of substituent effects by a combination of both resonance and inductive mechanisms. This is a key factor in tuning the covalent character of the Al-O interactions.

3.3.5 Proton and aluminum ion competition

So far, we have not considered the possible competition between Al(III) and proton(s) for ligand binding. In other words, the overall performance of a chelator at a given pH will be dictated not only by the stability of the corresponding aluminum-ligand complex, but also by the deprotonation capacity of a ligand at a certain pH. As a result, the experimental trends in *logβ* and pAl to characterize the performance of a given chelator can differ[27,78] (see Table 3.1). For instance, catechol shows a pAl value of 10.1, and the introduction of a nitro electron-withdrawing group raises this value up to 14.2, indicating better chelation properties[94]. However, as we have seen, 4-nitro-catecholate shows a lower *logβ* value than the unsubstituted catecholate (see Table 3.1). Conversely, in the case of salicylic acids, Nurchi et al.[199] reported that methoxy-substituted salicylic acids (an overall electron-donating group) show significant higher pAl values (9.6/10.2 for orto/para metoxy-salicylic acid) than the
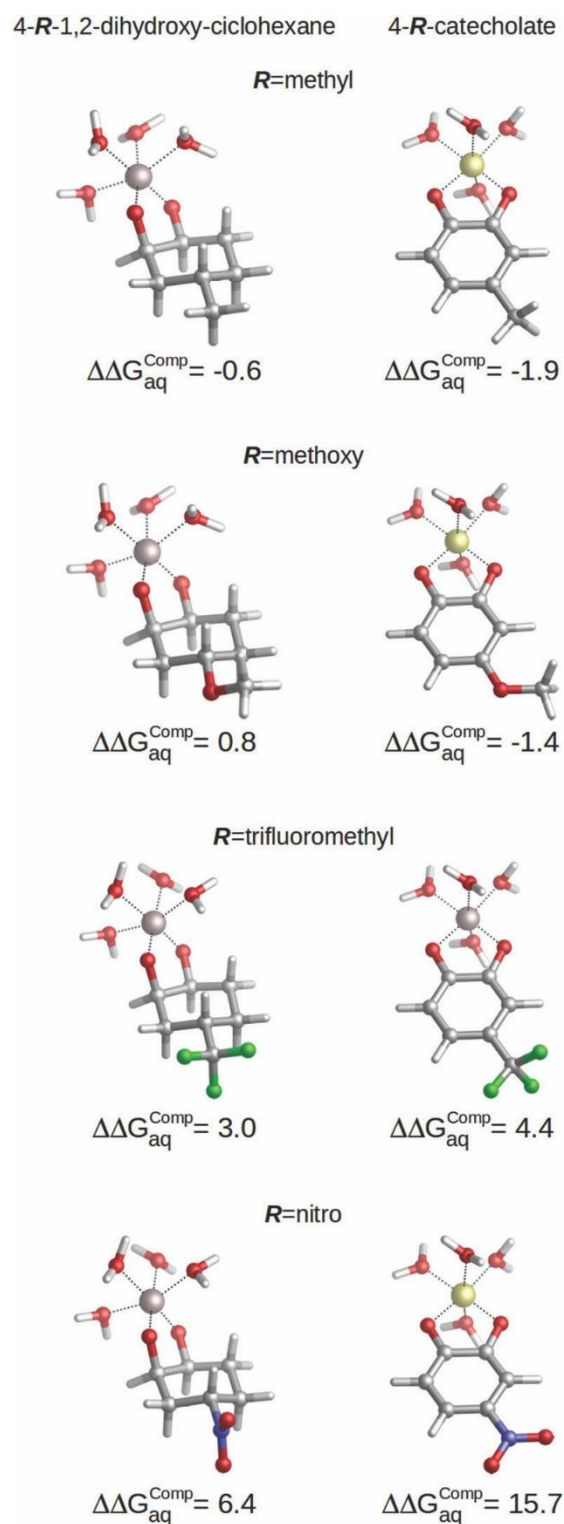
Fig. 3.8. Relative binding energies ($\Delta\Delta G_{aq}^{comp}$) of non-aromatic (4-**R**-1,2-dihydroxy-ciclohexane) and aromatic (4-**R**-chatecholate) chelators calculated with respect to their unsubstitued counterparts. **R** can be methyl, methoxy, nitro or trifluoromethyl. All energies are in kcal/mol.

unsubstituted one (8.2), while the introduction of a nitro group provokes only a moderate variation of

pAl, (8.4/8.7 for orto/para nitro-salicylic acid). What is the reason of these differential trends between salicylic acids and catechols, and between *logβ* and pAl in catechols? We have to take into account that whereas *logβ* is a measure of the stability of the complex with respect to the dissociation of unprotonated ligands, pAl takes into account additional factors, like proton/metal ion competition. Another important difference is that *logβ* is specific for each stoichiometry, while different stoichiometries and denticities contribute to a given value of pAl[28,78].

In order to account for proton/metal ion competition in our calculations, we have evaluated the relative proton affinities of the different ligands, and combine them with the relative aluminum affinities. The procedure is as follows: we evaluate the relative proton affinities of the ligands with a given functional group with respect to the unsubstituted catechol and salicylic acid, by the estimation of the following $\Delta\Delta G^{nh}(L_{subs}^{-2})$ reaction energy:

$$Cat^{2H,0} + Cat_{subs}^{-2} \xrightarrow{\Delta\Delta G^{2H}(L_{subs}^{-2})} Cat_{subs}^{2H,0} + Cat^{-2} \tag{3.4}$$

$$Sal^{1H,-1} + Sal_{subs}^{-2} \xrightarrow{\Delta\Delta G^{1H}(L_{subs}^{-2})} Sal_{subs}^{1H,-1} + Sal^{-2} \tag{3.5}$$
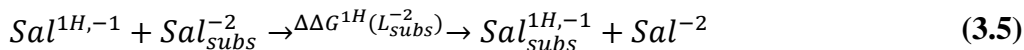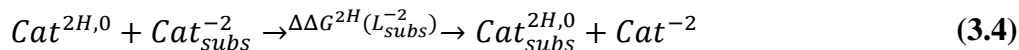
As one can see in these equations, there is an important difference between catechols and salicylic acids. The pK_a values of catechols (see Table 3.3 and ref.[94]) are such that at neutral pH both chelating positions are likely to be protonated and, therefore, Al(III) binding has to compete with the removal of two protons from the ligand.

However, the first pK_a^1 of salycilic acid is so low (see Table 3.3 and refs.[94,199]) that at neutral pH the carboxylic group is undoubtedly unprotonated; accordingly, the binding of the aluminum ion only involves the removal of the hydroxyl proton. Besides, we define a relative aluminum affinity of a given ligand in each family of compounds with respect to the unsubstituted ligand, using the ΔG_{aq}^{comp} values of Table 3.2, namely:

$$Al - lig^{-2} + Lig_{subs}^{-2} \xrightarrow{\Delta\Delta G^{Al}(L_{subs}^{-2})} Al - lig_{subs}^{-2} + Lig^{-2} \tag{3.6}$$
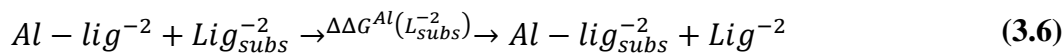
$$\Delta\Delta G^{Al}(L_{subs}^{-2}) = \Delta G_{aq}^{comp}(Al - L_{subs}^{-2}) - \Delta G_{aq}^{comp}(Al - L^{-2}) \tag{3.7}$$

with *Lig = Catecholate, Salicylate.* Combining the relative proton/aluminum ion affinities, we can estimate a value for the relative Al(III) affinity of a ligand that takes into account proton/metal ion competition, namely,

Ligand	$\Delta\Delta H_{subs}^{nH}$	$\Delta\Delta H_{subs}^{nH}$	pK_a^1(exp.)	pK_a^2(exp.)
$$Cat^{2H,0} + Cat_{subs}^{-2} \rightleftarrows Cat_{subs}^{2H,0} + Cat^{-2}$$				
Catechol	0.0	0.0	9.2	14.3
Electron Withdrawing Groups				
4-nitrocatechol	21.3	20.8	6.6	10.7
4,6-dinitrocatechol	36.0	36.0		
4,5,6-trinitrocatechol	47.6	46.9		
4-trifluoromethylcatechol	9.3	6.2		
4,6-trifluoromethilcatechol	18.7	19.0		
4,5,6-trifluoromethylcatechol	26.4	26.0		
Electron Donating Groups				
4-methylcatechol	-1.6	-3.0		
4,6-dimethylcatechol	-3.9	-4.8		
3,4,5,6-tetramethylcatechol	-9.1	-10.1		
4-methoxycatechol	-1.6	-1.6		
$$Sal^{1H,-1} + Sal_{subs}^{-2} \rightleftarrows Sal_{subs}^{1H,-1} + Sal^{-2}$$				
Salicylic acid	0.0	0.0	3.1	13.6
Electron Withdrawing Groups				
3-nitrosalicylic acid	10.8	10.5	1.5	9.9
5-nitrosalicylic acid	11.4	11.8	1.7	10.0
3,5-dinitrosalicylic acid	16.0	16.3	-0.1	7.0
3,4,5-trinitrosalicylic acid	18.9	18.9		
5-trifluoromethylsalicylic acid	5.2	2.9		
3,5-trifluoromethylsalicylic acid	9.7	9.4		
3,4,5-trifluoromethylsalicylic acid	12.7	12.6		
Electron Donating Groups				
4-methylsalicylic acid	-1.0	-1.3		
5-methylsalicylic acid	-1.1	-0.7		
6-methylsalicylic acid	2.5	1.5		
3,5-dimethylsalicylic acid	-2.4	-2.7		
4,6-dimethylsalicylic acid	1.5	1.4		
3,4,5-trimethylsalicilic acid	-3.4	-3.7		
3,5-dimethoxysalicylic acid	-2.1	-1.3		

Table 3.3 (previous page). Relative proton affinities with respect to catechols and salicylic acids in kcal/mol. Experimental protonation constants are taken from Ref.[94].

$$\Delta\Delta G^{Al}(Al - L_{subs}^{nH}) = \Delta\Delta G^{Al}(Al - L_{subs}^{-2}) - \Delta\Delta G^{nH}(L_{subs}^{-2}) \qquad \textbf{(3.8)}$$

with $n = 2$ for catechols, and $n = 1$ for salicylic acids. The results for $\Delta\Delta G^{nh}(L_{subs}^{-2})$can be found in Table 3.3 and Fig. 3.9-A, and the results for $\Delta\Delta G^{Al}(Al - L_{subs}^{nH})$ are also plotted in Fig. 3.9-B. As one can see in Fig. 3.9-A, EDGs lie at the top-right side of the diagram, whereas EWGs at the bottom-left side, manifesting that those ligands that have the largest affinities for aluminum, also display the largest affinities for protons. This is the case for both catechols and salicylic acids, but with an important difference. Catechols span a wider range of relative proton affinities than salicylic acids, a fact mainly attributed to the fact that two protons are removed in catechol and only one in salicylic acids. In order to estimate the aluminum relative binding affinity in the presence of protonated ligands (Fig. 3.9-B), we have to combine these two relative proton/aluminum affinities according to eq. 3.8, to yield $\Delta\Delta G^{Al}(Al - L_{subs}^{2H})$ (displayed in the y-axis of Fig. 3.9-B). Our data clearly shows an inverse trend between $\Delta\Delta G^{Al}(Al - L_{subs}^{2H})$ and $\Delta\Delta G^{Al}(Al - L_{subs}^{-2})$ for catechols, but not for salicylic acids. Our results for catechols suggest that the introduction of EWGs leads to a better Al(III) chelation performance upon competition with the removal of two protons, and this corresponds to the previously described experimental increase of pAl with nitro-substitution (Tables 3.1 and 3.3). In the case of salicylic acids, since we are only removing one proton upon aluminum binding, relative aluminum affinity is still the overall leading factor in chelator binding, and now it is the introduction of an EDG what clearly improves the performance of the chelator. This is again in agreement with the clear increase in the experimental pAl of salicylic acids upon the introduction of methoxy groups[199]. In summary, our results demonstrate that in the competition between aluminum binding and deprotonation, the latter factor dominates when the binding of Al(III) requires the removal of two protons from the ligand, whereas the former is dominant if only one proton has to be removed, in agreement with the experimental results for catechols and salicylic acids, respectively[94,199].

To complete our analysis, we provide a possible explanation of how the introduction of EWGs (i.e. nitro) in salicylic acids lead to similar albeit a bit higher pAl values. Our data for 1:1 complexes show a moderate decrease in $\Delta\Delta G^{Al}(Al - L_{subs}^{1H})$ for both 3 and 5-nitro-substitution (namely 1.5 kcal/mol), which in principle should point to a lower value of pAl. One aspect should be remarked in this regard: the experimental values of pAl doesn't take into account only 1:1 aluminum-ligand stoichiometry,

but different stoichiometrical complexes like 1:2 and 1:3. Therefore, we recalculated the differential binding free energies for 1:2 complexes, and 1:3 stoichiometries of the single nitro-substituted salicylic acids of Table 3.1, namely,

$$\Delta\Delta G^{Al}(Al - [L_{subs}^{1H}]_n) = \Delta\Delta G^{Al}(Al - [L_{subs}^{-2}]_n) + n\ \Delta\Delta G_{subs}^{1H} \qquad \textbf{(3.9)}$$

Where *n* is the number of ligands bound to aluminum. The results are as follows: for 1:1 complexes, we obtain values for $\Delta\Delta G^{Al}(Al - [L_{subs}^{1H}]_1)$ of 1.5 kcal/mol (3-nitro), 1.5 kcal/mol (5-nitro); for 1:2 complexes: 1.3 kcal/mol (3-nitro), -0.9 kcal/mol (5 nitro); finally, for 1:3 complexes, we found -9.8 kcal/mol (3-nitro), -9.6 kcal/mol (5-nitro). Thus, we can observe how the stoichiometry is an additional contributing factor in the modulation of the aluminum ion/proton competition for ligand binding, with higher stoichiometries favoring those substituents that lead to a more favorable deprotonation (i.e. EWGs), albeit lower interaction with aluminum itself. The overall result is that, for 1:3 complexes, the introduction of EWGs promotes their chelation to aluminum because of the lower protonation energies (i.e. lower protonation constants, Table 3.3), and would lead to higher pAl values; the case of 1:2 complexes lie in between 1:1 and 1:3-related behavior. The fact that the experimental data point only to a moderate increase in pAl upon nitro introduction in salicylic acids, suggests that different stoichimoetries with opposite effects are contributing to these values, and thus there is a partial cancelation and compensation of their effects. Finally, it is important to mention that both families of compounds, when protonated, form an intramolecular hydrogen bond between the two phenolates (catechol) and phenolate and carboxylate (salicylic acid), which is a further factor contributing to the modulation of the aluminum/proton competition.

3.3.6 Tuning the molecule: the role of substituents

The present paper provides the most complete and thorough theoretical study of the interaction of aluminum with catechols and salicylic acids chelating agents done so far. We have identified and rationalized important factors affecting ligand binding to aluminum, which are crucial to design new chelators of increased affinity. Namely, we have characterized the strength of the aluminum-ligand interactions, interpreted the binding strengths in terms of the electrostatic/covalent nature of the Al-O bonds, unveiled the role played by the aromaticity of these chelators, rationalized the modulation of the stability through addition of substituents and, finally, determined how aluminum/proton competition affects the overall activity of a chelator.

In this sense, our calculations demonstrate that although the bond is mainly electrostatic in nature, as it corresponds to a hard metal, the fine tuning of the stability in both families of chelators is mediated

through the modulation of the covalent character of the Al-O bonds.
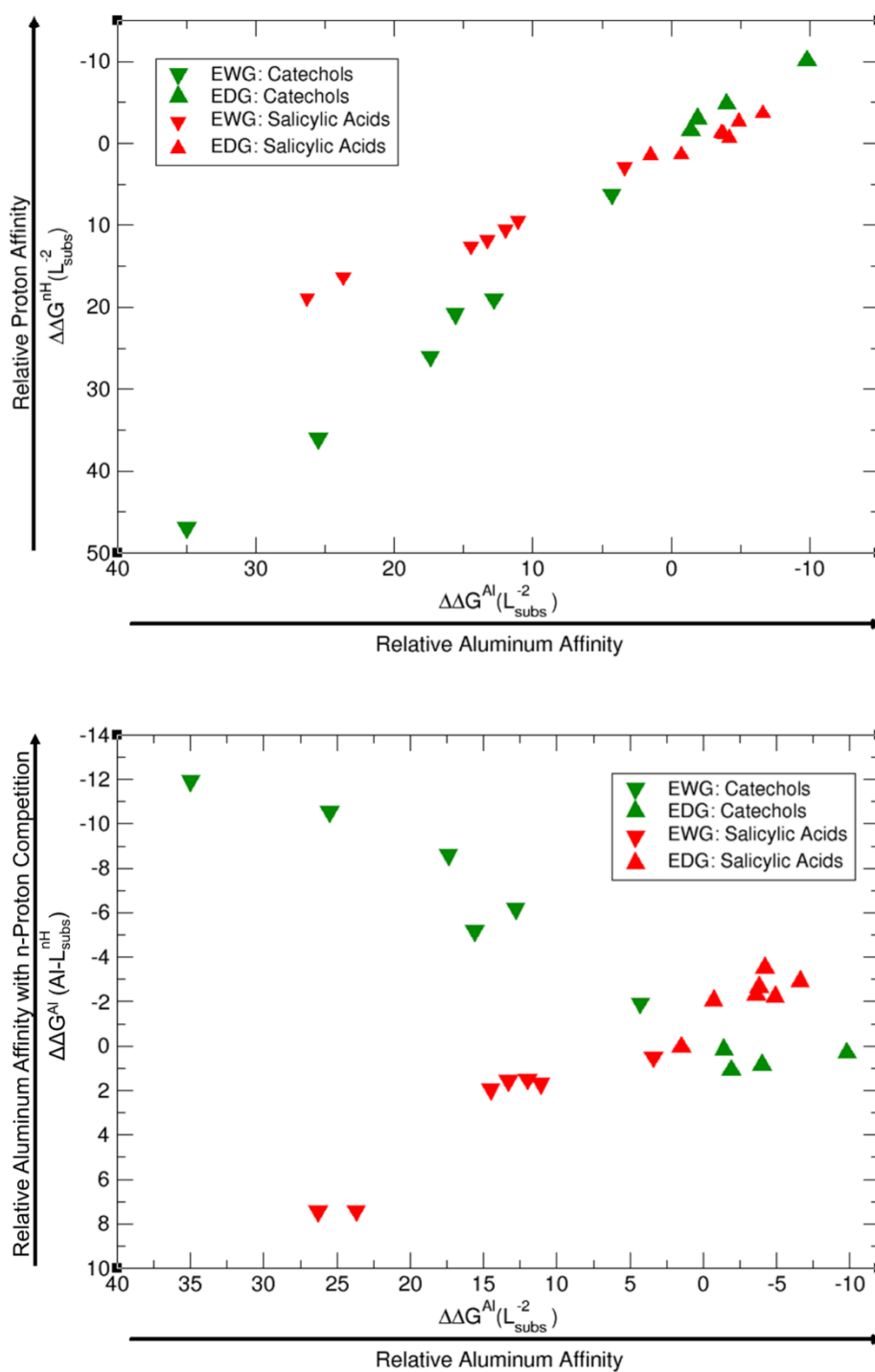
Fig. 3.9. Proton versus aluminum competition analysed as: (a) $\Delta\Delta G^{nH}\left(L_{subs}^{-2}\right)$ vs $\Delta\Delta G^{Al}\left(L_{subs}^{-2}\right)$ (top diagram). (b) $\Delta\Delta G^{Al}\left(Al - L_{subs}^{nH}\right)$ vs $\Delta\Delta G^{Al}\left(L_{subs}^{-2}\right)$ (bottom diagram). Terms are defined in the body text. All energies are in kcal/mol.

This covalent character can be classified as a dative bond from the lone pair of the oxygens to the 3s,

3p valence shell of Al(III). The increase in the dative Al-O bond character through the introduction of EDGs leads to complexes of higher stability, whereas EWGs lead to complexes of lower stability, in agreement with the experimental trends of *logβ* (Table 3.1). Such a picture is also coherent with the Pearson's Hard and Soft Acids and Bases (HSAB) principle[17]. Indeed, the two phenolate groups of catechol are harder Lewis bases than the carboxylate one of salicylic acid, because of the intrinsic resonance of the COO⁻ moiety, and therefore the former are expected to show higher affinity for hard Lewis acids such as Al(III). This is quite interesting considering that salicylates family shows, overall, a higher electrostatic interaction (three negatively charged oxygens) than the catecholate family, as shown by EDA results (Appendix A). Nevertheless, the catecholate family has a higher affinity for the trivalent metal, a fact that can be related to the more covalent Al-O bond as revealed by both QTAIM and EDA results and summarized in the electrostatic potential plots shown in Appendix A. We have also determined the role that the aromatic nature of these two families of chelators plays in the metal-ligand complexes. Aromaticity is only slightly affected upon aluminum binding, being more sensible to the introduction of EDG/EWG substituents in the ring. In both salicylates and catecholates, the introduction of both electron donating/withdrawing substituents leads to a lower aromatic character. Nevertheless, a significant degree of aromaticity is maintained in all complexes, which is pivotal to modulate and transmit some of the resonance-based substituent effects.

We should remark that, although the covalent character is the main driving factor in the modulation of the affinity toward aluminum for these two families of chelators, other factors can also affect the observed stability. For instance, in some of the complexes we found steric hindrances that put them out of the general trend in binding energy (see Table 3.2). Indeed, 6-methylsalicylate has a lower stability when compared with unsubstituted salicylic acid, despite the presence of an EDG, which should enhance its binding affinity. The optimized geometry for that compound shows that the six-membered ring formed by aluminum, the carboxylate and the enolate groups is slightly distorted from full planarity (by $16.8°$ and $20.9°$), suggesting a steric repulsion between methyl at the 6 position and the carboxylate group (m compound in Fig. 3.5). Such a situation leads to a decrease in binding affinity (Table 3.2). Moreover, If we consider 4,6-dimethylsalicylate (p compound in Fig. 3.5), we can see that the addition of a second methyl in position 4 partially recovers the stability and planarity of the complex ($12.6°$ and $15.6°$) when compared with salicylate (Table 3.2), because of the electron donating effect that counterbalances the steric repulsion of the methyl in position 6. However, the recovered stability is still not as stable as another di-substitued compound like 3,5-dimethylsalicylate ($0.1°$ and $0.1°$), where no steric effects are present (n compound in Fig. 3.5). This situation was also hypothesized by Dean et al.[201] for similar compounds. It is clear that, when considering new strategies toward the improvement and design of new Al(III) chelating agents, one should carefully consider

possible repulsive phenomena. Regarding proton/aluminum ion competition, we have been able to reproduce the inverse trends in ligand affinity when comparing *logβ* and pAl values for catechols (Table 3.1), and to explain how the introduction of an electron withdrawing group in catechols, but electron donating group in salicylic acids, enhances the chelation properties of the ligands upon competition with protonation. Taking into account that the metal/proton competition for ligand binding is critical to determine the performance of a given ligand in chelation therapy, as established by Hider et al.[27], complex stability is also important in order to compete with other endogenous ligands (like citrate) in an open biological environment[36]. Moreover, if the stablity of the Al(III)-chelator complex is too weak, then the metal may prefer to form the very stable $[Al(OH)_4]^-$ hydroxo complex[27,219]. We have found that those substituents that favor aluminum binding (in terms of *logβ*), they also favor protonation[27,94,199]. The overall effect is a balance between the Al(III)-ligand complex stability and the competition with H^+. In this sense, EWGs, by lowering the affinity toward aluminum, they also favor deprotonation (by lowering the protonation constants of the ligand), and this latter factor is the dominant one at a pH in which aluminum competes with two protons for ligand binding. Conversely, when only one proton has to be removed, like in salicylic acids at weakly acidic or neutral pH, the nature of the dominant factor shifts to aluminum complex stability. Other factors such as stoichiometry of the complex can also contribute to the proton/aluminum ion competition toward a given ligand. Our results suggest that higher stoichiometries favor deprotonation as a leading factor in the overall performance of a given chelator.

3.4 Conclusions

In the present work, we have developed, validated and applied a *state-of-the-art* theoretical protocol suitable for the investigation of two families of bidentate Al(III) chelating agents (catechols and salicylic acids). Trends in binding affinities show very good agreement with respect to available experimental data. We have rationalized our results analyzing the nature of the Al-O bonds, finding that the covalent part of a mainly ionic Al-O interaction is the driving force in the fine tuning of the stability of these complexes. Such covalent character is modulated by the opposite effect of the substituents: methyl and methoxy groups increase this covalency, leading to higher affinities, whereas the nitro and trifluoromethy groups decrease the covalent component leading to lower binding affinities. We have also determined how the overall performance of a chelator depends critically on the metal/proton competition toward ligand binding. In summary, the present work establishes a reliable and transferable theoretical protocol aimed to test the behavior of metal organic chelators, which would help in the future deign and tuning of novel chelating agents of increased efficacy.

Design of new efficient chelators of aluminum based on Mimosine-containing peptides

Jon I. Mujika, Gabriele Dalla Torre, Joanna I. Lachowicz and Xabier Lopez.
Phys. Chem. Chem. Phys., **submitted**.

Design of new efficient chelators of aluminum based on Mimosine-containing peptides

4.1 Introduction

Aluminum is the most abundant metal (about 8.3% by mass) in the Earth's crust[220], found in more than 270 different minerals in the insoluble form of hydroxy-aluminosilicates. It remained inaccessible for living matter for billions of years, until the acid rains started the massive export of aluminum from the crust of the earth to surface waters, putting vegetables, animals and humans in contact with absorbable cationic aluminium species, probably for the first time in their history[221].

In the 1970s, aluminum was recognized as a neurotoxin and since then, numerous scientific reports have linked aluminum to neurological disorders and bone and brain pathologies[222]. A role of aluminium in human pathology has been clearly established in at least three diseases: dialysis dementia[223], osteomalacia[224] and microcytic anaemia without iron deficiency[57,225]. The principal symptoms of aluminium toxicity are: diminished intellectual function, forgetfulness, inability to concentrate; speech and language impairment; personality changes, altered mood, depression; dementia; visual and/or auditory hallucinations; osteomalacia with fracturing; motor disturbances; weakness, fatigue, mainly related to microcytic anaemia; epileptic seizures.

In the case of aluminum intoxication, Al(III) chelation is performed to reduce Al(III) organ levels (especially in bone) and reduce toxicity of Al(III). This may benefit patients with end-stage renal disease or with neurodegenerative disorders as well as patients suffering from neurobehavioral toxicity due to prolonged occupational Al(III) exposure[226]. In chronic hemodialysis patients chelation therapy is indicated at serum Al(III) concentration higher than 80 μg/L[227]. Previously, the only available chelator for treating Al(III) overloaded patients was deferoxamine (DFO) originally developed for decorporation of iron in transfusional iron overload in thalassemia and sickle cell anemia patients. The hydrophilic chelator DFO is poorly absorbed in the gastrointestinal tract and must be administered parenterally, either subcutaneously, intramuscularly, or intravenously. DFO is not an ideal chelating agent due to the high frequency of side effects, the need for parenteral administration restricting off-clinic self-administration, and high price. However, despite the advent of alternative chelators for aluminum chelation, DFO still has an important role in treatment of Al intoxication[228]. An extensive body of evidence from *in vitro* and experimental animal studies demonstrates the potential of hydroxypyridinone derivatives from both series to reduce Al(III)

toxicity and promote Al(III) decorporation. The most promising compound among the hydroxypyridinones for iron chelation after extensive animal experimentation, 1,2-dimethyl-3-hydroxy-4-pyridone (deferiprone, DFP, see scheme 4.1) went into clinical trial initially for iron decorporation and is licenced in USA and Europe for treatment of iron overload in thalassemia major. Even if less efficient in aluminum coordination respect to DFO, DFP is orally administrated, somewhat less toxic, and much cheaper than DFO[16]. Nevertheless, there is an urgent need for other, more efficient, less toxic and cheaper aluminum chelator.

Mimosine [β-[N-(3-hydroxy-4-oxypyridyl)]-α-aminopropionic acid] (see scheme 4.1) is a non-protein amino acid found in the members of Mimosoideae family. It has been found to have various biological activities such as antibacteria, anti-cancer, antiinflammation, anti-fibrosis, anti-influenza, anti-virus, herbicidal and insecticidal activities[229]. In the 90's Mimosine was studied as an inducer of G1/S phase arrest[230] and over the past years of active research, Mimosine evolved as promising agent for the treatment of cancer disease. Mimosine dipeptides and tetrapeptides were synthesised as neuraminidase[231], tyrosinase[14,15] and cyclooxigenase[232] inhibitors.

The presence of the carbonyl and alcohol groups in the side chain of Mimosine makes this residue an effective ligand for binding metal ions, and thus Mimosine can bind divalent and tetravalent transition metal ions[233-235]. Due to its structural similarity to DFP it is expected a high affinity towards Al(III) as well. Moreover, joining three Mimosine residues in the same peptide could enhance significantly aluminum complex stability, and obtain new class of chelating agents based on non-proteinogenic amino acids. However, to the best of our knowledge this activity of Mimosine containing peptides has not been investigated yet.
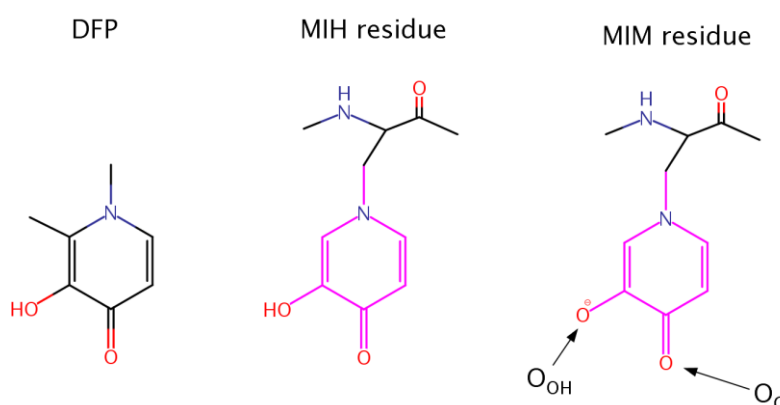
Scheme 4.1. Chemical structures of Deferiprone (DFP) and Mimosine residue in its neutral (MIH) and ionic (MIM) form. The labels of the two O atoms of Mimosine residue are also illustrated.

The present study aims to find the smallest Mimosine containing peptide that interacts tightly with Al(III), i.e., to find an efficient chelator of the cation. To do that, we employed state-of-the-art computational methods to characterize systematically the complexation of Al(III) to several peptides of different length that contain three Mimosine residues (shown in Fig. 4.1).

The geometric and energetic stabilities of all the Al(III)-peptide complexes were analyzed, paying special attention on the interactions between the cation and the peptide. All this information allows us to propose for the first time the shortest Mimosine-based peptide with the highest coordination stability toward Al(III) ions. This will certainly open the field to a new type of chelators, not only for aluminum, but for highly valent metals showing similar coordination features as Al(III).

4.2 Methodology

4.2.1 Systems set-up
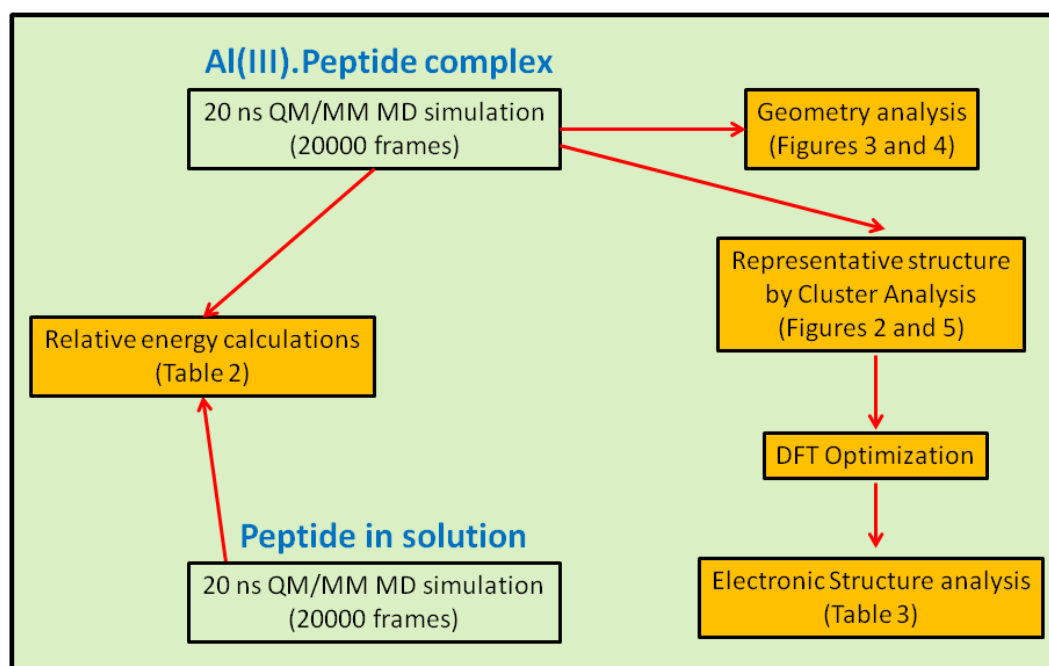
Scheme 4.2. Theoretical protocol used throughout this study (described in the Methodology section) for each of the structures shown in Fig. 4.1.

The complexation of Al(III) to eight Mimosine containing peptides of different length has been investigated following the protocol shown in scheme 4.2. All peptides contain three Mimosine residues (sequences presented in Fig. 4.1) and they differ in the two linkers connecting the Mimosine residues: the two longest peptides contain nine amino acids so that their two linkers are made of three

amino acids: in $Pept^9_{3G}$ the linker includes three glycine residues, whereas in $Pept^9_{GPG}$ a proline was inserted in the middle of the linkers. This is the only peptide containing a standard residue other than glycine, in order to check the effects that the insertion of a rigid amino acid such as proline may induce in the peptide's rigidity. Next, two eight residues-long peptides were built, what implies two different linkers: GG and GGG in $Pept^8_{2G-3G}$ and the reverse in $Pept^8_{3G-2G}$. Next, $Pept^7$ includes two symmetric linkers made of two glycine residue each. The six amino acid long peptides involve two asymmetric linkers, namely G and GG in $Pept^6_{G-2G}$ and the opposite in $Pept^6_{2G-G}$. Finally, $Pept^5$ is the shortest peptide, with just a glycine residue at each of the two linkers. In all peptides, the N- and C-terminals were neutralized by adding methyl groups.

The Al-$Pept^9_{3G}$ system was the first one to be built, for what the Fe(III)-N-derivatized 3-hydroxy-4-pyridiones complex[236] was used as initial template. Once the complex was set up and equilibrated by molecular dynamics simulation, its structure was used as template to build the initial structure for the complexes formed by $Pept^9_{GPG}$, $Pept^8_{2G-3G}$ and $Pept^8_{3G-2G}$. In a similar manner, previously equilibrated Al(III)-peptide structures were used to build the initial structures for the complexes of the remaining shorter peptides.

4.2.2 Molecular dynamics simulations

Each of the eight systems listed about was sampled by QM/MM molecular dynamics simulation using the Amber14 suite of programs[237]. The choice of running QM/MM MD simulations was based on two main reasons: a) lack of reliable MM parameters for the non-standard Mimosine amino acid, and b) description of the metal binding site by a quantum methods allows polarization, what it is expected to be relevant with a highly charged cation such as Al(III). The PM6 semiempirical method[238] was chosen to treat the Al(III) binding site, since it provides a good compromise between calculation speed and accuracy.

The LEaP program was used to build the topology of each system, for which Amber ff14SB all-atom force field parameters[239] were chosen for standard amino acids. The parameters for MIM needed to build the system (but not used during the QM/MM MD simulations) were obtained with Antechamber. Periodic boundary conditions were applied in all directions using an octahedron cell, with a minimal distance between the peptide and the wall of the cell set to 10 Å. The structures were solvated by a box of TIP3P-type water molecules[240].

First a MM minimization was carried out to relax the solvent, in which the Al(III)-Peptide complex was restrained. Then, in order to keep the initial rearrangement, a second minimization was performed restraining only the three Mimosine residues and Al(III). Next, the system was heated to 300 K by a 1ns-long equilibration defining a canonical thermodynamic ensemble (NVT), and using the Langevin

thermostat to couple the temperature of the system (collision frequency of 1.0 ps^{-1}). Again, the Al-Peptide solute was restrained. All this calculations were carried out at the MM level.

The QM part was treated with the PM6 semiempirical method and includes the side chains of the three unprotonated MIM residues (pink region depicted in scheme 4.1) and Al(III), so that the total charge of the QM part was always neutral. The Amber ff14SB force field was employed to describe the remaining part of the system.

Once the system was heated, the QM/MM MD simulations were carried out without applying any restraint and keeping the condition at the heating stage, that is, NVT ensemble and the Langevin thermostat to couple the temperature of the system (collision frequency of 1.0 ps^{-1}).
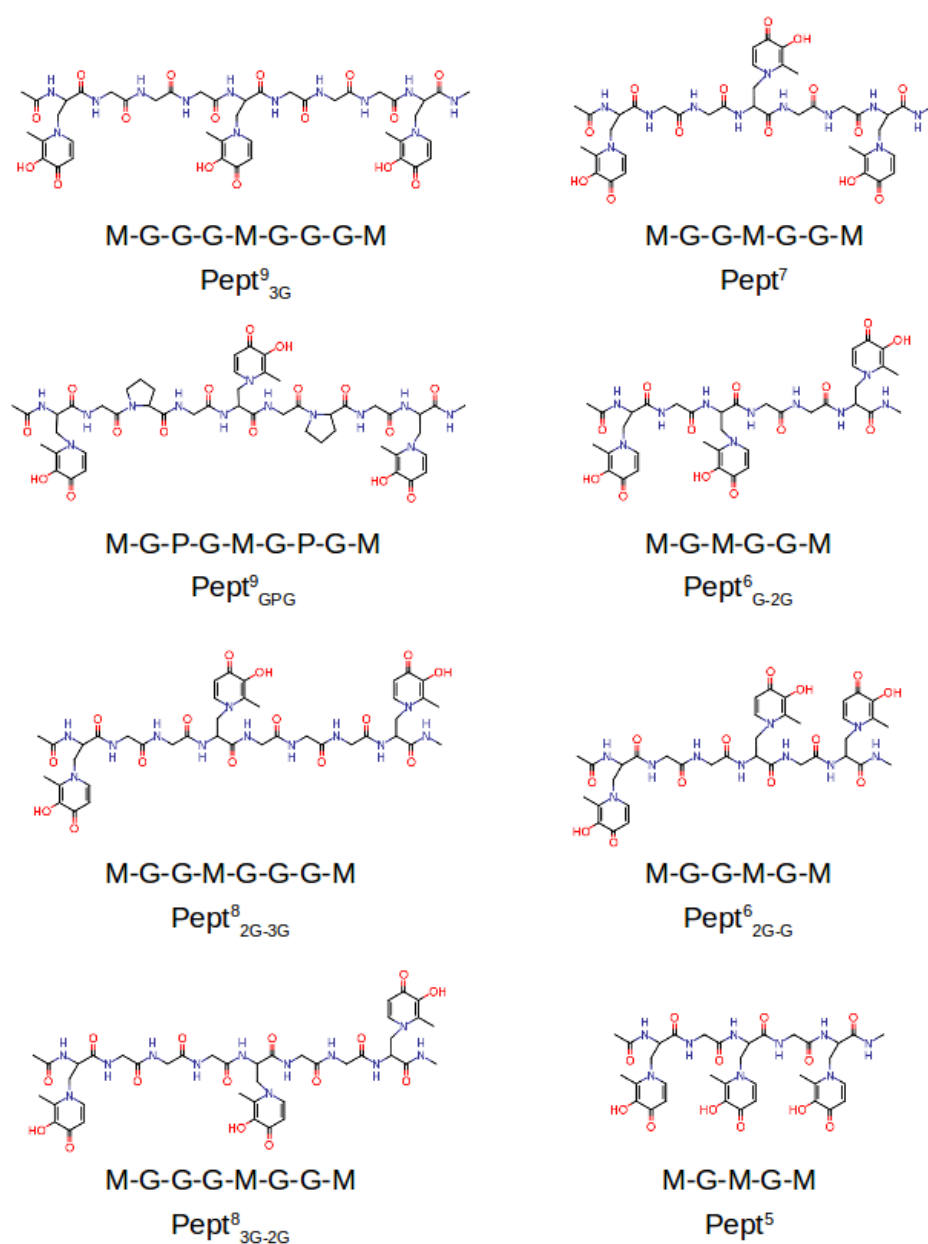
Fig. 4.1 Molecular structures of the eight Mimosine-containing peptides studied in this work.

All bonds involving hydrogens were constrained with the SHAKE algorithm[241], allowing for an integration time step of 2 fs. Long-range electrostatics were calculated using the smooth particle mesh Ewald (PME) method[242,243], and a cutoff of 8 Å was defined for all nonbonded interactions.

The first 1 ns of the QM/MM MD simulation were leave to equilibrate the system, whereas the remaining 20 ns of simulations were employed for the analysis. From each QM/MM MD simulation, representative structures were extracted by cluster analysis using the cpptraj utility in Amber14[244].

4.2.3 Relative Binding Energies

In order to estimate the absolute binding energy of Al(III) to a given peptide, we should calculate the binding energy of the next reaction:

$$[\text{Al}(\text{H}_2\text{O})_6]^{3+} + \text{Pept}_x(\text{MIH})_3 \rightleftarrows [\text{Al}.\text{Pept}_x(\text{MIM})] + 6\text{H}_2\text{O} + 3\text{H}^+ \tag{4.1}$$
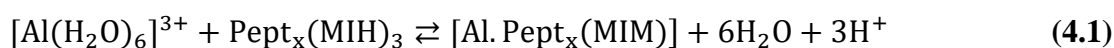
where Pept_x refers to any of the peptides considered herein and MIH and MIM refer to the protonated and deprotonated Mimosine residue, respectively (see scheme 4.1). However, this procedure includes many technical difficulties (how to deal with protons, difficulties defining the QM part, etc...). Alternatively, from a technical point of view the next reaction is easier to deal with:

$$[\text{Al}.\text{Pept}_x(\text{MIM})_3] + \text{Pept}_y(\text{MIH})_3 \rightleftarrows [\text{Al}.\text{Pept}_y(\text{MIM})_3] + \text{Pept}_x(\text{MIH})_3 \tag{4.2}$$

where Pept_x and Pept_y refer to peptides of different sequence. This reaction therefore will estimate the difference in energy between the interaction of Al(III) with Pept_x and Pept_y. In other words, it will give us the relative stability between the two complexes. Based on reaction 4.2, the relative binding enthalpies between the complexes formed by Pept_x and Pept_y with Al(III) are calculated as:

$$\Delta\Delta H_{bind}^{x-y} = (E)_{[\text{Al}.\text{Pept}_y(\text{MIM})_3]} + (E)_{\text{Pept}_x(\text{MIH})_3} - (E)_{[\text{Al}.\text{Pept}_x(\text{MIM})_3]} \\ - (E)_{\text{Pept}_y(\text{MIH})_3} \tag{4.3}$$

where (E) stands for the average potential energy calculated at the corresponding QM/MM MD simulation. A positive value of $\Delta\Delta H_{bind}^{x-y}$ will mean that Al(III) has a larger affinity towards Pept_x, whereas a negative value will suggest a larger affinity towards Pept_y. The $\text{Pept}^9{}_{3G}$ system was taken as reference.

Nevertheless, the computation of the $\Delta\Delta H_{bind}^{x-y}$ values is not straightforward since the number of explicit water molecules differs at each MD simulation (and therefore with unbalance number of

interactions), making unrealistic a direct comparison between them. In order to overcome this problem, the potential energies were determined replacing the explicit water molecules by a Generalized Born implicit solvent[245] as implemented in Amber14. The structures saved every 5 ps of each simulation were used to calculate the (*E*) average potential energies with implicit solvent.

The estimation of the relative binding energies (Equation 4.3) requires the energies of the apoform of the peptides as well. Thus, 20ns long QM/MM MD simulations were also performed for the eight apoform of the peptides using an implicit solvent. Note that unlike when the Mimosine residues interact with Al(III), we assume the Mimosine residues protonated in solution. This assumption relies on the pK$_a$ values estimated by cyclic voltammetry[246] for the two oxygen atoms of deferiprone: 3.5 and 10.2. Based on these values, it is clear that the two oxygen atoms should be as a keto and hydroxide group, respectively, and therefore, the later protonated. However, when they interact with Al(III), it is expected a significant drop of their pK$_a$ values, as computed for some oxygen-containing standard amino acids interacting with Al(III)[247]. Consequently, it is reasonable to assume that the hydroxide group is deprotonated when complexed to Al(III), but protonated in the apoform.

4.2.4 Electron delocalization indices

Electron delocalization indices (D.I.) were calculated on the most representative structures extracted by cluster analysis from the QM/MM MD simulations of all Al(III)-peptide complexes. These indices are a measure of the covariance between the population of two atoms A and B and, consequently, a measure of the number of electrons simultaneously fluctuating between these atoms:

$$\delta(A,B) = \int_A \int_B d\,1d2\rho_{xc}(1,2) = cov(N_A, N_B) \tag{4.4}$$

Where $\rho_{xc}(1,2)$ is the exchange-correlation density and it can be taken as the number of electron pairs shared between atoms A and B, i. e., the bond order[248,249]. The AIMAll v17.11.14 program[250] was used to carry out the QTAIM analysis[208] (what includes the characterization of D.I.) on the previously optimized structures. Wavefunctions for QTAIM analysis were obtained at the B3LYP/6-311++g(3df,2p) level of theory using the IEFPCM solvation model.

4.3 Results

The sequences of the eight peptides studied herein are shown in Fig. 4.1. The name of each peptide is composed by a superscript indicating the length of the peptide, and a subscript referring to the

linker sequences (one for symmetric peptides, and two for the asymmetric ones). For instance, the $Pept^9_{GPG}$ system is nine residues long and contains three Mimosine residues, which are spaced with GPG sequence linker. The two oxygen atoms of Mimosine residue are denoted as O_C and O_{OH}, and correspond to the carbonyl and hydroxyl oxygen atoms, respectively (scheme 4.1). Along the body text, the atom names include a subscript to specify the atom type and a superscript to refer to the residue number.

The RMSD computed on the QM/MM molecular dynamic simulations for the eight Al(III)-peptide complexes (shown in Appendix B) demonstrate that all systems are equilibrated during the 20-ns run of production. Representative snapshots of each simulation are shown in Fig. 4.2. First, the structural data of each complex is analysed, with special attention on the metal coordination shell. Then, the electronic structures of the Al(III) first coordination shell are described, and next the binding energy values of each Al(III).peptide complex presented. Finally, the structures of the Al.Pept complexes are compared with $Al.DFP_3$.

	MIM^A		MIM^B		MIM^C	
	$Al-O_C$	$Al-O_{OH}$	$Al-O_C$	$Al-O_{OH}$	$Al-O_C$	$Al-O_{OH}$
$Pept^9_{3G}$	1.961 (0.075)	1.922 (0.066)	1.969 (0.079)	1.935 (0.068)	1.957 (0.075)	1.931 (0.068)
$Pept^9_{GPG}$	1.969 (0.086)	1.921 (0.065)	1.982 (0.140)	1.936 (0.069)	1.950 (0.087)	1.931 (0.060)
$Pept^8_{2G-3G}$	1.970 (0.077)	1.923 (0.066)	1.972 (0.093)	1.939 (0.069)	1.955 (0.079)	1.931 (0.070)
$Pept^8_{3G-2G}$	1.961 (0.099)	1.931 (0.069)	1.967 (0.078)	1.934 (0.068)	1.962 (0.073)	1.927 (0.067)
$Pept^7$	1.934 (0.070)	1.934 (0.070)	2.514 (0.944)	1.917 (0.085)	1.938 (0.072)	1.932 (0.070)
$Pept^6_{G-2G}$	1.932 (0.069)	1.891 (0.059)	4.347 (0.197)	1.842 (0.057)	1.892 (0.062)	1.926 (0.066)
$Pept^6_{2G-G}$	1.903 (0.065)	1.913 (0.064)	4.252 (0.235)	1.836 (0.057)	1.935 (0.070)	1.896 (0.062)
$Pept^5$	1.917 (0.068)	1.911 (0.065)	4.112 (0.634)	1.839 (0.063)	2.090 (0.586)	1.889 (0.062)

Table 4.1. Average and standard deviation (in Å) of the six distances between the O_C and O_{OH} atoms of the three Mimosine residues and Al(III) computed along the QM/MM MD simulation trajectories of the Al-Pept

complexes. Since the indexes of the three Mimosine residues differ on the systems, they are referred to as A, B and C for the first, central and last Mimosine in the corresponding sequence shown in Fig. 4.1.

4.3.1 Structural stability of the first Al(III) coordination shell

The optimum coordination shell of Al(III) is the one presented in Al-DFP3 (see Appendix B)[251], with the cation octahedral and the three MIM residue bidentated through the O_C and O_{OH} atoms. In order to analyse the Mimosine layout, some geometrical parameters were analysed: i) distances between Al(III) and the six O atoms of the three MIM residues (Table 4.1 and Fig. 4.3), ii) all possible O-Al-O angles formed by the six oxygen atoms (Fig. 4.4 and Appendix B). The complexes are presented from the longest to the shortest peptides.

$Pept^9{}_{3G}$ $\qquad$ $Pept^9{}_{GPG}$ $\qquad$ $Pept^8{}_{2G-3G}$ $\qquad$ $Pept^8{}_{3G-2G}$

$Pept^7$ $\qquad$ $Pept^6{}_{G-2G}$ $\qquad$ $Pept^6{}_{2G-G}$ $\qquad$ $Pept^5$
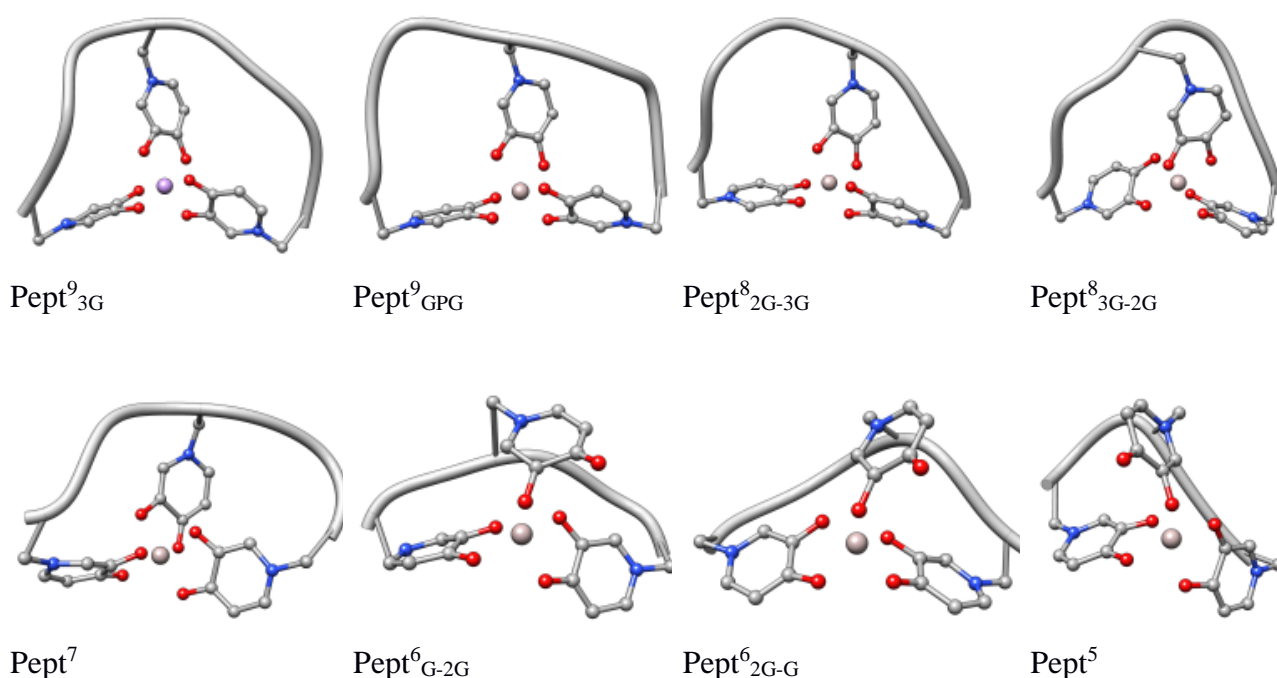
Fig. 4.2. Representative snapshot of the MD simulations of the eight Al(III)-peptide complexes determined by cluster analysis.

$Pept^9{}_{3G}$ and $Pept^9{}_{GPG}$: the two longest peptides form octahedral complexes with Al(III), as the values of the six Al-O Mim distances, which are very stable throughout the entire simulations (Table 4.1). Interestingly, although both oxygen atoms are deprotonated, the Al-Oxygen distances are not equivalent and O_C presents longest distances than O_{OH}: the average values of the Al-O_C and Al-O_{OH} distances are ca. 1.97 Å and 1.93 Å, respectively, with both $Pept^9$. Moreover, overall, the average distances are very similar with both $Pept^9$ peptides, except the Al-$O_C{}^5$ distance, which is about 0.02 Å longer for $Pept^9{}_{GPG}$ (1.982 Å).
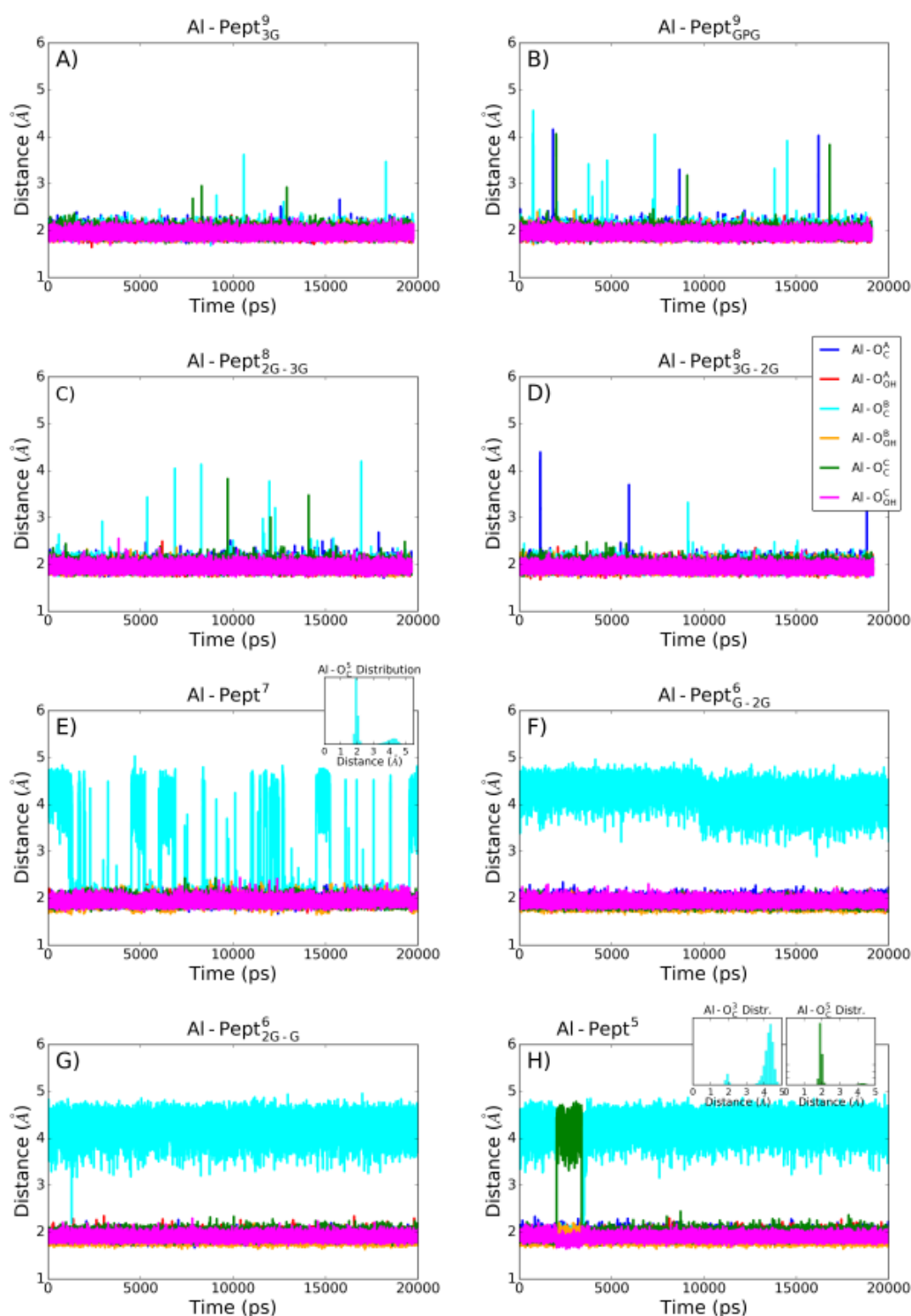
Fig. 4.3. 3 Evolution of the distances between Al(III) and the two O_C and O_{OH} atoms of the Mimosine residues during the QM/MM MD simulations. From left to right, upper line: A) $Pept^9_{3G}$, B) $Pept^9_{GPG}$, C) $Pept^8_{2G-3G}$, D) $Pept^8_{3G-2G}$; Bottom line: E) $Pept^7$, F) $Pept^6_{G-2G}$, G) $Pept^6_{2G-G}$, H) $Pept^5$. The colour scheme is shown in the D) panel. Since the indexes of the three Mimosine residues differ on the systems, they are referred to as A, B and C for the first, central and last Mimosine in the corresponding sequence shown in Fig.4.1.

The O^{Mim}-Al-O^{Mim} angles computed for the two Al-Pept[9] complexes confirm that Al complexes adopt a nearly octahedral arrangement. We can observe in Fig. 4.4 that O^{Mim}-Al-O^{Mim} angles are divided in two sets: a prevalent one centered on 90 degrees and a second one centered on 160 degrees, which correspond to equatorial and axial angles, respectively, in an octahedral arrangement. A deeper analysis of the angles (Appendix B) shows that during the simulation of the Al.Pept[9]$_{3G}$ complex, 11 out of the 15 angles are in the 86-92 degree range (the range is slightly wider for Al-Pept[9]$_{GPG}$: 82-94 degrees), very close to the ideal value of 90 degrees for equatorial angles. O_{OH}^1-Al-O_{OH}^9 is the only angle out of these ranges, with average values of 101 degrees on both complexes. On the other hand,

Pept[8]$_{2G-3G}$ and Pept[8]$_{3G-2G}$: the Al-O distances calculated for the complexes of these two peptides are similar to those of Pept[9] peptides, i. e., ca. 1.97 Å for the three Al-O_C distances and 1.93 Å for the Al-O_{OH} distances. Also the average values of the angles computed for the Al-Pept[8]$_{2G-3G}$ complex are very similar to the ones calculated for Pept[9] peptides: a maximum deviations of 7 degrees is observed with respect to the angles computed on the Al.Pept[9]$_{3G}$ complex. The similarity is maintained with the three axial angles. However, some differences are found in the Al-Pept[8]$_{3G-2G}$ complex, in which only seven angles lie between 86-95 degrees, and the remaining equatorial angles are in the 103-115 range, with larger standard deviations. Moreover, the values of the three axial angles are smaller, with larger standard deviation. The origin of these differences does not lie in the change of metal coordination mode, but rather in spatial rearrangement of the ligands, in the way that some equatorial angles become axial and the contrary. The metal complex structure remains octahedral and the distribution of the angles (Fig. 4.4) is invariable respect to Pept[9] peptides.

Pept[7]: the octahedral complexes of peptide Pept[7] are less stable compare to longer peptides and only five out of six oxygen atoms (of the three MIM residues) are tightly bound to Al(III). Al-O_{OH}^4 presents the shortest distance (1.917 Å), while the distances between Al(III) and the four oxygen atoms of MIM[1] and MIM[7] are 1.93 Å. Unlike with the two Pept[9] peptides, no clear difference between O_C and O_{OH} is observed. The remaining distance, Al-O_C^4, shows a significantly longer average value (2.514 Å), with a larger deviation (0.944 Å). As it can be observed in Fig. 4.3, the values of Al-O_C^4 distance fluctuates between 2 Å and 4.5 Å. As shown in the histogram of the distance (small panel in Fig. 4.3E), two clear peaks are centered on 2 Å and 4.5 Å, the former being predominant, without any significant intermediate value. Hence, MIM[4] does not bind Al(III) tightly and fluctuates between bidentate and monodentate (through O_{OH} atom) coordination modes. These two conformations are superimposed in Fig. 4.5C.

The distribution of the O-Al-O angles reflects such multiple conformations. Even if two clear peaks are located at 90 and 160 degrees, the angles population between these two peaks has increased, and it is not any more nearly zero (as in the simulations with larger peptides). Moreover, the peak of the axial angles has shifted to smaller values. At this point, the simulation suggests that Pept[7] presents less stable octahedral arrangement, even if this coordination mode is still the most prevalent one (see below).

Pept[6]G-2G, Pept[6]2G-G and Pept[5]: the three shortest peptides exhibit a similar pattern during the MD simulation: five out of six Mimosine oxygen atoms are tightly bound to Al(III), with average lengths of 1.8-1.9 Å. By contrast, the O_C atom of the central Mimosine residue (MIM[4] in the two Pept[6] peptides and MIM[3] in Pept[5]) is clearly out of the metal coordination shell, with an average length of ca. 4.2 Å. Even that $O_C{}^3$ atom interacts with Al(III) for a short period of time during the Al-Pept[5] simulation, during this period of simulation $O_C{}^5$ atom leaves the Al(III) first coordination shell. Therefore, Al(III) appears always pentacoordinated with these three peptide: the two terminal Mimosine residues coordinate metal ion bidentatedly, while the central one can bind Al(III) only monodentatedly.

Interestingly, in longer peptides Al-Oc distance of a Mimosine residue is around 0.3 Å longer than with its O_{OH} counterpairs. In the complexes of two Pept[6] asymmetric peptides this trend is maintained only by one of the two Mimosine residues bidentatedly bound to Al(III), whereas the Al-O_C distance is slightly shorter in the other Mimosine (Mim[3] in Pept[6]G-2G and Mim[4] in Pept[6]2G-G). This fact may be due to the shortness of the peptide backbone, too short to allow the Mimosine side chain positioning in a more suitable orientation and optimize their interactions with Al(III) (see Figure 5D).

The angles distribution computed on the MD simulations of the shortest three peptides are very similar and confirm that the octahedral arrangement of Al(III) is not possible due to the shortness of the peptides. The peak ascribed to the axial angles has lowered, and even if the peak located at around 90 degrees is still predominant, the angle distribution is significantly broader than with longer peptides.

4.3.2 Al(III) coordination mode

The analysis of the geometries has shown that the peptide length clearly influences the interaction of the peptide with Al(III). In order to quantify this trend, we calculated the coordination number (C.N.) of Al(III) along each MD simulation, which can be either 5 or 6. In order to do that, two alternative geometrical criteria were defined to consider a frame from a trajectory octahedral: i) six Al-O distances shorter than 2.5 Å, and ii) if three O-Al-O angles are larger than 150 degrees.
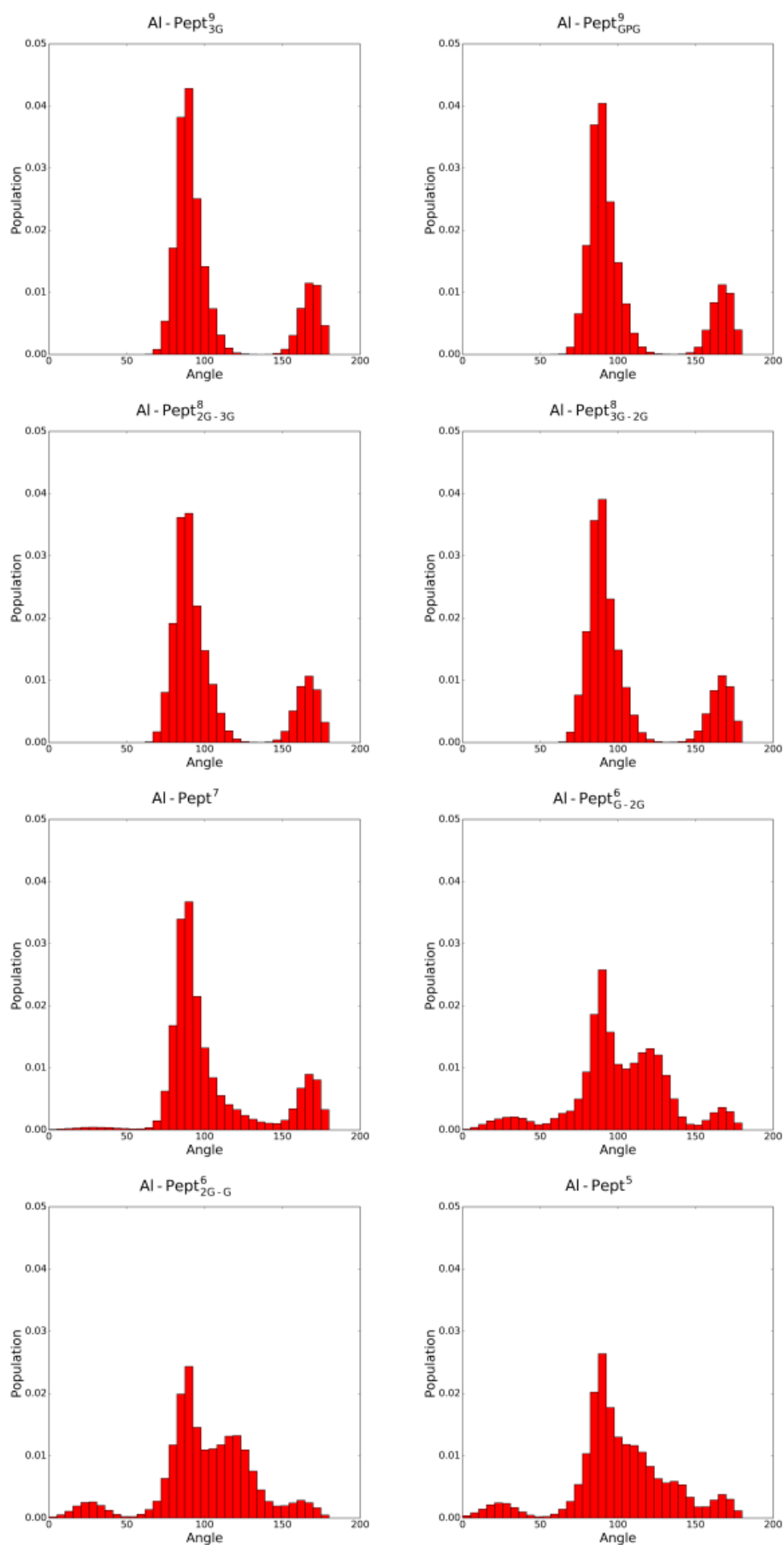
Fig. 4.4. Distribution of all O^{Mim}-Al-O^{Mim} angles computed along the QM/MM MD simulations trajectories of the eight Al.Pept complexes (sequences shown in Fig. 4.1).

The results (presented in Table 4.2) show the same trend for both criteria, although the percentage of C.N.= 6 are slightly lower with the angles criteria. During the corresponding QM/MM MD simulations, Pept[9] and Pept[8] bind Al(III) in the octahedral complex. According to the distance criterion, during almost all their simulations the C.N. is six.

The percentage is slightly lower according to the angle criterion, ca. 97% for the two Pept[9] peptides and 94% for the two Pept[8] peptides. The three shortest peptides, with five and six residues, do not form octahedral complexes with the Al(III) ion (the percentage of frames with C.N.= 6 is almost zero).

By contrast, the Al-Pept[7] complex is the borderline system, in which both C.N.= 5 and C.N.= 6 are significantly sampled. However, C.N.= 6 prevails during the MD simulation, with 72-75% of the structures with hexa coordination mode, while in the remaining 25-28% of snapshots the metal ion is pentacoordinated.

	% Oct (dist)	% Oct (angle)	$\Delta\Delta H_{bind}^{x-y}$
Pept[9]$_{3G}$	100.0	98.0	0.0
Pept[9]$_{GPG}$	99.6	96.5	1.8
Pept[8]$_{2G-3G}$	99.8	94.2	2.5
Pept[8]$_{3G-2G}$	99.9	93.1	1.7
Pept[7]	74.9	72.1	11.4	9.4 (C.N.=6) 17.3 (C.N.=5)
Pept[6]$_{G-2G}$	0.0	0.0	12.9
Pept[6]$_{2G-G}$	0.0	0.1	13.9
Pept[5]	0.1	2.2	20.0

Table 4.2. On the left section of the table, percentages of snapshots extracted from the QM/MM MD simulations of the Al-Pept complexes with an octahedral Al(III), determined based on two criteria: a) Al-O distances shorter than 2.5 Å, and b) presence of three axial angles (>150 degrees). On the right section of the table, relative binding enthalpies ($\Delta\Delta H_{bind}^{x-y}$, in kcal/mol) between the Mim-containing peptides of different sequence, taking the Al-Pept[9]$_{3G}$ complex as reference. In the case of Pept7, the relative energies between the two coordination modes observed during its MD simulation (Al(III) octahedral or pentacoordinated) are also shown.

4.3.3 Electronic structure of Al(III) coordination shell

Delocalization indices (D.I.) are a measure of the electron sharing between two atoms (see Methodology section). Although Al-O bonds are mainly electrostatic in nature, there are also important dative interactions from the lone pair of the oxygen atoms to the formally vacant 3s and 3p

orbitals of Al(III)[21]. Therefore, the higher the D.I. value, the stronger the covalent character of the bond between the two atoms. The D.I. were computed at the bonds formed by Al(III) and the six oxygen atoms of the three Mimosine residues in all Al-Pept complexes (Table 4.3).

Starting from the Al.Pept[9] complex, it can be observed that the D.I. values are ca 0.02 a.u. higher at Al-O_{OH} (ca 0.17 a.u.) than at Al-O_C (ca 0.15 a.u.).This is in agreement with the shorter bond distances of the formers (Table 4.1): the shorter the distance, the higher the D.I value due to the higher electron density. However, a closer analysis of the values indicates that the values are about 0.005 a.u. smaller at the central Mimosine residues. Even if the difference is very small, it suggests that the interaction with the central Mimosine is the weakest one among the three Mimosine residues (note this residue weakens its interaction with Al(III) with the shortest peptides). The total electron delocalization computed for the six Al-O bonds is 0.9590 a.u. These trends and values are maintained by Pept[9] and Pept[8] peptides, in which Al(III) is hexacoordinated, and in all of them the accumulated D.I. value is maintained in a narrow range between 0.9579-0.9590 a.u. We also add in Table 4.3, the values for the Al-DFP$_3$ complex, which demonstrates that the Al-Pept[9] complexes show a very similar binding patterns from the electronic point of view with respect to the aluminum-deferiprone complex. In this sense, the D.I. for Al-O_{OH} bonds are larger than for Al-O_C and the total D.I. is 0.9580. That is, the four Al-Pept[9] and Al-Pept[8] complexes have adopted the optimum interaction with respect to the three mimosine residues, and in this sense, an efficient chelation of the aluminum ion is expected for these polypeptides.

For the Al-Pept[7] complex two coordination modes were observed during the MD simulation of this complex and therefore two distinct structures were selected, with Al(III) hexa- or pentacoordinated. For Al(III) hexacoordinated structure, the D.I. values of Mim[4] and Mim[7] are very similar to the ones observed for the Pept[8] and Pept[9] peptides (again, the D.I. values are slightly smaller in the central Mimosine), while the two D.I. values computed on the first Mimosine residue are now almost the same (0.16 a.u.), although the accumulated D.I. maintains in the range of 0.958 a.u.

A different scenario emerges when Al(III) is pentacoordinated by Pept[7]. The D.I. value of Al-O_C^4 is almost vanished (0.0005 a.u.), since the O_C^4 atom is not present in the first coordination shell of the cation. Interestingly, the loss of O_C^4 atom interaction has strengthened the other five Al-O interactions, when comparing with the Al-Pept[7]$_{hexa}$ structure. For instance, the D.I. value of the Al(III)-O_{OH}^4 bond is increased up to 0.2228 a.u, 0.06 a.u. higher than the same bond in the hexacoordinated complex. The indices of the other Al-O bonds are also incremented, namely 0.04 a. u. at Al-O_{OH}^1, 0.03 a.u. at Al-O_C^7, ca 0.1 at Al-O_C^1 and 0.1 a.u. at Al-O_{OH}^7. As a consequence, the accumulated D.I. is equal to 0.9769 a.u., 0.02 a.u. higher than in its counterpair with a hexacoordinated Al(III). This pattern is maintained by the three shortest peptides, in which Al(III) is

pentacoordinated: the loss of one Al-O interaction has enlarged the indices of the other Al-O bond, and the accumulated D. I. value is ca. 0.98 in all of them.

In summary, the computed delocalization indices show that the reduction in the Al(III) coordination mode (from six to five) leads to an increment on the total dative interactions between Al(III) and the ligands. Nevertheless, note that this increment corresponds to the covalent part of the Al(III)-O bonds, and as we show in the next section this slightly enhanced covalent interactions between aluminum and mimosine can not compensate the loss of one Al-O electrostatic interaction in the first coordination shell when shifting from coordination number six to five.

Complex	L.. I. Al	D. I. Al-O_C	Al-O_{OH}	Al-O_C	Al-O_{OH}	Al-O_C	Al-O_{OH}	Total
Pept^9$_{3G}$	9.9493	0.1520	0.1722	0.1472	0.1641	0.1546	0.1689	0.9590
Pept^9$_{GPG}$	9.9494	0.1516	0.1720	0.1462	0.1632	0.1550	0.1704	0.9584
Pept^8$_{2G-3G}$	9.9498	0.1513	0.1694	0.1481	0.1627	0.1550	0.1714	0.9579
Pept^8$_{3G-2G}$	9.9496	0.1493	0.1665	0.1486	0.1648	0.1544	0.1749	0.9586
Pept^7 (hexa)	9.9498	0.1626	0.1659	0.1418	0.1628	0.1550	0.1700	0.9581
Pept^7 (penta)	9.9459	0.1744	0.2036	0.0005	0.2228	0.1875	0.1881	0.9769
Pept^6$_{G-2G}$	9.9475	0.1714	0.1999	0.0006	0.2290	0.1989	0.1798	0.9796
Pept^6$_{2G-G}$	9.9466	0.1924	0.1876	0.0005	0.2220	0.1734	0.2029	0.9789
Pept^5	9.9474	0.1973	0.1823	0.0006	0.2283	0.1666	0.2011	0.9761
Al-DFP$_3$		0.1540	0.1657	0.1522	0.1665	0.1531	0.1665	0.9580

Table 4.3. Electron localization index (L.I.) for the aluminum atom and electron delocalization indices (D. I.) for the aluminum-Mimosine oxygen bonds (a. u.). All structures were optimized in solution and refined at the B3LYP-D3(BJ)/6-311++G(3df,2p) - IEFPCMlevel of theory (see Methodology).

4.3.4 Relative stability of the Al-Pept complexes

As pointed out in the Methodology section, the Pept^9$_{3G}$ peptide was taken as reference to estimate the relative binding energies ($\Delta\Delta H_{bind}^{x-y}$) of the eight peptides, which were computed from the QM/MM MD simulations of the apoform and holoforms of free peptides. The results are presented in Table 4.2.

The $\Delta\Delta H_{bind}^{x-y}$ values indicate that there is a direct relationship between the length of the peptide, the stability of their Al(III)-Peptide complexes, and the coordination mode of Al(III): the complexes formed by the four longest peptides show similar energies and in all of them Al(III) is octahedral.

The Al-Pept$^9_{3G}$ complex is the most stable one, followed by Pept$^8_{3G-2G}$ ($\Delta\Delta H^{x-y}_{bind}$ = +1.7 kcal/mol), Pept$^9_{GPG}$ ($\Delta\Delta H^{x-y}_{bind}$ = +1.8 kcal/mol) and Pept$^8_{2G-3G}$ ($\Delta\Delta H^{x-y}_{bind}$ = +2.5 kcal/mol).

The remaining four complexes are significantly less stable. Among them, Al-Pept^7 is the most stable one, with $\Delta\Delta H^{x-y}_{bind}$ = +11.4 kcal/mol. It must be pointed out that this is the relative energy computed with consideration of all snapshots extracted from the MD simulation. As described above, in the Al-Pept^7 complex Al(III) can be either hexacoordinated (ca 72% of the structures) or pentacoordinated (ca 28%). When the relative energies are analysed separately, for each of the coordination modes, the $\Delta\Delta H^{x-y}_{bind}$ value of hexacoordinated structures reduces to +9.4 kcal/mol, whereas the $\Delta\Delta H^{x-y}_{bind}$ value of Al(III) pentacoordinated complex increases to +17.3 kcal/mol.

A) Pept$^9_{3G}$ (purple) vs Pept$^9_{GPG}$ (green)

B) Pept$^9_{3G}$ (purple) vs Pept$^7_{hexa}$ (white)

C) Pept$^7_{hexa}$ (white) vs Pept$^7_{penta}$ (orange)

D) Pept$^7_{hexa}$ (white) vs Pept$^6_{G-2G}$ (green)
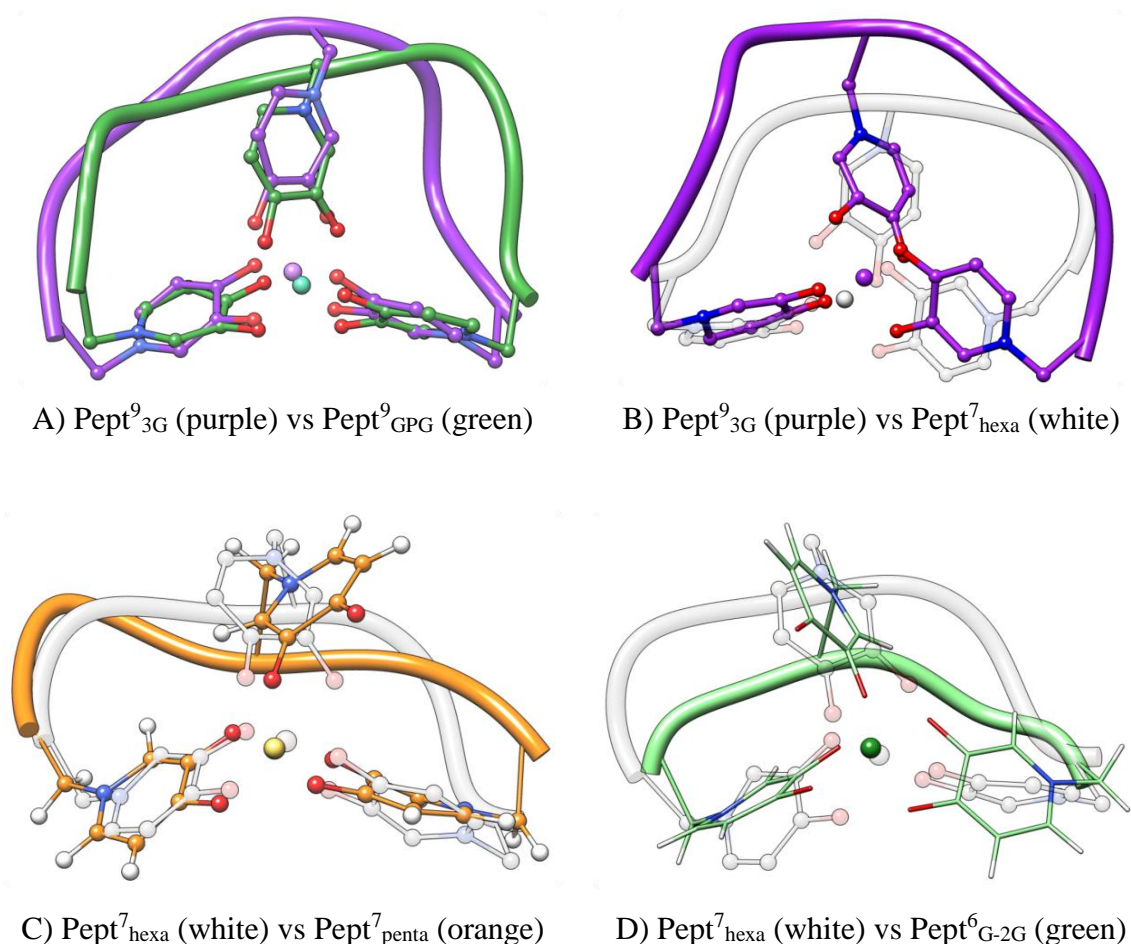
Fig. 4.5. Superposition between representative structures of QM/MM MD simulations of Al(III)-peptide complexes determined by cluster analysis.

The complexes formed by the two Pept[6] peptides present similar energies, with $\Delta\Delta H_{bind}^{x-y}$ values of +12.9 (Al-Pept[6]$_{G-2G}$) and +13.9 (Al-Pept[6]$_{2G-G}$) kcal/mol. The Al-Pept[5] is the less stable complex, with a $\Delta\Delta H_{bind}^{x-y}$ value of 20.0 kcal/mol.

4.3.5 Comparison with defriprone

The three pyrodine rings present in the Al-DFP$_3$ complex have no restraint to adopt an optimum orientation and maximize their interactions with Al(III). Consequently, the Al-DFP$_3$ complex is a good reference of the best interaction with aluminum that can be expected with the combination of three pyrodine rings. The comparison of the features of the Al-O bonds in Al-DFP$_3$ with those in the eight Al(III)-Peptide complexes can shed light on whether the geometrical constraints of the peptide backbone exerts a restraint to adopt the optimum coordination to maximize aluminum-pyrodine rings interactions. With this aim, we compare three different structures (shown in Appendix B): i) experimental structure of the Al-DFP$_3$ complex crystallized in water,[35] ii) the Al-DFP$_3$ complex optimized by a DFT high level quantum method, and iii) a DFT-optimized representative structure of the Al-Pep[9]$_{3G}$ complex. The distances and angles computed on these structures are shown in Appendix B.

Regarding the Al-DFP$_3$ complex, the six Al-O distances computed on the DFT optimized structures are systematically 0.02 Å longer than in the X-ray structure, and in both of them the Al-O$_C$ distances are 0.03 Å longer than the Al-O$_{OH}$ bonds. The computed angles are also very similar, with differences less than 1 degree between the experimental and theoretical Al-DFP$_3$ structures. On the other hand, the distances computed on the Al-DFP$_3$ and Al-Pept[9]$_{3G}$ structures optimized with DFT, are in general equivalent, with differences of ca 0.01 Å, except the Al-O$_C^5$ distance, which is 0.05 Å longer at the Al-Pept[9]$_{3G}$ complex. Nevertheless, the average Al-O distance and angle values computed along the QM/MM MD simulation of the Al.Pept[9]$_{3G}$ complex are in very good agreement with the Al-DFP$_3$ DFT-based structure, what may reinforce the importance of sampling different conformations of the peptide, with many possible conformations. This issue is not so problematic with the Al-DFP$_3$ complex due to the fewer number of degrees of freedom. Moreover, the delocalization indices computed on the Al-DFP$_3$ complex are also very similar to the ones computed on the complexes formed by the four longest peptides. All in all, all these evidences support the fact that the interactions between Al(III) and the four longest Mimosine-containing peptides are analogous to the interactions between Al(III) and three DFP molecules.

In order assess whether the Mimosine-containing peptides can chelate Al(III) as efficiently as DFP, we should consider not only their interactions with the cation, but also entropic effects, an issue

difficult to quantify. On one hand, it must be taken into account that the formation of the Al-DFP$_3$ complex may involve a larger entropic penalty due to the complexation of three molecules in three reaction steps (see chelate effect), while in the Mimosine-containing peptide the three chelating units belong to the same molecule. However, on the other hand, the formation of the Al-Peptide complex depends not only on the complex but also on the stability of the free peptide in solution (see Equation 4.1). The stability of the apoforms of the Mimosine-containing peptides is difficult to quantify accurately, because of the hugh amount of degrees of freedom that require an accurate and reliable sampling technique. However, we think that it is reasonable to assume that the formation of hydrogen bonds may contribute to their stability, and, therefore, the larger the number of hydrogen bonds formed by a free peptide in solution, the higher its stability (and the higher the energetic penalty required to deform the ligand in a conformation suitable to bind aluminum).. The list of all individual backbone hydrogen bond interactions during the QM/MM MD simulations of the peptides in solution and their lifetimes are shown in Appendix B. The data collected reveals the total number of hydrogen bonds is low, not surprising for such small peptides, although a clear trend is observed: the longest peptides form more intramolecular hydrogen bond interactions than the shorter ones. Among them, the number of interactions is larger for Pept$^9_{GPG}$ peptide due to the presence of the proline residues. In this case, the summation of lifetime of all hydrogen bonds identified is 23% of the QM/MM MD simulation (see Appendix B), whereas the summation reduces to 10-15% during the simulation of the complexes formed by Pep$^9_{3G}$ and the two Pept^8 peptides. The accumulated hydrogen bond lifetime reduces to ca. 5% on the complexes formed by the four shortest peptides. On the other hand, in none of the Al(III)-Peptide complexes intramolecular hydrogen bond interactions were detected. Thus, based on this data we can conclude that the number of hydrogen bonds is very small and therefore a small entropic penalty needs to be paid for the conformational change between the apoform and the metal-bound peptide.

4.4 Conclusions

In the present study we explore the suitability of a new family of high-valent metal chelators based on Mimosine-containing polypeptides that can be efficient chelator of Al(III). We analyze the structural and energetic stability of the complexes formed by Al(III) with several Mimosine-containing peptides of different length and sequence, going from the shortest polypeptide of five amino acids to the largest ones with nine residues.

Results reveal that with the longest four peptides, made of 9 and 8 residues, Al(III) shows no difficulties to interact in a hexadentate fashion with Mimosine sidechains. A comparative analysis of

the geometrical and electronic features characterized for these complexes reveals Al-O interactions very similar to the ones find in Al-DFP$_3$. The geometrical analysis indicates that the ligands of the cation are placced in a near-optimum octahedral arrangement, very similar to the disposition adopted by the aromatic rings in the Al-DFP$_3$ complex. On the other hand, the shortest three peptides, with only five or six residues, are too short to place the side chains of the three Mimosine residues in the proper arrangement to form six stable interactions with the cation. Consequently, the central Mimosine interacts in a mnodentate fashion with Al(III) so that only five Mimosine oxygen atoms interact with the ion. Finally, the Pept^7 peptide is the borderline case, since during the QM/MM MD simulation of the complex both coordination modes are sampled, that is, with Al(III) penta- or hexacoordinated. However, during the simulation the octahedral arrangement is clearly predominant, with >70% of the snapshots with this coordination mode.

The stabilities of the eight complexes characterized are directly related with the coordination mode of Al(III). Thus, the four complexes with the octahedral binding mode are clearly the most stable ones. The relative energies of all these complexes (see Table 4.2) are within the 2.5 kcal/mol range, Pept$^9_{3G}$ being the most stable one. On the other hand, with the remaining peptides, the shorter the peptide, the less stable the complex, so that the stability trend is: Pept^7>Pept^6>Pept^5. Among them, Pept^7 is the most stable one, 11.4 kcal/mol less stable than Pept$^9_{3G}$.

In summary, the computational study presented herein provides a deep description of the interaction between Al(III) and Mimosine-containing peptides, and provide significant atomistic details about the interaction between the peptide and the cation. The results clearly point to the longest peptides, and more in particular to Pept$^9_{3G}$ as the best potential Mimosine chelating agent suitable for Al(III), since this peptide provides an optimum interaction mode with the cation and forms the most stable complex. The present results can encourage further experimental characterization of these polypeptides which, we predict, potentially have promising properties to chelate not only aluminum, but also highly-charged metals such as Fe(III) that show octahedral coordination modes and for which Deferiprone is well known for being a good chelator.

PART II

Understanding the potential toxic roles of Al(III) in the biological environment

"Ain't no angel gonna greet me
It's just you and I my friend
And my clothes don't fit me no more
I walked a thousand miles
Just to slip this skin"

(B. Springsteen, Streets of Philadelphia)

Aluminum's preferential binding site in proteins: side chains of aminoacids versus backbone interactions

Jon I. Mujika, Gabriele Dalla Torre, Elena Formoso, Rafael Grande-Atzazi, Slowmir J. Grabowski, Christopher Exley and Xabier Lopez. *J. Inorg. Biochem.,* **2018***, 181,* 111-118.

Aluminum's preferential binding site in proteins: sidechain of amino acids versus backbone interactions

5.1. Introduction

During the last century, the massive introduction of aluminum in daily life has dramatically increased its bioavailability, altering the natural geochemical cycle that has consistently maintained the most abundant metal element in the Earth's crust absent from biota[180]. Unfortunately, the burden of aluminum we suffer is likely to have deep consequences, still not fully understood at the molecular level. Aluminum has been demonstrated to be involved in diseases such as dialysis encephalopaty[223], and this element is nowadays accepted as a risk factor in neurodegenerative diseases[4], such as Alzheimer disease (AD).

Due to its chemical properties, aluminum ion Al(III) has the capability of interacting with many biological molecules, which makes the mapping of these interactions difficult. Moreover, the complexes formed by aluminum with different biological building blocks are highly dependent on factors such as pH, concentration, *etc*... Therefore, the study of the interaction of biological molecules with aluminum (refer to aluminum speciation) is still challenging and presents inherent difficulties using experimental techniques alone. In this sense, theoretical methods have become a fundamental tool to characterize the structure and thermodynamics of aluminum compounds with biological molecules[115].

As a hard Lewis acid, aluminum shows preference towards oxygen donor ligands, such as carboxylates, phosphates, nucleotides (NADH, ATP,...) and nucleic acids such as DNA[252]. Similarly, polypeptides and proteins are a clear target of this cation and in fact aluminum has been proven to inhibit the activity of several proteins, mainly because of a strong interaction with a phosphate cofactor[253,254]. Aluminum may also contribute in the development of AD by promoting the formation and growing of the two most clear hallmarks in the disease[5,49,61,255]: i) intracellular neurofibrillary tangles (NFT) composed of hyperphosphorylated tau protein and ii) Amyloid-β (Aβ) fibrils, the main constituent in senile plaques, which are mainly made of aggregated Aβ peptides.

More recently, Song et al.[31], have suggested a new paradigm in the type of aluminum-protein interaction. They have proposed aluminum could directly interact with the backbone of the proteins, forming very stable structures with a characteristic 5-member ring, in which aluminum is directly coordinated to the carbonyl oxygen and a deprotonated peptide nitrogen, forming strong covalent

bonds. This type of binding motif would lead to a dramatic change on the secondary structure of the protein, altering its conformation and provoking its denaturation. However, the existence of this type of binding motif is difficult to reconcile with previous experimental[22,49] and theoretical[66,256] studies that have unequivocally established the propensity of aluminum to interact with amino acid sidechains with Al-O bonds of mainly electrostatic nature.

In the present paper, we apply different quantum methods to determine the thermodynamics of aluminum binding to the backbone of proteins. To do so, we consider a series of model structures based on the work of Song et al.[31], and we compare their binding energies to model structures in which aluminum is interacting with the sidechain of an amino acid. We also compare our results with previous calculations of model polypeptides in which the interaction is mediated through a variety of sidechains, including phosphorylated serines, known biological low-molecular-mass (LMM) chelators such as citrate, and a variety of phosphate molecules. Our results clearly point to a preference of aluminum to interact with amino acid sidechains, with backbone structures much less favorable and even endothermic for cases in which aluminum interacts with the peptide nitrogen.
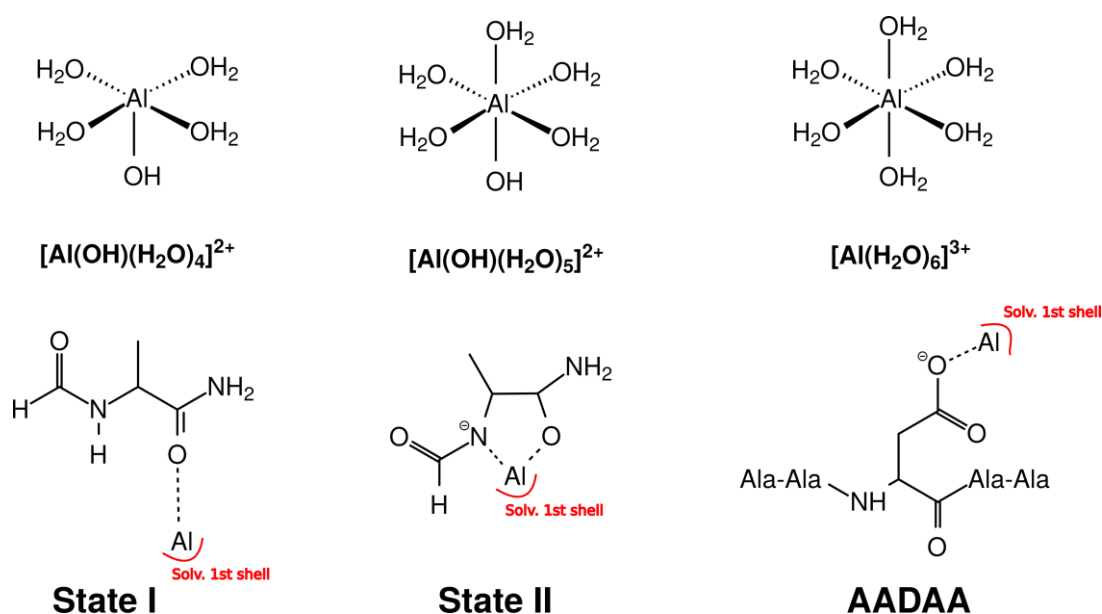
Fig. 5.1: Schematic representation of the structures characterized.

5.2. Methodology

Al(III) can form a large variety of different hydrated species[257]. Herein three hydrated Al(III) structures were considered (see Figure 1): i) Al(III) interacting with a hydroxide and four water molecules ($[Al(OH)(H_2O)_4]^{2+}$), ii) Al(III) interacting with a hydroxide and five water molecules

([Al(OH)(H$_2$O)$_5$]$^{2+}$) and iii) Al(III) interacting with six water molecules ([Al(H$_2$O)$_6$]$^{3+}$). Moreover, two Al(III)-peptide structures were optimized (see Figure 1): i) Al(III) interacts with the peptide bond carbonyl oxygen (referred to as State I) and ii) Al(III) interacts with the peptide bond carbonyl oxygen and the deprotonated N atom (referred to as State II). For these two structures, the coordination shell of Al(III) was fulfilled based on the three coordination shells considered for the hydrated Al(III), that is: i) pentacoordinated with one hydroxide in the coordination shell (as in ref, no subscript added) ii) pentacoordinated and shell completed with water molecules (the "1,5" subscript added) and iii) hexacoordinated and shell completed with water molecules (the "0,6" subscript added). All the structures are represented in Fig. 5.1 and the optimized geometries illustrated in Fig. 5.2.

All geometrical optimizations were carried out in aqueous phase using the Gaussian 09 program[258], B3LYP functional[132,259] and 6-31++G(d,p) basis set. To confirm that optimized structures were real minima on the potential energy surfaces, frequency calculations were carried out at the same level of theory. All structures showed positive force constants for all normal modes of vibration. The frequencies were then used to evaluate the zero-point vibrational energy (ZPVE) and thermal (T=298 K) vibrational corrections to the Gibbs free energies within the harmonic oscillator approximation. To calculate the entropy, the different contributions to the partition function were evaluated using the standard statistical mechanics expressions in the canonical ensemble and the harmonic oscillator and rigid rotor approximation. The solvent effect was introduced using the self-consistent reaction field (SCRF) method with the polarized continuum model (PCM), using the integral equation formalism variant (IEFPCM)[177].

The electronic energies were refined by single-point energy calculations at the B3LYP/6-311++G(3df,2p) level of theory, both in gas-phase and in solution, and then used to estimate energies in gas-phase (E$_{gas}$) and in solution (E$_{aq}$). On the other hand, the free energy contributions computed by the frequency calculations were added to E$_{aq}$ to determine the free energy in solution (G$_{aq}$). Moreover, single-point calculations at the MP2/6-311++G(3df,2p) level of theory were carried out both in the gas-phase and in aqueous environment in order to assess the accuracy of the results. In spite of some deviations between the relative energies computed with the B3LYP functional and MP2, in all cases the trends observed with the DFT functional are corroborated by the MP2 method, and for the sake of simplicity only the DFT results will be discuss in the body text.

5.3. Results

5.3.1 Interaction with the backbone of proteins

As a first approach, we follow the proposal of Song et al.[31], who employed a small model to analyze the interaction between Al(III) and the backbone of a peptide (an alanine capped by H atoms, shown in Fig. 5.1), with the reference structure for Al(III) in solution taken as a pentacoordinate $[Al(OH)(H_2O)_4]^{2+}$. Based on this model, they characterized two Al(III)-peptide structures (illustrated in Fig. 5.1 and 2 and referred to as State I and II in their paper and hereafter). In State I, Al(III) interacts with the peptide bond carbonyl oxygen, while in State II, both the carbonyl oxygen and the deprotonated peptide nitrogen interact with Al(III), forming a five-member ring. They evaluated the binding energies (ΔE) of State I and II according to the following reactions:

$$\textbf{State I}: [Al(OH)(H_2O)_4]^{2+} + C_4N_2O_2H_8$$
$$\rightarrow [Al(OH)(H_2O)_3(C_4N_2O_2H_8)]^{2+} + H_2O \tag{5.1}$$

$$\textbf{State II}: [Al(OH)(H_2O)_4]^{2+} + C_4N_2O_2H_8$$
$$\rightarrow [Al(OH)(H_2O)_2(C_4N_2O_2H_7)]^{1+} + H_2O + H_3O^+ \tag{5.2}$$
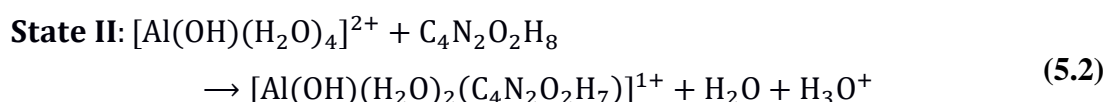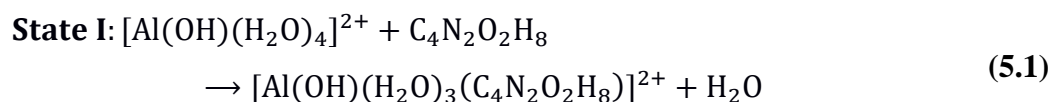
Their results pointed to a high stabilization of both States I and State II with ΔE values of -27.05 kcal/mol and -50.71 kcal/mol at the MP2 level of theory. Due to the high stability of State II, the authors concluded that Al(III) can indeed form five-member rings with the backbone of proteins. Furthermore, based on the analysis of orbitals and Mulliken charges the authors suggested a significant reduction of aluminum in State II, with a significant covalent nature of the bond between aluminum and the carbonyl oxygen and peptide nitrogen. This capacity of aluminum to form chemical bonds with the backbone of proteins would lead naturally to the formation of highly stable five-member ring structures with their backbone, provoking their denaturalization, and being an important molecular mechanism to understand aluminum toxicity.

However, these results were obtained based on binding energies computed in the gas-phase, and therefore a proper treatment of bulk solvent effects is needed to account for the possibility of the formation of these structures in a biological aqueous environment. On the other hand, the authors took as a reference in aqueous environment a pentacoordinated $[Al(OH)(H_2O)_4]^{2+}$ species[31]. However, both experiments[260,261] and computational[257] studies indicate that Al(III) shows preference towards being octahedral in aqueous solution, either coordinated to six water molecules, i.e. $[Al(H_2O)_6]^{3+}$, or with a combination of one hydroxide and five water molecules, $[Al(OH)(H_2O)_5]^{2+}$. Therefore, we decided to calculate the binding/formation energies for State I and II introducing i) bulk solvent effects through the use of a continuum model in the context of DFT level of theory, ii)

entropic effects by evaluating binding free energies (ΔG) and iii) using additionally, more reliable hydrated aluminum structures as reference so that three coordination shells are chosen: $[Al(OH)(H_2O)_4]^{2+}$ (used in ref.[31]), $[Al(OH)(H_2O)_5]^{2+}$, and $Al(H_2O)_6]^{3+}$.
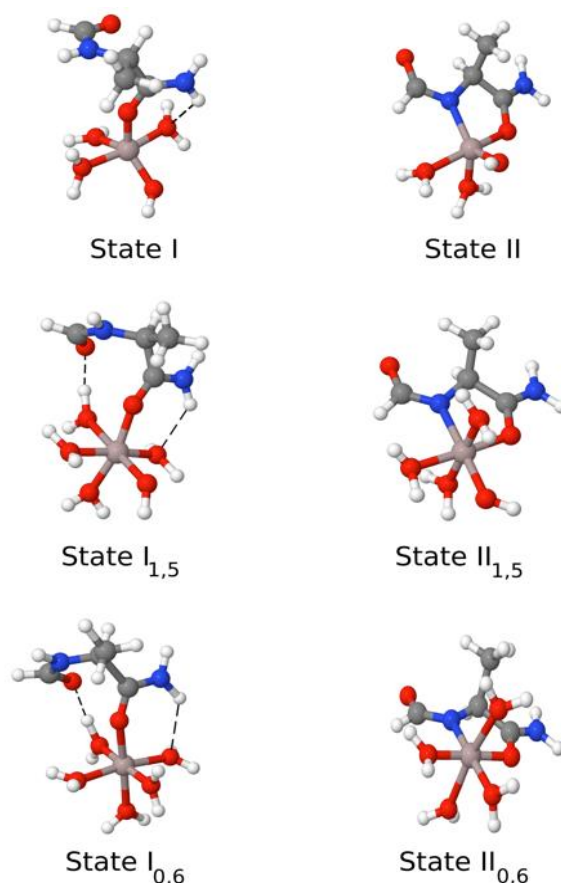
Fig. 5.2: State I corresponds to the binding of aluminum to the peptide bond carbonyl oxygen, whereas State II corresponds to the formation of an Al-N bond from State I. Both structures characterized considering three different coordination shells for Al(III) (nomenclature defined in Methodology section). Atoms represented as: O (red), H (white), C (grey) and N (blue).

In addition, we would like to note that dealing with a small charged molecule such as a hydronium ion involves some technical difficulties, mainly an accurate estimation of its solvation energy. In order to alleviate this shortcoming, the microsolvated hydronium model $[H_3O(H_2O)_3]$ and its neutral counterparts were used to calculate the energy of State II:

$$\text{State II: } [Al(OH)(H_2O)_4]^{2+} + C_4N_2O_2H_8 + H_2O(H_2O)_2$$
$$\rightarrow [Al(OH)(H_2O)_2(C_4N_2O_2H_7)]^{1+} + H_2O + [H_3O(H_2O)_3]^{+} \quad \textbf{(5.3)}$$
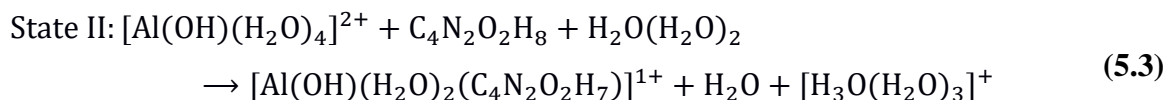
Results are summarized in Table 5.1 and all geometries characterized illustrated in Fig. 5.2.

	MP2			DFT		
	$\Delta E_{gas}^{(a)}$	$\Delta E_{gas}^{(b)}$	$\Delta E_{aq}^{(c)}$	$\Delta E_{gas}^{(d)}$	$\Delta E_{aq}^{(e)}$	$\Delta G_{aq}^{(e)}$
$[Al(OH)(H_2O)_4]^{2+}$						
State I[(1)]	-27.1	-40.2	-13.0	-38.9	-11.1	-7.6
State II[(2)]	-50.7	-44.9	17.2	-41.9	20.7	13.2
State II[(3)]	-	-112.6	-14.4	-110.5	-11.8	-8.0
$[Al(OH)(H_2O)_5]^{2+}$						
State I[(1)]	-	-41.6	-13.6	-39.5	-10.7	-2.9
State II[(2)]	-	-33.1	26.3	-29.0	30.7	25.0
State II[(3)]	-	-100.9	-5.4	-97.7	-1.8	3.7
$[Al(H_2O)_6]^{3+}$						
State I[(1)]	-	-70.7	-17.1	-69.4	-14.7	-11.1
State II[(2)]	-	-130.9	20.4	-127.9	24.0	20.7
State II[(3)]	-	-198.7	-11.3	-196.6	-8.6	-0.6

Table 5.1: Thermodynamics of Formation of State I and II. Reaction energies and free energies computed at different level of theories: a) MP2, taken from ref.[31]; b) MP2/6-311++G(3df,2p) in the gas-phase; c) MP2/6-311++G(3df,2p) in aqueous environment using the IEFPCM continuum model; d) B3LYP/6-311++G(3df,2p) in the gas-phase; e) B3LYP/6-311++G(3df,2p) in aqueous environment using the IEFPCM continuum model. Three different structure of hydrated aluminum are taken as reference for these two reactions: $[Al(OH)(H_2O)_4]^{2+}$, $[Al(OH)(H_2O)_5]^{2+}$ or $[Al(H_2O)_6]^{3+}$. For each state, the superscript corresponds to the label of the reaction used to calculate the energy of the corresponding compound.

We start comparing the results of State I and II according to reactions (1) and (2), that is, using the bare hydronium to evaluate the energies of State II. For gas phase calculations and taking the $[Al(OH)(H_2O)_4]^{2+}$ species as reference, we obtain similar gas phase energies as ref.[31] for State I and II, -38.9 kcal/mol and -41.9 kcal/mol, respectively. However, the introduction of solvent effects has a profound effect on the thermodynamics of these charged systems, and now although formation of

State I is still exothermic, -11.1 kcal/mol, State II is highly endothermic, 20.7 kcal/mol, and therefore unlikely to be formed in aqueous solution. The change of hydrated aluminum reference structure to $[Al(OH)(H_2O)_5]^{2+}$ or $[Al(H_2O)_6]^{3+}$ has a sizeable effect on the gas phase energetic and especially for the case of $[Al(H_2O)_6]^{3+}$, with a significant increase in the gas-phase exothermic behavior for the formation of States I and II. However, again the introduction of solvent effects yields an increase in the ΔE_{aq} values, with the result that only the formation of State I is moderately exothermic, while formation of State II is highly endothermic in all cases. Similarly, the computed ΔG_{aq} values confirm this trend, with values of State II between 13.2 to 25 kcal/mol depending on the hydrated aluminum structure taken as reference. Note that this is somehow expected, since State II requires the deprotonation of a peptide bond nitrogen, and this is a very unfavorable process in solution according to the high values of the pK$_a$ of amides.

Interestingly, the relative energies of State II decreases in ca. 20 kcal/mol (see Table 5.1) when its binding energies are evaluated using the microsolvated $H_3O(H_2O)_3$ model (reaction 3) instead of the bare hydronium ion, and consequently the difference between the energies of State I and State II shrinks. In spite of this modification, State II remains clearly less stable than State I when Al(III) presents any of the two octahedral arrangements, and only with Al(III) pentacoordinated the stability of the two compounds are similar. However, as pointed out above, this coordination mode is the most unlikely one for Al(III). More importantly, all these results confirm on one hand that special cautions should be taken evaluating binding energies and choosing the reference molecule, and on the other hand that the interaction of Al(III) with the backbone of a peptide bond (either State I or II) can not compete with the interaction of the cation with a negatively charged side chain (see below).

Song et al.[31] claimed that the energy required to deprotonate the peptide bond N atom could be somehow compensated by a strong binding of the carbonyl oxygen and peptide nitrogen to aluminum, with a significant degree of covalent character, and significant reduction of the aluminum oxidation state. Their analysis was based on the investigation of orbitals shapes and Mulliken charges, which shows inherent limitations[262]. We decided to analyze the bonding features of State I and II generated by the $[Al(OH)(H_2O)_4]^{2+}$ structure using the more accurate Quantum Theory of Atoms in Molecules (QTAIM)[208]. Briefly, the theory makes use of an unambiguous partition of electron density in atom basins based on Bader's definition of an atom in a molecule (zero-flux condition). In this context, the bonding between two atoms is characterized by the so-called bond critical point (BCP). Various properties at the BCPs characterize the type of bonding, in particular the value of the density ($\rho(r_{BCP})$), the Laplacian of the density ($\nabla^2\rho(r_{BCP})$), and the energy density ($H(r_{BCP})$) are commonly used to classify the type of bonding (covalent versus ionic) between a pair of atoms. In Table 5.2, we summarize the values obtained for all the Al-O and Al-N bonds found in State I and State II. Typical

covalent bonds show negative values of both the Laplacian and the energy density at the BCP. This indicates that the accumulation of the electronic charge at BCP leads to stabilization of the bonding interaction. On the contrary, ionic bonds show typically positive values of the Laplacian and the energy density[214]. As one can see in Table 5.2, all Al-O bonds of State I fall into the latter category. The formation of State II does not change the qualitative picture for Al-O bonds, whereas in the case of Al-N bonds, we find also a positive value of the Laplacian, and only a very small negative value of the energy density at the bond critical point. This can be related to very minor dative interactions from the nitrogen lone pair into the empty valence shell of aluminum, but not to a strong chemical bond due to the reduction of the aluminum oxidation state. In fact, the Bader atomic charges show only a very slight reduction of the charge of aluminum, from 2.578 to 2.546 a.u., when passing from State I to State II, another evidence of the mainly electrostatic nature of the bonding interactions between the peptide atoms and aluminum. Analogous results were obtained for the State I and II structures with Al(III) hexacoordinated.

	$\rho(r_{BCP})$	$\nabla^2\rho(r_{BCP})$	$H(r_{BCP})$		$\rho(r_{BCP})$	$\nabla^2\rho(r_{BCP})$	$H(r_{BCP})$
State I$_{1,5}$ (Q$_{Al}$ = +2.578 a.u.)				**State II$_{1,5}$ (QAl = +2.546 a.u.)**			
Al-O^{carb}	0.073	0.573	0.010	Al-N	0.076	0.449	-0.005
Al-O^{OH}	0.097	0.832	0.008	Al-O^{carb}	0.060	0.392	0.004
Al-O^{W1}	0.050	0.331	0.005	Al-O^{OH}	0.093	0.787	0.008
Al-O^{W2}	0.059	0.427	0.009	Al-O^{W1}	0.052	0.359	0.007
Al-O^{W3}	0.049	0.320	0.005	Al-O^{W2}	0.045	0.281	0.004
State I$_{0,6}$ (Q$_{Al}$ = +2.604 a.u.)				**State II$_{0,6}$ (QAl = +2.572 a.u.)**			
Al-O^{carb}	0.066	0.498	0.008	Al-N	0.075	0.426	-0.006
Al-O^{W1}	0.062	0.439	0.007	Al-O^{carb}	0.067	0.459	0.004
Al-O^{W2}	0.051	0.333	0.005	Al-O^{W1}	0.051	0.328	0.005
Al-O^{W3}	0.054	0.358	0.005	Al-O^{W2}	0.048	0.300	0.004
Al-O^{W4}	0.055	0.381	0.006	Al-O^{W3}	0.047	0.295	0.004
Al-O^{W5}	0.053	0.352	0.005	Al-O^{W4}	0.052	0.347	0.005

Table 5.2: QTAIM analysis of Al-O and Al-N bonding. Values of the electron density ($\rho(r_{BCP})$), Laplacian of electron density ($\nabla^2\rho(r_{BCP})$) and energy density ($H(r_{BCP})$) at the bond critical point for all Al-X (X=O,N) bonds in States I and II structures characterized considering the [1,5] and [0,6] coordination shells (defined in the Methodology section). All quantities in atomic units.

5.3.2 Interaction with amino acid sidechains

In summary, the calculations carried out in the model employed in ref.[31] do not support the idea of a strong interaction of Al(III) with the peptide backbone through the formation of 5-member rings (State II) in aqueous solution, although the interaction with the carbonyl oxygen (State I) could still be favorable thermodynamically. However, taking into account that the bond between aluminum and the carbonyl oxygen or nitrogen is mainly of electrostatic character, one could think that it could not compete with the interaction with other functional groups commonly present in residues, such as negatively charged carboxylic groups (Asp/Glu sidechains or C-terminals in proteins). In fact, it is well known that Al(III) has large affinity towards negatively charged carboxylic or phosphates groups[263]. To analyze this point, we evaluate the binding interaction energy of aluminum to a carboxylic sidechain in Ala-Ala-Asp-Ala-Ala (AADAA) pentapeptide (See Fig. 5.1 and 5.3). Results (shown in Table 5.3) clearly show a much larger exothermic character for the resultant structure with ΔG_{aq} values of -48.7 kcal/mol.

In addition, we also provide in Table 5.3, the thermodynamics of relevant structures found in our previous works, with similar quantum methods. For instance, in the case of the experimentally and theoretically studied GEGEGSGG octapeptide, we obtain different ΔG values depending on the coordination of aluminum[66]. We have chosen three paradigmatic cases: i) N1-GEGEGSGG where aluminum interacts with only one aspartate sidechain, -33.7 kcal/mol, N6-GEGEGSGG which shows one aspartate sidechain in the first coordination shell and a second carboxylate group in the second coordination sphere, -67.9 kcal/mol, and finally, P1-GEGEGSGG with a phosphorylated serine coordinating aluminum, -78.2 kcal/mol. All cases show a more favorable interaction than with the models in which aluminum is directly interacting with the peptide backbone. It is remarkable the enhancement of affinity obtained upon phosphorylation of the serine sidechain that increases the negative charge associated to the corresponding residue. Notice as well, the tendency of aluminum to favor structures in which several functional groups coordinate aluminum, (either in the first coordination sphere or in the second one). In this sense, the most favorable interaction is obtained for Aβ peptide[256], where three carboxylic groups (Glu3, Asp7 and Glu11) bind to aluminum in the first coordination shell. Thus, the simultaneous interaction with various negatively charged groups present in the Aβ peptide sequence makes this polypeptide to be highly favorable for aluminum binding[68].

The conclusion of our data is clear: in the aqueous phase, it is thermodynamically more favorable for Al(III) to interact with negative charged amino acid sidechains rather than with the backbone of proteins. Even with just one negatively charged amino acid sidechain, there is a substantial strengthening of the binding to aluminum with respect to only backbone interactions.

Are these sidechain interactions of sufficient strength as to be relevant in biological systems? To answer this question we need to compare our data with that obtained with similar methods for known low molecular mass biochelators of aluminum. In Table 5.3, we displays the thermodynamics of aluminum chelation by citrate, the main LMM chelator in blood serum, and by relevant biophosphates such as 2,3-DPG, glucose-6-phosphate (G6P), NADH, and ATP-like triphosphates (TriP). The order in binding energies is the following one: citrate (-124.9) > 2,3-DPG (-123.5) $\simeq$ G6P (-117.2) > TriP (-108.7) $\gg$ NADH (-54.0 kcal/mol). It is clear that based on these results and among the Al-peptide interactions shown in this work, only the Al-Aβ complex could be considered as a competitive strong chelator in biological systems.

Ligand	Ref.	Ligand Charge	Binding Mode	ΔH_{aq}	ΔG_{aq}
Interaction with the backbone					
State I$_{0.6}$	This work	0	Backbone O(C)	-14.7	-11.1
State II$_{0.6}$	This work	-1	Backbone N&O	24.0/-8.6	20.7/-0.6
Interaction with the sidechain of aminoacids					
AADAA	This work	-1	Asp	-	-48.7
GEGEGSGG	Ref[66].	-2	N1	-36.5	-33.7
			N6	-69.7	-67.9
GEGEGS(P)GG	Ref[66].	-4	P1	-81.0	-78.2
Aβ_{1-16} peptide	Ref[256].	-2	Glu3,Asp7,Glu11	-172.9[a]	-
Interaction with LMM Ligands					
Citrate	Ref[39,40].	-4	2 COO$^-$,O$^-$	-133.0	-124.9
2,3-DPG	Ref[40].	-5	Multiple	-118.9	-123.5
NADH	Ref[42].	-1	Multiple	-	-54.0
Glucose-6-Phosphate	Ref[41].	-3	Multiple	-116.5	-117.2
ATP-like, Triphosphate	Ref[45].	-4	α,β-Phosphate	-109.2	-108.7

(a) ΔE_{aq} value.

Table 5.3: Thermodynamics of the binding to Al(III) of i) peptide through its backbone (State I and II compounds) and ii) other relevant biological molecules. Reaction energies calculated according to equations (5.1) and (5.2) (taking [Al(H$_2$O)$_6$]$^{3+}$ as reference state), computed at B3LYP/6-311++G(3df,2p) with IEFPCM continuum model to include solvent effects.

Therefore, a high density of negative charged amino acid sidechains in a reduced sequence region seems to be a prerequisite for a polypeptide to have a high affinity for aluminum.
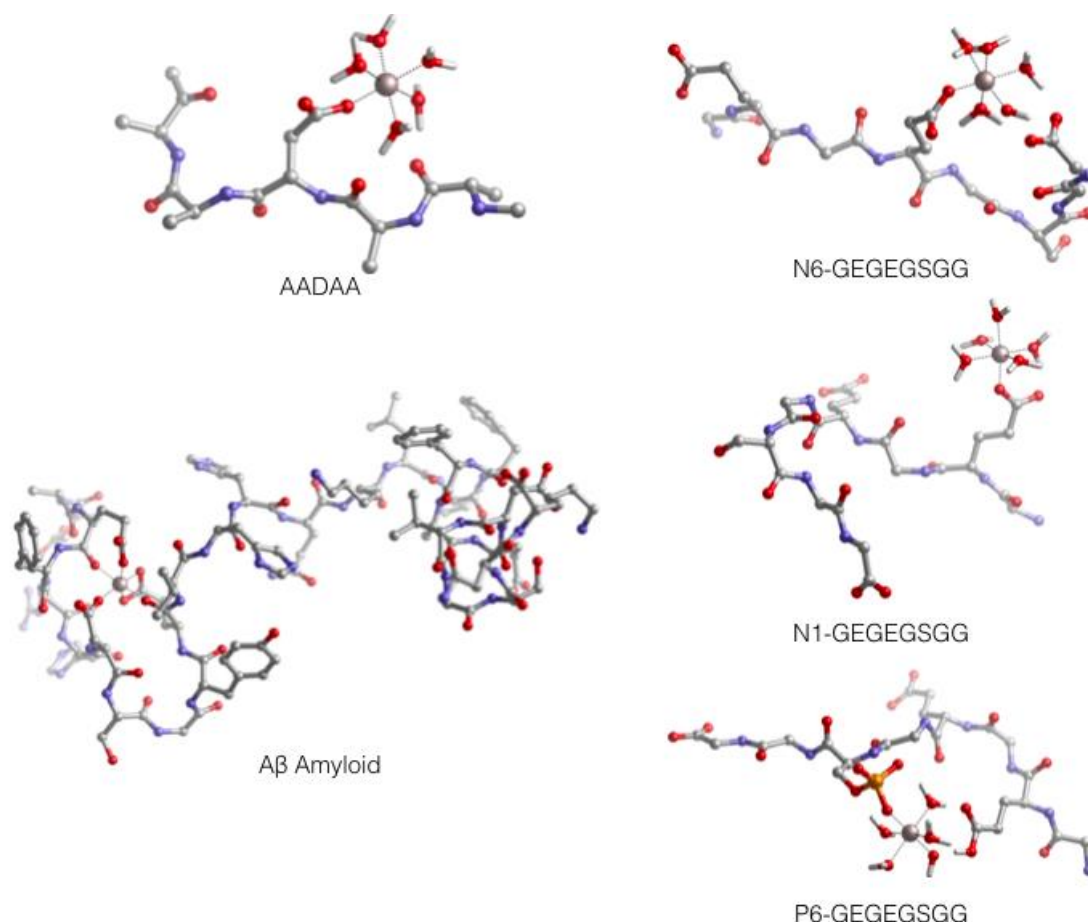
Figure 5.3: Structures of different polypeptide structures considered in Table 5.3. Note that for clarity hydrogen atoms are not displayed.

5.4 Conclusions

In this paper, we have revised the possibility of aluminum to interact with the backbone of proteins, using density functional theory in conjunction with continuum solvation models to treat bulk solvent effects. To do so, we have compared the thermodynamics of formation of Al(III)-backbone structures previously proposed in the literature, with those structures in which aluminum interacts with amino acid sidechains, and with known aluminum low molecular mass chelators in biological systems. We have found that in an aqueous environment aluminum shows a clear preference to interact with negatively charged amino acid sidechains, with aluminum-backbone structures being endothermic or much less exothermic than aluminum-sidechain structures. The comparison with known biochelators

of aluminum, like citrate or biophosphates, clearly indicates that only in cases in which there is a high density of negatively charged amino acid sidechains in proteins, such as in Aβ peptide, could a biomolecule be a competitive aluminum chelator in biological environment.

Aluminum and Fenton reaction: how can the reaction be modulated by speciation ? A computational study using citrate as test case

Jon I. Mujika, Gabriele Dalla Torre, and Xabier Lopez. *Phys. Chem. Chem. Phys.,* **2018***, 20,* 16256-16265

Aluminum and Fenton reaction: how can the reaction be modulated by speciation? A computational study using citrate as a test case

6.1 Introduction

Aluminum is the third most abundant element in Earth's crust, but complex geochemical cycles prevent its solubilization from lithosphere[1,180,264], maintaining this abundant metal out from essential biological cycles. Nevertheless, in the last century, aluminum has massively been extracted from soil due to its favorable properties (easy to manipulate, cheap and good *physico*-chemical properties) and myriad of applications (food additives, pharmaceuticals, Al-containers, etc.). As a consequence, aluminum is nowadays present in the biosphere, and humans are highly exposed to this metal[2,265]. Unfortunately, this is not without consequences, and this exposition to aluminum has been linked to various diseases[6,59,61,266], starting from early evidences of dialysis encephalopathy or osteodistrophy in patients with renal failure under dialysis treatment[223,267], to more recent evidences linking aluminum to several neurodegenerative diseases[59,61]. The high charge and small volume of aluminum make this metal a strong Lewis acid, with high affinity towards oxygen-containing and negatively-charged functional groups, such as phosphates or carboxylic groups. Therefore, aluminum has the potential ability to form strong interactions with important biomolecules such as proteins, phospholipids, ATP, NADH, RNA, DNA, etc...[115].

The pro-oxidant ability of aluminum is one of the main deleterious effects of aluminum, observed both *in-vitro* and *in-vivo* experiments[43,72]. This is a feature not expected for an element without a redox capability[52,268]. It was early hypothesized[43,52] that this pro-oxidant activity was due to the formation of a strong aluminum-superoxide complex, which leads to an increase of the lifetime of the superoxide radical species. In fact, Fukuzumi et al. reported a linear relationship between the strength of the metal-superoxide interaction, and the oxidant activity of the metal[269-271]. Based on this hypothesis, we demonstrated[51] the possibility of the formation of an aluminum-superoxide complex in solution, departing from various aluminum hydrolytic species. Further calculations confirmed that these aluminum-superoxide complexes may increase oxidative stress in biological environments by acting as promoting agents of the Fenton reaction[56] (see Fig. 6.1).

However, most of the aluminum present in the human organism is not free in solution, but forms stable complexes with low and high molecular mass biomolecules, and this could have a deep effect on the pro-oxidant activity of aluminum. Many attempts have been made to identify the molecules

interacting with aluminum in biological systems[34,36,272,273]. However, due to the complex chemistry of aluminum, its low total concentration, and the high risk of sample-contamination, the study of the speciation of aluminum is a complex task[36].
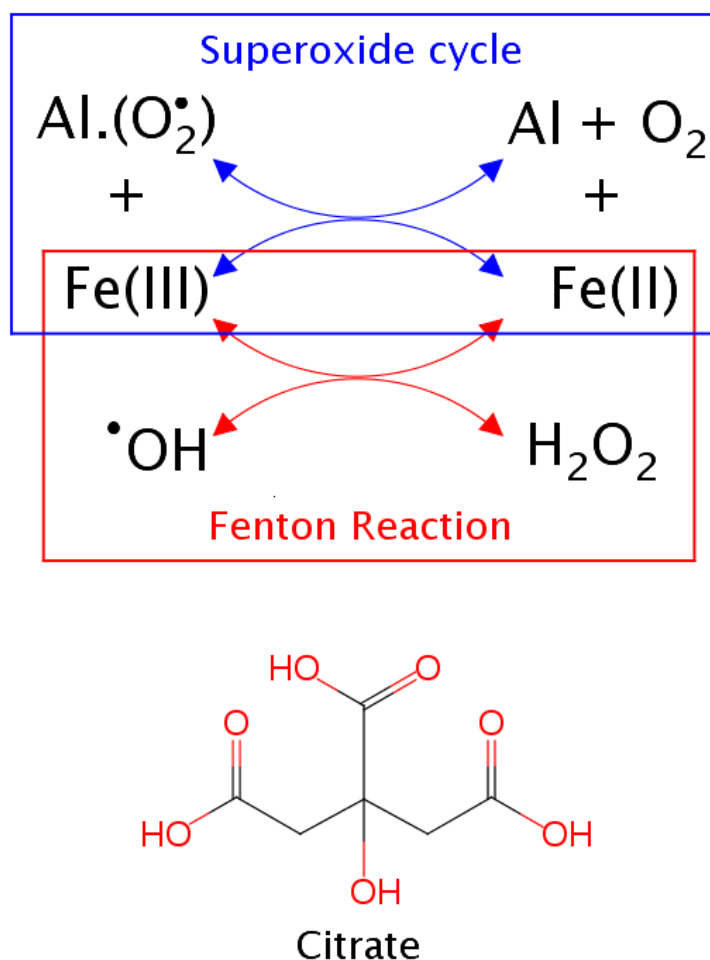
Fig. 6.1: Above, a possible route for the pro-oxidant activity of aluminum by the promotion of the Fenton reaction. Below, the molecular structure of citrate.

Nowadays it is accepted that the 90% of aluminum found in the blood serum is bound to serum transferrin protein, while citrate is the main low molecular weight chelator[83]. Alternatively, citrate is identified as the main chelator of aluminum in brain extracellular fluid[61]. This behavior is not surprising as the molecular composition of citrate with three carboxylic groups and an alcohol group (shown in Fig. 6.1) provides high affinity towards Al(III). Interestingly, in previous works, it was demonstrated that the formation of ternary complexes with citrate can show a protective role with respect to some of the deleterious effects of aluminum[40,186].

In the present study, our goal is to analyze how the interaction with citrate could alter i) the possibility

of formation of an aluminum-superoxide complexes and ii) the possibility of reducing Fe(III) to Fe(II), promoting the Fenton reaction. To do so, we evaluate the binding energies of Al(III) to superoxide and citrate, and the reaction free energy of iron reduction from Fe(III) to Fe(II) in the presence of aluminum-superoxide radical binary species and aluminum-citrate-superoxide ternary species. To be consistent, we also consider the changes in the corresponding energies when citrate is bound to iron. The study describes a complex scenario that ultimately depends on the relative concentrations of each species. However, the results point in general to a protective role of citrate with respect to the pro-oxidant ability of aluminum, specially in high-citrate concentration regimes.

6.2 Methodology

All geometries were optimized in solution at two level of theories using the 6-31++g(d,p) basis set: B3LYP/6-31++g(d,p) and B3LYP-D3(BJ)/6-31++g(d,p). In the latter level of theory D3 version of Grimme's dispersion[153] with Becke-Johnson damping[274] is included. To confirm that the optimized structures were real minima on the potential energy surfaces, frequency calculations were carried out at the same level of theory. All structures showed positive force constants for all the normal modes of vibration. The frequencies were then used to evaluate the zero-point vibrational energy (ZPVE) and the thermal (T = 298 K) vibrational corrections to the enthalpies and Gibbs free energies within the harmonic oscillator approximation. To calculate the entropy, the different contributions to the partition function were evaluated using the standard statistical mechanics expressions in the canonical ensemble and the harmonic oscillator and rigid rotor approximation. The solvent effect was introduced by using the self-consistent reaction field (SCRF) method with the polarized continuum model (PCM), using the integral equation formalism variant (IEFPCM)[177].

Once the geometries were optimized at the two level of theories stated above, the electronic energies were refined using the larger basis set 6-311++g(3df,2p) by two distinct single-point energy calculations: a) using the same functional as in the geometry optimization, or b) using the ωB97XD hybrid functional[275] with dispersion correction included in the functional form. Thus, for each reaction a set of four different energies are presented (energy evaluation//geometry optimization): i) B3LYP/TZ//B3LYP/DZ (ΔG_{aq}^{B3LYP}), ii) ωB97XD/TZ//B3LYP/DZ ($\Delta G_{aq}^{B3,wB97}$), iii) B3LYP-D3/TZ//B3LYP-D3/DZ (ΔG_{aq}^{B3-D3}), iv) ωB97XD/TZ//B3LYP-D3/DZ ($\Delta G_{aq}^{B3-D3,wB97}$), where TZ=6-311++g(3df,2p) and DZ=6-31++g(d,p). All these calculations were carried out using the Gaussian 09 and 16 packages[276].

As in our previous study[51], we considered different hydrated models for the Al-Citr complex, where

different number of waters and hydroxide molecules were included. Departing from each of these models, the substitution reaction of a water molecule (Equation 6.1) or a hydroxide (Equation 6. 2) by the superoxide to form a Al-Citr-$O_2^{.}$ complex was studied:

$$[\text{Al. Citr}(H_2O)_n(OH)_m]_{aq}^{(1-m)} + [O_2(H_2O)_2]_{aq}^{-} \longrightarrow$$
$$[\text{Al. Citr}(H_2O)_{n-1}(OH)_mO_2]_{aq}^{(2-m)} + [H_2O(H_2O)_2]_{aq} \tag{6.1}$$

$$[\text{Al. Citr}(H_2O)_n(OH)_m]_{aq}^{(1-m)} + [O_2(H_2O)_2]_{aq}^{-} \longrightarrow$$
$$[\text{Al. Citr}(H_2O)_n(OH)_{m-1}O_2]_{aq}^{(1-m)} + [OH(H_2O)_2]_{aq}^{-} \tag{6.2}$$
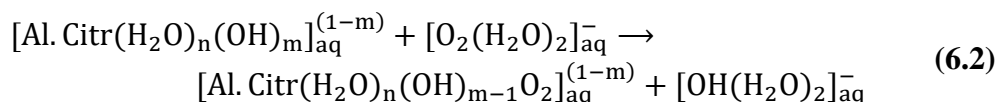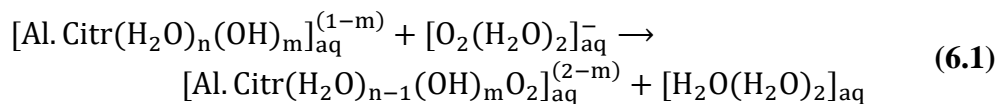
were *n* and *m* are the number of water and hydroxide molecules, respectively. Note that in concordance with some test calculations carried out previously[51], the small ligands (superoxide, water molecule and hydroxide) were micro-solvated with two explicit water molecules to improve their solvation energy. Moreover, citrate was considered completely deprotonated with a net charge of -4 (see below).

The free energies in solution corresponding to these two reactions are calculated as:

$$\Delta G_{aq} = G_{aq}(Al.\,Citr(H_2O)_{n-1}(OH)_mO_2) + G_{aq}(H_2O(H_2O)_2)$$
$$- G_{aq}(Al.\,Citr(H_2O)_n(OH)_m) - G_{aq}(O_2(H_2O)_2) \tag{6.3}$$

Or

$$\Delta G_{aq} = G_{aq}(Al.\,Citr(H_2O)_n(OH)_{m-1}O_2) + G_{aq}(OH(H_2O)_2)$$
$$- G_{aq}(Al.\,Citr(H_2O)_n(OH)_m) - G_{aq}(O_2(H_2O)_2) \tag{6.4}$$

The ΔG_{aq} values were computed at the four level of theories described above. All these values are presented in Table 6.1, 6.2 and 6.3, but since the overall trends are maintained, only the ΔG_{aq}^{B3-D3} values are discussed throughout the body text.

For all aluminum containing structures we also calculated delocalization Indices (D.I.). These are a measure of the covariance between the population of two atoms and and, consequently, a measure of the number of electrons simultaneously fluctuating between these atoms[248,249],

$$\delta(A,B) = \int_A \int_B d\,1d2\rho_{xc}(1,2) = cov(N_A, N_B) \tag{6.5}$$

where $\rho_{xc}(1,2)$ is the exchange-correlation density[277]. It can be taken as the number of electron pairs

shared between atoms and , i.e., the bond order[278]. The AIMAll v11.08.23 program[250] was used to carry out the QTAIM analysis (what includes the characterization of D.I.) on the previously optimized structures. Wavefunctions for QTAIM analysis were obtained at the B3LYP/6-311++g(3df,2p) level of theory using the IEFPCM solvation model.

6.3 Results and discussion

6.3.1 Incorporation of the $O_2^{\cdot}$ superoxide radical

In our previous work, we investigated the incorporation of O_2^- to first coordination shell of aluminum hydrolytic species[51]. In particular the displacement of either a water molecule or an hydroxide from the first coordination shell was analyzed by evaluating the ΔG_{aq} of one of the next reactions:

$$[Al(H_2O)_n(OH)_m]_{aq}^{3-m} + [O_2]_{aq}^- \longrightarrow [Al(H_2O)_{n-1}(OH)_mO_2]_{aq}^{(2-m)} + [H_2O]_{aq} \tag{6.6}$$

$$[Al(H_2O)_n(OH)_m]_{aq}^{3-m} + [O_2]_{aq}^- \longrightarrow [Al(H_2O)_n(OH)_{m-1}O_2]_{aq}^{(3-m)} + [OH]_{aq}^- \tag{6.7}$$
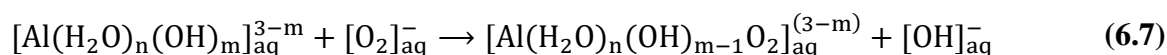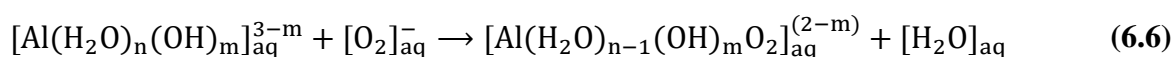
where Equation 6.6 implies the substitution of a water molecule by the superoxide anion, and Equation 6.7 the substitution of an hydroxide. The subscripts *n* and *m* refer to the number of water molecules and hydroxides present in the complexes. Note that these reactions are analogous to reactions 6.1 and 6.2, but without the presence of citrate.

	ΔG_{aq}^{B3LYP}	$\Delta G_{aq}^{B3,wB97}$	ΔG_{aq}^{B3-D3}	$\Delta G_{aq}^{B3-D3,wB97}$
$[Al(H_2O)_6]^{3+} + [O_2]^- \longrightarrow [Al(O_2)(H_2O)_5]^{2+} + H_2O$	-24.7	-25.9	-19.5	-19.9
$[Al(OH)(H_2O)_5]^{2+} + [O_2]^- \longrightarrow [Al(O_2)(OH)(H_2O)_4]^+ + H_2O$	-24.6	-24.1	-17.9	-18.3
$[Al(OH)_2(H_2O)_4]^+ + [O_2]^- \longrightarrow [Al(O_2)(OH)_2(H_2O)_3] + H_2O$	-18.7	-18.6	-17.6	-17.4
$[Al(OH)_3(H_2O)_3] + [O_2]^- \longrightarrow [Al(O_2)(OH)_3(H_2O)_2]^- + H_2O$	-16.4	-17.4	-8.5	-8.6
$[Al(OH)_4]^- + [O_2]^- \longrightarrow [Al(O_2)(OH + OH^-$	31.1	30.5	21.5	22.1

Table 6.1. Reaction free energies in solution (in kcal/mol) evaluated for the substitution of a water molecule (Equation 6.6) or hydroxide (Equation 6.7) located in the aluminum first coordination shell of aluminum hydrolytic species by the O_2^* superoxide radical computed at the four level of theories described in

Methodology: B3LYP/TZ//B3LYP/DZ (ΔG_{aq}^{B3LYP}), wB97XD/TZ//B3LYP/DZ ($\Delta G_{aq}^{B3,wB97}$), B3LYP-D3/TZ//B3LYP-D3/DZ (ΔG_{aq}^{B3-D3}) and wB97XD/TZ/B3LYP-D3/DZ ($\Delta G_{aq}^{B3-D3,wB97}$).

The results clearly indicated that the substitution of a water molecule by the superoxide radical anion was energetically favorable (data shown in Table 6.1), whereas the substitution of an hydroxide was unfavorable in all cases. Besides, we concluded that the charge of the complex is a contributing factor, as the larger the number of negatively charged hydroxides in the first coordination shell, the less negative the ΔG_{aq} value for the displacement of water molecules by the superoxide radical.

Now, we will analyze whether aluminum can form a stable complex with the superoxide radical anion in the presence of citrate, a ligand composed by three carboxylic groups and an alcohol group (see Fig. 6.1). Previously, pK$_a$ values of -14.5, -8.0, 0.6 and 3.6 were computed for the four titratable groups of an aluminum-bound citrate molecule[39], which are in concordance with the two known experimental values, the two highest ones: 2.3 and 3.6[34]. Therefore, we assume that, at physiological conditions, the Al(III)-bound citrate is fully deprotonated. Note that the pK$_a$ values of free citrate in solution (2.9, 4.3, 5.6 and 11.6/14.4) suggest a different protonation state, with the alcohol group protonated[39]. Different coordination modes between citrate and Al(III) were also compared[39], concluding that citrate interacts tridentately with aluminum.

	ΔG_{aq}^{B3LYP}	$\Delta G_{aq}^{B3,wB97}$	ΔG_{aq}^{B3-D3}	$\Delta G_{aq}^{B3-D3,wB97}$
$[Al.Citr(H_2O)_3(H_2O)_{10}]^- + [O_2]^- \rightarrow$ $[Al.Citr(H_2O)_2(O_2)(H_2O)_{10}]^{2-} + H_2O$	-7.2	-5.5	-4.0	-5.2
$[Al.Citr(H_2O)_2(OH)(H_2O)_{10}]^{2-} + [O_2]^- \rightarrow$ $[Al.Citr(H_2O)(OH)(O_2)(H_2O)_{10}]^{3-} + H_2O$	-4.4	-4.2	-3.9	-4.5
$[Al.Citr(H_2O)(OH)_2(H_2O)_{10}]^{3-} + [O_2]^- \rightarrow$ $[Al.Citr(OH)_2(O_2)(H_2O)_{10}]^{4-} + H_2O$	4.1	7.4	6.2	6.6
$[Al.Citr(H_2O)_2(OH)(H_2O)_{10}]^{2-} + [O_2]^- \rightarrow$ $[Al.Citr(H_2O)_2(O_2)(H_2O)_{10}]^{2-} + [OH]^-$	15.5	16.3	16.5	17.5
$[Al.Citr(H_2O)(OH)_2(H_2O)_{10}]^{3-} + [O_2]^- \rightarrow$ $[Al.Citr(H_2O)(OH)(O_2)(H_2O)_{10}]^{3-} + [OH]^-$	16.6	16.1	14.0	14.8
$[Al.Citr(OH)_3(H_2O)_{10}]^- + [O_2]^{4-} \rightarrow$ $[Al.Citr(OH)_2(O_2)(H_2O)_{10}]^{4-} + [OH]^-$	3.2	5.2	4.1	5.2

Table 6.2. Reaction free energies in solution (in kcal/mol) evaluated for the substitution of a water molecule (Equation 6.1) or a hydroxide ion (Equation 6.2) located in the aluminum first coordination shell of Al-Citr complexes by the O$_2^*$ superoxide radical (structures shown in Fig. 6.2). ΔG_{aq} values computed at the level of

theories described in Methodology: B3LYP/TZ//B3LYP/DZ (ΔG_{aq}^{B3LYP}), wB97XD/TZ//B3LYP/DZ ($\Delta G_{aq}^{B3,wB97}$), B3LYP-D3/TZ//B3LYP-D3/DZ (ΔG_{aq}^{B3-D3}) and wB97XD/TZ/B3LYP-D3/DZ ($\Delta G_{aq}^{B3-D3,wB97}$).
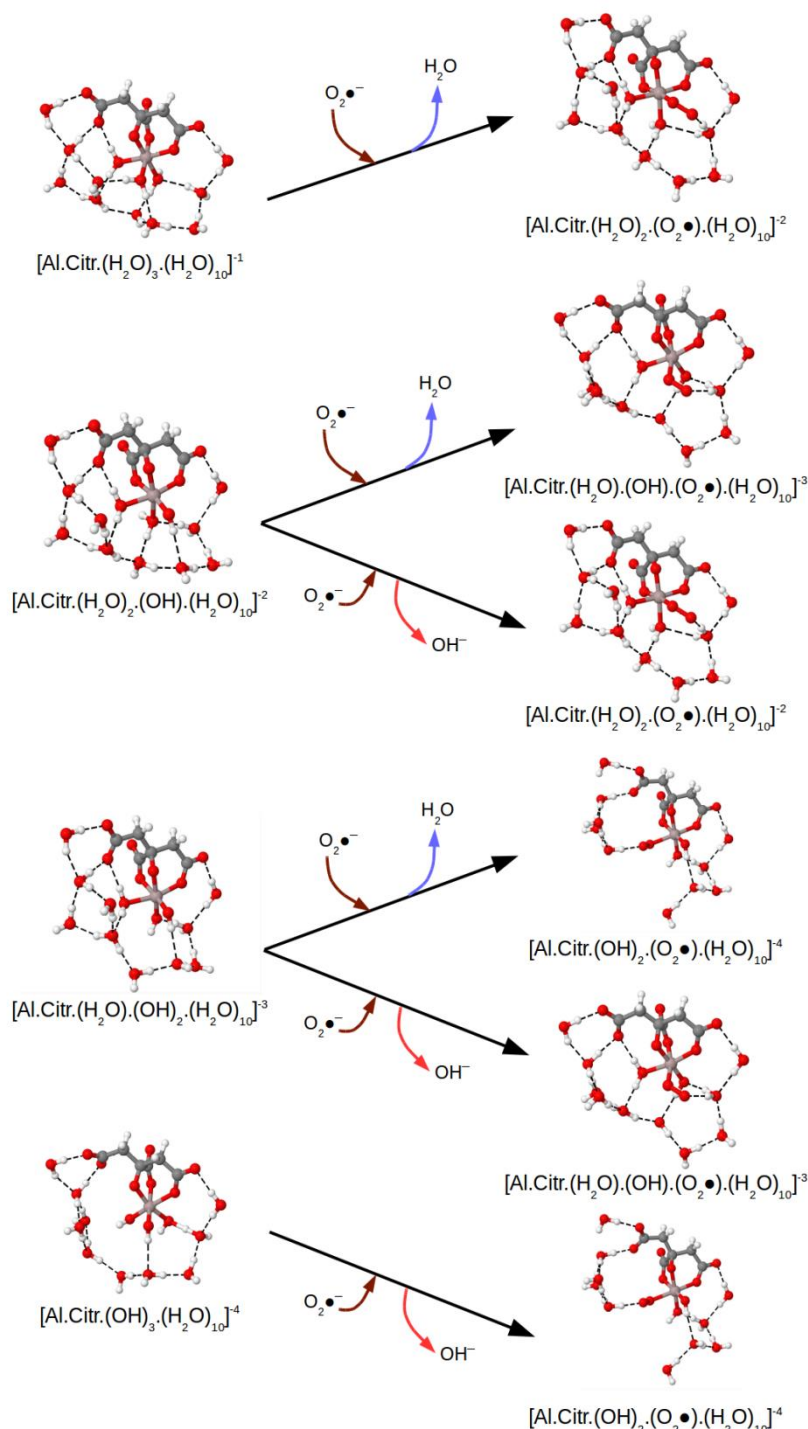
Fig. 6.2. Density Functional Theory structures optimized at B3LYP/6-31++g(d,p) level of theory. On the left, initial Al-Citr complexes with different number of H_2O/OH^- molecules (according to Equations 6.1 and 6.2). On the right, Al-Citr-O_2^- complexes formed by the substitution of either a H_2O or a OH^- molecule by O_2^-.

Different solvation models were considered for the aluminum-citrate complexes, varying in the number of water/hydroxide molecules. In all of them, aluminum presents an octahedral arrangement, with three of the six first coordination shell positions occupied by citrate, and three of them available for water or hydroxide molecules. All possible combinations were taken into account, giving rise to a total of four structures (see Fig. 6.2). In addition, our previous calculations demonstrated the importance of including the second solvation sphere explicitly in order to obtain reliable solvation energies[247]; therefore, ten water molecules were placed in the second coordination shell, mainly around the water/hydroxide molecules. All these structures are shown in Fig. 6.2.

We found that the substitution of a water molecule by the superoxide radical anion is thermodynamically favorable in solution, when at least two water molecules are found in the first coordination shell. Thus, the formation of $[\text{Al.Citr}(H_2O)_2(O_2^{\cdot})(H_2O)_{10}]^{-2}$ and $[\text{Al.Citr}(H_2O)(OH)(O_2^{\cdot})(H_2O)_{10}]^{-3}$ shows ΔG_{aq} values of -4.0 and -3.9 kcal/mol, respectively. In contrast, the ΔG_{aq} for the formation of $[\text{Al.Citr}(OH)_2(O_2^{\cdot})(H_2O)_{10}]^{-4}$ is positive, 6.2 kcal/mol. Thus, the amount of negatively charged groups in the first coordination shell influences the final stability of the aluminum-citrate-superoxide ternary complexes.

On the other hand, none of the substitution of an hydroxide anion by the superoxide radical is thermodynamically favorable. The formation of $[\text{Al.Citr}(H_2O)_2(O_2^{\cdot})(H_2O)_{10}]^{-}$ and $[\text{Al.Citr}(H_2O)(OH)(O_2^{\cdot})(H_2O)_{10}]^{-3}$ species show values of 16.5 and 14.0 kcal/mol, respectively. However, departing from the $[\text{Al.Citr}(OH)_3(H_2O)_{10}]^{-4}$ species, the formation of the $[\text{Al.Citr}(OH)_2(O_2^{\cdot})(H_2O)_{10}]^{-4}$ complex is less endoergic, with a ΔG_{aq} value of 4.1 kcal/mol.

In summary, as in the case of the absence of citrate, the interaction of superoxide with aluminum can lead to thermodynamically favorable species, with negative formation energies, only in the case of substitution of water molecules in the first-coordination shell around aluminum, whereas the substitution of hydroxides is highly unfavorable. As expected, the presence of other negatively-charged groups in the first-coordination shell of aluminum leads to less favorable formation of an aluminum-superoxide complex, both in binary and ternary compounds. In this sense, the presence of citrate, with a total charge of -4, has a sizable effect on the substitution reactions. The addition of more negative charge by the incorporation of a superoxide radical is energetically less favorable than in the absence of citrate. For instance, in the absence of citrate, the exchange of a water molecule with the superoxide shows a ΔG_{aq} value of -19.5 kcal/mol, while the same reaction in the presence of citrate shows a value of -4.0 kcal/mol. However, although the binding of aluminum to citrate makes less favorable the interaction of the metal with the superoxide, the formation of a ternary aluminum-citrate-superoxide complex is still thermodynamically favorable, and therefore a ternary complex of

this kind could also take part in the promotion of the Fenton reaction. In the next section, we evaluate how the inclusion of citrate influences the thermodynamics of the resultant redox reaction.

6.3.2 Fenton reaction

	ΔG_{aq}^{B3LYP}	$\Delta G_{aq}^{B3,wB97}$	ΔG_{aq}^{B3-D3}	$\Delta G_{aq}^{B3-D3,wB97}$
Absence of Citrate and Aluminum				
$[FeW_6]^{3+} + [O_2^*]^- \rightarrow [FeW_6]^{2+} + O_2$	-54.7	-57.8	-50.0	-55.7
Absence of Citrate[a]				
$[FeW_6]^{3+} + [AlW_5(O_2^*)]^{2+} \rightarrow [FeW_6]^{2+} + [AlW_5(O_2)]^{3+}$	-19.6	-16.7	-9.2	-12.7
$[FeW_6]^{3+} + [AlW_5(O_2^*)]^{2+} + H_2O \rightarrow [FeW_6]^{2+} + [AlW_6]^{3+} + O_2$	-30.0	-31.9	-30.5	-35.8
$[FeW_6]^{3+} + [Al(OH)W_4(O_2^*)]^+ + H_2O \rightarrow [FeW_6]^{2+} + [Al(OH)W_5]^{2+} + O_2$	-30.1	-33.7	-32.1	-37.4
$[FeW_6]^{3+} + [Al(OH)_2W_3(O_2^*)] + H_2O \rightarrow [FeW_6]^{2+} + [Al(OH)_2W_4]^+ + O_2$	-1.6	-3.9	-32.4	-38.4
Citrate interacting only with Aluminum				
$[FeW_6]^{3+} + [Al.CitrW_2(O_2^*)]^{-2} \rightarrow [FeW_6]^{2+} + [Al.CitrW_2(O_2)]^-$	-10.2	-4.8	-4.9	-2.6
$[FeW_6]^{3+} + [Al.CitrW_2(O_2^*)]^{2+} + H_2O \rightarrow [FeW_6]^{2+} + [Al.CitrW_3]^- + O_2$	-37.9	-30.6	-36.1	-41.2
$[FeW_6]^{3+} + [Al.Citr(OH)W(O_2^*)]^{3-} + H_2O \rightarrow [FeW_6]^{2+} + [Al.Citr(OH)W_2]^{2-} + O_2$	-40.6	-31.8	-36.5	-42.1
Citrate interacting only with Iron				
$[Fe.CitrW_3]^- + [AlW_5(O_2^*)]^{2+} \rightarrow [Fe.CitrW_3]^{2-} + [AlW_5(O_2)]^{3+}$	28.2	28.7	34.0	30.2
$[Fe.CitrW_3]^- + [AlW_5(O_2^*)]^{2+} + H_2O \rightarrow [Fe.CitrW_3]^{2-} + [AlW_6]^{3+} + O_2$	17.8	26.0	12.7	7.0
$[Fe.CitrW_3]^- + [Al(OH)W_4(O_2^*)]^+ + H_2O \rightarrow [Fe.CitrW_3]^{2-} + [Al(OH)W_5]^{2+} + O_2$	17.7	24.2	11.1	5.5
Citrate interacting with both Aluminum and Iron				
$[Fe.CitrW_3]^- + [Al.CitrW_2(O_2^*)]^{2-} \rightarrow [Fe.CitrW_3]^{2-} + [Al.CitrW_2(O_2)]^-$	37.7	40.7	38.3	40.3
$[Fe.CitrW_3]^- + [Al.CitrW_2(O_2^*)]^{2-} + H_2O \rightarrow [Fe.CitrW_3]^{2-} + [Al.CitrW_3]^- + O_2$	10.0	14.9	7.0	1.7
$[Fe.CitrW_3]^- + [Al.Citr(OH)W(O_2^*)]^{3-} + H_2O \rightarrow [Fe.CitrW_3]^{2-} + [Al.Citr(OH)W_2]^{2-} + O_2$	7.3	13.7	6.6	0.7

[a] Data taken from ref.[51].

Table 6.3. Reaction free energies in solution (in kcal/mol) evaluated for the reduction of Fe(III) in presence of different forms of the Al-O$_2^*$ or Al-Citr-O$_2^*$ complex. As reference, the Fenton reaction in absence of Al(III)

is also included. ΔG_{aq} values computed at the level of theories described in Methodology: B3LYP/TZ//B3LYP/DZ (ΔG_{aq}^{B3LYP}), wB97XD/TZ//B3LYP/DZ ($\Delta G_{aq}^{B3,wB97}$), B3LYP-D3/TZ//B3LYP-D3/DZ (ΔG_{aq}^{B3-D3}) and wB97XD/TZ/B3LYP-D3/DZ ($\Delta G_{aq}^{B3-D3,wB97}$).

Previously[56], it was shown that an aluminum-superoxide complex could promote thermodynamically the Fenton reaction by reducing Fe(III) (sextuplet spin state) to Fe(II) (pentuplet spin state) through the following redox reaction:

$$[Fe^{3+} + [Al(O_2^*)]^{2+} \longrightarrow Fe^{2+} + Al^{3+} + O_2 \qquad \textbf{(6.8)}$$
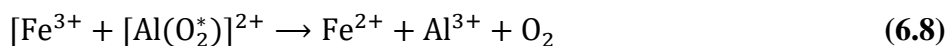
As shown in Table 6.3, this reaction is thermodynamically favorable with a ΔG_{aq} value of -30.5 kcal/mol when the superoxide is forming the $[Al(O_2^*)]^{2+}$ complex, and the reaction is even more favorable with the $[Al(OH)(O_2^*)]^+$ and $[Al(OH)_2(O_2^*)]$ species, -32.1 and -32.4 kcal/mol, respectively. Note that the reaction is significantly less exothermic than when O_2^* does not interact with Al(III) (-50.0 kcal/mol, see Table 6.3). Nevertheless, the formation of a stable Al(III)-O_2^* complex may increase the lifetime of O_2[52], a very reactive species, what ultimately favors the Fenton reaction[51]. Now, we analyze the effect in the thermodynamics of the redox reaction caused by the coordination of citrate to aluminum (Table 6.3).

Taking into account the most stable aluminum-citrate-superoxide ternary complex (Al.Citr(H$_2$O)$_2$(O$_2^*$)(H$_2$O)$_{10}$]$^{2-}$) as reference, the ΔG_{aq} value of reaction in Equation 8 is -36.1 kcal/mol, thus, 6 kcal/mol more stable than in the absence of citrate. A very similar exothermicity is found (ΔG_{aq} value of -36.5 kcal/mol) when the [Al.Citr(H$_2$O)(OH)(O$_2^*$)(H$_2$O)$_{10}$]$^{3-}$ complex is taken as reference. Thus, the formation of a ternary aluminum-citrate-superoxide complex favors the redox reaction that reduces Fe(III) to Fe(II). In this sense, the presence of citrate would enhance the ability of aluminum to promote the Fenton reaction. The reason for that behavior is that the presence of a highly-negative charged citrate in the coordination shell of aluminum makes the loss of an electron in superoxide, and therefore reduction of its negative charge, more likely.

However, citrate is not only a good chelator for aluminum in biological systems, but also a good chelator of Fe(III). In fact, the binding free energy of the citrate-Fe(III) complex is -133 kcal/mol, 10 kcal/mol more stable than those of the citrate-Al(III) complex. Therefore, we also investigated the possibility of iron reduction with complexes in which iron is also chelated to citrate. We consider two possibilities: i) reduction of Fe(III)-Citrate to Fe(II)-Citrate by an aluminum-superoxide binary species and ii) the reduction of Fe(III)-Citrate to Fe(II)-Citrate by an aluminum-citrate-superoxide ternary complex. In both cases and for all the complexes considered, the redox reaction is

thermodynamically unfavorable. For instance in the case that both iron and aluminum are chelated by citrate, the ΔG_{aq} value of the redox reaction 7 is 7.0 kcal/mol when the $[Al.Citr(H_2O)_2(O_2{}^*)(H_2O)_{10}]^{2-}$ complex is taken as reference, and 6.6 kcal/mol with $[Al.Citr(H_2O)(OH)(O_2{}^*)(H_2O)_{10}]^{3-}$. Therefore, the high stabilization of Fe(III) by citrate is a dominant factor with respect to the loss of an electron by the superoxide and stabilization of the aluminum-citrate complex. Thus, the chelation of iron by citrate has a protective effect with respect to the generation of Fe(II), and the promotion of Fenton reaction.

Overall from our calculations a complex picture emerges on the role of citrate in the thermodynamic promotion/inhibition of aluminum pro-oxidant activity, which is summarized in the scheme of Fig. 6.3. Aluminum hydrolytic species can form stable complexes with superoxide, leading to stable binary aluminum-superoxide and ternary aluminum-citrate-superoxide complexes. Both type of complexes have the ability to reduce Fe(III) to Fe(II) from a thermodynamic point of view. Moreover, the presence of citrate in ternary complexes promotes the loss of an electron from the superoxide, thus, increasing the iron-reduction ability of the aluminum ternary complexes with respect to binary ones. However, if iron is also chelated to citrate, the possibility of iron reduction is compromised, leading in all cases to endothermic redox reactions.
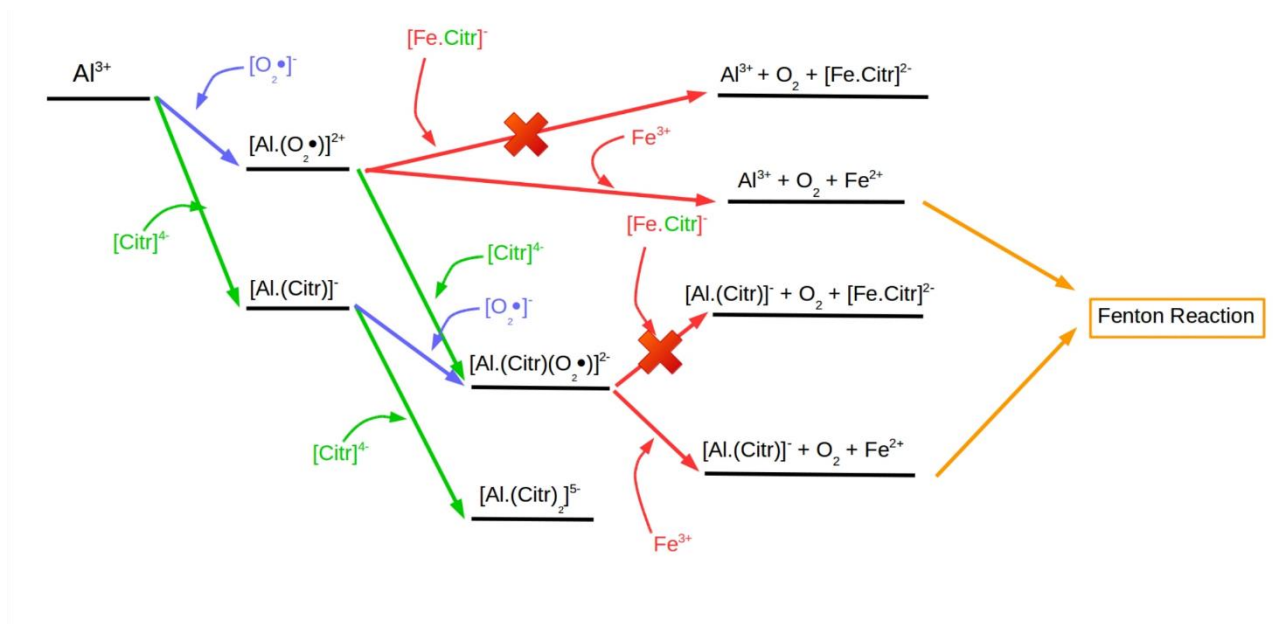
Fig. 6.3. Schematic representation of how citrate modulates the promotion of Fenton reaction by Al(III).

Finally, we should also take into account that in excess of citrate and formation of the $[Al-Citr_2]$ complex, in which all coordination positions of aluminum are occupied by citrate, there would be no

possibility of stabilization of superoxide by aluminum, and therefore, no possibility to reduce iron from the thermodynamic point of view.

Therefore, an overall sophisticated scenario is drawn from these calculations, where, depending on the type of complexes formed (binary/ternary), and the relative concentrations of citrate/aluminum/iron, one could observe a promotion or an inhibition of the pro-oxidant activity of aluminum. In addition, the reactions of oligonuclear and/or mixed hydroxo complexes of Al(III) can be extremely slow, resulting in long-lived non-equilibrium states of Al(III)-ligand complexes[20,83], which in the current context could imply that aluminum could exert its pro-oxidant activity from the ternary species characterized in this work, even at conditions in which there is an excess of citrate.

6.3.3 Delocalization Indices and ligand affinity

The effects of different functional groups considered herein (i.e. H_2O, OH^-, O_2^*, and the alkoxide and carboxylate groups of citrate) on the Al-O interactions are analyzed by calculating the delocalization indices (D.I.) for all the Al-O bonds in 17 structures: five aluminum hydrolytic species, five binary aluminum-superoxide complexes, four binary aluminum-citrate complexes and three ternary aluminum-superoxide-citrate complexes. Within each family of compounds, the complexes differ by the number of H_2O/OH^- ligands in the first solvation shell of aluminum. Most of the structures correspond to hexacoordinated species, but there are also examples of structures penta-($[Al(H_2O)_2(OH)_3]$) and tetra-coordinated ($[Al(OH)_4]^-$). In all cases, the structures consider a double layer of explicit waters around aluminum, embedded in an implicit solvation model. The results are summarized in Fig. 6.4 and in Table 6.4.

Delocalization indices (D.I.) are a measure of the degree of electron sharing between two atoms (see Methodology section). Although Al-O bonds are mainly electrostatic in nature, there are also important dative interactions[20] from the lone pair of the oxygen donors to the formally vacant 3s and 3p orbitals of Al(III). For functional groups/ligands of similar charge, like in the case of hydroxide, alkoxide, carboxylate and superoxide, the analysis of D.I. can help in the rationalization of the specific aluminum-binding affinities of the different oxygen donors. Among the 17 structures analyzed, we find a consistent pattern with the D.I. decreasing in the following order: $Al-OH^- > Al-CO^- > Al-COO^- > Al-O_2^{.-} > Al-H_2O$. There are several aspects to highlight in the following trends, which allow for a clear rationalization of the ligand affinities described in the previous sections.

The D.I. for $Al-O_2^{.-}$ bonds are the lowest among charged ligands/groups, but higher than that for water.

Aluminum Hydrolytic Species

Complex						
$[Al(H_2O)_6]^{3+}$	0.1614 (W)	0.1536 (W)	0.1383 (W)	0.1560 (W)	0.1507 (W)	0.1545 (W)
$[Al(H_2O)_5(OH)]^{2+}$	0.1476 (W)	0.1386 (W)	0.1454 (W)	0.1385 (W)	0.1378 (W)	0.2160 (OH)
$[Al(H_2O)_4(OH)_2]^{+}$	0.1269 (W)	0.1240 (W)	0.1130 (W)	0.1238 (W)	0.2075 (OH)	0.2428 (OH)
$[Al(H_2O)_2(OH)_3]$	0.1094 (W)	0.1081 (W)	0.2707 (OH)	0.2395 (OH)	0.2709 (OH)	
$[Al(OH)_4]^{-}$	0.2693 (OH)	0.2694 (OH)	0.2393 (OH)	0.2583 (OH)		

Aluminum-Superoxide Complexes

Complex							ρO_2^*	ρO_2^{*Al}
$[Al(H_2O)_5 O_2^*]^{2+}$	0.1561 (W)	0.1533 (W)	0.1459 (W)	0.1453 (W)	0.1515 (W)	0.1715 (SO)	0.6723	0.3164
$[Al(H_2O)_4(OH)O_2^*]^{+}$	0.1326 (W)	0.1344 (W)	0.1478 (W)	0.1444 (W)	0.2265 (OH)	0.1500 (SO)	0.6577	0.3251
$[Al(H_2O)_3(OH)_2 O_2^*]$	0.1217 (W)	0.1161 (W)	0.1320 (W)	0.2197 (OH)	0.2123 (OH)	0.1384 (SO)	0.6103	0.3828
$[Al(H_2O)(OH)_3 O_2^*]^{-}$	0.1148 (W)	0.2589 (OH)	0.2539 (OH)	0.2336 (OH)		0.1344 (SO)	0.6024	0.3880
$[Al(OH)_3 O_2^*]^{2-}$	0.2869 (OH)	0.2771 (OH)	0.2860 (OH)			0.1774 (SO)	0.6322	0.3599

Aluminum-Citrate Complexes

Complex						
$[Al.\,Citr(H_2O)_3]^{-}$	0.2232 (CA)	0.1645 (CCC)	0.1596 (CCT)	0.1240 (W)	0.1480 (W)	0.1333 (W)
$[Al.\,Citr(H_2O)_2(OH)]^{2-}$	0.2134 (CA)	0.1410 (CCC)	0.1417 (CCT)	0.1072 (W)	0.1097 (W)	0.2428 (OH)
$[Al.\,Citr(H_2O)(OH)_2]^{3-}$	0.1947 (CA)	0.1266 (CCC)	0.1305 (CCT)	0.0936 (W)	0.1894 (OH)	0.2197 (OH
$Al.\,Citr(OH)_3]^{4-}$	0.1845 (CA)	0.1125 (CCC)	0.1059 (CCT)	0.1930 (OH)	0.1996 (OH)	0.1593 (OH)

Aluminum-Superoxide-Citrate Complexes

Complex							ρO_2^*	ρO_2^{*Al}
$[Al.\,Citr(H_2O)_2 O_2^*]^{2-}$	0.2159 (CA)	0.1610 (CCC)	0.1574 (CCT)	0.1244 (W)	0.1348 (W)	0.1613 (SO)	0.5814	0.4012
$[Al.\,Citr(H_2O)(OH)O_2^*]^{3-}$	0.1985 (CA)	0.1455 (CCC)	0.1455 (CCT)	0.1111 (W)	0.2211 (OH)	0.1326 (SO)	0.5496	0.4310
$[Al.\,Citr(OH)_2 O_2^*]^{4-}$	0.1872 (CA)	0.1318 (CCC)	0.1263 (CCT)	0.2199 (OH)	0.1827 (OH)	0.1102 (SO)	0.5306	0.4484

Table 6.4. Delocalization Indices (in a.u.) obtained at the B3LYP/6-311++G(3df,2p) level of theory using the IEFPCM solvation model calculated for the Al-O interactions on aluminum complexes. The molecule of each oxygen atom is specified in parenthesis as: W: water (O^{H_2O}); OH: hydroxide (O^{OH}); SO: superoxide ($O^{O_2^*}$);

CA: citrate alkoxide (O^{CO}); CCC: citrate central carboxylate (O^{COOc}); citrate terminal carboxylate (CTC) (O^{COOt}). The Mulliken spin densities computed at the same level of theory for the two oxygen atoms of O_2^* are also reported (ρO_2^*), ρO_2^{*Al} referring to the O atom interacting with Al(III).
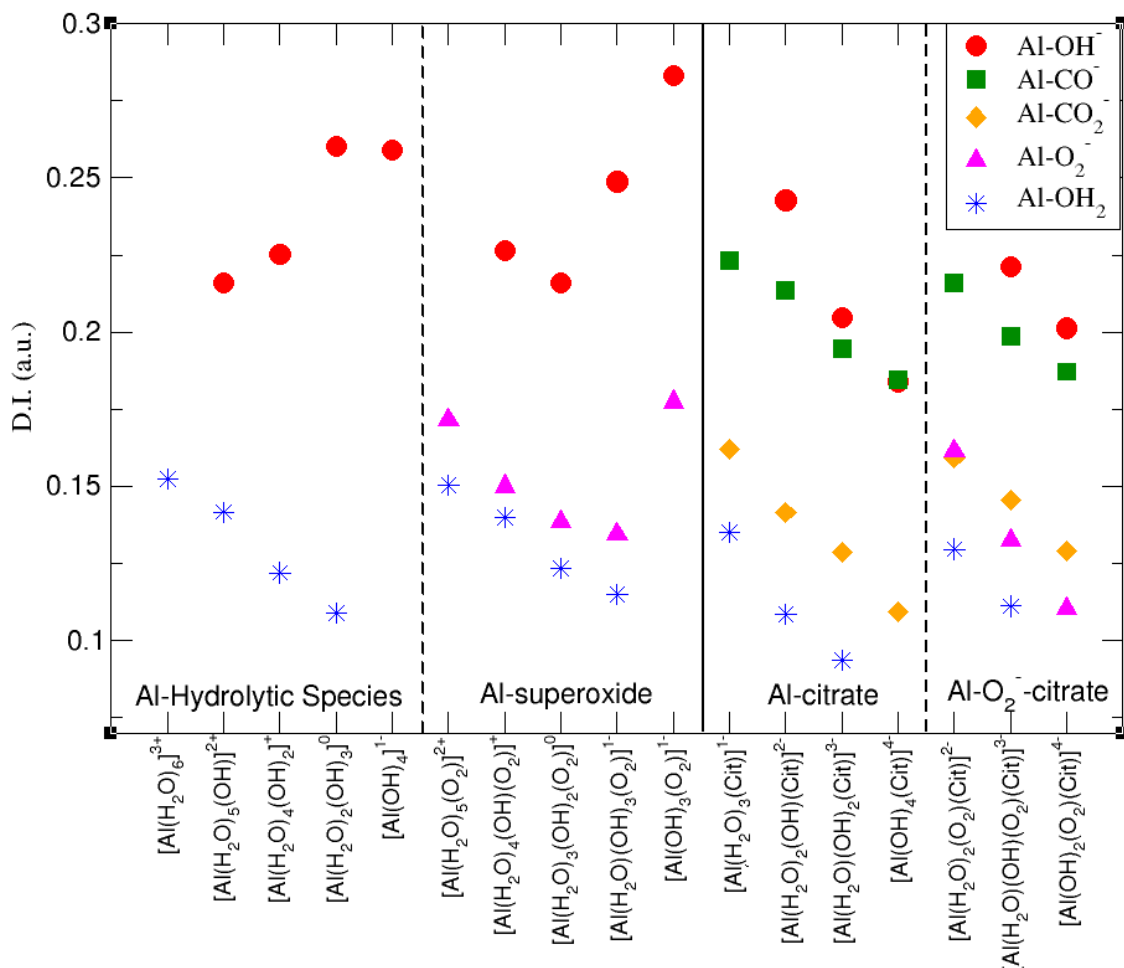
Fig. 6.4.: The delocalization indices for the Al-O bonds of various aluminum hydrolytic species, aluminum-superoxide and aluminum-citrate binary complexes and ternary aluminum-superoxide-citrate complexes with different number of H_2O/OH filling the first-coordination shell of aluminum. The D.I. are classified according to the different functional groups: hydroxide (Al-OH$^-$), alkoxide (Al-CO$^-$), acetate (Al-CO$_2^-$), superoxide (Al-O_2^*) and water (Al-OH$_2$). In the case that for a given structure several Al-O bonds with the same functional groups are present, the average value is provided in the figure.

This is in agreement with the favorable substitution of a water molecule by superoxide, and the unfavorable substitution of a charged ligand like hydroxide characterized in our previous work[51] and showed in Table 6.1.

On the other hand, the highest Al-O delocalization indices correspond to the interaction of aluminum with hydroxides, with alkoxide having similar but smaller values. This is in agreement with the fact that hydrogen being less electronegative than carbon, makes OH^- to be a better Lewis base than alkoxide.

However, the D.I. for carboxylate groups are substantially lower, due to the resonance of the COO^- moiety, which leads to a less dative oxygen. Finally, considering superoxide, the higher electronegativity of oxygen compared to carbon and hydrogen makes O_2^- the poorest Lewis base among the charged functional groups/ligands of the present work.

We should also remark that the strong $Al-OH^-$ interaction characterized in our structures is in agreement with the inherent stability of hydroxides at the first solvation layer around aluminum[279]. Moreover, the presence of hydroxides has a sizable effect on the strength of the rest of Al-O bonds with other ligands and functional groups, leading to a weakening of the rest of Al-O bonds, and therefore, a lowering of their D.I.. This is also in agreement with the known fact that the presence of hydroxides leads to a depleting of the toxicity of aluminum, by hindering the direct interaction of aluminum with bioligands. This leads to a low toxicity of aluminum at neutral pH at the limit of chemical equilibrium, i.e., when all aluminum is in the $[Al(OH)_4]^-$ form. However, as Exley et al.[83] has established, one should always bear in mind that non-equilibrium aluminum species could be highly relevant in the biological effects of this metal.

Finally, when we compare similar structures in the presence or in the absence of citrate, we encounter that the presence of citrate leads consistently to lower D.I. for aluminum-superoxide bonds, in agreement with the lower affinity for superoxide displayed by aluminum-citrate complexes with respect to aluminum hydrolytic species. However, the D.I. of superoxide are still higher than the ones of water, and therefore the displacement of a water molecule by a O_2^* remains favorable. This decrease in aluminum-superoxide interaction with the presence of citrate also explains the fact that the aluminum-citrate-superoxide ternary complex is a better reductant than an aluminum-superoxide binary complex, since the loss of an electron and therefore the loss of an aluminum-superoxide interaction is energetically less unfavorable for the former than for the latter.

Similar conclusions can be reached based on the analysis of the Mulliken spin densities (ρ) at the two oxygen atoms of the O_2^* molecule. It should be pointed out that the spin densities computed based on the Mulliken atom partition are physically unsound, but they can be useful to determine qualitatively where the radical character is located and to describe trends in similar structures. The spin densities at the two oxygen atoms of O_2^* are shown in Table 6.4. For instance, the ρ values at the two oxygen atoms of O_2^* in the $[Al(H_2O)_5(O_2^*)]^{2+}$ structure are 0.6723 and 0.3164. So, the sum of these two values is approximately 1, but the spin density is mainly located at the O atom not interacting with

Al(III). In other words, the molecule is highly polarized by the cation. However, the ρ values computed on other structures show that: 1) the inclusion of OH$^-$ radicals on the Al(III) first coordination shell leads to a small but consistent decrease of the polarization, and b) this effect is more effective when Al(III) interacts with citrate.

6.4 Conclusions

We have presented a thorough computational study on the influence of citrate, the main low-molecular-mass chelator of aluminum, on the pro-oxidant activity of this metal. We have found that from the thermodynamic point of view stable ternary aluminum-citrate-superoxide complexes can be formed in aqueous solution, which can in turn promote the Fenton reaction by reducing Fe(III) to Fe(II). The presence of citrate has a two-fold effect: it reduces the affinity of aluminum towards superoxide, although it is still thermodynamically favorable to form aluminum-citrate-superoxide compounds, and thermodynamically, it favors the redox reaction in which iron is reduced from Fe(III) to Fe(II). However, we also found that citrate has a protective role in two ways: if iron is linked to citrate, the Fe(III) oxidation state is highly stabilized, and the reduction of iron is not longer thermodynamically favorable, irrespective of whether we depart from an aluminum-superoxide binary complex or an aluminum-superoxide-citrate ternary one. In addition, in excess of citrate the formation of very stable 1:2 aluminum-citrate compounds is predicted to outcompete thermodynamically the formation of aluminum-superoxide-citrate complexes. In conclusion, we would like to remark that the use of delocalization indices, and in general of the QTAIM theory, is a powerful tool for the clear and full rationalization of the observed trends in complex stability, allowing us to establish an order of affinity of aluminum towards the different functional groups/ligands analyzed in the present work: Al-OH$^-$ > Al-CO$^-$ > Al-COO$^-$ > Al-O$_2^-$ > Al$-$H$_2$O.

The interaction of aluminum with catecholamine-based neurotransmitters: can the formation of these species be considered a potential risk factor for neurodegenerative diseases?

Gabriele Dalla Torre, Jon I. Mujika, Joanna I. Lachowicz, Maria J. Ramos and Xabier Lopez. *Dalton Trans.,* **accepted.**

The interaction of aluminum with catecholamine-based neurotransmitters: can the formation of these species be considered a potential risk factor for neurodegenerative diseases?

7.1 Introduction

The possible toxicity of aluminum is a highly controversial issue[3]. Although scientific literature on the adverse health effects of aluminum is extensive[5,14,49], the exact molecular mechanisms of aluminum toxicity are not sufficiently understood[59,61]. Among the possible detrimental effects of aluminum, we can mention the promotion of oxidative stress[51,52,56], the inhibition of the normal function of several enzymes (such as hexokinase[184], glutamate dehydrogenase[185-187], etc), the interference with several key cell metabolism cycles[188-190], as well as alteration of the structure and chemistry of important metabolites[115,186] and cofactors[42]. Moreover, since it has been pointed out that aluminum can cross the blood-brain barrier and accumulate in cerebral tissues[63], special concerns have been raised on the possibility of local toxic effects caused by the presence of the aluminum ion. In fact, aluminum is widely recognized as a potential neurotoxic element[191]. Early studies supported this hypothesis, linking aluminum to the formation of neurofibrillary tangles (NFT)[192], and more recent experimental and theoretical studies have underlined the ability of aluminum to bind to phosphorylated peptides[66,193] and to promote hyperphosphorylation of normal neurofilaments[194]. In addition, the ability of aluminum to contribute to Aβ-amyloid aggregation has been recently demonstrated[48,49,256], and growing evidence is linking aluminum as a decisive contributing factor in Alzheimers disease[4,5].

Another proposed route for aluminum neurotoxicity is the alteration of signaling processes in which neurotransmitters are somehow affected by the presence of this exogenous metal. Due to the possibility of aluminum to bind catechols, that bear two of the hardest Lewis base oxygen donors to Al(III)[20], an obvious target would be catecholamine-based neurotransmitters[7,22,195-197]. As a matter of fact, it has been shown that aluminum affects the signaling process mediated by these neurotransmitters[198], altering their content in animal models[195], and interfering with enzymatic activities in which these neurotransmitters are involved[76].

Catechol-aluminum interactions have been extensively studied in the framework of aluminum chelation therapy[6,16,20,21,94], because of their strong binding affinity towards high valence metals and

their low molecular mass. Although several experimental efforts have been made in this sense, the clear and complete understanding of the properties and behavior of these metal-ligand complexes is still a challenging task. Accordingly, computational chemistry has raised as a very powerful tool to complement the available experimental data and help towards their rationalization and clear understanding. The use of *state-of-the-art* theoretical approaches can provide fundamental knowledge and valuable insights on the properties of these systems, unattainable by other means. In this sense, we have recently proposed and applied a validated computational protocol[21] to account for the binding affinity of a wide set of catechols and salicylates towards Al(III), finding a good qualitative agreement with respect to experimental stability constants. Moreover, the use of the Bader's Quantum Theory of Atoms in Molecules (QTAIM) and the Energy Decomposition Analysis (EDA) approach allowed us to characterize the *physico*-chemical features of the Al-O bonds and rationalize the effects of different substituents towards the modulation of the binding affinities. In this sense, we have stressed how electron withdrawing/donating effects can modulate the strength of the Al-O bonds by means of their efficient transmission through the aromatic rings of these compounds[21].

In the present work, we apply a similar methodology to investigate the stability of complexes formed by aluminum and catecholamine-based neurotransmitters (Fig. 7.1). Four catecholamines are considered in different metal-ligand stoichiometries: L-DOPA, dopamine, noradrenaline (norepinephrine) and adrenaline (epinephrine). Furthermore, and more importantly, we carefully analyze the proton/aluminum ion competition for the binding to these neurotransmitters, comparing our results with those previously published for catechol and 4-nitrocatechol[21], as well as other known low-molecular-mass (LMM) Al(III) chelators such as citrate, deferiprone (1,2-dimetil-3-hydroxy-4(1H)-piridinone) and ethylenediaminetetraacetic acid (EDTA) (Fig. 7.1). In particular, citrate was chosen as a reference compound of endogenous aluminum chelators because of its well established high affinity for Al(III) in human serum[36,39,280]; deferiprone was chosen as reference of exogenous Al(III) chelators since it is the most efficient LMM drug currently employed in aluminum and iron chelation therapy[6,28]. Finally, the choice of EDTA as reference compound is due to its high affinity for trivalent and divalent metal ions, which is also the reason of its controversial role in chelation therapy[112,114]. It is important to note that these polydentate ligands span different binding modes (tridentate for citrate, bidentate for deferiprone and hexadentate for EDTA, Fig. 7.1), leading to different stoichimetric complexes with different entropic contributions, therefore are very suitable choices to compare the thermodynamics of formation of catecholamines.

Our results show that, although the formation of different Al-catecholamines complexes show favourable complexation energies compared to catechol, due to the electron withdrawing (EW) effect of the positively charged amino group, the overall stability is not competitive with the formation of

other species in solution. Indeed, Al-catecholamine complexes can only barely compete, from a thermodynamic point of view, with the formation of $[Al(OH)_4^-]$ species in solution, in agreement with the available experimental data. Al-hydroxide is widely recognized as the most stable Al(III) hydrolytic species at physiological pH[7,22]. Moreover, in an open biological environment, the formation of Al-catecholamine complexes is not as stable as the formation of other metal-ligand complexes such as Al-citrate, Al-Defriprone and Al-EDTA.

In summary, we rule out the possibility that the interaction of aluminum with these neurotransmitters in an open biological environment could explain the experimentally assessed toxic effects of Al(III) with neuronal processes involving catechol-based neurotransmitters. Other possibilities are examined and discussed in light of an up-to-date view of the catecholamines biosynthesis pathway.
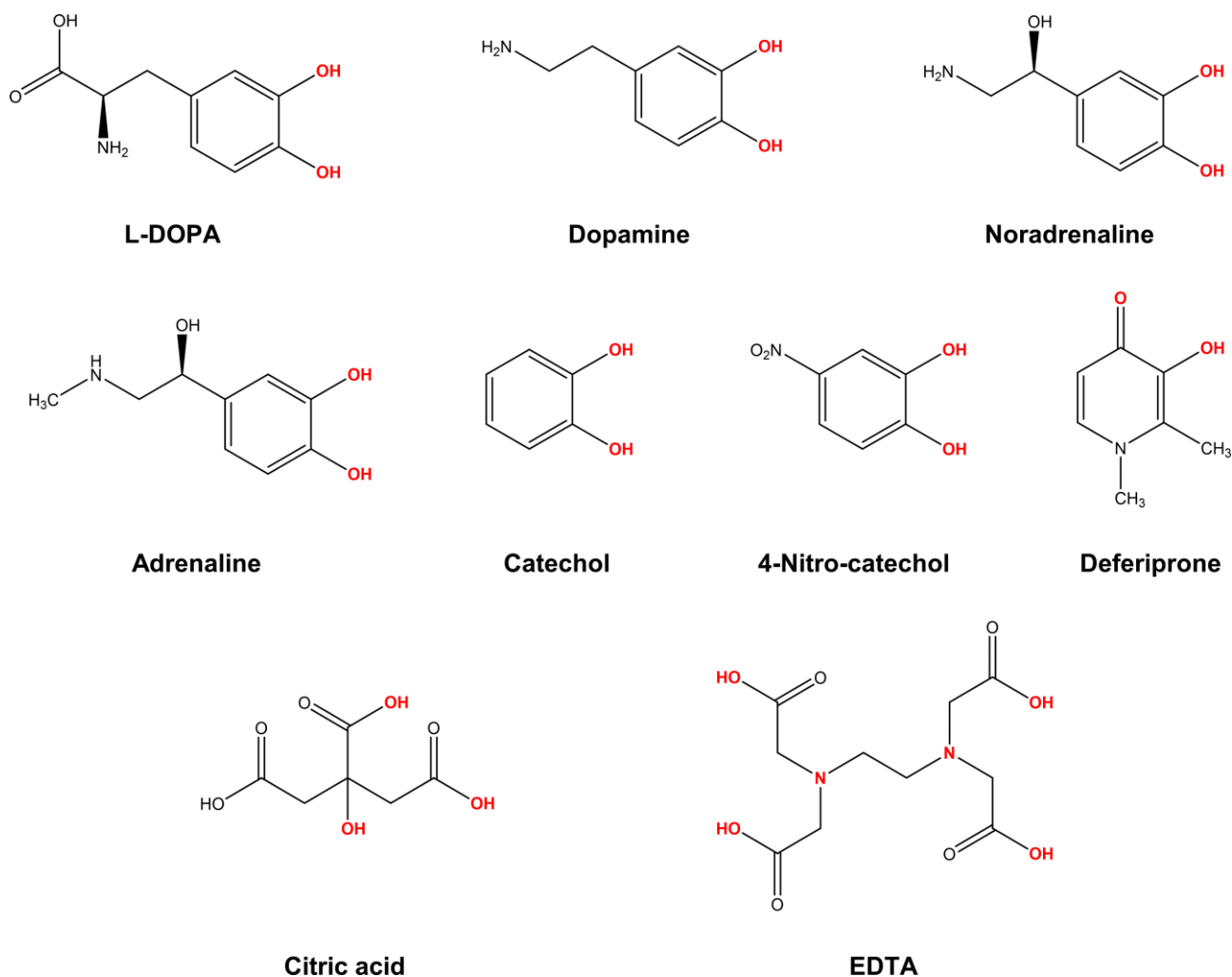
Fig. 7.1. Structures of the compounds considered in the present work: L-DOPA, dopamine, noradrenaline (norepinephrine), adrenaline (epinephrine), catechol, 4-nitro catechol, deferiprone (Ferriprox®), citric acid, ethylenediaminetetraacetic acid (EDTA). In red, atoms that form the aluminum coordination site.

7.2. Methodology

7.2.1 Cluster-continuum approach

In order to investigate the thermodynamics of these Al-catecholamine complexes, a cluster-continuum approach is employed[115,204,205]. The first coordination shell of aluminum is surrounded by explicit water molecules in an octahedral fashion; the effect of the remaining solvent is treated using the self-consistent reaction field (SCRF) method with the polarized continuum model (PCM), using the integral equation formalism variant (IEFPCM)[177]. All geometrical optimizations were carried out in aqueous phase using the Gaussian 16 Rev.A03 suite of programs[276], the B3LYP functional[132,259] and 6-31++G(d,p) basis set. Additionally, we added Grimme's D3 dispersion correction[153], along with the Becke-Johnson (BJ) damping function[274], that was shown to further increase accuracy[155,156,281].

To confirm that the optimized structures were real minima on the potential energy surfaces, frequency calculations were carried out at the same level of theory. All structures showed positive force constants for all the normal modes of vibration. The frequencies were then used to evaluate the zero-point vibrational energy (ZPVE) and the thermal ($T = 298$ K) vibrational corrections to the enthalpies and Gibbs free energies within the harmonic oscillator approximation. To calculate the entropy, the different contributions to the partition function were evaluated using the standard statistical mechanics expressions in the canonical ensemble and the harmonic oscillator and rigid rotor approximation.

The electronic energies were refined by single-point energy calculations at the B3LYP-D3(BJ)/6-311++G(3df,2p) level of theory. Single point calculations with other dispersion corrected DFT functionals, as well as MP2, were also performed to validate the methodology, with similar results (Appendix C).

7.2.2 Definition of binding affinities

We characterized Al(III)-Lig complexes with 1:1, 1:2 and the 1:3 stoichiometry. The formation stability of these complexes was studied following the ligand substitution reaction shown in (eq. 7.1):

$$\text{Al(H}_2\text{O)}_6]^{3+}_{(aq.,1M)} + \text{L}^{-q}_{r(aq.1M)} \rightleftarrows \text{Al(H}_2\text{O)}_{6-m}\text{L}_r]^{3-q}_{(aq,1M)} + m\text{H}_2\text{O}_{(aq,1M)} \qquad \textbf{(7.1)}$$
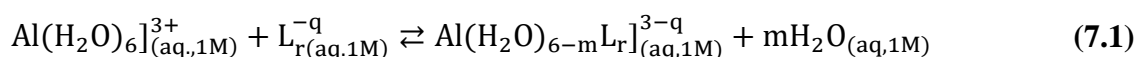
where q is the net charge of the ligand L, r is the number of ligands and m depends on the stoichiometry of the complex, such as $m=2$, $m=4$ and $m=6$ for 1:1, 1:2 and 1:3 complexes, respectively. Notice that we consider the ligand's coordinating groups in their unprotonated form, which is the state considered when evaluating experimental logβ.

The enthalpy in solution corresponding to the binding of the ligand to Al(III) is therefore calculated as:

$$\Delta H_{aq}^{comp} = H_{aq}Al(H_2O)_{6-m}L_r + mH_{aq}(H_2O) - H_{aq}[Al(H_2O)_6] - H_{aq}(L)_r \\ + \Delta nRTln(24.46)$$

(7.2)

Since the enthalpies are determined using an ideal gas at 1 atm as the standard state, the last term in eq. (7.2) corresponds to the volume change due to the transformation from 1 atm to 1 M in solution, where Δn refers to the change in the number of species in the reaction[207]. In a similar way, the free energy of the complexes is determined as:

$$\Delta G_{aq}^{comp} = G_{aq}Al(H_2O)_{6-m}L_r + mG_{aq}(H_2O) - G_{aq}[Al(H_2O)_6] - G_{aq}(L)_r \\ + \Delta nRTln(24.46) + mRTln(55.34)$$

(7.3)

where the last term is the entropic factor that accounts for the concentration of 55.34 M of water in liquid water[207].

In order to take into account the influence of the protonation constants at the coordination site, we also define a free energy at physiological pH values that takes into account the energy penalty associated to the deprotonation of the two phenoxide groups of these catechol-based ligands at physiological pH (7.4), defined as:

$$\Delta G_{aq}^{Phys} = \Delta G_{aq}^{comp} + \Delta G_{aq}^{deprot}$$

(7.4)

The last term in Eq. 4 corresponds to the free energy of deprotonation of a given ligand at physiological pH (7.4). This is calculated according to the experimental values for the titratable groups (phenolate) of the ligands. pK_a values for catechol and 4-nitro catechol were taken from ref.[94]; for L-DOPA, dopamine, noradrenaline and adrenaline were taken from ref.[196].

$$\Delta G^{deprot} = 2.303RT \sum_i (pK_a^i - pH)$$

(7.5)

where pK_a^i is the experimental pK_a and pH is taken as 7.4.

7.2.3 Al-ligand formation energies

A strategy to take into account the aluminum ion/proton competition for the ligand's binding site is presented. Formation energies for aluminum-ligand complexes of different stoichiometries were considered according to the general equilibria:

$$Al(H_2O)_6^{3+} + L_{nH}^0 \rightarrow AlL(H_2O)_{6-m}^+ + nH_3O^+ + (m-n)H_2O \qquad (7.6)$$
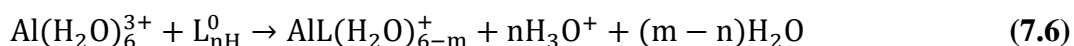
Where n is the number of protons in the coordination site of a given ligand at physiological pH; m depends on the stoichiometry and the binding mode (bidentate, tridentate, hexadentate) of the ligand considered (Table 7.2).

As pointed out by Jensen[30], the calculation of binding energies in solution is a challenging task from a computational point of view. This is mainly due to the inaccurate prediction of solvation energies of small charged ions with continuum solvation models such as IEFPCM. In order to alleviate this problem, the Gibbs free energies of the hydronium and hydroxide ions were calculated as:

$$G_{aq}(H_3O)^+ = G_{gas}(H_3O)^+ + \Delta G_{solv}(H_3O)^+ \qquad (7.7)$$

$$G_{aq}(OH)^- = G_{gas}(OH)^- + \Delta G_{solv}(OH)^- \qquad (7.8)$$

Where G_{gas} is calculated at the DFT level; ΔG_{solv} are the experimental solvation energies of the hydronium and hydroxide ions (-103.45 and -106.40 kcal/mol, respectively) taken from ref.[282].

Moreover, a correction term in the free energies is introduced to account for the pH as:

$$G_{pH} = m(-pH)RTLn(10) \qquad (7.9)$$

where physiological pH is 7.4 and m is the number of hydroniums.

In the case of the calculation of the formation free energy of $[Al(OH)_4^-]$ hydrolytic species a similar correction term was introduced to account for pOH:

$$G_{pOH} = m(-pOH)RTLn(10) \qquad (7.10)$$

7.2.4 pAl calculation

Experimental pAl values of L-DOPA, dopamine, noradrenaline and adrenaline were calculated by means of the Hyperquad simulation and speciation (HySS) program[283] using speciation data from ref.[196].

7.2.5 QTAIM and Delocalization Indices (D.I.)

The Quantum Theory of Atoms in Molecules (QTAIM)[208] was used to perform a topological analysis of the electron density, providing the critical points of the electron density and the atomic boundaries that define the atomic partition of the molecular space. The so-called bond critical points (BCP) are saddle points of the electron density that usually occur between two bonded atoms and provide important information about the nature of the bonding. Closed-shell interactions (such as van der Waals, ionic and hydrogen bonds) and metal-metal interactions are characterized by small values of the density, charge depletion and positive energy densities (i.e., small $\rho(r_{BCP})$, $\nabla^2\rho(r_{BCP}) > 0$ and $H(r_{BCP}) > 0$). Conversely, covalent interactions are characterized by large electron density values, charge concentration and negative energy densities (i.e., large $\rho(r_{BCP})$, $\nabla^2\rho(r_{BCP}) < 0$ and $H(r_{BCP}) < 0$)[208,214,216]. However, it has been pointed out that for some interactions which may be classified as covalent bonds, the Laplacian is positive and the total energy density at the BCP ($H(r_{BCP})$) is negative. Such a situation is often observed for strong AH···B hydrogen bonds classified as partly covalent in nature ($H(r_{BCP}) < 0$)[284].

Delocalization Indices (D.I.) are a measure of the covariance between the population of two atoms A and B and, consequently, a measure of the number of electrons simultaneously fluctuating between these atoms[248,249],

$$\delta(A,B) = \int_A \int_B d\,1d2\rho_{xc}(1,2) = cov(N_A, N_B) \tag{7.11}$$

where $\rho_{xc}(1,2)$ is the exchange-correlation density[277]. It can be taken as the number of electron pairs shared between atoms A and B, i.e., the bond order[278].

The AIMAll v11.08.23 program[250] was used to carry out the QTAIM analysis on the previously optimized structures at the B3LYP-D3(BJ)/6-311++G(3df,2p) level of theory.

7.2.6 Energy Decomposition Analysis (EDA)

The energy decomposition analysis (EDA) is a state-of-the-art tool for a quantitative interpretation of chemical bonds[285]. The EDA scheme based on the theory developed by Ziegler and Rauk[210] and by Morokuma[209] was carried out using the ADF2017 suite of programs. In order to perform the EDA analysis, all 1:1 Al-ligand complexes previously optimized at the B3LYP-D3(BJ)/6-31++G(d,p) IEFPCM level with Gaussian16 were split in two fragments: the aluminum ion surrounded by four water molecules and the unprotonated ligand. Single-point energies for the EDA analysis were calculated using the B3LYP-D3(BJ) functional and the very robust full electron even-tempered quadruple-ζ basis set[176,286] (ET-QZ3P-1DIFFUSE) provided by ADF2017[287-289]. All EDA calculations were performed in gas phase.

The EDA decomposes the instantaneous interaction energy ΔE_{int} between two fragments A and B in a molecule AB into three well defined terms that can be interpreted in chemical meaningful ways:

$$\Delta E_{int} = \Delta E_{elstat} + \Delta E_{Pauli} + \Delta E_{oi} \tag{7.12}$$

These terms are (1) the quasi-classical electrostatic interaction energy between the charge densities of the fragments, ΔE_{elstat} (2) the exchange/repulsion between the fragments due to Pauli's principle, ΔE_{Pauli}, and (3) the energy gain due to orbital mixing of the fragments, ΔE_{oi}.

Considering that EDA calculations are usually carried out in the framework of density functional theory, if an explicit correction term for dispersion interaction is employed (such as Grimme's D3 method), then EDA numerical results remain unchanged but the dispersion correction appears as an extra term:

$$\Delta E_{int} = \Delta E_{elstat} + \Delta E_{Pauli} + \Delta E_{oi} + \Delta E_{disp} \tag{7.13}$$

7.3 Results and discussion

7.3.1 Binding affinities of 1:1, 1:2 and 1:3 Al-catecholamines with respect to reference catechol

In Fig. 7.2, we depict the structures characterized in the present work for 1:1, 1:2 and 1:3 aluminum-catecholamines complexes along with our previously determined structures for catechol and 4-nitro catechol ligands[21]. Very similar structures are obtained with respect to catechol, indicating that the

different amine substituents have a little effect on the coordination mode of aluminum to the catechol moiety.

In Table 7.1, we can find the binding energies of catecholamines compared to catechol and 4-nitro catechol chosen as reference structures of our previous work[21]. Two states have been considered for the amino group: protonated and unprotonated. Although the estimation of Kiss et al.[196] is that at physiological pH these amines will be protonated, we have decided to consider both possibilities in order to gain more insights into the thermodynamics of binding energies and the role played by the positively charged amino group. It is worth to emphasize that the theoretical methodology employed in this work has been recently thoroughly validated for a wide dataset of catechols and salicylates using different density functionals, the MP2 method and experimental data[21]. In Fig. 7.3, we compare the binding free energies, ΔG_{aq}^{comp}, of the catecholamines along with the previously obtained values for catechol and 4-nitro catechol with respect to experimental stability constants (logβ) finding a remarkable good correlation coefficient of 0.9909, which confirms the validity of our approach. It is important to mention, at this stage, that experimental logβ values were taken from two different sources: those of catecholamines from an old paper by Kiss et al.[196] and those of catechol and 4-nitro catechol from a more recent paper by Nurchi et al.[94]. Binding energies with different functionals (M06-2X[290] and ωB97X-D[275]) as well as the MP2 method[291,292] can be found in Appendix C giving very similar correlation coefficients when compared with experimental stability constants.

We first discuss results for N-protonated catecholamines, as this is the most likely situation at physiological pH. In general, catecholamines show lower ΔG_{aq}^{comp} (in absolute values) than catechol, in agreement with the lower experimental stability constants (Table 7.1). However, these binding affinities are higher than the one of 4-nitro catechol; this compound was chosen as reference system to evaluate the electron withdrawing (EW) effect of substituents in the catechol ring. Accordingly, the introduction of a positively charged amino tail in catecholamines has an EW effect, which is smaller than the one provoked by the 4-nitro substituent. This can be explained considering that, as assessed in our previous work[21], the strong EW effect of the NO_2 group added to a catecholate ring is mediated through both resonance and inductive mechanisms of action. On the other hand, the EW effect of the protonated amino group of catecholamines is mediated only by the electron attracting behavior of the positive charge. Among catecholamines, L-DOPA and dopamine show, in general, higher ΔG_{aq}^{comp} than adrenaline and noradrenaline. In this sense, we should bear in mind that protonated L-DOPA has a higher total negative charge (-2) than the rest of catecholamines (-1) due to the presence of the carboxylate group (Fig. 7.1); therefore, its interaction with the trivalent

1:1 Al-(L-DOPA) **1:2 Al-(L-DOPA)** **1:3 Al-(L-DOPA)**

1:1 Al-Dopamine **1:2 Al-Dopamine** **1:3 Al-Dopamine**

1:1 Al-Noradrenaline **1:2 Al-Noradrenaline** **1:3 Al-Noradrenaline**

1:1 Al-Adrenaline **1:2 Al-Adrenaline** **1:3 Al-Adrenaline**

1:1 Al-Catechol **1:2 Al-Catechol** **1:3 Al-Catechol**

1:1 Al-(4-Nitro-catechol) **1:2 Al-(4-nitro-catechol)** **1:3 Al-(4-Nitro-catechol)**
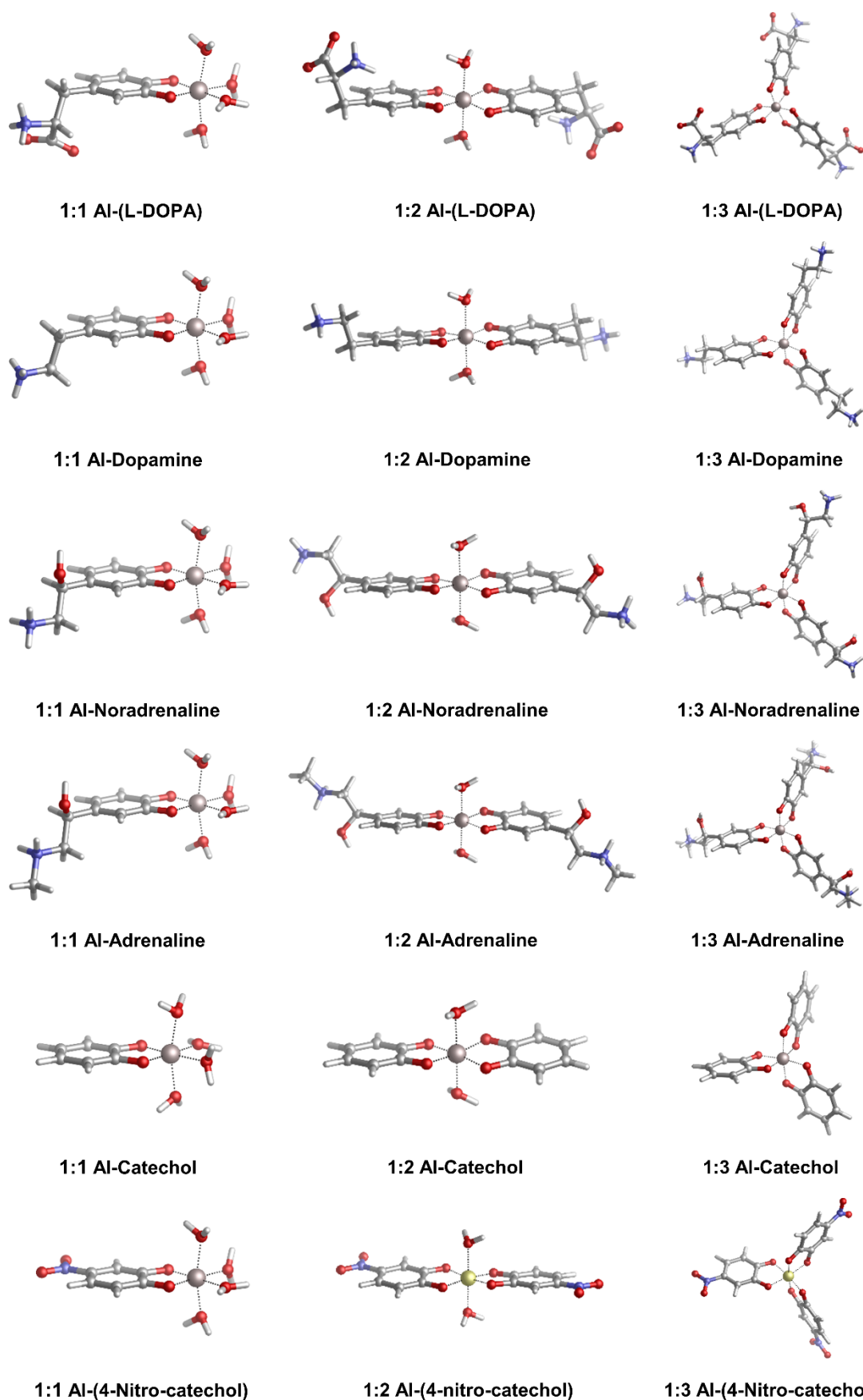
Fig.7.2. Optimized geometries in aqueous solution of 1:1, 1:2 and 1:3 complexes of aluminum with L-DOPA, dopamine, noradrenaline (norepinephrine), adrenaline (epinephrine), catechol and 4-nitro catechol.

		Theoretical						Experimental[a]		
		ΔH_{aq}^{comp}	ΔG_{aq}^{comp}	ΔG_{aq}^{Phys}	ΔH_{aq}^{comp}	ΔG_{aq}^{comp}	ΔG_{aq}^{Phys}	$\log\beta$	$\log\beta_{Cond.}$	pAl
Ligands		*Protonated Amine*			*Unprotonated Amine*					
L-DOPA	1:1	-88.3	-92.8	-82.7	-91.8	-95.2	-81.9	16.0	8.1	
	1:2	-160.0	-166.6	-146.4	-160.3	-165.6	-138.8	29.2	13.3	10.8
	1:3	-182.8	-193.5	-163.3	-187.7	-195.7	-155.5	38.4	14.5	
Dopamine	1:1	-85.7	-88.6	-78.8	-89.5	-92.8	-78.9	15.6	8.0	
	1:2	-148.4	-154.7	-135.1	-153.6	-161.6	-133.8	28.6	13.4	10.8
	1:3	-181.8	-190.0	-160.6	-186.2	-195.2	-153.5	37.6	14.7	
Noradrenaline	1:1	-83.1	-87.2	-77.8	-88.3	-91.8	-79.8	15.6	8.3	
	1:2	-143.0	-150.7	-131.8	-148.5	-157.0	-133.0	28.6	14.0	11.4
	1:3	-177.5	-186.1	-157.7	-179.2	-189.8	-153.8	37.9	16.0	
Epinephrine	1:1	-83.0	-87.2	-78.1	-88.2	-91.5	-78.7	15.6	8.2	
	1:2	-143.0	-150.7	-132.5	-146.4	-154.6	-129.3	28.6	13.9	11.3
	1:3	-176.4	-187.2	-159.2	-178.4	-186.3	-148.0	37.9	15.8	
Catechol	1:1	-88.4	-91.4	-79.6				16.3	8.2	
	1:2	-151.8	-157.7	-134.1				31.7	13.2	10.1
	1:3	-183.1	-191.7	-156.6				41.1	13.5	
4-nitro Catechol	1:1	-71.6	-75.8	-71.2				13.3	-	
	1:2	-124.0	-130.8	-121.7				24.8	-	14.2
	1:3	-183.1	-164.6	-150.8				33.7	-	

Table 7.1. DFT binding enthalpies (ΔH_{aq}^{comp}), binding energies (ΔG_{aq}^{comp}) and physiological binding energies (ΔG_{aq}^{Phys}) with available experimental stability constant ($\log\beta$, $\log\beta_{Cond}$) and pAl data for the whole dataset of catechol-based ligands. Notice that cumulative stability constants ($\log\beta$) are comparable with ΔG_{aq}^{comp}, while conditional stability constants ($\log\beta_{Cond}$) are comparable with ΔG_{aq}^{Phys}, since the last two quantities take into account the influence of protonation constants. [a]Experimental pK_a and parameters values for L-DOPA, dopamine, noradrenaline and adrenaline are taken and calculated (pAl) using data from ref.[196]; for catechol and 4-nitro catechol are taken from ref.[94]. All energies in kcal/mol are calculated at the B3LYP-D3(BJ)/6-311++G(3df,2p) - IEFPCM level of theory.

aluminum ion is expected to be stronger. Besides, the higher Al(III) affinity of dopamine compared to noradrenaline and adrenaline can be explained considering that the latter two compounds contain a hydroxyl group in the alkyl chain, which has an EW effect. These aspects will be discussed in detail in the next section through chemical bond analysis.

In order to check the effect of the positive charge of the amine towards binding affinities, we re-evaluated ΔG_{aq}^{comp} values considering the unprotonated amino groups. In all cases, there is an increase of absolute ΔG_{aq}^{comp} values (Table 7.1), which is due to the higher total negative charge of N-

unprotonated catecholamines. Interestingly, now L-DOPA and dopamine show larger binding energies than catechol. Again, L-DOPA bears a higher total negative charge (-3) than catechol (-2) and the other catecholamines (-2), that explains its stronger aluminum affinity. However, in the case of dopamine, the presence of the alkyl tail acts as an electron donating group (ED) by induction, although such an effect is weakened by the presence of the EW effect (by induction) of NH_2. Moreover, when a second EW group is added to the alkyl chain, namely, $-OH$ in noradrenaline and adrenaline, the overall EW effect prevails over the ED one, lowering the binding ability of these two catecholamines with respect to catechol (Table 7.1).

In summary, the positive charge at the amino group plays a major role in the modulation of the binding affinities in these aluminum-ligand complexes, although the presence of other substituents also influence the overall stability.

In order to confirm these speculations and to get a more physically sound picture of the substituent effects, as well as to investigate the bonding nature of these complexes, we decided to perform a detailed chemical bond analysis based on both QTAIM and EDA analysis which is presented in the next section.
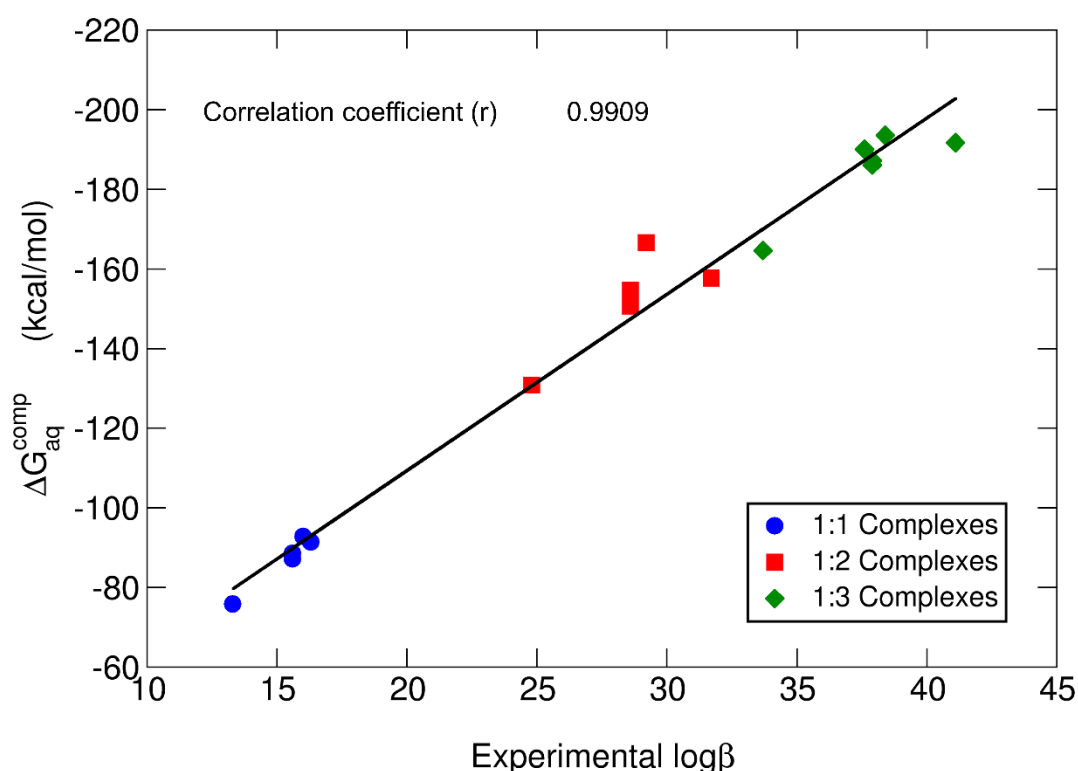
Fig. 7.3. B3LYP-D3(BJ) binding energies (ΔG_{aq}^{comp}) versus experimental stability constants ($\log\beta$)[94,196]. A correlation coefficient of 0.9909 is obtained. All amino groups are considered in their protonated state.

7.3.2 Analysis of Al-O bonds

The Bader's Quantum Theory of Atoms in Molecules (QTAIM, Appendix C) allows us to get more insight into the *physico*-chemical properties of these Al-ligand interactions. For simplicity, we will focus our discussion on 1:1 complexes, considering both N-protonated and N-unprotonated catecholamines. Similarly as reported in our previous work on the interaction of aluminum with substituted catechols and salicylic acids[21], we find positive values of the Laplacian of the electron density, $\nabla^2\rho(r_{BCP})$, and small but negative values of the energy density, $H(r_{BCP})$, consistently for all Al-O bond critical points. According to the Bader's criteria, positive values of $\nabla^2\rho(r_{BCP})$ and $H(r_{BCP})$ are indicative of closed-shell interactions (i.e. ionic or electrostatic bonds), while negative values for both quantities indicate the presence of shared (covalent) interactions. The mixed situation present in our results, previously reported for bonds involving metals[214], suggests that, although Al-O bonds are mainly of ionic nature, they also contain a small degree of covalency, due to their dative nature. To provide a more accurate analysis of these aluminum-ligand interactions, Al-O delocalization indices ($D.I._{Al-O}$) were also calculated. Delocalization indices are a measure of the average number of electron pairs shared between two atoms, therefore they have been related to the measure of the covalent character of a given bond[278].

As previously hypothesized, the results seem to confirm the electron withdrawing effect mediated by the positively charged amino group (Appendix C) that decreases the electron density from the two Al-O bonds; a more detailed albeit speculative analysis of the $D.I._{Al-O}$ values is presented and thorougly discussed in Appendix C.

In summary, the Bader's analysis confirmed the hybrid nature of the Al-O interactions, and has been proven to be a powerful tool to rationalize the effects that the different chemical environments of these catechol-based compounds have on their binding affinity trend.

The EDA approach was also used to characterize the degree of the ionic/covalent character of the Al-O bonds (Appendix C) by splitting the total interaction energy (ΔE_{Int}) into the electrostatic (ΔE_{elstat}), orbital interaction (ΔE_{oi}) and Pauli repulsion (ΔE_{Pauli}) terms. EDA results confirm the previous QTAIM analysis, pointing to a mainly ionic bond with a smaller but significant covalent character. As expected, there are pronounced differences in the electrostatic contributions to the bond depending on the total charge of the ligand. In this sense, unprotonated catecholamines show higher ΔE_{elstat} values than protonated ones (Appendix C). Moreover, N-protonated L-DOPA, catechol and 4-nitro catechol show larger electrostatic energies than protonated dopamine, noradrenaline and adrenaline, in agreement with their higher negative charge. One has to take into account that a lower ΔE_{elstat} will be compensated with a lower de-solvation energy when forming the complex, and therefore the

big differences in ΔE_{elstat} and ΔE_{int} shown in Table S5 of Appendix C are not reflected in the actual ΔG_{aq}^{comp} trend (Table 7.1), due to the lack of solvation effects in EDA analysis. Also, this puts a word of caution in the use of EDA with no-solvation effects when comparing ligands of different total charge.

In general, protonated catecholamines show lower orbital interaction energies (ΔE_{oi}) than the protonated counterparts, in agreement with the previous Delocalization Indices analysis (Appendix C), indicating a lower covalent contribution. However, among different compounds a clear trend in orbital and interaction energies with respect to binding energies (ΔG_{aq}^{comp}) could not be established. Therefore, we remark again that EDA results should be taken only with caution, since no solvation is introduced in this energy decomposition scheme; we already reported the paramount importance of considering solvation effects when dealing with charged complexes in solution[24].

7.3.3 Aluminum ion/proton competition for ligand binding

Unlike logβ, conditional (apparent) stability constants (logβ$_{Cond}$) are weighted by taking into account the influence of the protonation constants of a given ligand[78]. That is, their calculation considers the ligand in all of its possible forms in solution[78]; accordingly, logβ$_{Cond}$ takes into account the proton/aluminum ion competition for ligand's coordination site. This is due to the fact that both Al(III) and $H^+$are hard Lewis acids and, therefore, compete for the binding of hard Lewis bases, coherently with the Pearson's Hard and Soft Acids and Bases (HSAB) principle[17].

A comparison between the experimental values of logβ and logβ$_{Cond}$ points to a change in chelation performance between catechol and catecholamines (Table 7.1). Thus, whereas in general higher values of logβ are found for catechol with respect to catecholamines, the opposite is true when considering conditional stability constants, indicating that when proton competition is taken into account catecholamines are better aluminum chelators than catechol. The reason relies on the lower pK$_a$ values of the two hydroxyl groups of the catechol ring of catecholamines[196] compared with those of catechol[94]. In Table 7.1, we report the values of physiological binding energies (ΔG_{aq}^{Phys}), calculated by taking into account the energetic penalty that Al(III) has to pay in order to deprotonate the ligands, based on their experimental pK$_a$ values (see Methodology section). In agreement with the experimental logβ$_{Cond}$ data, we also observe a change in the trend between ΔG_{aq}^{Phys} and ΔG_{aq}^{comp}, with catecholamines showing slightly higher ΔG_{aq}^{Phys} values than catechol but smaller ΔG_{aq}^{comp}(Table 7.1).

The estimation of ΔG_{aq}^{Phys} is a first approach to understand the chelation performance towards Al(III). However, the fact that both theoretical and experimental information are combined in the evaluation of ΔG_{aq}^{Phys} partially jeopardize the usefulness of this approach; both contributions to the final binding

Ligands	Reaction equilibria	$\Delta G_{aq,L_{nH}}^{Phys}$	$\Delta\Delta G_{aq,L_{nH}}^{Phys}$	pAl
Hydroxide	$Al(H_2O)_6^{3+} + 4OH^- \rightarrow Al(OH)_4^- + 6H_2O$	-59.0	**0.0**	12.1[a]
L-DOPA	$Al(H_2O)_6^{3+} + L_{2H}^0 \rightarrow AlL(H_2O)_4^+ + 2H_3O^+$	-40.1	**18.9**	10.8[b]
	$Al(H_2O)_6^{3+} + 2L_{2H}^0 \rightarrow AlL_2(H_2O)_2^- + 4H_3O^+$	-61.1	**-2.1**	
	$Al(H_2O)_6^{3+} + 3L_{2H}^0 \rightarrow AlL_3^{3-} + 6H_3O^+$	-31.9	**27.1**	
Dopamine	$Al(H_2O)_6^{3+} + L_{2H}^+ \rightarrow AlL(H_2O)_4^{2+} + 2H_3O^+$	-39.0	**20.0**	10.8[b]
	$Al(H_2O)_6^{3+} + 2L_{2H}^+ \rightarrow AlL_2(H_2O)_2^+ + 4H_3O^+$	-55.5	**3.4**	
	$Al(H_2O)_6^{3+} + 3L_{2H\rightarrow}^+ \rightarrow AlL_3^0 + 6H_3O^+$	-41.3	**17.7**	
Adrenaline	$Al(H_2O)_6^{3+} + L_{2H}^+ \rightarrow AlL(H_2O)_4^{2+} + 2H_3O^+$	-41.3	**17.7**	11.3[b]
	$Al(H_2O)_6^{3+} + 2L_{2H}^+ \rightarrow AlL_2(H_2O)_2^+ + 4H_3O^+$	-59.0	**0.0**	
	$Al(H_2O)_6^{3+} + 3L_{2H}^+ \rightarrow AlL_3^0 + 6H_3O^+$	-48.5	**10.5**	
Noradrenaline	$Al(H_2O)_6^{3+} + L_{2H}^+ \rightarrow AlL(H_2O)_4^{2+} + 2H_3O^+$	-42.1	**16.9**	11.4[b]
	$Al(H_2O)_6^{3+} + 2L_{2H}^+ \rightarrow AlL_2(H_2O)_2^+ + 4H_3O^+$	-60.6	**-1.6**	
	$Al(H_2O)_6^{3+} + 3L_{2H}^+ \rightarrow AlL_3^0 + 6H_3O^+$	-52.1	**6.9**	
Catechol	$Al(H_2O)_6^{3+} + L_{2H}^0 \rightarrow AlL(H_2O)_4^+ + 2H_3O^+$	-39.6	**19.4**	10.1[c]
	$Al(H_2O)_6^{3+} + 2L_{2H}^0 \rightarrow AlL_2(H_2O)_2^- + 4H_3O^+$	-54.0	**5.0**	
	$Al(H_2O)_6^{3+} + 3L_{2H}^0 \rightarrow AlL_3^{3-} + 6H_3O^+$	-36.2	**22.8**	
4-nitro Catechol	$Al(H_2O)_6^{3+} + L_{2H}^0 \rightarrow AlL(H_2O)_4^+ + 2H_3O^+$	-45.2	**13.8**	14.2[c]
	$Al(H_2O)_6^{3+} + 2L_{2H}^0 \rightarrow AlL_2(H_2O)_2^- + 4H_3O^+$	-70.4	**-11.4**	
	$Al(H_2O)_6^{3+} + 3L_{2H}^0 \rightarrow AlL_3^{3-} + 6H_3O^+$	-74.6	**-15.6**	
Deferiprone	$Al(H_2O)_6^{3+} + L_H \rightarrow AlL(H_2O)_4^{2+} + H_2O + H_3O^+$	-43.4	**15.6**	15.4[d]
	$Al(H_2O)_6^{3+} + 2L_H \rightarrow AlL_2(H_2O)_2^+ + 2H_2O + 2H_3O^+$	-71.2	**-12.2**	
	$Al(H_2O)_6^{3+} + 3L_H \rightarrow AlL_3^0 + 3H_2O + 3H_3O^+$	-84.0	**-25.0**	
Citrate	$Al(H_2O)_6^{3+} + L_H^{3-} \rightarrow AlL(H_2O)_4^- + 2H_2O + H_3O^+$	-80.0	**-21.0**	14.4[a]
	$Al(H_2O)_6^{3+} + 2L_H^{3-} \rightarrow AlL(H_2O)_4^{5-} + 3H_2O + 3H_3O^+$	-91.8	**-32.8**	
EDTA	$Al(H_2O)_6^{3+} + L_H^{3-} \rightarrow AlL + 5H_2O + H_3O^+$	-121.9	**-62.9**	16.4[a]

Table 7.2. DFT and experimental (pAl) proton/aluminum ion competition for ligand binding, compared to hydroxide formation used as reference. Ligands are considered in their physiological protonation state. [a] Data taken from ref.[7]. [b] Calculated with the HySS program using data from ref.[196]. [c] Data taken from ref.[94]. [d] Calculated with the HySS program using data from ref.[111]. All energies in kcal/mol are obtained at the B3LYP-D3(BJ)/6-311++(3df,2p)-IEFPCM level of theory.

energy are not evaluated at the same level and the procedure depends on the availability of experimental pK_a values for the ligands. In order to overcome these limitations, we decided to calculate binding energies of Al-ligand complexes departing from protonated ligands. In this way, the proton/aluminum ion competition for ligand binding is intrinsically considered in the definition of the corresponding reaction equilibria (see Methodology section). We will refer to these free energies as $\Delta G_{aq,L_{nH}}^{Phys}$, where the subscript L_{nH} stands for the protonation state of a given ligand L at physiological pH. Results can be found in Table 7.2; we have considered that both hydroxyl groups of the catechol moiety in all compounds are protonated and that the amino groups of catecholamines are also in their protonated state. We have observed that, irrespective of the stoichiometry and of the catecholamine, we obtain in all cases substantial negative $\Delta G_{aq,L_{nH}}^{phys}$ values. This suggests that, in all cases, aluminum is able to displace the protons from the catechol moieties and form stable Al-ligand complexes.

In summary, both experimental and theoretical results point to the importance of considering properly the effect of ligand's deprotonation in order to evaluate the overall performance of a given ligand towards aluminum binding. In fact, the order in relative binding affinity can be altered when deprotonation energies of the ligands are taken into account. Nevertheless, the interaction between aluminum and catechol/catecholamines is strong enough to displace the protons from the ligand, leading to potentially stable complexes.

7.3.4 Comparison between different ligands towards aluminum binding and aluminum hydroxide formation in solution

In an open biological environment, in order to bind to a given ligand, the aluminum ion has to compete not only with protons, but also with other endogenous (and eventually exogenous) chelators. Moreover, the speciation of the Al(III) ion in solution is a complex task[7]; indeed, at physiological pH, there exist several Al(III)-hydroxide species, with $[Al(OH)_4]^-$ being the most stable one[7]. Accordingly, we also need to consider the possibility of the hydroxide binding competition, in order to evaluate the chelation performance of a given ligand.

In this sense, the main shortcoming in the use of $\log\beta_{Cond}$ as a criterion to evaluate chelation properties is the fact that conditional stability constants depend on the stoichiometries of the corresponding metal-ligand complexes[28,78]. For this reason, stability constant values of ligands displaying different denticities (e.g. bidentate, tridentate, hexadentate etc.) cannot be directly compared because of different entropic contributions of their chelate effect[28].

In order to overcome such limitations, the pM parameter has been introduced as a general criterion to compare the chelation performance between different ligands[109]. This is defined as $-\log[M_F]$ usually taken at $[M_T] = 1 \times 10^{-6}$ M and $[L_T] = 1 \times 10^{-5}$ M at pH 7.4, where $[M_F]$ is the concentration of free metal in solution (in this case aluminum), and $[M_T]$ and $[L_T]$ are the total concentration of the metal and the ligand, respectively[78]. Such experimental parameter is very useful to assess the potential competitiveness of different ligands towards Al(III) in an open biological environment, and it will be used in this section for the discussion of the Al(III) binding efficiency of different ligands (see Table 7.2 and Fig. 7.5).

1:1 Al-Deferiprone **1:2 Al-Deferiprone** **1:3 Al-Deferiprone**

1:1 Al-Citrate **1:2 Al-Citrate** **1:1 Al-EDTA**
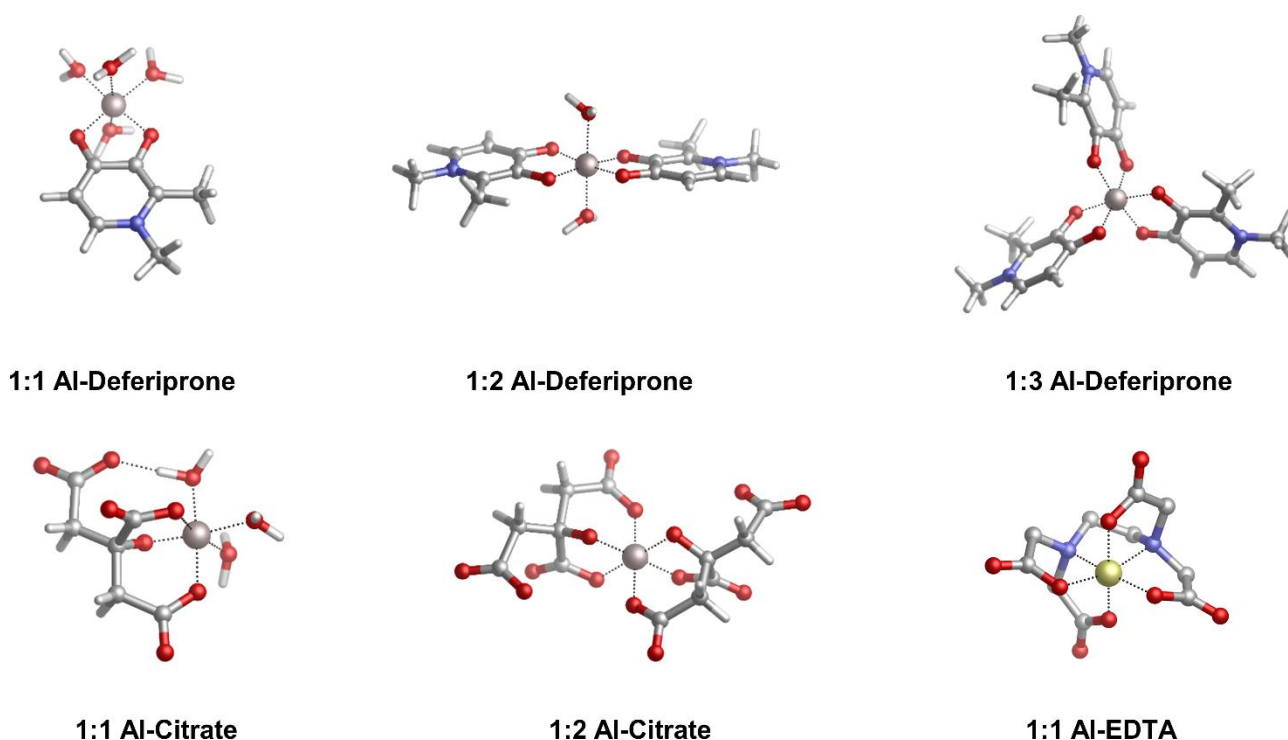
Fig. 7.4. Optimized geometries in aqueous solution of aluminum bound to different reference ligands: deferiprone (Ferriprox®), citrate and ethylenediaminetetraacetic acid (EDTA). Notice that deferiprone, citrate and EDTA are, respectively, bidentate, tridentate and hexadentate aluminum chelators.

In Table 7.2, and Fig. 7.5, we compare the formation energies of the catechol-based ligands with those of some reference compounds displaying different denticities, namely: citrate, the main biochelator of aluminum in blood serum[36,39,280]; deferiprone, one of the main drugs used in Al(III) chelation therapy[6,28,86]; EDTA, one of the most powerful Al(III) chelating agents[112,114] (Fig. 7.1 and 7.4). As in the previous section, all ligands are considered at their most likely protonation states at physiological pH (Table 7.2): citrate with hydroxyl group protonated and the three carboxylates unprotonated; deferiprone with the hydroxyl group protonated, and EDTA with one amine protonated

and the four carboxylates unprotonated. In addition, relative formation energies ($\Delta\Delta G_{aq,L_{nH}}^{phys}$) for each ligand are calculated with respect to the formation energy of $[Al(OH)_4]^-$ hydrolytic species, which represents the competition of hydroxide for aluminum binding in solution (Table 7.2). We depict both theoretical and experimental pAl data in Fig. 7.5. Notice that the vertical line at pAl=12.1 indicates the threshold for an efficient competition with aluminum hydroxide formation; the same is true for the horizontal line at $\Delta G_{aq,L_{nH}}^{phys}$ = -59.0 kcal/mol, which marks the theoretical limit for a given ligand to be able to compete with hydroxide formation at physiological pH (Table 7.2).
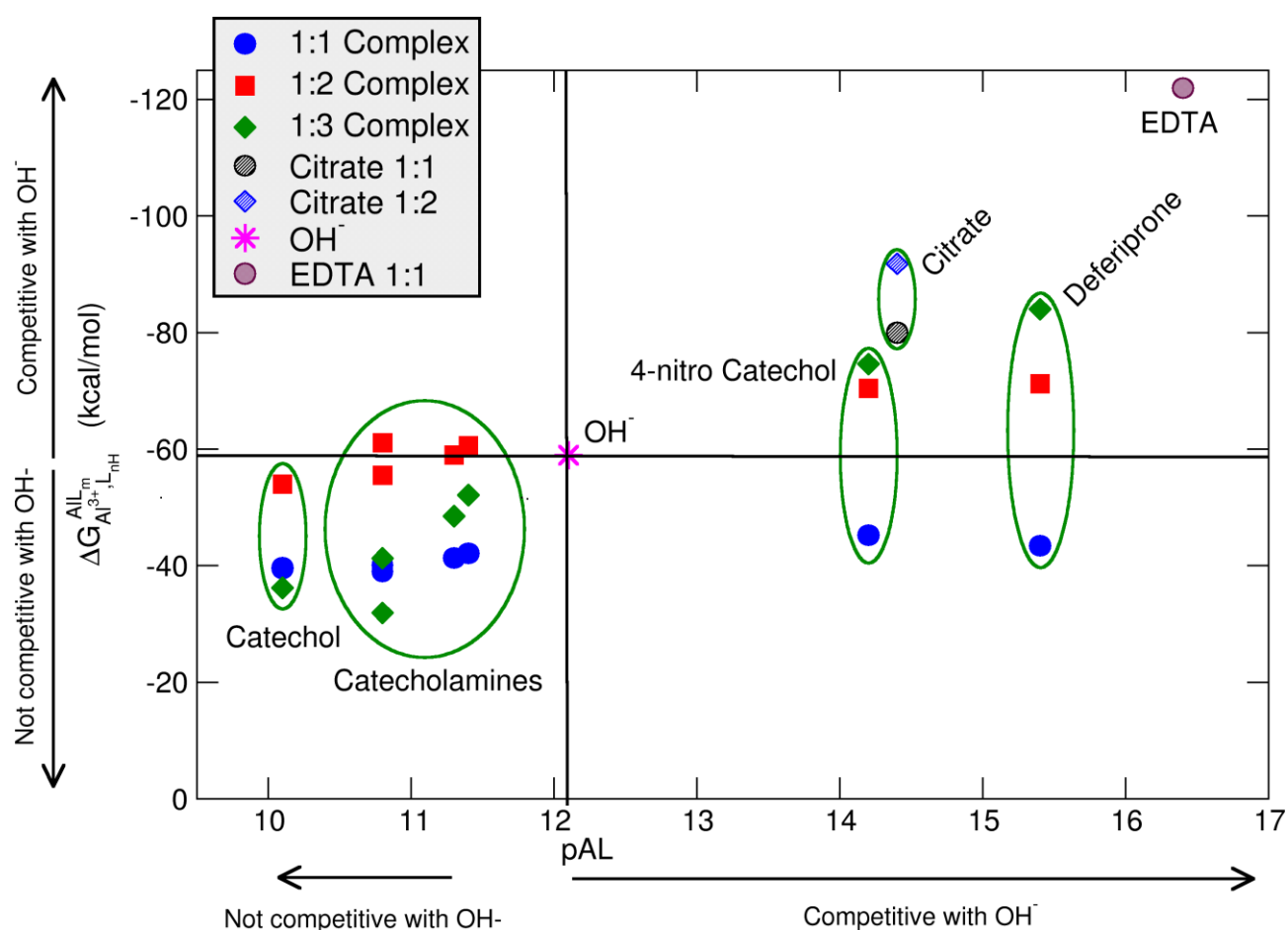
Fig. 7.5. Proton versus aluminum ion competition for different ligands at different stoichiometries. On the x-axis, experimental pAl values. On the y-axis, DFT formation energies. Aluminum hydroxide $[Al(OH)_4]^-$ formation is used as threshold for positive/negative Al-ligand competition. All Al-ligand reaction equilibria are presented in Table 7.2.

Looking at Fig. 7.5 we see that, although all catecholamines and catechol compounds show negative formation energies, only 4-nitro catechol at 1:2 and 1:3 stoichiometries is able to outcompete in an effective way hydroxide at physiological pH (Fig. 7.5). This is coherent with an experimental pAl

value of 14.2 for 4-nitro catechol, similar to the 14.4 value of citrate. Likewise, citrate, deferiprone and EDTA lie in the top-right region of Fig. 7.5, the region where they can form more stable complexes than $[Al(OH)_4]^-$ according to both theoretical and experimental data. The $\Delta G_{aq,L_{nH}}^{phys}$ values of catechol, irrespective of the stoichiometry, are lower (in absolute values) than -59.0 kcal/mol, the calculated formation free energy of $[Al(OH)_4]^-$ hydrolytic species (Table 7.2). This is in agreement with the lower pAl value of Al-catechol, 10.2, than those of Al-hydroxide, 12.1. Catecholamines lie in an intermediate situation between that of catechol and 4-nitro catechol, but both theoretical and experimental results restrain them in an area of low competitiveness with respect to hydroxide formation (Fig. 7.5). Indeed, only 1:2 Al-L-DOPA and Al-noradrenaline seem to be barely competitive with Al-hydroxide, showing $\Delta G_{aq,L_{nH}}^{Phys}$ values of -61.1 and -60.6 kcal/mol, respectively (Table 7.2). Interestingly, among bidentate compounds, all Al-catecholamines complexes, as well as all Al-catechol ones (but not Al-4-nitrocatechol nor Al-deferiprone) show a preference towards the formation of the 1:2 metal-ligand complex (Fig. 7.5). This is in agreement with the speciation diagram for Al-adrenaline depicted by Kiss et al.[196], where they found that the 1:2 Al-adrenaline complex is the prevalent one in the 5-8 pH range.

The overall low competitive situation of all catecholamines is reflected by their pAl values around 10-11, that we calculated using the speciation data of Kiss et al.[196]. They are close but lower than thE pAl value of Al-hydroxide, 12.1 (Table 7.2), although Martin[7] has reported a generic and single pAl value for all catecholamines of 12.8, which seems to be only barely competitive compared with Al-hydroxide formation.

In summary, despite catecholamines display in principle favorable proton/aluminum ion competition with an enhanced affinity with respect to catechol, this is not sufficient to transform them into potential strong aluminum binders in aqueous solution at physiological pH; they can only barely compete with aluminum-hydroxide formation. Moreover, as demonstrated by our calculations and by the available experimental data, other well known aluminum chelators such as citrate, deferiprone and EDTA, are much more prompt to bind to Al(III) than catecholamines in an open biological environment. Accordingly, we can classify these neurotransmitters as overall poor aluminum binders; the impact of these findings in light of the catecholamine biosynthesis pathway will be discussed in the next section.

7.4 Biological implications of the results

The catechol moiety is the building block of catecholamines, a class of neurotransmitters and hormones of fundamental importance for the correct homeostasis and function of both the central (CNS) and peripheral (PNS) nervous systems, where they exert a wide range of tasks[293-295]. Within the CNS, these neurotransmitters, are involved in many cognitive, motor, emotional, neuronal plasticity and memory-related functions. In the PNS, as hormones they find their way in the correct behavior of both the sympathetic and parasympathetic systems, where they play an important role in the fight-or-flight response and, in general, in the body's response to stress[296]. L-DOPA, dopamine, noradrenaline (norepinephrine) and adrenaline (epinephrine) are synthesized from the amino acid L-tyrosine (Fig. 7.6); the resulting catecholamines biosynthesis pathway involves several enzymes, substrates, cofactors, metal ions and regulatory mechanisms that are highly intertwined with other metabolic pathways, leading to a complex and finely controlled network[294]. Hence, the perturbation, interference or impairment of such an intricate network is associated to the development of severe clinical phenotypes and neurometabolic disorders[294].
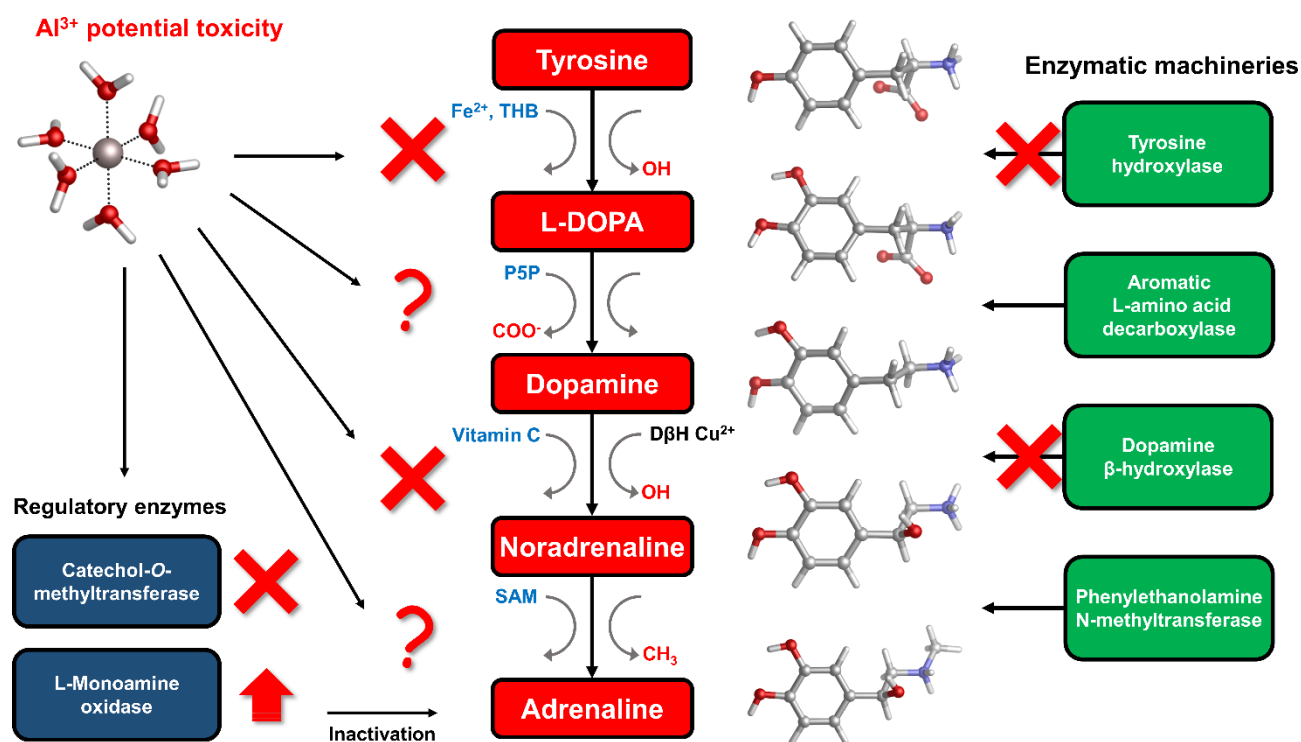
Fig. 7.6. Schematic representation of the catecholamine biosynthesis pathway with sites of aluminum interference according to the literature. Cofactors involved in each specific enzymatic reaction are highlighted in blue, while functional groups that are added/removed in red. THB=Tetrahydrobiopterin; P5P=Pyridoxal phosphate; SAM=S-Adenosyl methionine; vitamin C=ascorbic acid; Dβ H=Dopamine β -Hydroxylase.

As introduced in the beginning, Al(III) is believed to play a role in the insurgence of neurodegenerative diseases (in particular the Alzheimer's Disease[4]) as well as in the impairment of several key neuronal processes[5]. Indeed, it has been shown that this exogenous metal affects the signaling process mediated by catecholamines[198], it alters their content in animal models[195], and interferes with enzymatic activities that involve these neurotransmitters[64,76,297,298]. Moreover, it has been demonstrated that the ingestion of aluminum affects catecholamine levels in different brain tissues[299,300].

Therefore, a relationship between the presence of aluminum in the brain and interferences with the metabolic routes involving catecholamines has been established. Does the interaction of aluminum with catecholamines, and the resulting metal-neurotransmitter complexes, play a direct and crucial role that could be considered a potential risk factor for neurodegenerative phenotypes? Our calculations clearly support the formation of stable complexes between aluminum and catecholamines, with favorable complexation energies even when proton displacement is taken into account. However, in solution the resultant complexes are only barely competitive with the formation of $[Al(OH)_4]^-$ hydrolytic species at physiological pH. Additionally, both theoretical and available experimental data point to a very low competitiveness of all Al-neurotransmitter complexes with respect to other endogenous biochelators such as citrate, or with respect to other ligands like deferiprone and EDTA.

As a consequence, the direct interaction of a free aluminum in solution with catecholamines does not seem to be a likely factor that could interfere with these metabolic pathways. Based on our thermodynamic data, the formation of strong aluminum-catecholamine complexes must fulfill two conditions: i) a solvent-free environment that protects from hydroxide attack or prevents hydroxide formation, and ii) the absence of other efficient aluminum chelators. Some authors have already suggested that the formation of aluminum-catecholamine complexes requires a citrate-free environment[7,196], although they did not discuss carefully the effect of hydroxide molecules.

In light of these considerations, what is the experimentally assessed detrimental role of aluminum within the catecholamines route?

To answer this question, in the rest of the section we will collect and discuss (to the best of our knowledge) the literature regarding Al(III) and catecholamines, and evaluate some other possible mechanisms of Al(III) interference that could be assessed in future. For that purpose, an up-to-date representation of the catecholamine biosynthesis pathway with sites of aluminum influence (according to the literature) is proposed in Fig. 7.6.

There are three enzymes whose activity has been reported to be inhibited by the presence of aluminum: tyrosine hydroxylase (TH)[297,298], dopamine β-hydroxylase (DBH)[64,76] and catechol-O-

methyltransferase (COMT)[301,302]. Tyrosine hydroxylase is responsible for the synthesis of L-DOPA using the amino acid L-tyrosine as substrate and Fe(II) and tetrahydrobiopterin (THB) as cofactors. Dopamine β-hydroxylase, an enzyme that contains Cu(II) metal ions in its active site, converts dopamine to noradrenaline using vitamin C as cofactor. Finally, catechol-O-methyltransferase is involved in the regulation (inactivation) of catecholamine levels by methylation of their hydroxyl groups, using Mg(II) and S-adenosil methionine (SAM) as cofactors (Fig. 7.6).

Interestingly, all of these three enzymes make use of divalent metal ions (iron, copper and magnesium) in order to perform the redox reactions required by their active sites. Al(III) is well known for being a non-redox metal[51,52,56], therefore can have a direct and strong influence on the reaction mechanisms catalyzed by these enzymes. Aluminum has been shown to be able to bind to Fe(III)-loaded transferrin[46,47,181,303]. Accordingly, aluminum might be able to displace the copper ion from the active site of DBH and, due to its different ionic radius, impair the activity of that enzyme from a conformational point of view. Alternatively, another possibility is that the non-redox behavior of Al(III) alters the reaction mechanism of DBH leading to its inactivation.

Similarly, Al(III) might compete with Fe(II) and Mg(II) being utilized as cofactor by TH and COMT, respectively, thus affecting their normal behavior.

Quite interestingly, Al(III) inhibits O-methylation (COMT) but no N-methylation (phenylalanine N-methyltransferase, PNMT) of catecholamines[301,302]. PNMT is the enzyme in charge of the synthesis of adrenaline through N-methylation of noradrenaline (Fig. 7.6). These findings were interpreted in terms of the formation of strong and stable Al-catecholamine complexes, in which the methylation at the oxygen atoms of the catecholate would be affected by the binding of the metal, whereas the methylation at the terminal amino group of noradrenaline would be unaffected since this group is not directly bound to aluminum[301,302]. In line with this interpretation, authors showed that the use of a potent chelating agent such as deferoxamine (DFO) is able to reverse the Al(III)-induced inhibition of COMT[302], in agreement with the much higher Al(III) affinity of EDTA and deferiprone characterized in this work. They also reported that an excess of DFO inhibits again COMT, because of the removal of magnesium ions that are required as cofactors[302].

Our results would further support this hypothesis, since in COMT, contrary to PNMT, there is a well-defined Mg(II) binding site that can protect aluminum from hydroxide formation, due to the lack of solvent molecules. Therefore, such an environment could favor the formation of a strong aluminum-catecholamine complex that, ultimately, impair the normal functioning of COMT. In this sense, Sparta and Alexandrova investigated the effects of various divalent and trivalent metal ions towards the enzymatic activity of COMT by means of QM/MM simulations[304]. They found that trivalent metal ions such as Fe(III) impair the reaction mechanism by increasing the activation energy needed for the

methyl transfer reaction; this is due to the higher electrophilic nature of Fe(III) that reduces the basicity of the oxygen donors of the catechol-based substrate, rather than to an iron-induced conformational change of the enzyme[304]. Aluminum could certainly play a similar role since it also shows a strong electrophilic nature according to its high charge and small size.

Regarding the non-inhibition of PNMT, it is important to note that while COMT requires metal ions as cofactors, PNMT does not rely on metal ions[305]. The unfavorable competition of Al-adrenaline complexes with respect to Al-hydroxide formation in absence of a protective metal ion binding site might explain its non-sensitivity to the presence of Al(III) reported in literature[302].

The catecholamine pathway contains two main enzymatic regulators that ensure the correct homeostasis of the levels of these neurotransmitters: one is the previously discussed catechol-O-methyltransferase, and the second one is monoamine oxydase (MAO, Fig. 7.6). MAO enzymes catalyze the oxidative deamination of biological monoamines using flavin adenine dinucleotide (FAD) as cofactors, thus leading to their inactivation. Different mechanisms of action (at least four) have been proposed for MAO catalytic activity, although the exact one is still not well understood[306]. Interestingly, while Al(III) inhibits COMT, some authors reported, by means of kinetic studies in rat brain, that this metal is instead able to increase the activity of MAO, in particular the B isotype[307,308]. Hyperactivation of monoamine oxidase enzymatic activity is one of the hallmarks of both Alzheimer's[309] and Parkinson's[310] diseases. However, it is hard to hypothesize what could be the role of aluminum in the overactivation of MAO, considering the lack of a clear reaction mechanism.

So far we have discussed the role that aluminum might have with respect to the enzymatic machineries acting on the catecholamines pathway. However, there are many low-molecular-mass organic cofactors that are pivotal for the correct behavior of these enzymes and therefore could be important targets of this metal (Fig. 7.6).

In this sense, there is evidence that aluminum affects the metabolism of tetrahydrobiopterin (THB[84,311,312]). THB is an essential cofactor employed by many enzymes, including tyrosine hydroxylase. Impaired THB metabolism by aluminum has been related in particular with dialysis dementia[84]. One hypothesis that has been made, is that Al(III) might interfere with the activity of dihydrobiopterin reductase[312], an enzyme that employs the nicotinamide adenine dinucleotide phosphate (NADPH) cofactor to catalyze the production of tetrahydrobiopterin from dihydrobiopterin. However, such a hypothesis was not further investigated. Quite interestingly, computational studies proved the ability of Al(III) to alter the conformation of NADH[42], a cofactor closely related to NADPH. Although still unclear, Al(III) interference with THB metabolism might be another possibility to explain the metal-induced inhibition of TH.

Vitamin C, also known as ascorbic acid, is an essential vitamin required as cofactor by DBH for the conversion of dopamine into noradrenaline (Fig. 7.6). Perturbation of Vitamin C metabolism in the brain has been related to the occurrence of severe neurodegenerative diseases[313]. Moreover, several studies highlight the chelation properties of vitamin C and its interaction with aluminum has been investigated[314-317]. In this sense, the structure and binding mode of the Al-ascorbate complexes in solution have been unveiled and clarified by means of both experimental and DFT computations[317]. Therefore, vitamin C might be a potential Al(III) target, and the resulting complex might be involved in the impairment of DHB activity (Fig. 7.6).

7.5 Conclusions

We have investigated the possibility of the formation of complexes between aluminum and an important class of catecholamine-based neurotransmitters: L-DOPA, dopamine, noradrenaline (norephinephrine) and adrenaline (ephinephrine). Chemical bond analyses confirmed the main ionic nature of the Al-O interaction, but a singnificant degree of covalent character. Then, we have determined that aluminum can clearly displace the protons of the hydroxyl groups of the catechol moiety forming stable aluminum-catecholamine complexes. However, in solution the estimated binding affinities are lower than the formation energies of aluminum-hydroxide, and much lower than the Al(III) affinities of other ligands such as citrate, deferiprone and EDTA. According to these results, we can rule out that the formation of aluminum-cathecolamine complexes in an open biological environment, considering the competition with other endogenous/exogenous ligands, might be behind the toxic role attributed to this metal ion within the catecholamine biosynthesis pathway.

Other possible mechanisms are discussed; aluminum could interfere/compete with the homeostasis of other metal ions required as cofactors of the enzymes involved in the catecholamines route. It could bind within the active site of metal-dependent enzymes, where the presence of a protective metal-ion binding site, like in the case of COMT, would provide the necessary conditions for the formation of strong aluminum-catecholamine complexes. It could bind to other organic cofactors such as vitamin C and it could interfere with the upstream metabolic routes of other cofactors. Again, it is worth to emphasize that little-to-nothing is known about the molecular basis of aluminum's behavior in these neurotransmitter pathways; therefore, much more basic knowledge in this sense must be gained in future. The present paper certainly helps in this regard, and also encourages further theoretical and experimental works.

SCIENTIFIC IMPACT OF THE PROJECT

"Well they closed down the auto plant in Mahwah late that month
Ralph went out lookin' for a job but he couldn't find none
He came home too drunk from mixin'
Tanqueray and wine
He got a gun shot a night clerk now they call 'm Johnny 99"

(B. Springsteen, Johnny 99)

8.1 Training schools and international courses

1. Doctorate Core Course (Autonomous University of Madrid) – 28/09/2015 – 09/09/2015, Madrid, Spain.

2. School on Parallel Computing (University of Barcelona and Barcelona Supercomputing Center) – 25/01/2016 – 31/01/2016, Barcelona, Spain.

3. Tutorial on ADF (University of Groningen and Software for Chemistry & Materials) – 26/04/2016 – 02/05/2016, Amsterdam, Netherlands.

4. Short Course *"The chemical bond"* by Prof. Gernot Frenking (University of Marburg) – 0502/2016 – 28/03/2016, Donostia, Spain.

5. Short Course *"New tools for chemical bond analysis"* by Dr. Eduard Matito (Donostia International Physics Center -DIPC) – 02/06/2016 – 28/06/2016, Donostia, Spain.

6. Dynapeutics International Summer School – 26/09/2016 – 30/09/2016, Donostia, Spain. Poster contribution: *A theoretical approach to aluminum chelation therapy: insights from computational chemistry.*

7. Tutorial on SHARC (University of Vienna) – 03/10/2016 – 07/10/2016, Vienna, Austria.

8. School on Scientific Visualization (Cineca) – 16/01/2017 – 20/01/2017, Rome, Italy.

9. School on Open Cloud Science (University of Perugia) – 01/06/2017 – 07/06/2017, Perugia, Italy.

10. Course on Project Management (KU Leuven) – 19/07/2017 – 21/07/2017, Leuven, Belgium.

11. Theoretical Methods in Quantum Chemistry (Zaragoza Scientific Center for Advanced Modelling and University of Tolouse) – 02/10/2017 – 05/10/2017, Zaragoza, Spain.

12. Manuel Yanez's workshop (Donostia International Physics Center) – 26/10/2017 – 27/10/2017, Donostia, Spain.

8.2 International conferences and workshops contributions

1. 1st ITN Annual Workshop (University Pierre et Marie Curie Paris VI) 18/07/2016 – 21/07/2016, Paris, France..
    a. Oral communication: *Computational approach to Al(III) chelation therapy: insights from computational chemistry.*
    b. Poster contribution: *Computational approach to Al(III) chelation therapy: insights from computational chemistry.*

2. ITN Mid-Term Meeting – 16/12/2016, Madrid, Spain.
    a. Oral communication: *Aluminum biochemistry.*
    b. Poster contribution: *Theoretical approach to aluminum biochemistry: a computational approach.*

3. 12th Keele's Meeting on Aluminum – 04/03/2017 – 08/03/2017, Vancouver, Canada.
    a. Poster contribution: *Characterization of Substituent Effects and Binding Features of different Al(III)-Chelator Complexes*. **(Metallomics Poster Prize)**

4. Workshop on Computational Studies applied in Biological Sciences (University of Cagliari) – 02/04/2017, Cagliari, Italy.
    a. Oral communication: *Theoretical approach to aluminum chelation therapy: characterization of the Al(III)-Ligand binding features.*

5. 8th Theoretical Biophysics International Symposium – 26/06/2017 – 30/06/2017, Donostia, Spain.
    a. Oral communication: *Computational approach to Aluminum biochemistry.*
    b. Poster contribution: *Aluminum, a walk on part in the war or a lead role in a cage ?*

6. 2nd ITN Annual Workshop (KU Leuven) – 16/07/2017 – 19/07/2017, Leuven, Belgium.
    a. Oral communication: *Computational approach to Aluminum biochemistry.*
    b. Poster contribution: *Aluminum, a walk on part in the war or a lead role in a cage ?*

7. 11th European Conference on Theoretical and Computational Chemistry (EUCO) – 04/09/2017 – 07/09/2017, Barcelona, Spain.

   a. Poster contribution: *The Dark Side of aluminium chelation therapy: characterization of Al(III)-ligand binding features.*

8. 16th International Congress of Quantum Chemistry (ICQC) – 18/06/2018 – 23/06/2018, Menton, France.

   a. Poster contribution: *Towards new and reliable Al(III) chelating agents.*

9. 3rd ITN Annual Workshop (University of Pisa) – 23/07/2018 – 25/07/2018, Pisa, Italy.

   a. Oral communication: *Computational approach to Aluminum biochemistry and development of new chelation strategies.*

   b. Poster contribution: *Aluminum: a mysterious metal ion.*

10. 14th European Biological Inorganic Chemistry Conference – 26/08/2018 – 30/08/2018, Birmingham, U.K.

   a. Poster contribution: *Computational Approach to Al(III) Chelation Therapy.*

8.3 Outreach activities

1. "Meet the Prof" event with Nobel Laureates Prof. Dudley R. Herschbach, Passion for Knowledge Festival – 26/09/2016 – 01/10/2016, Donostia, Spain. (http://p4k.dipc.org/en/home)

2. 7th Encuentro "Vidas Cientifica" (Eureka! Science Museum) 23/10/2017, Donostia, Spain. (Career meeting for high school students).

   a. Oral communication: *Computational chemistry: beyond the dark side of science.*

   b. Poster contribution: *Computational chemistry: beyond the dark side of science.*

3. Co-supervisor of a Bachelor thesis project focused on aluminium biochemistry, degree in Chemistry, University of the Basque Country (Spain).

   a. Defense: 22/07/2016.

      b. Title of the dissertation: *Estudio Teórico de la Interacción del Aluminio con Moléculas de Interés Biológico.*

4. Publication of a dissemination article for general audience, about the controversy of aluminium biochemistry, in the Mapping the Ignorance blog (https://mappingignorance.org/2016/10/28/dark-side-aliii-chelation-therapy-new-computational-hope/).

      a. Article title: *The Dark Side of Al(III) chelation therapy: A new computational hope.*

8.4 Publications

1. Gabriele Dalla Torre, Jon I. Mujika, Elena Formoso, Eduard Matito, Maria J. Ramos and Xabier Lopez. *Tuning the affinity of catechols and salicylic acids toward Al(III): characterization of Al-chelator interactions.*
   Dalton Trans., **2018**, *47*, 9592-9607. **(Front cover article)**

2. Jon I. Mujika, Gabriele Dalla Torre, Joanna I. Lachowicz and Xabier Lopez. *Design of new efficient chelators of aluminum based on Mimosine-containing peptides.*
   Phys. Chem. Chem. Phys., submitted.

3. Jon I. Mujika, Gabriele Dalla Torre, Elena Formoso, Rafael Grande-Atzazi, Slowmir J. Grabowski, Christopher Exley and Xabier Lopez. *Aluminum's preferential binding site in proteins: side chains of aminoacids versus backbone interactions.*
   J. Inorg. Biochem., **2018**, *181*, 111.

4. Jon I. Mujika, Gabriele Dalla Torre, and Xabier Lopez. *Aluminum and Fenton reaction: How can the reaction be modulated by speciation ? A computational study using citrate as test case.*
   Phys. Chem. Chem. Phys., **2018**, *20*, 16256.

5. Gabriele Dalla Torre, Jon I. Mujika, Joanna I. Lachowicz, Maria J. Ramos and Xabier Lopez. *The interaction of aluminum with catecholamine-based neurotransmitters: Can the formation of these species be considered a potential risk factor for neurodegenerative diseases?*

   Dalton Trans., accepted.

6. Gabriele Dalla Torre, Xabier Lopez and Maria J. Ramos. *Benchmarking approximate exchange-correlation functionals and sempiempirical methods towards binding energies and geometries of different Al-ligand complexes in solution.*
   In preparation.

8.5 Awards

1. Metallomics Poster Award. The 12TH Keele's Meeting on aluminum: living the aluminum age. Vancouver, Canada.

CONCLUSIONS

"They declared me unfit to live said into that great void my soul'd be hurled
They wanted to know why I did what I did
Well sir I guess there's just a meanness in this world."

(B. Springsteen, Nebraska)

9.1 Concluding remarks

The present PhD dissertation aimed to shed light on the properties and the behaviour of Al(III), an exogenous and non-essential metal ion, that became an important part of our daily lives in the so-called Aluminum Age.

In particular, three different but tightly connected areas were covered, that are summarized below with the main findings previously discussed in the results chapters.

9.1.1 Chelation therapy and development of new chelation strategies

In the first paper, we have investigated how different substituents (electron donating/withdrawing groups) with different mechanisms of actions (induction and/or resonance) can tune and modulate the properties of a given chelating agent towards Al(III). For that purpose, we have used two well known families of chelators for which different sources of experimental data are available, so that to calibrate our computational protocol and to be able to investigate all their features.

Our results showed that, depending on the properties of the chelator (e.g. aromaticity, presence of substituents) and the aluminum/protons competition for binding the coordination site, these substituents can alter the chelation performance in different extents. When aluminum has to compete with only one proton for biding the ligand, then electron donating groups (methyl, methoxy) are able to increase the binding affinity of the chelator; conversely, when aluminum has to compete with two protons, then the addition of electron withdrawing groups (e.g. nitro and trifluoromethyl) provide the better chelation performance. Moreover, the aromatic nature of the chelating agent is also pivotal; in the case of aromatic chelators, those substituents that work through resonance or both induction/resonance mechanisms of action are able to provide a higher effect in terms of chelation performance of the ligand. Therefore, we propose that, when the aromatic nature of the ligand is low (for instance, pyridine-based ligands), then those substituents that work through induction should be more suitable to tune the binding properties of a given ligand.

Interestingly, the modulation of these binding properties is mediated by the minor covalent character of the Al(III)-ligand interactions, rather than their prevalent electrostatic nature. Indeed, such an effect is exerted through the modulation of the electron density at the coordination site of the ligand, as revealed by the QTAIM and EDA analyses.

Overall, we developed a computational approach suitable to investigate and predict the properties of low-molecular-mass Al(III) chelators, that we beliece it wll be a useful tool to design improved compounds to be used in aluminum chelation therapy.

In our second paper (chapter 4), we developed a new family of peptide-based chelating agents whose chelation unit is composed of Mimosine amino acids. The reason of such a choice relies on the similarity between Mimosine and deferiprone, a well-known and performant Al(III) chelating agent. We designed eight peptidic sequence that differ by the number (from five to nine) and the nature (glycine and proline) of he amino acids of the linker sequences.

QM/MM simulations showed that those peptide sequences that are too short (five, six and seven amino acids) fail to bind aluminum in a octahedral fashion. Conversely, sequences composed of eight and nine amino acid are able to properly coordinate Al(III) filling all the six coordination sites.

The comparison with the x-ray structure of the 1:3 aluminum-deferiprone complex allowed us to speculate that the nine peptide long sequences coordinate in a very similar fashion the former complex, leading to an optimum complexation with the trivalent metal, as highlighted by the calculated binding enthalpies.

These results would encourage further experimental synthesis and characterization of our newly developed family of aluminum chelating agents.

9.1.2 The potential toxic role of aluminum in the biological environment

The second part of this thesis project was focused on the understanding the molecular basis of the (potential) detrimental role of Al(III) within the cellular life of the human organism.

The first paper (chapter 5) investigated a recent paradigm that has been proposed regarding the interaction of aluminum with proteins: backbone versus sidechains.

Indeed, in a recent paper, some authors proposed that aluminum is able to bind strongly, through covalent interactions, the backbone of proteins, thus leading to their denaturation.

However, our calculations (in agreement with the vast majority of the literature in that respect) showed that, from a thermodynamic point of view, Al(III) interaction with protein side chains is much more favoured than the interaction with the backbone. The latter situation is therefore way less competitive and aluminum prefers to bind the negatively charged side chains of amino acids, in agreement with the Pearson's Hard and Soft Acids and Basis (HSAB) principle. The reason relies on the fact that the aluminum-ligand interactions are mainly of electrostatic nature, although the minor covalent character can be important in some situations, as discussed in chapter 3.

In chapter 6, we investigated the role of citrate, the main low-molecular-mass aluminum chelator in blood serum, in the context of the Fenton reaction. Although Al(III) is a non-redox metal, it has been assessed that it is nevertheless able to promote the Fenton reaction, by stabilizing the superoxide radical. The inclusion of the Al-citrate complex in the thermodynamic cycle of the Fenton reaction

leads to a complex scenario, where depending on the relative concentrations of aluminum, citrate and iron, citrate can have both a promotion and protective role with respect to aluminum.

Moving to the role of Al(III) in the brain (chapter 7), since it has been linked to several neurodegenerative disorders, we assessed whether its binding to catecholamines (e.g. L-DOPA, dopamine, adrenaline and noradrenaline) can lead to the formation of strong complexes that can potentially contribute to the severe phenotypes associated to the interference of Al(III) within the catecholamine biosynthesis pathway.

Our results highlighted that, differently than what it has been proposed in previous papers, the Al(III)-catecholamine complex is not competitive in solution when compared to Al-hydroxide formation (the most stable aluminum species at physiological pH) and with other endogenous and exogenous chelators such as citrate, deferiprone and EDTA.

Accordingly, we discussed other hypotheses that could be behind the detrimental role of aluminum in the catecholamines route, such as the impairment of enzymatic reactions in the catalytic pocket of key enzymes, and would encourage further experimental and computational works in the near future.

9.1.3 Improvement and calibration of the theoretical methods

The major developments in this area are spread through all the previous chapters, as we have updated and improved our "standard" computational protocol (see Fig. 3.2) in order to adapt it to the different systems under investigation and to calibrate it according to the fitting with the available experimental data.

As a result, we have been able to understand and well reproduce both the main experimental criteria that evaluate the chelation performance in solution (e.g. stability constants and pAl, see section 1.2.3). This is of pivotal importance in order to produce reliable results and to compare them with what it has been proposed in literature, as well as to propose new potentially therapeutic compounds.

Moreover, since the huge developments of the last years in the fields of DFT and semiempirical methods allowed to introduce some important corrections and upgrades, we are currently working on an accurate benchmark of the performance of DFT and semiempirical methods towards the evaluation of binding energies of Al-chelator complexes in solution, according to eq. 3.4.

The purpose is to evaluate the accuracy of DFT exchange/correlation functionals (spanning the whole DFT Jacob's ladder) in light of the two most important developments in this area: dispersion corrections and range separation (see section 2.2.2 and 2.2.3), with respect to aluminum-containing systems.

We have chosen seven different 1:1 aluminum-ligand systems (catechol, deferiprone, kojic acid, four hydroxypyridincarboxylic acids (HPCs) bearing different protonation states and substituents, see Fig.

1.11) because they span different donors to aluminum (e.g. carboxyl, hydroxyl, carboxylate) and different chemical environments (e.g. phenyl, pyridine, pyrone) as well as for the presence of the electron donating methyl group. In this way, a significant modulation of the chelation properties is expected, allowing for a good diversification of the dataset and a more reliable calibration of different methods.

The reference energies are calculated at the CCSD(T)/CBS//MP2/aug-cc-pVTZ level of theory using the popular extrapolation schemes developed by Helgaker and Halkier for the correlated and uncorrelated energies, respectively.

Although still work in prograss, some preliminary results with selected methods are presented in table 9.1 that allows for some important observations.

Method	MUE
CCSD(T)/CBS	
MP2=FULL	1.60
MP2	2.03
B3LYP	1.61
B3LYP-D3	1.44
B3LYP-D3(BJ)	0.78
CAM-B3LYP-D3(BJ)	0.55
M06-2X	1.41
M06-2X-D3	1.12
TPSS	1.30
TPSS-D3(BJ)	0.60
PBE	3.44
PBE-D3(BJ)	2.96
LC-wHPBE-D3/BJ)	0.76
ωB97XD	1.02
AM1	12.91
PM3	33.14
PM6	12.28
PM7	12.91
PM7R8	12.84

Table 9.1. Mean unsigned errors (MUEs) in kcal/mol for the physiological binding energies calculated for the seven different 1:1 aluminum-ligand complexes discussed above. DFT and MP2 single point energies are calculated with the 6-311++G(3df,2p) basis set. All geometry optimizations were carried out at the MP2/aug-cc-pVTZ level of theory.

1) The inclusion of dispersion clearly leads to more accurate results; the D3(BJ) scheme is more accurate than the D3 one (see section 2.2.3). Moreover, the inclusion of range-separation corrections in addition to dispersion (see section 2.2.2) such as the CAM-B3LYP-D3(BJ) and LC-wHPBE-D3(BJ) methods further increases the accuracy.

2) The B3LYP-D3(BJ) functional is one of the best performers among the methods displayed in table 9.1 (that were chosen herein since they represent the most accurate ones among all the tested functonals that are not reported for simplicity). Likewise, the PM6 method is the most accurate among all semiempirical Hamiltonians tested.
This confirms the suitability of the choice of these two methods that were extensively used in the present PhD project.

3) Regarding semiempirical methods, it is reasonable to hypothesize that the addition of dispersion corrections, when available in the specific package, would lead to a significant improvement of the performance of the method, leading to more accurate results. The same speculations might be extended to the newly developed hydrogen bond corrections (see section 2.2.3).

4) The MP2 *ab initio* method is clearly a worse performer when compared to most of DFT functionals, even when the full electron basis set is used.
This situation may be due to the bad estimation of dispersion energy by the MP2 method, which is a well known issue. However, these results highlight that this method is not suitable for the investigation of the thermodynamics of aluminum-containing systems, and put a word of caution on its use in that regard (see chapter 5).

9.2 Future perspectives

Overall, the results presented in the present dissertation provide a significant contribution in the computational approach to aluminum biochemistry. The overall accuracy of the protocol has been increased, and the various aspects that determine an increment of the failure of that accuracy were identified.

Clearly, this means that in future higher accuracy can be reached, and an even closer fitting with experimental criteria is a goal that must the pursued, also trying to investigate other variables that influence the accuracy of the computational protocol (e.g. solvation models, pK_a prediction, free ions in solution).

Besides, novel knowledge has been provided with respect to the development of novel chelating agents to be used in aluminum-based chelation therapy. A novel family of potentially well performing peptide-based chelator has been proposed. Moreover, following the findings of chapter 3, we expect to further increase the performance of these chelators by tuning the chemical environment with the proper electron donating/withdrawing substituents.

The role of citrate and aluminum in the case of the Fenton reaction has been elucidated, refining previous results found in our group.

Finally the interaction of aluminum with catecholamine-based neurotransmitters was assessed, and new hypotheses on the role of Al(III) within the catecholamine biosynthesis pathway were formulated, providing new substrate for near-future computational works.

APPENDIX A

"I love to see the cottonwood blossom
In the early spring
I love to see the message of love
That the bluebird brings
But when I see you walkin' with him
Down along the strand
I wish I were blind
When I see you with your man"

(B. Springsteen, I Wish I Were Blind)

Appendix A

Tuning the Affinity of Catechols and Salicylic Acids towards Al(III): Characterization of Al-Chelator Interactions

- **Table S1:** Binding enthalpies and free energies of 1:1,1:2,1:3 complexes with the ωB97XD functional.

- **Table S2:** Binding enthalpies and free energies of 1:1,1:2,1:3 complexes with MP2.

- **Table S3:** Binding enthalpies and free energies of 1:1,1:2,1:3 complexes with the M06-2X functional.

- **Table S4:** Binding enthalpies and free energies of 1:1,1:2,1:3 complexes with PBE0-D3(BJ) functional.

- **Table S5:** Binding enthalpies and free energies of 1:1,1:2,1:3 complexes with TPSS-D3(BJ) functional.

- **Figure S1:** comparison of all DFT functionals as well as the MP2 method with respect to B3LYP-D3(BJ) binding energies.

- **Figure S2:** comparison of all DFT functionals as well as the MP2 method with respect to experimental stability constants.

- **Table S6:** characteristics of all Al-O Bond Critical Points (BCPs) for the whole dataset of 27 compounds.

- **Figure S3:** comparison of binding energies (ΔG_{aq}^{comp}) with respect to the sum of the electron density for all Al-O BCPs.

- **Figure S4:** comparison of binding energies (ΔG_{aq}^{comp}) with respect to the sum of the Laplacian of the electron density for all Al-O BCPs.

- **Figure S5:** comparison of binding energies (ΔG_{aq}^{comp}) with respect to the sum of the total energy density for all Al-O BCPs.

- **Table S7:** values for all Al-O Delocalization Indices (D.I.) as well as the charge of the two oxygens directly interacting with aluminum for all the dataset of 27 compounds.

- **Table S8:** Values of the electrostatic term (ΔE_{elstat}), the orbital interaction term (ΔE_{oi}), the Pauli repulsion term (ΔE_{Pauli}) the dispersion term (ΔE_{disp}) and the total interaction energy (ΔE_{int}), for all the 27 compunds, calculated in gas phase.

- **Table S9:** Aromaticity indices according to the I$_{ring}$ and MCI aromatic descriptors computed on the free ligand (Lig) and aluminum-ligand complexes (Al-Lig).

- **Figure S6:** Electrostatic Potential maps (ESP) summarizing the effects of EDGs and EWGs toward the modulation of the covalent character of the bond.

Specific computational details

Density Functional Theory calculations

All geometrical optimizations were carried out in aqueous phase using the B3LYP functional and 6-31++G(d,p) basis set. Additionally, we added Grimme's D3 dispersion correction, since dispersion may play an important role in describing intra-/inter-ligand interactions in the aromatic compounds. Moreover, we included the Becke-Johnson (BJ) damping function that was shown to further increase accuracy by allowing the correct treatment of short-, medium- and long-range dispersion energies. In general, the addition of methods that properly take into account dispersion energies in DFT has been proven to improve the precision of computed non-covalent interactions and $\pi - \pi$ stacking systems. Unless otherwise specified, D3 refers to the D3(BJ) scheme. Other dispersion corrected DFT functionals, as well as the MP2 method were also employed to validate the methodology, with similar results (see Supplementary tables S1 to S5 and Figures S1 and S2).

To confirm that the optimized structures were real minima on the potential energy surfaces, frequency calculations were carried out at the same level of theory. All structures showed positive force constants for all the normal modes of vibration. The frequencies were then used to evaluate the zero-

point vibrational energy (ZPVE) and the thermal (T = 298 K) vibrational corrections to the enthalpies and Gibbs free energies within the harmonic oscillator approximation. To calculate the entropy, the different contributions to the partition function were evaluated using the standard statistical mechanics expressions in the canonical ensemble and the harmonic oscillator and rigid rotor approximation. The solvent effect was introduced using the self-consistent reaction field (SCRF) method with the polarized continuum model (PCM), using the integral equation formalism variant (IEFPCM). The electronic energies were refined by single-point energy calculations at the B3LYP-D3/6- 311++G(3df,2p) level of theory. Single point calculations with different methods (M06-2X, PBE0 and TPSS with the D3(BJ) dispersion correction scheme, ωB97XD and MP2) were carried out with the same triple-ζ basis set and IEFPCM solvation model at the B3LYP-D3/6-31++G(d,p) optimized geometries.

The NBO 3.1 program included in the Gaussian 09 package was used to carry out full Natural Orbital Theory population analysis of the orbitals involved in the metal-chelator interaction. Population analysis was performed on the SCF density at the B3LYP-D3/6-311++G(3df,2p) level.

QTAIM and Delocalization Indices

The Quantum Theory of Atoms in Molecules (QTAIM) was used to perform a topological analysis of the electron density, providing the critical points of the electron density and the atomic boundaries that define the atomic partition of the molecular space. The so-called bond critical points (BCP) are saddle points of the electron density that usually occur between two bonded atoms and provide important information about the nature of the bonding. Closed-shell interactions (such as van der Waals, ionic and hydrogen bonds) are characterized by small values of the density, charge depletion and positive energy densities (*i.e.*, small $\rho(r_{BCP})$, $\nabla^2\rho(r_{BCP}) > 0$ and $H(r_{BCP}) > 0$). Conversely, covalent interactions are characterized by large electron density values, charge concentration and negative energy densities (*i.e.*, large $\rho(r_{BCP})$, $\nabla^2\rho(r_{BCP}) < 0$ and $H(r_{BCP}) < 0$). However, it has been pointed out that for some interactions which may be classified as covalent bonds, the Laplacian is positive and the total energy density at the BCP ($H(r_{BCP})$) is negative. Such a situation is often observed for strong AH$\cdots$B hydrogen bonds classified as partly covalent in nature ($H(r_{BCP}) < 0$).

Delocalization Indices (D.I.) are a measure of the covariance between the population of two atoms A and B and, consequently, a measure of the number of electrons simultaneously fluctuating between these atoms,

$$\delta(A,B) = \int_A \int_B d\, 1 d2 \rho_{xc}(1,2) = cov(N_A, N_B) \tag{1}$$

where $\rho_{xc}(1,2)$ is the exchane-correlation density. It can be taken as the number of electron pairs shared between atoms A and B, *i.e.*, the bond order.

The AIMAll v11.08.23 program was used to carry out the QTAIM analysis on the previously optimized structures at the B3LYP-D3/6-311++G(3df,2p) level of theory. The ESI was employed to perform the calculation of the D.I..

Aromaticity Indices

Aromaticity indices provide a computational tool to assess the effect of the aromaticity in ring structures, molecules and large conjugated circuits. Among the different aromaticity indices available in the literature, the multicenter indices are among the most reliable ones for organic and inorganic systems. In particular, for a ring structure A composed of n atoms, $A = \{A_1, \dots, A_n\}$, we have chosen I_{ring},

$$I_{ring}(A) = 2^{n-1} \sum_{i_1 i_2 \dots i_n} S_{i_1 i_2}(A_1) \cdots S_{i_n i_1}(A_n) \tag{2}$$

and MCI

$$MCI(A) = \frac{1}{2n} \sum_{P(A)} I_{ring}(A) \tag{3}$$

where $S_{ij}(A_1)$ is the atomic overlap matrix (AOMs) of atom A_1,

$$S_{ij}(A_1) = \int_{A_1} d\, r \phi_i(r) \phi_j(r) \tag{4}$$

$\phi_i(r)$ is a molecular orbital. I_{ring} depends on the order of the atoms in the string for $n > 3$. The MCI is related to the n-center electron sharing index (nc-ESI), which is the n-center generalization of the covariance (eq. 1). These indices provide an electronic-based description of aromaticy, which is the most suitable one to investigate the effect of different substituents (EDGs and EWGs) in terms of electron density analysis, which is consistent with the D.I. and the topological analysis provided by the QTAIM.

All the aromaticity calculations were performed using the ESI-3D program and the AOMs obtained from AIMall.

Energy decomposition analysis (EDA)

The energy decomposition analysis (EDA) is a powerful tool for a quantitative interpretation of chemical bonds. The EDA scheme based on the energy decomposition analysis developed by Ziegler and Rauk and by Morokuma was carried out using the ADF2016 suite of programs. In order to perform the EDA analysis, all 1:1 Al-chelator complexes previously optimized at the B3LYP-D3(BJ)/6-31++G(d,p) IEFPCM level with Gaussian 09 were splitted in two fragments: aluminum surrounded by four water molecules and the unprotonated chelator. Single-point energies for the EDA analysis were calculated using the B3LYP-D3(BJ) functional and the very robust full electron (no frozen core) even-tempered quadruple-ζ basis set (ET-QZ3P-1-DIFFUSE) provided by ADF2016. All EDA calculations were performed both in gas phase and with the COSMO solvation model using the dielectric constant of water. However, it should be noted that a proper description of the solvent effect within the EDA scheme is not yet implemented in the ADF Modelling suite, and we have decided for an EDA analysis without solvent but at the solvent-including geometry.

The EDA decomposes the instantaneous interaction energy ΔE_{int} between two fragments A and B in a molecule AB into three well defined terms that can be interpreted in chemical meaningful ways:

$$\Delta E_{int} = \Delta E_{elstat} + \Delta E_{Pauli} + \Delta E_{oi} \tag{5}$$

These terms are (1) the quasiclassical electrostatic interaction energy between the charge densities of the fragments, ΔE_{elstat} (2) the exchange/repulsion between the fragments due to Pauli's principle, ΔE_{Pauli}, and (3) the energy gain due to orbital mixing of the fragments, ΔE_{oi}.

Considering that EDA calculations are usually carried out in the framework of density functional theory, if an explicit correction term for dispersion interaction is employed (such as Grimme's D3 method), then EDA numerical results remain unchanged but the dispersion correction appears as an extra term:

$$\Delta E_{int} = \Delta E_{elstat} + \Delta E_{Pauli} + \Delta E_{oi} + \Delta E_{disp} \tag{6}$$

Comparison of different Density Functional Theory and *Ab initio* methods

All the DFT functionals tested herein account for dispersion energies, though in different extents. As we can notice in Fig. S2, all functionals give very similar binding energies (ΔG_{aq}^{comp}) when compared with B3LYP-D3(BJ) energies; the same is true for MP2, with some slight fluctuations.

If we compare the binding energies for all the methods with respect to the experimental stability constants, we can see that the correlation coefficients (r) obtained for all different DFT functionals don't show significant variations, and the same is true if we consider the MP2 method (see Fig. S3). In this regard, we should mention that MP2 is well known to overestimate dispersion interactions. Indeed, as reported by these authors, MP2 poorly describes aromatic-containing systems and $\pi - \pi$ stacking interactions, while dispersion corrections improve such non-covalent interactions. Accordingly, the small differences between DFT methods and MP2 shown in Fig. S3 may be due to the presence of dispersion corrections which are supposed to improve the description of the behavior of these aluminum-ligand complexes.

The following tables show the values of binding energies (ΔG_{aq}^{comp}) and binding Enthalpy (ΔG_{aq}^{comp}) for all the methods, namely PBE0 and TPSS with the D3(BJ) dispersion correction scheme, ωB97XD, M06-2X, and MP2.

Stochiometry	Ligand		Theoretical		Exp.
			ΔH_{aq}^{comp}	ΔG_{aq}^{comp}	$\log\beta$
1:1 Complexes	Catecholates	Cathecolate	-88.7	-91.8	16.3
		4-nitrocatecholate	-74.7	-78.8	13.3
	Salicylates	Salicylicate	-75.3	-77.3	13.3
		3-nitrosalicylicate	-64.1	-66.6	9.5
		5-nitrosalicylicate	-64.0	-66.1	9.3
		3,5-dinitrosalicylicate	-55.6	-57.8	6.9
1:2 Complexes	Catecholates	Cathecolate	-152.3	-158.4	31.7
		4-nitrocatecholate	-129.1	-135.9	24.8
	Salicylates	Salicylicate	-128.9	-135.0	24.2
		3-nitrosalicylicate	-110.9	-114.9	17.7
		5-nitrosalicylicate	-110.7	-115.8	17.7
		3,5-dinitrosalicylicate	-96.9	-102.5	13.3
1:3 Complexes	Catecholates	Cathecolate	-184.1	-192.7	41.1
		4-nitrocatecholate	-160.1	-170.0	33.7
	Salicylates	Salicylicate	-158.5	-165.4	32.1
		3-nitrosalicylicate	-140.0	-146.0	23.7
		5-nitrosalicylicate	-139.6	-143.5	23.7
		3,5-dinitrosalicylicate	-127.4	-129.5	18.5
Total Correlation coefficient				0.9698	

Table S1: Binding enthalpies (ΔH_{aq}^{comp}) and free energies (ΔG_{aq}^{comp}) in kcal/mol computed at the ωB97XD level of theory for the 1:1, 1:2 and 1:3 complexes, and experimental $\log\beta$.

Stochiometry	Ligand	Theoretical		Exp.
		ΔH_{aq}^{comp}	ΔG_{aq}^{comp}	logβ
1:1 Complexes	Catecholates	Cathecolate	-88.4	-91.4	16.3
		4-nitrocatecholate	-74.9	-79.1	13.3
	Salicylates	Salicylicate	-73.9	-75.9	13.3
		3-nitrosalicylicate	-64.1	-66.6	9.5
		5-nitrosalicylicate	-63.4	-65.5	9.3
		3,5-dinitrosalicylicate	-55.8	-57.9	6.9
1:2 Complexes	Catecholates	Cathecolate	-152.4	-158.5	31.7
		4-nitrocatecholate	-130.2	-137.0	24.8
	Salicylates	Salicylicate	-126.6	-132.7	24.2
		3-nitrosalicylicate	-111.6	-115.6	17.7
		5-nitrosalicylicate	-109.5	-114.5	17.7
		3,5-dinitrosalicylicate	-97.5	-103.1	13.3
1:3 Complexes	Catecholates	Cathecolate	-186.8	-195.4	41.1
		4-nitrocatecholate	-163.4	-173.3	33.7
	Salicylates	Salicylicate	-159.5	-166.5	32.1
		3-nitrosalicylicate	-147.8	-153.9	23.7
		5-nitrosalicylicate	-142.2	-146.1	23.7
		3,5-dinitrosalicylicate	-137.6	-139.7	18.5
Total Correlation coefficient			0.9579	

Table S2: Binding enthalpies (ΔH_{aq}^{comp}) and free energies (ΔG_{aq}^{comp}) in kcal/mol computed at the MP2 level of theory for the 1:1, 1:2 and 1:3 complexes, and experimental logβ.

Stochiometry	Ligand		Theoretical		Exp.
			ΔH_{aq}^{comp}	ΔG_{aq}^{comp}	logβ
1:1 Complexes	Catecholates	Cathecolate	-88.0	-91.7	16.3
		4-nitrocatecholate	-73.2	-77.4	13.3
	Salicylates	Salicylicate	-75.3	-77.3	13.3
		3-nitrosalicylicate	-63.3	-65.8	9.5
		5-nitrosalicylicate	-63.4	-65.6	9.3
		3,5-dinitrosalicylicate	-54.4	-56.5	6.9
1:2 Complexes	Catecholates	Cathecolate	-154.7	-157.0	31.7
		4-nitrocatecholate	-130.1	-133.1	24.8
	Salicylates	Salicylicate	-132.3	-134.5	24.2
		3-nitrosalicylicate	-109.0	-113.0	17.7
		5-nitrosalicylicate	-113.1	-114.4	17.7
		3,5-dinitrosalicylicate	-97.8	-99.7	13.3
1:3 Complexes	Catecholates	Cathecolate	-182.7	-191.2	41.1
		4-nitrocatecholate	-155.4	-165.3	33.7
	Salicylates	Salicylicate	-158.9	-165.9	32.1
		3-nitrosalicylicate	-138.4	-144.4	23.7
		5-nitrosalicylicate	-138.4	-142.2	23.7
		3,5-dinitrosalicylicate	-125.0	-127.0	18.5
Total Correlation coefficient				0.9717	

Table S3: Binding enthalpies (ΔH_{aq}^{comp}) and free energies (ΔG_{aq}^{comp}) in kcal/mol computed at the M06-2X level of theory for the 1:1, 1:2 and 1:3 complexes, and experimental logβ.

Stochiometry	Ligand	Theoretical		Exp.
		ΔH_{aq}^{comp}	ΔG_{aq}^{comp}	logβ
1:1 Complexes	Catecholates	Cathecolate	-89.1	-92.1	16.3
		4-nitrocatecholate	-73.3	-77.5	13.3
	Salicylates	Salicylicate	-76.7	-78.7	13.3
		3-nitrosalicylicate	-64.7	-67.1	9.5
		5-nitrosalicylicate	-64.0	-66.1	9.3
		3,5-dinitrosalicylicate	-55.5	-57.7	6.9
1:2 Complexes	Catecholates	Cathecolate	-152.9	-159.0	31.7
		4-nitrocatecholate	-126.9	-133.7	24.8
	Salicylates	Salicylicate	-130.9	-136.9	24.2
		3-nitrosalicylicate	-111.4	-115.4	17.7
		5-nitrosalicylicate	-110.3	-115.4	17.7
		3,5-dinitrosalicylicate	-96.2	-101.8	13.3
1:3 Complexes	Catecholates	Cathecolate	-185.1	-193.7	41.1
		4-nitrocatecholate	-158.4	-168.2	33.7
	Salicylates	Salicylicate	-161.0	-168.0	32.1
		3-nitrosalicylicate	-140.9	-147.0	23.7
		5-nitrosalicylicate	-143.3	-139.4	23.7
		3,5-dinitrosalicylicate	-126.7	-128.8	18.5
Total Correlation coefficient			0.9718	

Table S4: Binding enthalpies (ΔH_{aq}^{comp}) and free energies (ΔG_{aq}^{comp}) in kcal/mol computed at the PBE0-D3(BJ) level of theory for the 1:1, 1:2 and 1:3 complexes, and experimental logβ.

Stochiometry	Ligand		Theoretical		Exp.
			ΔH_{aq}^{comp}	ΔG_{aq}^{comp}	$\log\beta$
1:1 Complexes	Catecholates	Cathecolate	-89.0	-92.1	16.3
		4-nitrocatecholate	-71.6	-75.8	13.3
	Salicylates	Salicylicate	-77.1	-79.1	13.3
		3-nitrosalicylicate	-64.1	-66.6	9.5
		5-nitrosalicylicate	-63.0	-65.1	9.3
		3,5-dinitrosalicylicate	-54.4	-56.5	6.9
1:2 Complexes	Catecholates	Cathecolate	-152.7	-158.8	31.7
		4-nitrocatecholate	-124.2	-131.0	24.8
	Salicylates	Salicylicate	-131.3	-137.3	24.2
		3-nitrosalicylicate	-110.1	-114.1	17.7
		5-nitrosalicylicate	-108.4	-113.5	17.7
		3,5-dinitrosalicylicate	-94.0	-99.6	13.3
1:3 Complexes	Catecholates	Cathecolate	-184.6	-193.2	41.1
		4-nitrocatecholate	-155.7	-165.6	33.7
	Salicylates	Salicylicate	-161.5	-168.4	32.1
		3-nitrosalicylicate	-140.0	-146.0	23.7
		5-nitrosalicylicate	-137.6	-141.4	23.7
		3,5-dinitrosalicylicate	-124.8	-126.9	18.5
Total Correlation coefficient				0.9726	

Table S5: Binding enthalpies (ΔH_{aq}^{comp}) and free energies (ΔG_{aq}^{comp}) in kcal/mol computed at the TPSS-D3(BJ) level of theory for the 1:1, 1:2 and 1:3 complexes, and experimental $\log\beta$.
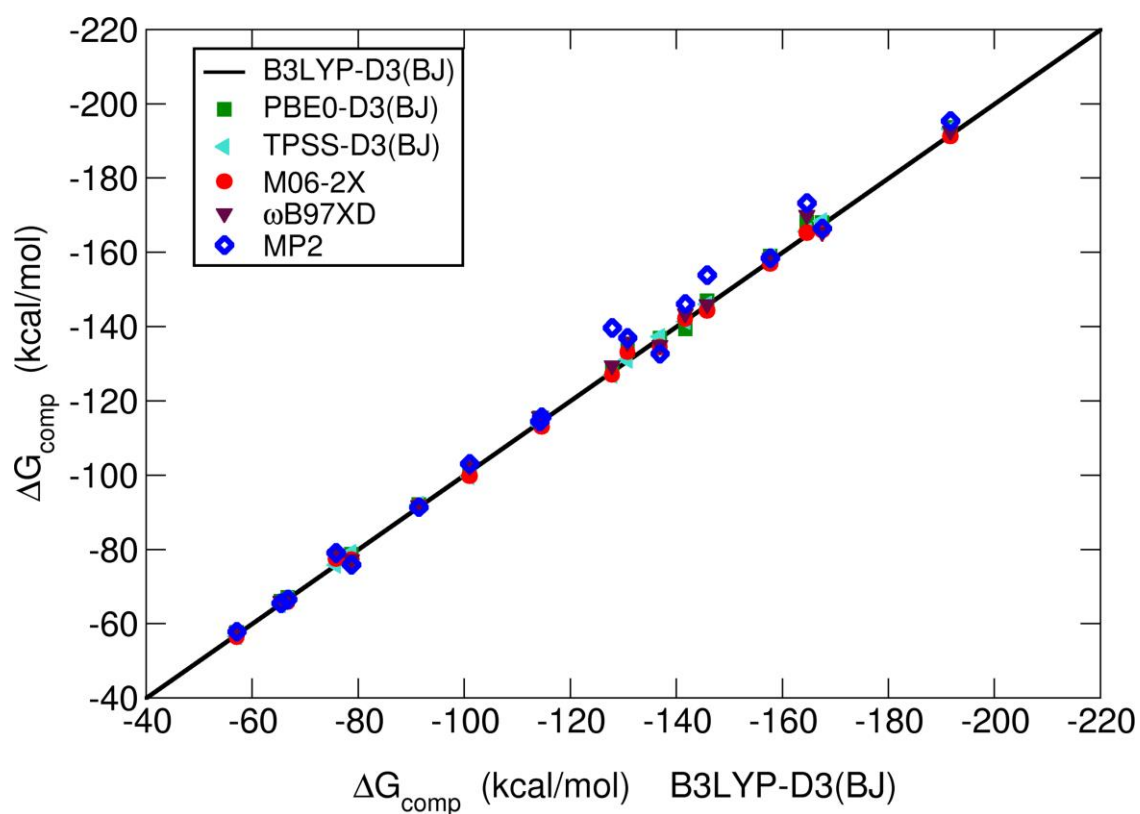
Figure S1: B3LYP-D3(BJ) Free binding energies (ΔG_{aq}^{comp}) compared with other dispersion corrected functionals:PBE0-D3(BJ), TPSS-D3(BJ), M06-2X, ωB97XD and the MP2 method. All single point calculations were performed with the 6-311++G(3df,2p) basis set on the B3LYP-D3(BJ)/6-31++G(d,p) optimized geometries using the self-consistent reaction field (SCRF) method with the polarized continuum model (PCM) with the integral equation formalism variant (IEFPCM). All energies are in kcal/mol.
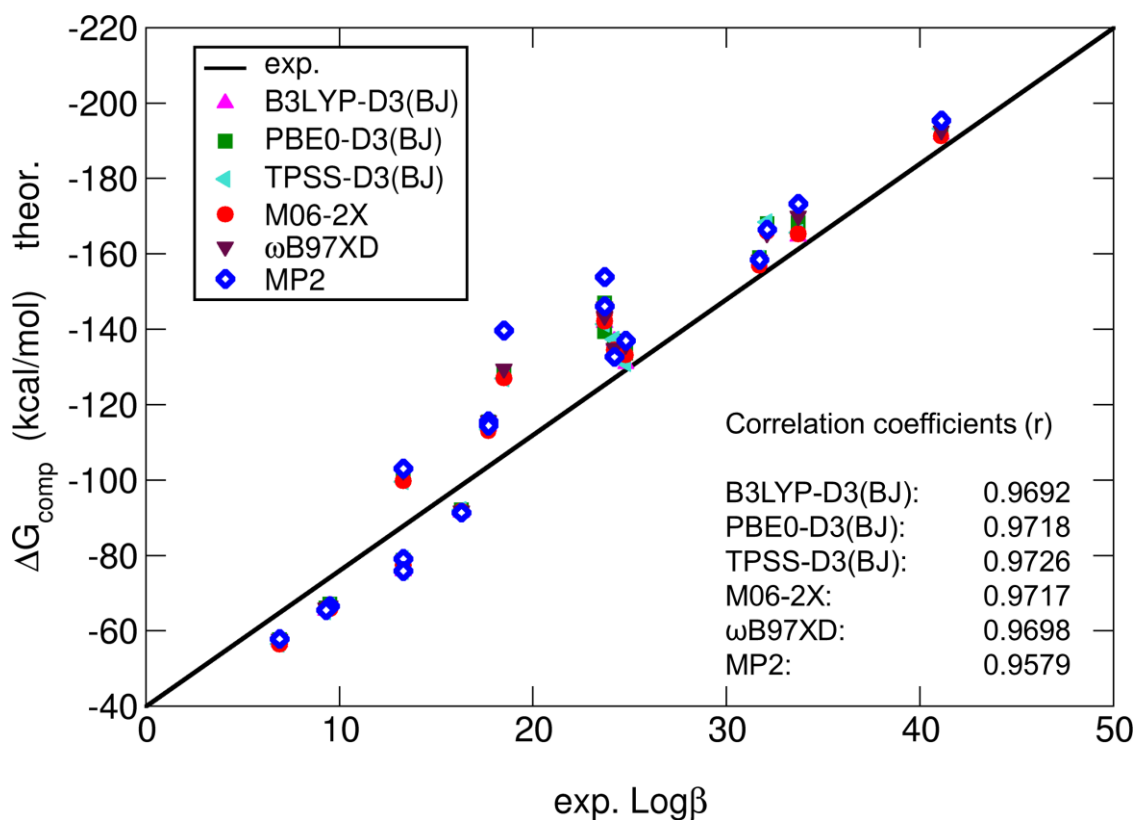
Figure S2: Different DFT and ab initio methods (B3LYP-D3(BJ), PBE0-D3(BJ), TPSS-D3(BJ), M06-2X,ωB97XD and MP2) compared with experimental stability constants. All single point calculations were performed with the 6-311++G(3df,2p) basis set on the B3LYP-D3(BJ)/6-31++G(d,p) optimized geometries using the self-consistent reaction field (SCRF) method with the polarized continuum model (PCM) with the integral equation formalism variant (IEFPCM).All energies are in kcal/mol.

Ligand	Al − O $_1$			Al − O $_2$		
	$\rho(r_{BCP})$	$\nabla^2\rho(r_{BCP})$	$H(r_{BCP})$	$\rho(r_{BCP})$	$\nabla^2\rho(r_{BCP})$	$H(r_{BCP})$
Catecholates						
Catecholate	0.0858	0.5271	-0.0078	0.0847	0.5193	-0.0074
Electron Withdrawing Groups						
4-nitrocatecholate	0.0846	0.5189	-0.0073	0.0802	0.4838	-0.0062
4,6-dinitrocatecholate	0.0842	0.5196	-0.0070	0.0764	0.4581	-0.0050
4,5,6-trinitrocatecholate	0.0752	0.4488	-0.0047	0.0815	0.4966	-0.0064
4-trifluoromethylcatecholate	0.0848	0.5207	-0.0074	0.0830	0.5059	-0.0069
4,6-trifluoromethilcatecholate	0.0841	0.5151	-0.0072	0.0806	0.4899	-0.0061
4,5,6-trifluoromethylcatecholate	0.0827	0.5057	-0.0067	0.0803	0.4887	-0.0059
Electron Donating Groups						
4-methylcatecholate	0.0857	0.5263	-0.0078	0.0853	0.52436	-0.0076
4,6-dimethylcatecholate	0.0860	0.5283	-0.0079	0.0858	0.5279	-0.0078
3,4,5,6-tetramethylcatecholate	0.0877	0.5444	-0.0082	0.867	0.5377	-0.0078
4-methoxycatecholate	0.0851	0.5214	-0.0076	0.0858	0.5273	-0.0078
Salicylates						
Salicylic acid	0.0842	0.5515	-0.0042	0.0887	0.5822	-0.0060
Electron Withdrawing Groups						
3-nitrosalicylicate	0.0840	0.5513	-0.0041	0.0850	0.5613	-0.0042
5-nitrosalicylicate	0.0834	0.5465	-0.0039	0.0844	0.5491	-0.0046
3,5-dinitrosalicylicate	0.0832	0.5458	-0.0038	0.0814	0.5334	-0.0031
3,4,5-trinitrosalicylicate	0.0790	0.5128	-0.0026	0.0823	0.5399	-0.0035
5-trifluoromethylsalicylicate	0.0866	0.5659	-0.0053	0.0836	0.5477	-0.0040
3,5-trifluoromethylsalicylicate	0.0835	0.5475	-0.0039	0.0847	0.5550	-0.0044
3,4,5-trifluoromethylsalicylicate	0.0834	0.5480	-0.0038	0.0827	0.5418	-0.0037
Electron Donating Groups						
3-methylsalicylicate	0.0847	0.5546	-0.0045	0.0884	0.5826	-0.0057
4-methylsalicylicate	0.0847	0.5542	-0.0045	0.0879	0.5764	-0.0057
5-methylsalicylicate	0.0846	0.5540	-0.0044	0.0884	0.5807	-0.0059
6-methylsalicylicate	0.0853	0.5623	-0.0045	0.0885	0.5823	-0.0059
3,5-dimethylsalicylicate	0.0848	0.5552	-0.0045	0.0890	0.5873	-0.0059
4,6-dimethylsalicylicate	0.0860	0.5694	-0.0046	0.0891	0.5886	-0.0059
3,4,5-trimethylsalicilicate	0.0851	0.5571	-0.0046	0.0893	0.5915	-0.0059
3,5-dimethoxysalicylicate	0.0842	0.5511	-0.0043	0.0892	0.5899	-0.0059

Table S6 (previous page): Characteristics of the Al-O Bond Critical Points (in a.u.) for the aluminum-chelator interactions: the electron density at the BCP ($\rho(r_{BCP})$), the Laplacian of electron density ($\nabla^2\rho(r_{BCP})$), and the total energy density at the BCP ($H(r_{BCP})$). All structures were optimized and refined at the B3LYP-D3(BJ)/6-311++G(3df,2p) level of theory as reported in the methods section. All calculations take into account implicit solvent effects according to the IEFPCM formalism.
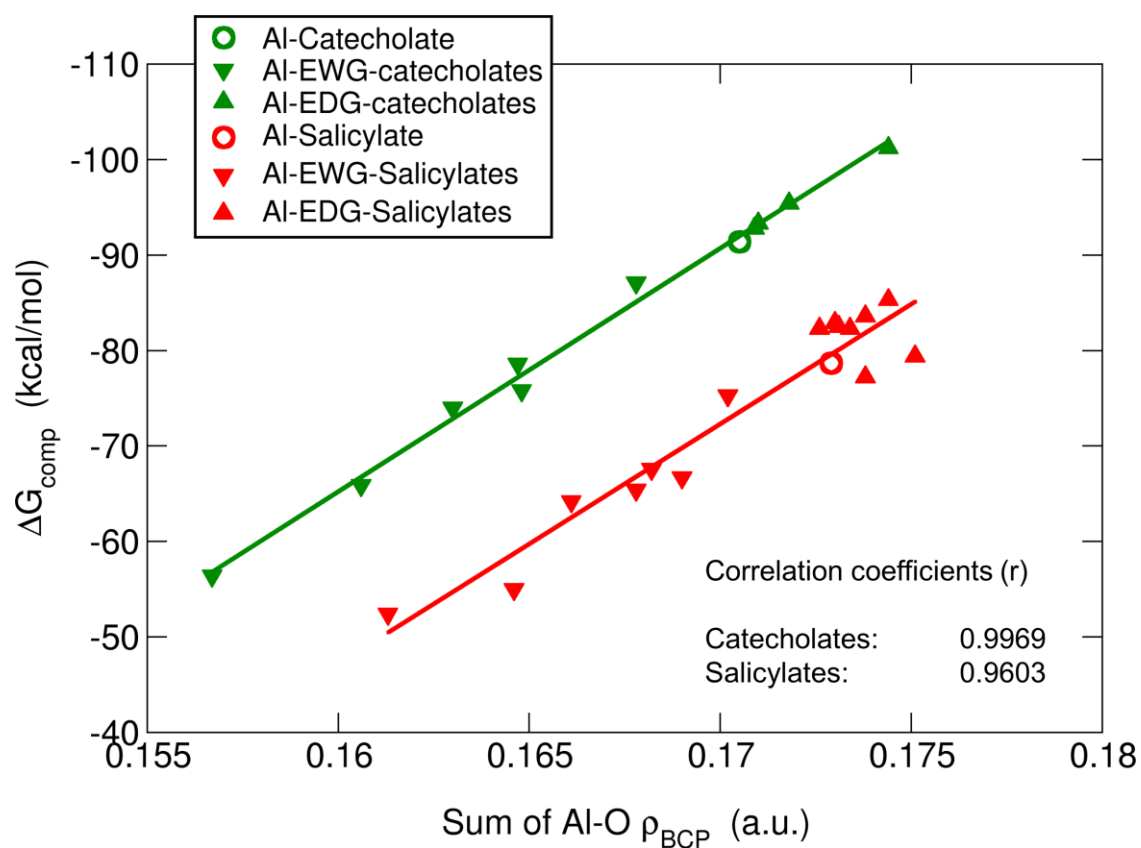
Figure S3: Free binding energies (ΔG_{aq}^{comp}) versus the sum of the electron density for all Al-O bond critical points $\rho(r_{BCP})$.
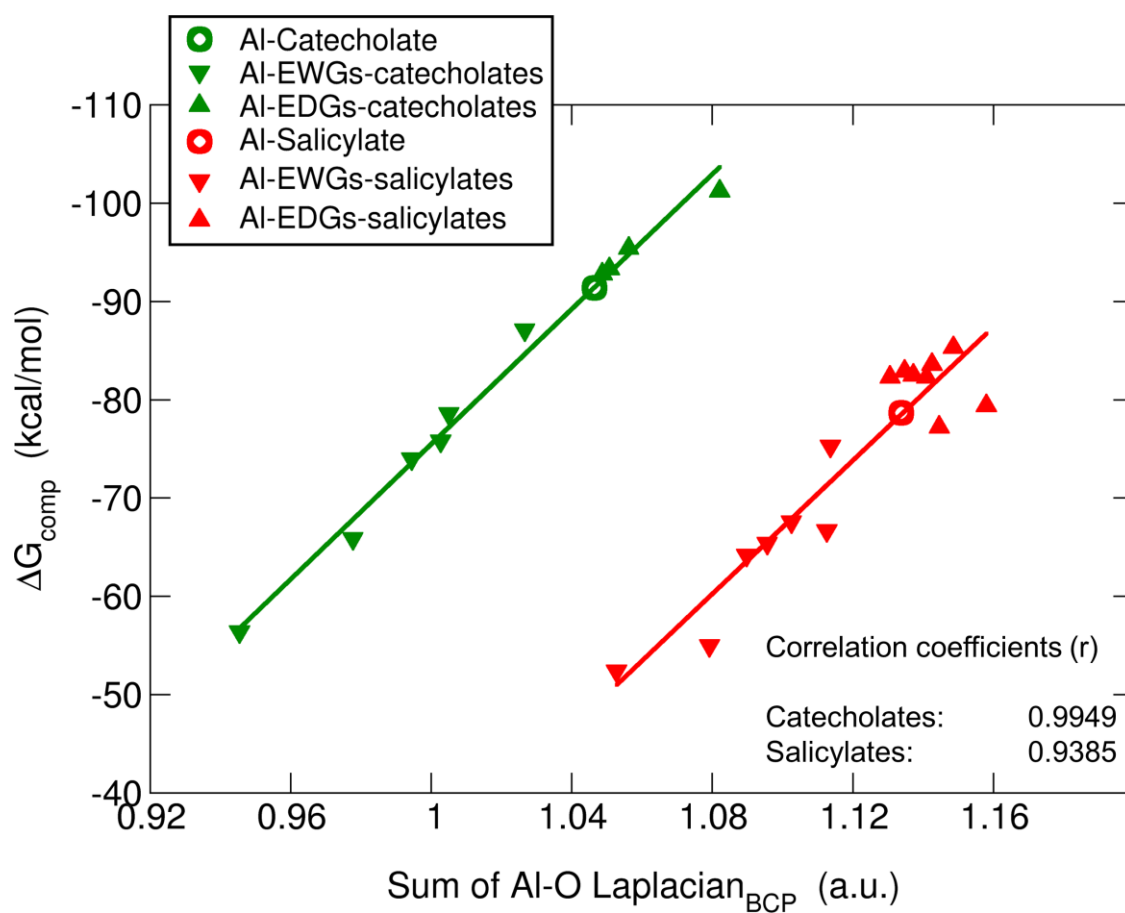
Figure S4: Free binding energies (ΔG_{aq}^{comp}) versus the sum of the Laplacian of the electron density for all Al-O bond critical points $\nabla^2 \rho(r_{BCP})$.
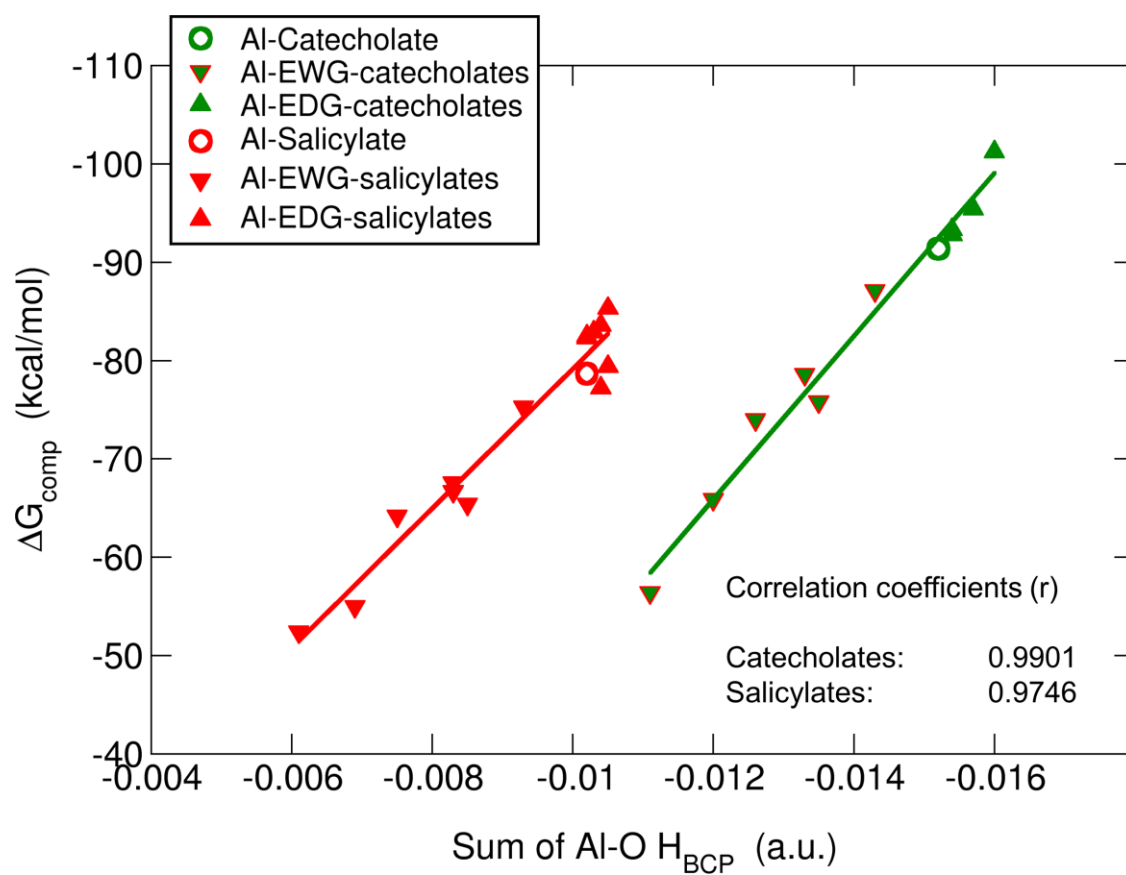
Figure S5: Free binding energies (ΔG_{aq}^{comp}) versus the sum of the total energy density for all Al-O bond critical points $H(r_{BCP})$.

Structure	L.I. (a.u.) Al	D.I.(a.u.) Al-O$_1$	Al-O$_2$	q(Bader, a.u.) qAl	qO$_1$	qO$_2$
Catecholates						
Catecholate	9.9433	0.2228	0.2208	2.5623	-1.3469	-1.3440
Electron Withdrawing Groups						
4-nitrocatecholate	9.9427	0.2183	0.2065	2.5658	-1.3239	-1.3337
4,6-dinitrocatecholate	9.9419	0.2151	0.1926	2.5686	-1.3250	-1.2877
4,5,6-trinitrocatecholate	9.409	0.2080	0.1900	2.5698	-1.3133	-1.2895
4-trifluoromethylcatecholate	9.9429	0.2193	0.2154	2.5644	-1.3378	-1.3385
4,6-trifluoromethilcatecholate	9.9426	0.2171	0.2064	2.5661	-1.3314	-1.3197
4,5,6-trifluoromethylcatecholate	9.9422	0.2119	0.2041	2.5670	-1.3237	-1.3099
Electron Donating Groups						
4-methylcatecholate	9.9433	0.2226	0.2226	2.5628	-1.3446	-1.3489
4,6-dimethylcatecholate	9.9433	0.2231	0.2230	2.5623	-1.3463	-1.3478
3,4,5,6-tetramethylcatecholate	9.9429	0.2262	0.2248	2.5616	-1.3465	-1.3499
4-methoxycatecholate	9.9433	0.2209	0.2246	2.5624	-1.3423	-1.3491
Salicylates						
Salicylic acid	9.9395	0.2065	0.2187	2.5743	-1.3593	-1.3600
Electron Withdrawing Groups						
3-nitrosalicylicate	9.9387	0.2047	0.2038	2.5768	-1.3551	-1.3338
5-nitrosalicylicate	9.9394	0.2041	0.2067	2.5763	-1.3551	-1.3407
3,5-dinitrosalicylicate	9.9386	0.2019	0.1943	2.5788	-1.3514	-1.3190
3,4,5-trinitrosalicylicate	9.9388	0.1901	0.1998	2.5780	-1.3122	-1.3491
5-trifluoromethylsalicylicate	9.9395	0.2130	0.2054	2.5751	-1.3517	-1.3569
3,5-trifluoromethylsalicylicate	9.9390	0.2055	0.2038	2.5768	-1.3350	-1.3546
3,4,5-trifluoromethylsalicylicate	9.9390	0.2019	0.2019	2.5770	-1.3284	-1.3514
Electron Donating Groups						
3-methylsalicylicate	9.9392	0.2086	0.2183	2.5758	-1.3593	-1.3590
4-methylsalicylicate	9.9395	0.2093	0.2187	2.5746	-1.3596	-1.3614
5-methylsalicylicate	9.9395	0.2090	0.2200	2.5746	-1.3594	-1.3624
6-methylsalicylicate	9.9389	0.2090	0.2182	2.5751	-1.3592	-1.3614
3,5-dimethylsalicylicate	9.9392	0.2091	0.2199	2.5755	-1.3598	-1.3608
4,6-dimethylsalicylicate	9.9389	0.2110	0.2192	2.5746	-1.3618	-1.3626
3,4,5-trimethylsalicilicate	9.9393	0.2102	0.2214	2.5742	-1.3606	-1.3642
3,5-dimethoxysalicylicate	9.9393	0.2079	0.2211	2.5745	-1.3581	-1.3538

Table S7: Localization and Delocalization Indices (D.I.), in a.u., for the aluminum-oxygen bonds in the Al.chelator complex dataset. Localization Index (L.I.), in a.u., for the aluminum atom. Bader's atomic charges, in a.u., are also provided. All structures were optimized and refined at the B3LYP-D3(BJ)/6-311++G(3df,2p)

level of theory as reported in the methods section. All calculations take into account implicit solvent effects according to the IEFPCM formalism

Structure	ΔE_{elstat}	(%)	ΔE_{oi}	(%)	ΔE_{Pauli}	ΔE_{disp}	ΔE_{int}
Al-Catecholates							
Catecholate	-610.4	(64.9)	-329.7	(35.1)	149.9	-6.5	**-796.7**
Electron Withdrawing Groups							
4-nitrocatecholate	-647.1	(72.4)	-247.1	(27.6)	147.2	-6.5	**-753.5**
4,6-dinitrocatecholate	-610.0	(71.7)	-240.9	(28.3)	139.0	-6.7	**-718.6**
4,5,6-trinitrocatecholate	-583.4	(70.9)	-239.4	(29.1)	133.6	-6.7	**-695.9**
4-trifluoromethylcatecholate	-571.2	(63.1)	-333.8	(36.9)	144.4	-6.5	**-767.2**
4,6-trifluoromethilcatecholate	-578.0	(65.4)	-306.4	(34.6)	141.3	-6.7	**-749.8**
4,5,6-trifluoromethylcatecholate	-589.1	(67.5)	-283.3	(32.5)	144.9	-6.8	**-734.3**
Electron Donating Groups							
4-methylcatecholate	-601.0	(64.0)	-337.6	(36.0)	149.6	-6.4	**-795.4**
4,6-dimethylcatecholate	-601.1	(63.9)	-339.3	(36.1)	151.1	-6.7	**-796.0**
3,4,5,6-tetramethylcatecholate	-593.5	(62.9)	-350.8	(37.1)	153.1	-6.9	**-798.0**
4-methoxycatecholate	-590.1	(63.2)	-343.8	(36.2)	148.8	-6.5	**-791.6**
Al-Salicylates							
Salicylic acid	-659.8	(70.6)	-274.7	(29.4)	153.6	-7.7	**-788.7**
Electron Withdrawing Groups							
3-nitrosalicylicate	-654.8	(73.0)	-241.9	(27.0)	148.0	-8.2	**-757.0**
5-nitrosalicylicate	-634.8	(72.0)	-246.6	(27.0)	146.8	-7.8	**-742.4**
3,5-dinitrosalicylicate	-610.2	(71.6)	-241.9	(28.4)	141.4	-8.3	**-718.9**
3,4,5-trinitrosalicylicate	-588.8	(71.2)	-238.3	(28.8)	136.6	-8.2	**-698.8**
5-trifluoromethylsalicylicate	-615.7	(68.2)	-287.5	(31.8)	148.5	-7.8	**-762.4**
3,5-trifluoromethylsalicylicate	-620.1	(70.1)	-263.9	(29.9)	145.3	-8.3	**-746.9**
3,4,5-trifluoromethylsalicylicate	-629.3	(72.6)	-238.1	(27.4)	143.7	-8.4	**-732.1**
Electron Donating Groups							
3-methylsalicylicate	-651.5	(70.2)	-276.8	(29.8)	153.5	-8.1	**-782.9**
4-methylsalicylicate	-639.5	(68.8)	-289.7	(31.2)	152.8	-7.7	**-784.1**
5-methylsalicylicate	-642.0	(69.0)	-288.4	(31.0)	153.1	-7.7	**-785.0**
6-methylsalicylate	-652.3	(70.7)	-279.1	(29.3)	153.5	-7.9	**-758.8**
3,5-dimethylsalicylicate	-642.2	(69.1)	-287.8	(30.9)	153.8	-8.1	**-784.3**
4,6-dimethylsalicylicate	-638.3	(68.4)	-295.0	(31.4)	154.2	-7.9	**-786.9**
3,4,5-trimethylsalicilicate	-637.4	(68.4)	-295.0	(31.6)	154.4	-8.2	**-786.1**
3,5-dimethoxysalicylicate	-626.4	(67.1)	-306.8	(32.9)	152.1	-7.9	**-789.0**

Table S8: Energy Decomposition Analysis, values obtained at the full electron (no frozen core) B3LYP-D3(BJ)/ET-QZ3P-1DIFFUSE level of theory in gas phase, using the ADF2016 modelling suite of programs.

Structure	I_{ring}			MCI		
	Al-Lig	Lig	($\Delta_{Arom.}$)	Al-Lig	Lig	($\Delta_{Arom.}$)
Benzene		0.0472			0.0705	
Ciclohexane		0.0003			0.0003	
Al-Catecholates						
Catechol		0.0374			0.0551	
Catecholate	0.0345	0.0235	(0.0110)	0.0503	0.0322	(0.0181)
Electron Withdrawing Groups						
4-nitrocatecholate	0.0258	0.0128	(0.0130)	0.0353	0.0150	(0.0203)
4,6-dinitrocatecholate	0.0211	0.0096	(0.0115)	0.0283	0.0116	(0.0167)
4,5,6-trinitrocatecholate	0.0207	0.0074	(0.0133)	0.0280	0.0086	(0.0194)
4-trifluoromethylcatecholate	0.0308	0.0193	(0.0115)	0.0440	0.0257	(0.0183)
4,6-trifluoromethilcatecholate	0.0279	0.0159	(0.0120)	0.0396	0.0212	(0.0184)
4,5,6-trifluoromethylcatecholate	0.0258	0.0136	(0.0122)	0.0363	0.0181	(0.0182)
Electron Donating Groups						
4-methylcatecholate	0.0331	0.0227	(0.0104)	0.0480	0.0310	(0.0170)
4,6-dimethylcatecholate	0.0320	0.0224	(0.0096)	0.0463	0.0307	(0.0156)
3,4,5,6-tetramethylcatecholate	0.0302	0.0216	(0.0086)	0.0436	0.0297	(0.0139)
4-methoxycatecholate	0.0308	0.0218	(0.0090)	0.0447	0.0297	(0.0150)
Al-Salicylates						
Salicylic acid		0.0353			0.0510	
Salycilicate	0.0351	0.0306	(0.0045)	0.0510	0.0436	(0.0074)
Electron Withdrawing Groups						
3-nitrosalicylicate	0.0295	0.0187	(0.0108)	0.0419	0.0248	(0.0171)
5-nitrosalicylicate	0.0284	0.0185	(0.0099)	0.0395	0.0232	(0.0163)
3,5-dinitrosalicylicate	0.0255	0.0154	(0.0101)	0.0353	0.0196	(0.0157)
3,4,5-trinitrosalicylicate	0.0249	0.0156	(0.0093)	0.0345	0.0199	(0.0146)
5-trifluoromethylsalicylicate	0.0323	0.0259	(0.0064)	0.0462	0.0355	(0.0107)
3,5-trifluoromethylsalicylicate	0.0305	0.0229	(0.0076)	0.0437	0.0311	(0.0126)
3,4,5-trifluoromethylsalicylicate	0.0294	0.0214	(0.0080)	0.0421	0.0291	(0.0130)
Electron Donating Groups						
3-methylsalicylate	0.0332	0.0295	(0.0037)	0.0478	0.0419	(0.0059)
4-methylsalicylicate	0.0327	0.0294	(0.0033)	0.0469	0.0416	(0.0053)
5-methylsalicylicate	0.0334	0.0301	(0.0033)	0.0482	0.0428	(0.0054)
6-methylsalicylicate	0.0333	0.0296	(0.0037)	0.0481	0.0419	(0.0062)
3,5-dimethylsalicylicate	0.0317	0.0291	(0.0026)	0.0454	0.0414	(0.0040)
4,6-dimethylsalicylate	0.0310	0.0284	(0.0026)	0.0443	0.0401	(0.0035)
3,4,5-trimethylsalicilicate	0.0305	0.0282	(0.0026)	0.0436	0.0401	(0.0035)
3,5-dimethoxysalicylicate	0.0271	0.0254	(0.0017)	0.0387	0.0360	(0.0027)

Table S9: Aromaticity indices according to the I_{ring} and MCI aromatic descriptors computed on the free ligand (Lig) and aluminum-ligand complexes (Al-Lig). Relative aromatic changes from aluminum-bound to unbound state ($\Delta_{arom.}$) are also provided. Benzene is used as reference for an aromatic compound, ciclohexane for a non-aromatic one. All indices are in a.u.

Al-dimethylcatecholate

Al-dinitrocatecholate

Al-dimethylsalicylate

Al-dinitrosalicylate
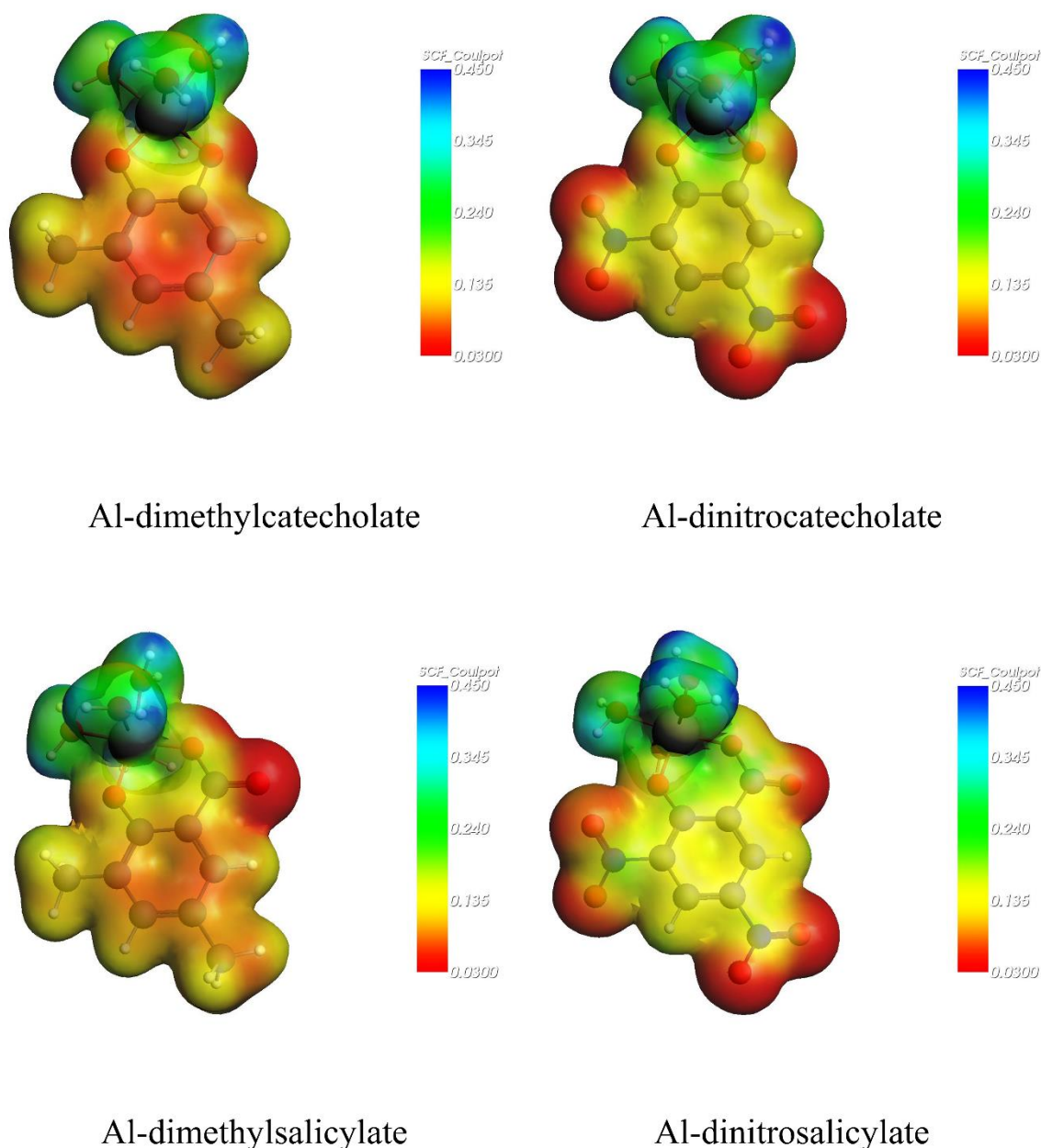
Fig. S10: Electrostatic potential surfaces obtained from the SCF density calculated at the B3LYP-D3(BJ)/ET-QZ3P-1DIFFUSE level of theory using the ADF2016 suite of programs. Red areas account for negative charge distribution (low potential, high electron density), while blue areas account for positive charge distribution

(high potential, low electron density). The introduction of a methyl group increases the electron density, while the introduction of a nitro group leads to the decrease of the electron density. In general, catecholates show higher electron density (covalent character) than salicylates.

APPENDIX B

"I come from down in the valley
where mister when you're young
They bring you up to do like your daddy done
Me and Mary we met in high school
when she was just seventeen
We'd ride out of this valley down to where the fields were green"

(B. Springsteen, The River)

Appendix B

Design of New Efficient Chelators of Aluminum Based on Mimosine Containing Peptides

- **Figure S1:** Crystal structure of Al(III)-DFP$_3$.

- **Figure S2:** DFT structures of Al.DFP$_3$ and Al.Pept$^9_{3G}$.

- **Figure S3:** RMSD of all Al-Peptide complexes.

- **Table S1:** geometries on Al-DFP$_3$ and Al.Pept$^9_{3G}$ structures.

- **Table S2:** radius of gyrations computed on all QM/MM MD simulations.

- **Table S3:** Average values of all possible O^{Mim}-Al-O^{Mim} angles.

- **Table S4-S11:** all individual hydrogen bonds during the QM/MM MD simulations of the apoforms of the eight peptides.
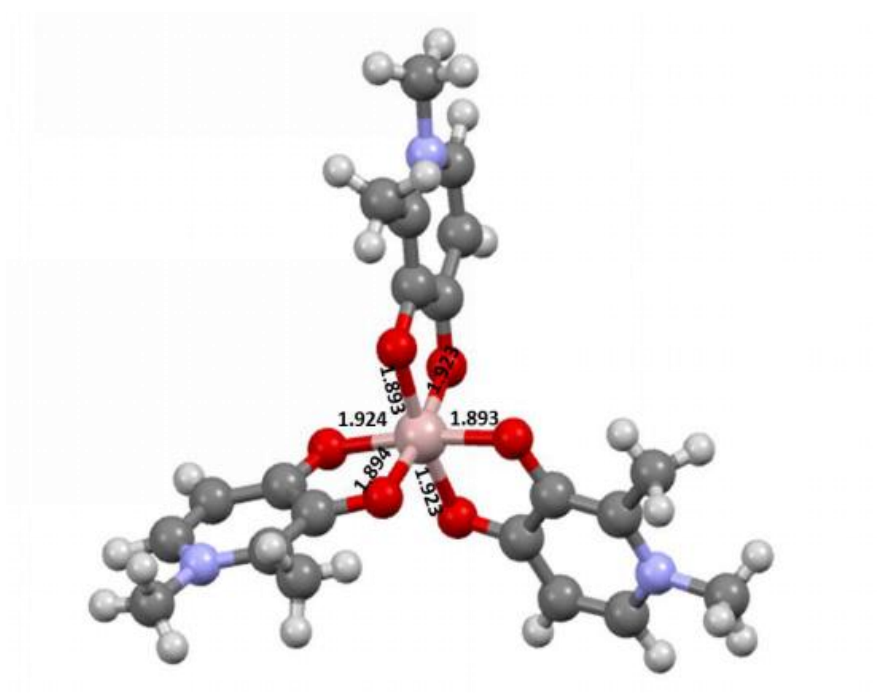
Figure S1. Crystal structure of Al(III)-DFP$_3$. Al-O distances (Å).
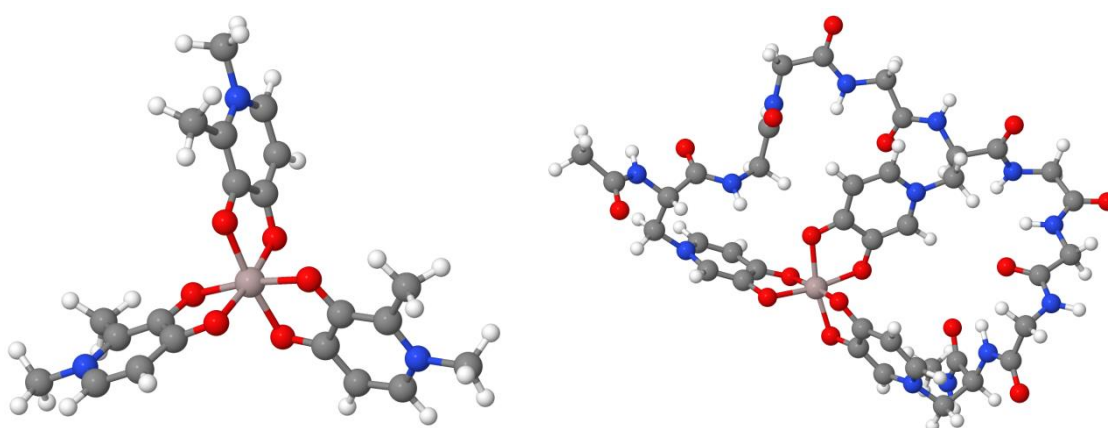
Figure S2. DFT structures of Al(III)-DFP$_3$ (left) and Al-Pept$^9_{3G}$ (right).
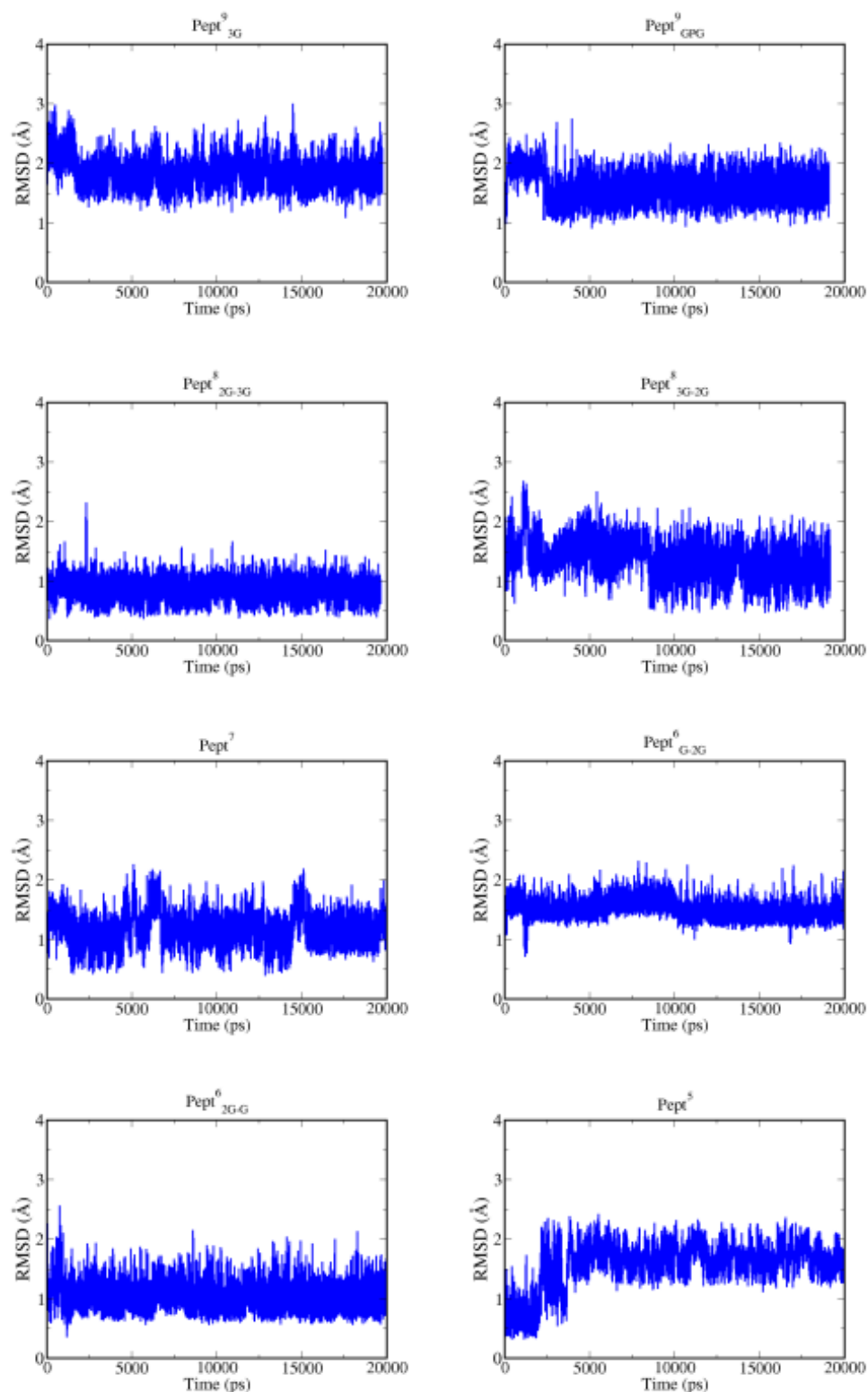
Figure S3. Root mean square deviations (RMSD, in Å) computed on the QM/MM MD simulations. From left to right: $Pept^9_{3G}$, $Pept^9_{GPG}$, $Pept^8_{2G-3G}$ and $Pept^8_{3G-2G}$, $Pept^7$, $Pept^6_{G-2G}$, $Pept^6_{2G-G}$ and $Pept^5$.

			Al-DFP₃		Al-Pept⁹₃G
			X-ray	**DFT**	**DFT**
	Atom1	**Atom2**			
	Al	O_C^A	1.924	1.951	1.943
	Al	O_H^A	1.894	1.916	1.903
	Al	O_C^B	1.923	1.946	1.990
	Al	O_H^B	1.893	1.914	1.913
	Al	O_C^C	1.923	1.945	1.954
	Al	O_H^C	1.893	1.918	1.908
Atom1	**Atom2**	**Atom3**			
Al1	O_C^A	C_C^A	112.22	112.18	109.76
Al1	O_H^A	C_H^A	111.97	112.85	109.81
Al1	O_C^B	C_C^B	112.19	111.77	110.20
Al1	O_H^B	C_H^B	112.22	112.32	111.66
Al1	O_C^C	C_C^C	111.97	112.02	108.96
Al1	O_H^C	C_H^C	112.00	112.44	108.87
O_C^A	Al	C_H^A	84,23	83.57	83.90
O_C^A	Al	C_C^B	89,83	90.66	92.73
O_C^A	Al	C_H^B	171,91	172.55	93.53
O_C^A	Al	C_C^C	89,79	94.12	175.22
O_C^A	Al	O_H^C	95.65	90.05	95.10
O_H^A	Al	O_C^B	95.73	94.45	88.59
O_H^A	Al	O_H^B	90,87	91.52	170.87
O_H^A	Al	O_C^C	171,82	91.20	91.631
O_H^A	Al	O_H^C	90,84	171.69	100.96
O_C^B	Al	O_H^B	84,25	84.12	82.77
O_C^B	Al	O_C^C	89,82	172.98	88.85
O_C^B	Al	O_H^C	171,85	90.94	168.22
O_H^B	Al	O_C^C	95,68	91.58	91.15
O_H^B	Al	O_H^C	90,83	95.33	87.98
O_C^C	Al	O_H^C	84,19	83.92	84.05

Table S1. Distances (in Å) and angles (in degrees) computed on the crystal structure of Al(III)-DFP$_3$, and the DFT structures of Al(III)-DFP$_3$ and Al-Pept$^9_{3G}$.

	Apoform	Al(III)-Peptide
Pept$^9_{3G}$	7.68 (1.14)	6.78 (0.10)
Pept$^9_{GPG}$	7.04 (0.97)	7.05 (0.11)
Pept$^8_{2G-3G}$	7.15 (1.01)	6.56 (0.09)
Pept$^8_{3G-2G}$	7.12 (0.92)	6.43 (0.12)
Pept^7	6.49 (0.77)	6.25 (0.11)
Pept$^6_{G-2G}$	6.36 (0.69)	5.71 (0.15)
Pept$^6_{2G-G}$	6.43 (0.70)	5.89 (0.13)
Pept^5	5.90 (0.50)	5.32 (0.18)

Table S2 Average and standard deviation (in Å) radius of Gyration computed along the QM/MM MD simulation trajectories of the apoform of the peptides in solution and Al-Pept complexes.

	$Pept^9_{3G}$	$Pept^9_{GPG}$	$Pept^8_{2G\text{-}3G}$	$Pept^8_{3G\text{-}2G}$	$Pept^7$	$Pept^6_{G\text{-}2G}$	$Pept^6_{2G\text{-}G}$	$Pept^5$
Oc^A-Al-O_{OH}^A	88.1 (3.6)	87.8 (3.7)	87.6 (3.7)	87.2 (4.0)	88.3 (3.6)	88.8 (3.5)	89.0 (3.6)	88.2 (3.7)
Oc^A-Al-Oc^B	91.5 (8.1)	93.7 (7.9)	98.8 (8.1)	86.0 (7.8)	92.6 (16.5)	101.7 (27.1)	126.8 (9.2)	129.4 (25.7)
Oc^A-Al-O_{OH}^B	90.6 (8.6)	87.5 (8.3)	84.8 (7.6)	103.6 (25.5)	134.9 (35.0)	93.1 (8.4)	112.3 (10.6)	129.5 (16.8)
Oc^A-Al-Oc^C	168.2 (6.2)	167.3 (6.5)	166.5 (6.5)	156.5 (24.8)	92.5 (11.4)	89.7 (8.1)	84.6 (6.6)	84.6 (8.6)
Oc^A-Al-O_{OH}^C	89.1 (8.5)	85.9 (7.8)	84.9 (7.7)	95.0 (12.7)	122.8 (31.9)	165.4 (7.7)	128.9 (13.6)	116.2 (19.4)
O_{OH}^A-Al-Oc^B	85.9 (7.0)	82.3 (6.4)	80.7 (6.0)	114.8 (37.1)	107.5 (32.8)	121.3 (11.4)	120.5 (7.8)	111.2 (11.3)
O_{OH}^A-Al-O_{OH}^B	167.3 (6.3)	164.3 (7.2)	161.9 (6.9)	135.4 (35.4)	94.3 (14.7)	125.5 (8.9)	103.7 (9.0)	95.3 (12.1)
O_{OH}^A-Al-Oc^C	90.6 (8.1)	94.2 (8.5)	96.7 (8.2)	84.5 (7.5)	144.9 (30.4)	117.8 (10.6)	158.8 (11.4)	155.7 (24.9)
O_{OH}^A-Al-O_{OH}^C	100.7 (8.4)	101.1 (8.9)	103.5 (8.5)	107.3 (23.9)	89.6 (16.5)	83.4 (6.8)	83.5 (7.2)	94.1 (10.2)
Oc^B-Al-O_{OH}^B	87.3 (3.7)	86.8 (4.2)	86.9 (3.8)	84.5 (7.5)	72.4 (25.2)	29.9 (11.3)	26.2 (9.9)	28.4 (18.8)
Oc^B-Al-Oc^C	91.8 (9.4)	92.7 (9.0)	89.1 (8.5)	107.1 (25.8)	98.6 (17.3)	111.7 (17.2)	77.2 (10.7)	86.5 (23.8)
Oc^B-Al-O_{OH}^C	167.3 (6.2)	168.3 (6.3)	168.1 (6.1)	127.2 (42.8)	135.6 (36.1)	87.7 (25.4)	98.7 (9.4)	103.5 (12.5)
O_{OH}^B-Al-Oc^C	91.3 (7.9)	91.8 (7.9)	92.6 (8.0)	89.3 (8.9)	108.9 (32.8)	115.7 (9.3)	95.2 (9.7)	98.7 (14.9)
O_{OH}^B-Al-O_{OH}^C	86.5 (7.0)	90.1 (8.1)	89.6 (7.5)	110.3 (35.0)	94.6 (13.1)	96.7 (7.9)	117.6 (8.9)	112.6 (10.6)
Oc^C-Al-O_{OH}^C	87.9 (3.7)	88.0 (3.8)	87.3 (3.8)	88.3 (3.6)	88.0 (3.8)	89.5 (3.6)	88.9 (3.6)	85.2 (16.5)

Table S3. Average values (and their standard deviations) of all possible O^{Mim}-Al-O^{Mim} angles computed along the standard MD simulation trajectories of the Al-Pept complexes. Since the indices of the three Mimosine residues differ on the systems, they are referred to as A, B and C for the first, central and last Mimosine in the corresponding sequence shown in Fig. 4.1.

Acceptor	DonorH	Donor	Frames	Frac	AvgDist	AvgAng
GLY_3@O	GLY_5@H	GLY_5@N	215	0.0108	2.8785	146.3374
GLY_7@O	GLY_9@H	GLY_9@N	212	0.0107	2.8822	146.6055
MIH_2@O	GLY_4@H	GLY_4@N	115	0.0058	2.9048	144.1116
GLY_3@O	GLY_7@H	GLY_7@N	108	0.0054	2.8808	155.7838
MIH_6@O	GLY_8@H	GLY_8@N	108	0.0054	2.9069	145.295
GLY_4@O	GLY_8@H	GLY_8@N	105	0.0053	2.8992	148.6666
GLY_7@O	NME_11@H	NME_11@N	103	0.0052	2.9102	158.7487
GLY_5@O	GLY_8@H	GLY_8@N	88	0.0044	2.9053	151.2934
MIH_6@O	GLY_9@H	GLY_9@N	83	0.0042	2.9332	149.4445
MIH_2@O	GLY_5@H	GLY_5@N	79	0.004	2.9273	150.6268
GLY_8@O	GLY_5@H	GLY_5@N	76	0.0038	2.8772	152.9991
GLY_8@O	MIH_10@H	MIH_10@N	74	0.0037	2.8827	143.9258
GLY_3@O	MIH_6@H	MIH_6@N	70	0.0035	2.9301	153.4352
GLY_4@O	MIH_6@H	MIH_6@N	67	0.0034	2.8916	143.8881
GLY_7@O	MIH_10@H	MIH_10@N	65	0.0033	2.9414	155.0316
ACE_1@O	GLY_4@H	GLY_4@N	61	0.0031	2.9071	151.0677
GLY_3@O	GLY_8@H	GLY_8@N	57	0.0029	2.8701	147.764
GLY_4@O	GLY_9@H	GLY_9@N	47	0.0024	2.8802	150.0839
GLY_9@O	NME_11@H	NME_11@N	40	0.002	2.9071	142.9866
GLY_5@O	GLY_7@H	GLY_7@N	38	0.0019	2.9128	143.2313
GLY_5@O	GLY_9@H	GLY_9@N	36	0.0018	2.8748	154.2794
ACE_1@O	GLY_8@H	GLY_8@N	35	0.0018	2.8871	155.9333
GLY_9@O	GLY_4@H	GLY_4@N	33	0.0017	2.8694	154.1742
ACE_1@O	GLY_3@H	GLY_3@N	32	0.0016	2.9065	145.3006
GLY_3@O	GLY_9@H	GLY_9@N	30	0.0015	2.885	148.2627
GLY_3@O	NME_11@H	NME_11@N	25	0.0013	2.9134	159.6403
GLY_9@O	GLY_5@H	GLY_5@N	23	0.0012	2.8768	153.1714
GLY_4@O	GLY_7@H	GLY_7@N	19	0.001	2.9105	151.6243
GLY_9@O	GLY_3@H	GLY_3@N	18	0.0009	2.8835	152.2386
GLY_8@O	GLY_4@H	GLY_4@N	18	0.0009	2.8916	153.0775
ACE_1@O	GLY_5@H	GLY_5@N	18	0.0009	2.8945	153.0308
MIH_6@O	MIH_2@H	MIH_2@N	18	0.0009	2.9474	155.769
ACE_1@O	GLY_7@H	GLY_7@N	16	0.0008	2.8653	156.489
GLY_7@O	GLY_4@H	GLY_4@N	16	0.0008	2.91	160.0729
GLY_8@O	GLY_3@H	GLY_3@N	14	0.0007	2.8735	154.0044
ACE_1@O	GLY_9@H	GLY_9@N	10	0.0005	2.8745	155.7919

ACE_1@O	NME_11@H	NME_11@N	10	0.0005	2.8876	164.7855
GLY_8@O	NME_11@H	NME_11@N	9	0.0005	2.8826	161.073
GLY_5@O	MIH_2@H	MIH_2@N	9	0.0005	2.9112	159.5201
GLY_7@O	GLY_3@H	GLY_3@N	9	0.0005	2.9287	147.5528
GLY_9@O	MIH_6@H	MIH_6@N	9	0.0005	2.9326	161.5631
GLY_5@O	NME_11@H	NME_11@N	8	0.0004	2.9105	152.8098
MIH_6@O	MIH_10@H	MIH_10@N	8	0.0004	2.9398	149.5473
MIH_6@O	GLY_3@H	GLY_3@N	7	0.0004	2.908	156.0943
MIH_2@O	MIH_10@H	MIH_10@N	7	0.0004	2.9193	154.3373
ACE_1@O	MIH_10@H	MIH_10@N	7	0.0004	2.9381	155.7219
MIH_10@O	GLY_7@H	GLY_7@N	7	0.0004	2.9427	153.8193
MIH_10@O	GLY_4@H	GLY_4@N	6	0.0003	2.8829	150.1012
GLY_4@O	MIH_10@H	MIH_10@N	5	0.0003	2.8669	158.2397
MIH_10@O	MIH_6@H	MIH_6@N	4	0.0002	2.8581	154.516
GLY_4@O	NME_11@H	NME_11@N	4	0.0002	2.8599	164.25
GLY_8@O	MIH_6@H	MIH_6@N	4	0.0002	2.9029	147.6096
MIH_2@O	NME_11@H	NME_11@N	4	0.0002	2.9237	146.8696
MIH_10@O	GLY_5@H	GLY_5@N	3	0.0002	2.861	147.852
MIH_2@O	GLY_8@H	GLY_8@N	3	0.0002	2.8987	143.7901
ACE_1@O	MIH_6@H	MIH_6@N	3	0.0002	2.9012	158.9874
MIH_2@O	MIH_6@H	MIH_6@N	3	0.0002	2.929	145.2159
MIH_2@O	GLY_7@H	GLY_7@N	3	0.0002	2.9306	151.2682
GLY_7@O	GLY_5@H	GLY_5@N	3	0.0002	2.9482	164.0803
GLY_8@O	MIH_2@H	MIH_2@N	3	0.0002	2.9585	151.8144
GLY_7@O	MIH_2@H	MIH_2@N	2	0.0001	2.8744	145.217
GLY_4@O	MIH_2@H	MIH_2@N	2	0.0001	2.9244	148.2908
GLY_3@O	MIH_10@H	MIH_10@N	2	0.0001	2.9429	170.6483
MIH_10@O	MIH_2@H	MIH_2@N	2	0.0001	2.9467	164.2435
MIH_10@O	GLY_3@H	GLY_3@N	1	0.0001	2.9103	137.865
GLY_9@O	MIH_2@H	MIH_2@N	1	0.0001	2.9395	144.758
MIH_6@O	NME_11@H	NME_11@N	1	0.0001	2.9558	173.4173
		Total	**11.79**			

Table S4. List of all hydrogen bonds identified during the QM/MM MD simulation of the Pept$^9_{3G}$ apoform with implicit solvent. From left to right, the columns refer to: hydrogen bond acceptor atom, hydrogen bond donor hydrogen atom, donor heavy atom, number of frames in which a given hydrogen bond was detected (note the total number of frames is approximately 20000), fraction of time (from 0 to 1) in which a given hydrogen bond was detected, average donor-acceptor distance (in Å), and average donor-H-acceptor angle (in

degrees). Note the accumulated lifetime is given at the end of the table. Note as well residue numbers 1 (residue ACE) and 11 (residue NME) correspond to the two terminal methyl groups, and therefore the residue IDs are +1 with respect to the residue IDs discussed in the main manuscript.

Acceptor	DonorH	Donor	Frames	Frac	AvgDist	AvgAng
GLY_3@O	GLY_7@H	GLY_7@N	1958	0.1018	2.88	158.3044
GLY_3@O	MIH_6@H	MIH_6@N	645	0.0335	2.9143	153.7117
GLY_7@O	NME_11@H	NME_11@N	511	0.0266	2.8869	155.9729
GLY_7@O	MIH_10@H	MIH_10@N	346	0.018	2.9199	155.4973
PRO_4@O	GLY_9@H	GLY_9@N	174	0.009	2.8823	146.9834
GLY_7@O	GLY_9@H	GLY_9@N	111	0.0058	2.8501	144.9871
PRO_4@O	MIH_6@H	MIH_6@N	87	0.0045	2.8943	144.1337
PRO_8@O	MIH_10@H	MIH_10@N	70	0.0036	2.8935	143.1248
GLY_3@O	GLY_5@H	GLY_5@N	62	0.0032	2.8747	145.3162
GLY_3@O	NME_11@H	NME_11@N	44	0.0023	2.8821	158.9585
GLY_7@O	GLY_3@H	GLY_3@N	43	0.0022	2.9058	159.7418
MIH_10@O	GLY_5@H	GLY_5@N	33	0.0017	2.9146	154.8955
MIH_6@O	GLY_9@H	GLY_9@N	33	0.0017	2.9287	147.7181
GLY_9@O	GLY_3@H	GLY_3@N	31	0.0016	2.8865	158.5505
ACE_1@O	GLY_9@H	GLY_9@N	27	0.0014	2.868	151.8591
MIH_2@O	GLY_9@H	GLY_9@N	27	0.0014	2.9029	153.7497
PRO_4@O	GLY_7@H	GLY_7@N	26	0.0014	2.9099	150.8733
GLY_9@O	NME_11@H	NME_11@N	25	0.0013	2.9142	142.2446
ACE_1@O	GLY_3@H	GLY_3@N	24	0.0012	2.933	143.2126
MIH_2@O	MIH_10@H	MIH_10@N	21	0.0011	2.9393	148.7389
GLY_7@O	GLY_5@H	GLY_5@N	20	0.001	2.8781	151.2832
MIH_10@O	GLY_7@H	GLY_7@N	17	0.0009	2.8736	154.7412
GLY_9@O	GLY_5@H	GLY_5@N	15	0.0008	2.895	157.5342
GLY_7@O	MIH_2@H	MIH_2@N	15	0.0008	2.8985	157.9786
PRO_8@O	NME_11@H	NME_11@N	13	0.0007	2.8961	153.712
GLY_5@O	GLY_7@H	GLY_7@N	13	0.0007	2.9011	144.3597
PRO_4@O	NME_11@H	NME_11@N	12	0.0006	2.9109	158.0943
MIH_2@O	GLY_5@H	GLY_5@N	12	0.0006	2.9299	147.889
MIH_6@O	GLY_3@H	GLY_3@N	12	0.0006	2.936	152.2779
PRO_4@O	MIH_10@H	MIH_10@N	11	0.0006	2.9064	155.0446
MIH_10@O	GLY_3@H	GLY_3@N	11	0.0006	2.907	149.9275

GLY_3@O	GLY_9@H	GLY_9@N	11	0.0006	2.9311	148.8482
MIH_10@O	MIH_2@H	MIH_2@N	10	0.0005	2.9149	151.3628
GLY_3@O	MIH_10@H	MIH_10@N	8	0.0004	2.9028	151.6664
MIH_10@O	MIH_6@H	MIH_6@N	8	0.0004	2.9356	156.3425
MIH_6@O	MIH_2@H	MIH_2@N	7	0.0004	2.9368	152.4178
MIH_2@O	NME_11@H	NME_11@N	7	0.0004	2.9508	145.2459
ACE_1@O	NME_11@H	NME_11@N	6	0.0003	2.9075	159.0805
GLY_5@O	NME_11@H	NME_11@N	6	0.0003	2.9109	152.9593
GLY_9@O	MIH_2@H	MIH_2@N	4	0.0002	2.9145	150.8553
PRO_8@O	MIH_2@H	MIH_2@N	3	0.0002	2.9136	160.2622
GLY_9@O	MIH_6@H	MIH_6@N	3	0.0002	2.9233	157.5447
MIH_2@O	MIH_6@H	MIH_6@N	3	0.0002	2.95	155.0058
ACE_1@O	GLY_7@H	GLY_7@N	1	0.0001	2.7774	145.0489
ACE_1@O	MIH_10@H	MIH_10@N	1	0.0001	2.8831	159.7035
MIH_2@O	GLY_7@H	GLY_7@N	1	0.0001	2.9581	142.4575
PRO_4@O	MIH_2@H	MIH_2@N	1	0.0001	2.9693	136.4532
GLY_7@O	MIH_6@H	MIH_6@N	1	0.0001	2.9836	144.6059
MIH_6@O	MIH_10@H	MIH_10@N	1	0.0001	2.9965	166.3753

Total 23.59

Table S5. List of all hydrogen bonds identified during the QM/MM MD simulation of the Pept^9$_{GPG}$ apoform with implicit solvent. From left to right, the columns refer to: hydrogen bond acceptor atom, hydrogen bond donor hydrogen atom, donor heavy atom, number of frames in which a given hydrogen bond was detected (note the total number of frames is approximately 20000), fraction of time (from 0 to 1) in which a given hydrogen bond was detected, average donor-acceptor distance (in Å), and average donor-H-acceptor angle (in degrees). Note the accumulated lifetime is given at the end of the table. Note as well residue numbers 1 (residue ACE) and 11 (residue NME) correspond to the two terminal methyl groups, and therefore the residue IDs are +1 with respect to the residue IDs discussed in the main manuscript.

Acceptor	DonorH	Donor	Frames	Frac	AvgDist	AvgAng
GLY_6@O	GLY_8@H	GLY_8@N	248	0.0128	2.8873	145.1479
GLY_6@O	NME_10@H	NME_10@N	210	0.0108	2.889	159.8586
GLY_3@O	GLY_7@H	GLY_7@N	187	0.0096	2.8841	150.9704
GLY_3@O	GLY_8@H	GLY_8@N	171	0.0088	2.8873	151.8764
MIH_2@O	GLY_4@H	GLY_4@N	107	0.0055	2.9141	144.1075
GLY_3@O	MIH_5@H	MIH_5@N	96	0.0049	2.9002	143.7966
MIH_5@O	GLY_8@H	GLY_8@N	95	0.0049	2.9182	150.0832
MIH_5@O	GLY_7@H	GLY_7@N	93	0.0048	2.8982	144.9737
GLY_6@O	MIH_9@H	MIH_9@N	82	0.0042	2.9048	152.6675
GLY_7@O	MIH_9@H	MIH_9@N	78	0.004	2.8999	144.4584
GLY_4@O	GLY_7@H	GLY_7@N	66	0.0034	2.9005	148.7571
MIH_2@O	MIH_5@H	MIH_5@N	66	0.0034	2.9291	154.457
GLY_3@O	GLY_6@H	GLY_6@N	53	0.0027	2.9116	148.7328
ACE_1@O	GLY_4@H	GLY_4@N	45	0.0023	2.8944	151.9484
GLY_6@O	GLY_3@H	GLY_3@N	44	0.0023	2.891	158.822
MIH_2@O	GLY_6@H	GLY_6@N	36	0.0019	2.9259	152.5658
GLY_8@O	NME_10@H	NME_10@N	30	0.0015	2.9277	143.0043
GLY_4@O	GLY_6@H	GLY_6@N	28	0.0014	2.904	145.7611
ACE_1@O	GLY_3@H	GLY_3@N	27	0.0014	2.925	144.2819
ACE_1@O	GLY_8@H	GLY_8@N	21	0.0011	2.9	157.7117
GLY_7@O	GLY_4@H	GLY_4@N	18	0.0009	2.9207	151.1105
GLY_4@O	GLY_8@H	GLY_8@N	17	0.0009	2.8906	153.0675
MIH_2@O	GLY_7@H	GLY_7@N	16	0.0008	2.898	146.4786
GLY_7@O	GLY_3@H	GLY_3@N	14	0.0007	2.8657	155.8258
GLY_3@O	MIH_9@H	MIH_9@N	14	0.0007	2.9133	152.3677
GLY_3@O	NME_10@H	NME_10@N	14	0.0007	2.9288	162.9838
GLY_7@O	MIH_2@H	MIH_2@N	12	0.0006	2.8819	165.9856
GLY_8@O	GLY_3@H	GLY_3@N	11	0.0006	2.8759	155.5976
GLY_8@O	GLY_4@H	GLY_4@N	11	0.0006	2.8935	156.9359
MIH_5@O	MIH_2@H	MIH_2@N	11	0.0006	2.9488	155.4122
GLY_4@O	MIH_9@H	MIH_9@N	10	0.0005	2.8999	154.341
GLY_7@O	NME_10@H	NME_10@N	10	0.0005	2.9141	147.8452
MIH_9@O	GLY_6@H	GLY_6@N	9	0.0005	2.9176	146.6791
ACE_1@O	GLY_6@H	GLY_6@N	7	0.0004	2.8864	163.9489
GLY_4@O	NME_10@H	NME_10@N	7	0.0004	2.8937	158.9534
ACE_1@O	GLY_7@H	GLY_7@N	6	0.0003	2.8577	149.7698

MIH_5@O	MIH_9@H	MIH_9@N	6	0.0003	2.8958	152.0844
MIH_2@O	GLY_8@H	GLY_8@N	6	0.0003	2.9162	141.6467
MIH_9@O	GLY_3@H	GLY_3@N	5	0.0003	2.9291	145.9894
MIH_9@O	MIH_5@H	MIH_5@N	5	0.0003	2.9515	157.0493
GLY_8@O	MIH_2@H	MIH_2@N	4	0.0002	2.8319	158.1465
GLY_8@O	MIH_5@H	MIH_5@N	4	0.0002	2.8552	156.8847
ACE_1@O	NME_10@H	NME_10@N	4	0.0002	2.8561	154.8016
GLY_8@O	GLY_6@H	GLY_6@N	4	0.0002	2.9012	159.6242
MIH_9@O	GLY_4@H	GLY_4@N	4	0.0002	2.9171	146.3207
MIH_2@O	NME_10@H	NME_10@N	4	0.0002	2.9184	143.9855
MIH_2@O	MIH_9@H	MIH_9@N	4	0.0002	2.933	160.2773
ACE_1@O	MIH_9@H	MIH_9@N	3	0.0002	2.836	153.5137
MIH_5@O	NME_10@H	NME_10@N	3	0.0002	2.9165	147.2706
ACE_1@O	MIH_5@H	MIH_5@N	3	0.0002	2.9632	140.0127
MIH_5@O	GLY_3@H	GLY_3@N	2	0.0001	2.7482	141.7097
GLY_4@O	MIH_2@H	MIH_2@N	2	0.0001	2.9692	159.8182
GLY_6@O	GLY_4@H	GLY_4@N	1	0.0001	2.9701	137.0208
MIH_9@O	MIH_2@H	MIH_2@N	1	0.0001	2.9742	151.3305

Total	**10.5**

Table S6. List of all hydrogen bonds identified during the QM/MM MD simulation of the Pept$^8_{2G\text{-}3G}$ apoform with implicit solvent. From left to right, the columns refer to: hydrogen bond acceptor atom, hydrogen bond donor hydrogen atom, donor heavy atom, number of frames in which a given hydrogen bond was detected (note the total number of frames is approximately 20000), fraction of time (from 0 to 1) in which a given hydrogen bond was detected, average donor-acceptor distance (in Å), and average donor-H-acceptor angle (in degrees). Note the accumulated lifetime is given at the end of the table. Note as well residue numbers 1 (residue ACE) and 10 (residue NME) correspond to the two terminal methyl groups, and therefore the residue IDs are +1 with respect to the residue IDs discussed in the main manuscript.

Acceptor	DonorH	Donor	Frames	Frac	AvgDist	AvgAng
GLY_3@O	GLY_7@H	GLY_7@N	754	0.0371	2.8779	158.0234
GLY_3@O	GLY_8@H	GLY_8@N	373	0.0184	2.8862	152.1049
GLY_3@O	MIH_6@H	MIH_6@N	275	0.0135	2.9169	153.2689
GLY_3@O	GLY_5@H	GLY_5@N	188	0.0093	2.8767	146.7852
GLY_4@O	GLY_8@H	GLY_8@N	132	0.0065	2.8929	148.0462
MIH_2@O	GLY_4@H	GLY_4@N	115	0.0057	2.9064	145.7169
MIH_6@O	GLY_8@H	GLY_8@N	108	0.0053	2.9102	144.6828
GLY_5@O	GLY_8@H	GLY_8@N	89	0.0044	2.8939	152.3736
MIH_2@O	GLY_5@H	GLY_5@N	89	0.0044	2.9253	150.4109
GLY_7@O	MIH_9@H	MIH_9@N	70	0.0034	2.8882	144.4823
GLY_4@O	MIH_6@H	MIH_6@N	66	0.0032	2.8969	143.983
MIH_6@O	MIH_9@H	MIH_9@N	63	0.0031	2.9374	153.1904
GLY_4@O	MIH_9@H	MIH_9@N	53	0.0026	2.9069	151.0583
GLY_8@O	GLY_5@H	GLY_5@N	51	0.0025	2.8768	157.1594
ACE_1@O	GLY_4@H	GLY_4@N	40	0.002	2.9045	150.4863
GLY_5@O	GLY_7@H	GLY_7@N	39	0.0019	2.9054	142.3242
GLY_8@O	NME_10@H	NME_10@N	38	0.0019	2.8974	142.5205
GLY_4@O	NME_10@H	NME_10@N	32	0.0016	2.8986	156.9252
GLY_8@O	GLY_4@H	GLY_4@N	31	0.0015	2.8739	156.8424
ACE_1@O	GLY_3@H	GLY_3@N	30	0.0015	2.9048	141.9304
GLY_7@O	GLY_4@H	GLY_4@N	23	0.0011	2.8877	157.1277
GLY_4@O	GLY_7@H	GLY_7@N	23	0.0011	2.9003	153.5001
GLY_3@O	NME_10@H	NME_10@N	19	0.0009	2.9168	161.7408
GLY_3@O	MIH_9@H	MIH_9@N	18	0.0009	2.8883	150.0677
MIH_2@O	MIH_9@H	MIH_9@N	15	0.0007	2.9102	152.5233
ACE_1@O	GLY_8@H	GLY_8@N	12	0.0006	2.8828	162.1359
MIH_9@O	GLY_4@H	GLY_4@N	12	0.0006	2.9078	146.3489
MIH_6@O	NME_10@H	NME_10@N	11	0.0005	2.9035	157.8823
MIH_6@O	GLY_3@H	GLY_3@N	11	0.0005	2.9111	152.5976
GLY_8@O	GLY_3@H	GLY_3@N	10	0.0005	2.8566	156.4978
ACE_1@O	NME_10@H	NME_10@N	10	0.0005	2.8869	157.5946
MIH_9@O	MIH_2@H	MIH_2@N	10	0.0005	2.93	157.4721
MIH_2@O	NME_10@H	NME_10@N	9	0.0004	2.9107	155.7627
MIH_9@O	MIH_6@H	MIH_6@N	9	0.0004	2.9145	155.2164
MIH_9@O	GLY_5@H	GLY_5@N	8	0.0004	2.8747	149.6254
GLY_8@O	MIH_2@H	MIH_2@N	8	0.0004	2.8939	161.4626

MIH_2@O	MIH_6@H	MIH_6@N	7	0.0003	2.9287	151.2034
ACE_1@O	GLY_5@H	GLY_5@N	6	0.0003	2.8594	149.8754
GLY_7@O	NME_10@H	NME_10@N	6	0.0003	2.9096	154.6404
GLY_5@O	MIH_2@H	MIH_2@N	5	0.0002	2.8755	147.8595
MIH_9@O	GLY_3@H	GLY_3@N	5	0.0002	2.917	148.1186
GLY_7@O	MIH_2@H	MIH_2@N	5	0.0002	2.927	154.0848
ACE_1@O	MIH_9@H	MIH_9@N	4	0.0002	2.8645	158.72
MIH_2@O	GLY_8@H	GLY_8@N	4	0.0002	2.9498	163.5209
MIH_2@O	GLY_7@H	GLY_7@N	3	0.0001	2.9018	143.1263
ACE_1@O	MIH_6@H	MIH_6@N	3	0.0001	2.9166	154.1501
GLY_8@O	MIH_6@H	MIH_6@N	3	0.0001	2.9461	144.9694
GLY_7@O	GLY_3@H	GLY_3@N	2	0.0001	2.8768	148.5593
MIH_6@O	MIH_2@H	MIH_2@N	2	0.0001	2.9286	155.9171
ACE_1@O	GLY_7@H	GLY_7@N	2	0.0001	2.931	161.2361
GLY_7@O	GLY_5@H	GLY_5@N	2	0.0001	2.9482	161.8298
GLY_5@O	MIH_9@H	MIH_9@N	1	0	2.9257	163.0251
GLY_5@O	NME_10@H	NME_10@N	1	0	2.9809	163.5218

Total	**14.24**

Table S7. List of all hydrogen bonds identified during the QM/MM MD simulation of the $\underline{Pept^8_{2G\text{-}3G}\ apoform}$ with implicit solvent. From left to right, the columns refer to: hydrogen bond acceptor atom, hydrogen bond donor hydrogen atom, donor heavy atom, number of frames in which a given hydrogen bond was detected (note the total number of frames is approximately 20000), fraction of time (from 0 to 1) in which a given hydrogen bond was detected, average donor-acceptor distance (in Å), and average donor-H-acceptor angle (in degrees). Note the accumulated lifetime is given at the end of the table. Note as well residue numbers 1 (residue ACE) and 10 (residue NME) correspond to the two terminal methyl groups, and therefore the residue IDs are +1 with respect to the residue IDs discussed in the main manuscript.

Acceptor	DonorH	Donor	Frames	Frac	AvgDist	AvgAng
GLY_3@O	GLY_7@H	GLY_7@N	170	0.0092	2.8977	148.9097
MIH_5@O	GLY_7@H	GLY_7@N	124	0.0067	2.9076	144.4154
MIH_5@O	MIH_8@H	MIH_8@N	98	0.0053	2.9312	151.6136
GLY_3@O	MIH_5@H	MIH_5@N	81	0.0044	2.899	144.4622
MIH_2@O	GLY_4@H	GLY_4@N	81	0.0044	2.9005	145.4876
GLY_6@O	MIH_8@H	MIH_8@N	76	0.0041	2.892	143.8784
MIH_2@O	MIH_5@H	MIH_5@N	76	0.0041	2.9325	153.2701
GLY_4@O	GLY_7@H	GLY_7@N	67	0.0036	2.9203	150.902
ACE_1@O	GLY_4@H	GLY_4@N	59	0.0032	2.8874	149.5484
GLY_3@O	MIH_8@H	MIH_8@N	57	0.0031	2.9194	151.9448
MIH_2@O	GLY_6@H	GLY_6@N	42	0.0023	2.9079	156.0776
GLY_4@O	GLY_6@H	GLY_6@N	34	0.0018	2.9045	144.2805
GLY_3@O	GLY_6@H	GLY_6@N	32	0.0017	2.9055	148.7617
GLY_7@O	NME_9@H	NME_9@N	32	0.0017	2.921	142.9699
MIH_5@O	NME_9@H	NME_9@N	28	0.0015	2.9225	156.9073
ACE_1@O	GLY_3@H	GLY_3@N	26	0.0014	2.9162	142.4152
GLY_3@O	NME_9@H	NME_9@N	23	0.0012	2.9045	160.4789
MIH_8@O	GLY_4@H	GLY_4@N	13	0.0007	2.8836	147.0329
MIH_8@O	MIH_2@H	MIH_2@N	13	0.0007	2.9253	158.122
MIH_8@O	GLY_3@H	GLY_3@N	11	0.0006	2.8877	148.3853
GLY_6@O	NME_9@H	NME_9@N	11	0.0006	2.9268	153.3033
ACE_1@O	NME_9@H	NME_9@N	10	0.0005	2.9177	160.3734
ACE_1@O	GLY_7@H	GLY_7@N	9	0.0005	2.8705	157.9581
GLY_7@O	GLY_3@H	GLY_3@N	9	0.0005	2.9412	155.5651
GLY_4@O	MIH_8@H	MIH_8@N	8	0.0004	2.8788	153.2212
MIH_5@O	MIH_2@H	MIH_2@N	8	0.0004	2.9329	160.2779
MIH_2@O	NME_9@H	NME_9@N	7	0.0004	2.9017	153.7408
MIH_8@O	MIH_5@H	MIH_5@N	7	0.0004	2.9077	147.7103
MIH_2@O	GLY_7@H	GLY_7@N	7	0.0004	2.9253	145.9651
GLY_4@O	NME_9@H	NME_9@N	6	0.0003	2.8417	147.9796
GLY_7@O	MIH_2@H	MIH_2@N	6	0.0003	2.9405	153.85
ACE_1@O	MIH_8@H	MIH_8@N	4	0.0002	2.8922	149.3166
GLY_6@O	GLY_3@H	GLY_3@N	4	0.0002	2.9107	157.9424
GLY_7@O	MIH_5@H	MIH_5@N	3	0.0002	2.9077	150.4977
GLY_7@O	GLY_4@H	GLY_4@N	2	0.0001	2.8335	142.8448
ACE_1@O	MIH_5@H	MIH_5@N	1	0.0001	2.7792	139.917

GLY_4@O	MIH_2@H	MIH_2@N	1	0.0001	2.9069	172.5264
ACE_1@O	GLY_6@H	GLY_6@N	1	0.0001	2.9183	149.7025
GLY_6@O	GLY_4@H	GLY_4@N	1	0.0001	2.9631	157.5588
			Total	**6.75**		

Table S8. List of all hydrogen bonds identified during the QM/MM MD simulation of the Pept[7] apoform with implicit solvent. From left to right, the columns refer to: hydrogen bond acceptor atom, hydrogen bond donor hydrogen atom, donor heavy atom, number of frames in which a given hydrogen bond was detected (note the total number of frames is approximately 20000), fraction of time (from 0 to 1) in which a given hydrogen bond was detected, average donor-acceptor distance (in Å), and average donor-H-acceptor angle (in degrees). Note the accumulated lifetime is given at the end of the table. Note as well residue numbers 1 (residue ACE) and 9 (residue NME) correspond to the two terminal methyl groups, and therefore the residue IDs are +1 with respect to the residue IDs discussed in the main manuscript.

Acceptor	DonorH	Donor	Frames	Frac	AvgDist	AvgAng
MIH_4@O	GLY_6@H	GLY_6@N	151	0.0074	2.9008	143.0568
MIH_2@O	MIH_4@H	MIH_4@N	131	0.0064	2.9108	142.9848
GLY_3@O	GLY_6@H	GLY_6@N	110	0.0054	2.9042	151.6088
MIH_4@O	MIH_7@H	MIH_7@N	88	0.0043	2.9415	153.682
GLY_5@O	MIH_7@H	MIH_7@N	74	0.0036	2.9013	144.1374
MIH_4@O	NME_8@H	NME_8@N	54	0.0027	2.9221	151.3264
GLY_3@O	GLY_5@H	GLY_5@N	47	0.0023	2.8913	144.0601
MIH_7@O	MIH_2@H	MIH_2@N	33	0.0016	2.9228	153.792
MIH_2@O	GLY_6@H	GLY_6@N	32	0.0016	2.9318	145.408
ACE_1@O	GLY_3@H	GLY_3@N	28	0.0014	2.8948	144.0492
GLY_6@O	NME_8@H	NME_8@N	26	0.0013	2.9062	145.2781
GLY_6@O	MIH_2@H	MIH_2@N	24	0.0012	2.9325	159.1319
MIH_7@O	MIH_4@H	MIH_4@N	20	0.001	2.9205	157.7276
GLY_5@O	MIH_2@H	MIH_2@N	16	0.0008	2.9169	155.0697
ACE_1@O	GLY_5@H	GLY_5@N	13	0.0006	2.8988	153.3561
GLY_6@O	GLY_3@H	GLY_3@N	11	0.0005	2.9025	153.1315
GLY_3@O	MIH_7@H	MIH_7@N	10	0.0005	2.9396	152.6466
MIH_7@O	GLY_3@H	GLY_3@N	8	0.0004	2.8474	152.7994
GLY_6@O	MIH_4@H	MIH_4@N	8	0.0004	2.9232	155.8506
GLY_5@O	NME_8@H	NME_8@N	8	0.0004	2.9491	150.2356
MIH_2@O	GLY_5@H	GLY_5@N	6	0.0003	2.9148	144.6319
ACE_1@O	MIH_4@H	MIH_4@N	6	0.0003	2.9418	155.3531
MIH_4@O	MIH_2@H	MIH_2@N	5	0.0002	2.902	160.4888
MIH_2@O	NME_8@H	NME_8@N	5	0.0002	2.9102	145.793
MIH_2@O	MIH_7@H	MIH_7@N	5	0.0002	2.9584	148.6413
GLY_3@O	NME_8@H	NME_8@N	1	0	2.8016	169.7221
ACE_1@O	NME_8@H	NME_8@N	1	0	2.9319	141.9541
MIH_7@O	GLY_5@H	GLY_5@N	1	0	2.9348	142.3034
ACE_1@O	GLY_6@H	GLY_6@N	1	0	2.9541	147.8889
			Total	**4.5**		

Table S9. List of all hydrogen bonds identified during the QM/MM MD simulation of the Pept^6$_{\text{G-2G}}$ apoform with implicit solvent. From left to right, the columns refer to: hydrogen bond acceptor atom, hydrogen bond donor hydrogen atom, donor heavy atom, number of frames in which a given hydrogen bond was detected (note the total number of frames is approximately 20000), fraction of time (from 0 to 1) in which a given hydrogen bond was detected, average donor-acceptor distance (in Å), and average donor-H-acceptor angle (in

degrees). Note the accumulated lifetime is given at the end of the table. Note as well residue numbers 1 (residue ACE) and 8 (residue NME) correspond to the two terminal methyl groups, and therefore the residue IDs are +1 with respect to the residue IDs discussed in the main manuscript.

Acceptor	DonorH	Donor	Frames	Frac	AvgDist	AvgAng
MIH_5@O	MIH_7@H	MIH_7@N	127	0.0063	2.9082	144.9952
MIH_7@O	GLY_4@H	GLY_4@N	124	0.0061	2.9123	147.5652
MIH_2@O	GLY_4@H	GLY_4@N	121	0.006	2.9068	144.2411
GLY_3@O	MIH_5@H	MIH_5@N	82	0.004	2.9095	143.6877
MIH_2@O	GLY_6@H	GLY_6@N	82	0.004	2.9252	154.9145
MIH_2@O	MIH_5@H	MIH_5@N	62	0.0031	2.9261	154.3665
ACE_1@O	GLY_4@H	GLY_4@N	52	0.0026	2.9231	153.6765
GLY_3@O	NME_8@H	NME_8@N	49	0.0024	2.8967	157.6187
GLY_4@O	GLY_6@H	GLY_6@N	31	0.0015	2.9201	143.0025
ACE_1@O	GLY_3@H	GLY_3@N	27	0.0013	2.9142	145.4752
GLY_3@O	MIH_7@H	MIH_7@N	24	0.0012	2.9199	151.945
MIH_7@O	GLY_3@H	GLY_3@N	21	0.001	2.9201	147.0023
GLY_4@O	MIH_7@H	MIH_7@N	19	0.0009	2.9069	150.5797
GLY_6@O	NME_8@H	NME_8@N	19	0.0009	2.9244	143.367
GLY_3@O	GLY_6@H	GLY_6@N	16	0.0008	2.8923	149.3829
MIH_5@O	MIH_2@H	MIH_2@N	13	0.0006	2.8781	152.0273
MIH_5@O	NME_8@H	NME_8@N	9	0.0004	2.9257	146.0922
ACE_1@O	GLY_6@H	GLY_6@N	9	0.0004	2.9469	152.4124
ACE_1@O	MIH_5@H	MIH_5@N	7	0.0003	2.9539	158.3778
MIH_7@O	MIH_5@H	MIH_5@N	6	0.0003	2.9163	156.5813
GLY_4@O	NME_8@H	NME_8@N	6	0.0003	2.9287	157.2526
MIH_7@O	MIH_2@H	MIH_2@N	5	0.0002	2.8991	151.8919
ACE_1@O	NME_8@H	NME_8@N	3	0.0001	2.8847	154.2694
MIH_2@O	MIH_7@H	MIH_7@N	2	0.0001	2.9162	157.6013
GLY_4@O	MIH_2@H	MIH_2@N	2	0.0001	2.934	149.0547
GLY_6@O	GLY_4@H	GLY_4@N	1	0	2.9444	137.7786
			Total	**4.49**		

Table S10. List of all hydrogen bonds identified during the QM/MM MD simulation of the Pept$^6_{2G\text{-}G}$ apoform with implicit solvent. From left to right, the columns refer to: hydrogen bond acceptor atom, hydrogen bond donor hydrogen atom, donor heavy atom, number of frames in which a given hydrogen bond was detected (note the total number of frames is approximately 20000), fraction of time (from 0 to 1) in which a given hydrogen bond was detected, average donor-acceptor distance (in Å), and average donor-H-acceptor angle (in degrees). Note the accumulated lifetime is given at the end of the table. Note as well residue numbers 1 (residue ACE) and 8 (residue NME) correspond to the two terminal methyl groups, and therefore the residue IDs are +1 with respect to the residue IDs discussed in the main manuscript.

Acceptor	DonorH	Donor	Frames	Frac	AvgDist	AvgAng
MIH_6@O	MIH_2@H	MIH_2@N	158	0.0079	2.9189	156.8119
MIH_4@O	MIH_6@H	MIH_6@N	136	0.0068	2.9137	144.2391
MIH_2@O	MIH_4@H	MIH_4@N	120	0.006	2.9172	143.5579
MIH_6@O	GLY_3@H	GLY_3@N	101	0.0051	2.9067	148.0095
GLY_5@O	NME_7@H	NME_7@N	31	0.0016	2.9042	144.3577
GLY_5@O	MIH_2@H	MIH_2@N	29	0.0015	2.8944	153.3918
ACE_1@O	GLY_5@H	GLY_5@N	25	0.0013	2.891	155.3835
GLY_3@O	GLY_5@H	GLY_5@N	23	0.0012	2.9244	143.6728
ACE_1@O	GLY_3@H	GLY_3@N	20	0.001	2.9083	145.2975
ACE_1@O	MIH_4@H	MIH_4@N	14	0.0007	2.9484	154.6062
MIH_4@O	MIH_2@H	MIH_2@N	13	0.0007	2.9373	145.0839
GLY_3@O	MIH_6@H	MIH_6@N	8	0.0004	2.9423	161.4659
MIH_6@O	MIH_4@H	MIH_4@N	6	0.0003	2.9324	151.7514
MIH_2@O	NME_7@H	NME_7@N	5	0.0003	2.9603	138.5456
MIH_2@O	MIH_6@H	MIH_6@N	2	0.0001	2.863	142.462
MIH_2@O	GLY_5@H	GLY_5@N	2	0.0001	2.9528	164.4862
GLY_3@O	NME_7@H	NME_7@N	2	0.0001	2.9804	154.6807
MIH_4@O	NME_7@H	NME_7@N	2	0.0001	2.9916	154.4958
			Total	**3.52**		

Table S11. List of all hydrogen bonds identified during the QM/MM MD simulation of the Pept[5] apoform with implicit solvent. From left to right, the columns refer to: hydrogen bond acceptor atom, hydrogen bond donor hydrogen atom, donor heavy atom, number of frames in which a given hydrogen bond was detected (note the total number of frames is approximately 20000), fraction of time (from 0 to 1) in which a given hydrogen bond was detected, average donor-acceptor distance (in Å), and average donor-H-acceptor angle (in degrees). Note the accumulated lifetime is given at the end of the table. Note as well residue numbers 1 (residue ACE) and 7 (residue NME) correspond to the two terminal methyl groups, and therefore the residue IDs are +1 with respect to the residue IDs discussed in the main manuscript.

APPENDIX C

"Down in the shadow of the penitentiary
Out by the gas fires of the refinery
I'm ten years burning down the road
Nowhere to run ain't got nowhere to go"

(B. Springsteen, Born in the U.S.A)

Appendix C

The interaction of aluminum with catecholamine-based neurotransmitters: can the formation of these species be considered a potential risk factor for neurodegenerative diseases?

- **Table S1:** Binding enthalpies and free energies of 1:1, 1:2 ,1:3 Al-ligand complexes with MP2.

- **Table S2**: Binding enthalpies and free energies of 1:1, 1:2, 1:3 Al-ligand complexes with the M06-2X functional.

- **Table S3:** Binding enthalpies and free energies of 1:1, 1:2, 1:3 Al-ligand complexes with the ωB97XD functional.

- **Figure S1:** Binding free energies of 1:1, 1:2, 1:3 Al-ligand complexes calculated with different methods compared with experimental stability constants (logβ).

- **Table S4:** Characteristics of the Al-O Bond Critical Points (BCPs) and Delocalization Indices (D.I.$_{Al-O}$).

- **Figure S2:** Delocalization Indices compared with binding enthalpies for 1:1 Al-ligand complexes.

- **Table S5:** Energy Decomposition Analysis (EDA) results.

		ΔH_{aq}^{comp}	ΔG_{aq}^{comp}	$\log\beta$
Ligands		*Protonated Amine*		
	1:1	-88.1	-92.6	16.0
L-DOPA	1:2	-160.6	-167.2	29.2
	1:3	-187.4	-193.6	38.4
	1:1	-85.5	-88.4	15.6
Dopamine	1:2	-148.9	-155.1	28.6
	1:3	-185.1	-193.3	37.6
	1:1	-83.3	-87.4	15.6
Noradrenaline	1:2	-144.3	-152.0	28.6
	1:3	-180.8	-191.7	37.9
	1:1	-83.3	-87.5	15.6
Epinephrine	1:2	-144.3	-152.0	28.6
	1:3	-181.7	-190.3	37.9
	1:1	-88.4	-91.4	16.3
Catechol	1:2	-152.4	-158.5	31.7
	1:3	-186.8	-195.4	41.1
	1:1	-74.9	-79.1	13.3
4-nitro Catechol	1:2	-130.2	-137.0	24.8
	1:3	-163.4	-173.3	33.7

Table S1: Binding enthalpies (ΔH_{aq}^{comp}) and binding energies (ΔG_{aq}^{comp}) with available experimental stability constant ($\log\beta$) obtained with single point energy calculations at the MP2/6-311++G(3df,2p) - IEFPCM level of theory.

		ΔH_{aq}^{comp}	ΔG_{aq}^{comp}	$\log\beta$
Ligand		*Protonated Amine*		
	1:1	-87.7	-92.2	16.0
L-DOPA	1:2	-157.8	-164.5	29.2
	1:3	-182.7	-189.0	38.4
	1:1	-85.1	-88.0	15.6
Dopamine	1:2	-147.2	-153.4	28.6
	1:3	-180.5	-188.7	37.6
	1:1	-83.1	-87.2	15.6
Noradrenaline	1:2	-142.8	-150.5	28.6
	1:3	-176.5	-187.3	37.9
	1:1	-83.2	-87.3	15.6
Epinephrine	1:2	-142.8	-150.5	28.6
	1:3	-177.4	-186.0	37.9
	1:1	-88.1	-91.2	16.3
Catechol	1:2	-151.0	-157.0	31.7
	1:3	-182.7	-191.2	41.1
	1:1	-73.2	-77.4	13.3
4-nitro Catechol	1:2	-126.3	-133.1	24.8
	1:3	-155.4	-165.3	33.7

Table S2: Binding enthalpies (ΔH_{aq}^{comp}) and binding energies (ΔG_{aq}^{comp}) with available experimental stability constant ($\log\beta$) obtained with single point energy calculations at the M06-2X/6-311++G(3df,2p) - IEFPCM level of theory.

		ΔH_{aq}^{comp}	ΔG_{aq}^{comp}	$\log\beta$
Ligand		*Protonated Amine*		
	1:1	-88.7	-93.2	16.0
L-DOPA	1:2	-160.1	-166.7	29.2
	1:3	-185.1	-191.3	38.4
	1:1	-86.2	-89.1	15.6
Dopamine	1:2	-149.3	-155.5	28.6
	1:3	-182.9	-191.2	37.6
	1:1	-84.1	-88.2	15.6
Noradrenaline	1:2	-144.8	-152.5	28.6
	1:3	-178.6	-189.5	37.9
	1:1	-84.1	-88.2	15.6
Epinephrine	1:2	-144.7	-152.3	28.6
	1:3	-179.5	-188.1	37.9
	1:1	-88.7	-91.8	16.3
Catechol	1:2	-152.3	-158.4	31.7
	1:3	-184.1	-192.7	41.1
	1:1	-74.7	-78.8	13.3
4-nitro Catechol	1:2	-129.1	-135.9	24.8
	1:3	-160.1	-170.0	33.7

Table S3: Binding enthalpies (ΔH_{aq}^{comp}) and binding energies (ΔG_{aq}^{comp}) with available experimental stability constant ($\log\beta$) obtained with single point energy calculations at the ωB97X-D/6-311++G(3df,2p) - IEFPCM level of theory.
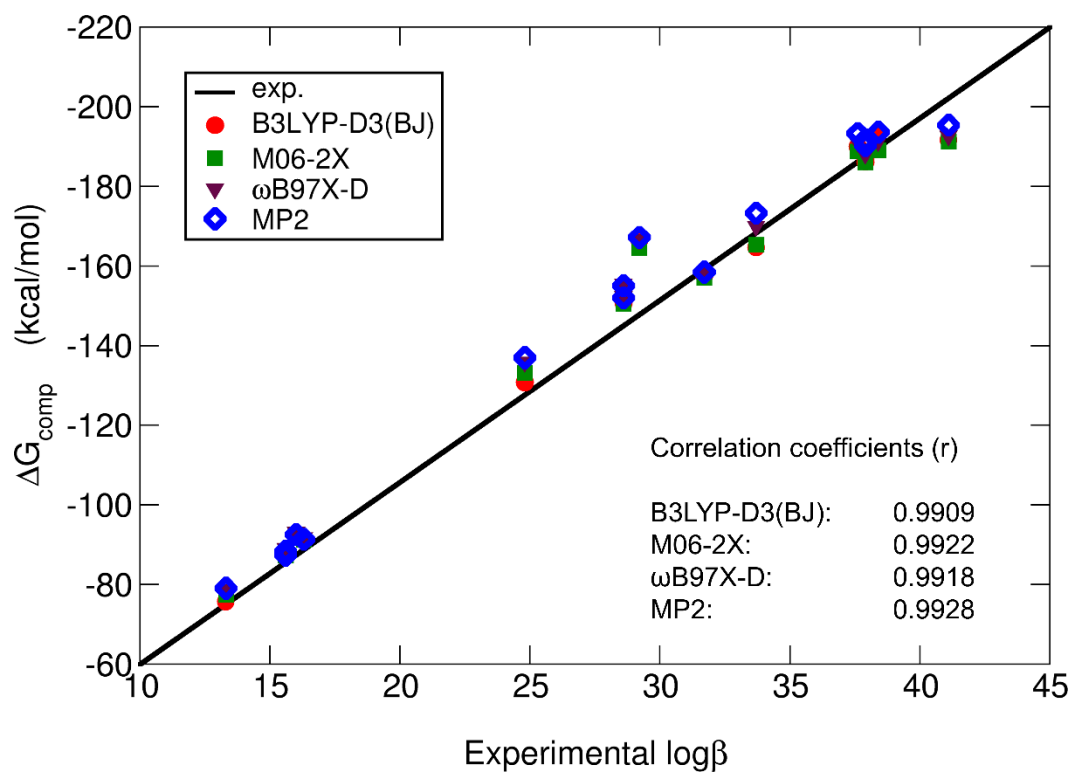
Figure S1. Binding energies (ΔG_{aq}^{comp}) calculated with dfferent functionals (B3LYP-D3(BJ, M06-2X, B97XD) and with the MP2 method compared with experimental stability constants (logβ). All single point calculations are performed using the 6-311++G/3df,2p) basis set on geometries optimized at the B3LYP-D3(BJ)/6-31++G(d,p) level of theory. All calculations include solvation e#ects through the IEFPCM model.

Bader's Quantum Theory of Aroms in Molecules (QTAIM)

Delocalization indices are a measure of the average number of electron pairs shared between two atoms, therefore they have been related to the measure of the covalent character of a given bond. Results are reported in Table S4, while in Fig. S2 we represent the sum of the two D.I.$_{Al-O}$ of each bidentate complex versus their binding enthalpies (ΔH_{aq}^{comp}).

Delocalization indices of protonated catecholamines are slightly smaller than those of their unprotonated counterparts and of catechol, although differences are quite small. As previously hypothesized, this confirms the electron withdrawing effect mediated by the positively charged amino group (Fig. S2) that decreases the electron density from the two Al-O bonds. This effect, in turn, lowers the covalent character of these interactions, leading to lower binding enthalpies (Fig. S2). In both N-protonated and N-unprotonated cases, noradrenaline and adrenaline show smaller D.I.$_{Al-O}$ and smaller binding affinities than L-DOPA, dopamine and catechol; this is due to the presence of an EW hydroxyl group in noradrenaline and adrenaline. Interestingly, N-unprotonated neurotransmitters L-DOPA and dopamine bear higher D.I.$_{Al-O}$ than catechol. While, as discussed before, L-DOPA bears a higher total negative charge (-3) which is the main responsible of the stronger binding affinity to aluminum, in the case of dopamine the inductive ED effect of the alkyl chain increases the covalency of its Al-O interactions compared to catechol (table S4). Despite the unprotonated dopamine also contains an EW group (NH_2), the effect of the alkyl chain prevails leading to an overall electron donating behavior. The addition of a second EW group such as OH, in addition to NH_2, in the alkyl chain of noradrenaline and adrenaline shifts the overall behavior to an electron withdrawing one, making these two compounds the poorest aluminum binders in both protonated and unprotonated forms (Table S4).

Finally, it is important to mention that 4-nitro catechol shows the lowest D.I.$_{Al-O}$ values as well as the lowest binding enthalpy (Table S4 and Fig. S2) in our dataset. As thoroughly discussed in our previous work, the EW nitro group added to an aromatic ring works through both inductive and resonance mechanisms of action, with resonance that prevails over induction. Therefore, the overall electron withdrawing nature of NO_2 is much more pronounced than than the inductive ones mediated by OH and/or *NH$_2$* in catecholamines (Fig. S2).

Ligand	Al-O$_1$			Al-O$_2$			D.I. (a.u.)	
	$\rho_{(BCP)}$	$\nabla^2\rho_{(BCP)}$	$H_{(BCP)}$	$\rho_{(BCP)}$	$\nabla^2\rho_{(BCP)}$	$H_{(BCP)}$	Al-O$_1$	Al-O$_2$
Catecholamines with Protonated Amines								
L-DOPA	0.0845	0.5174	-0.0074	0.0856	0.5260	-0.0077	0.2221	0.2199
Dopamine	0.0854	0.5241	-0.0077	0.0843	0.5160	-0.0073	0.2218	0.2200
Noradrenaline	0.0841	0.5143	-0.0072	0.0849	0.5205	-0.0075	0.2198	0.2188
Adrenaline	0.0850	0.5210	-0.0075	0.842	0.5154	-0.0073	0.2204	0.2194
Catecholamines with Unprotonated Amines								
L-DOPA	0.0849	0.5207	-0.0075	0.0860	0.5283	-0.0079	0.2236	0.2216
Dopamine	0.0860	0.5287	-0.0078	0.0848	0.5195	-0.0075	0.2239	0.2212
Noradrenaline	0.0856	0.5255	-0.0077	0.0847	0.5192	-0.0074	0.2220	0.2207
Adrenaline	0.0856	0.5254	-0.0077	0.0847	0.5189	-0.0074	0.2224	0.2209
Catecholate	0.0858	0.5271	-0.0078	0.0847	0.5193	-0.0074	0.2228	0.2208
4-nitro catechol	0.0846	0.5189	-0.0073	0.0802	0.4838	-0.0062	0.2183	0.2065

Table S4. Characteristics of the Al-O Bond Critical Points (in a.u.) for the aluminum-chelator interactions: the electron density at the BCP ($\rho_{(BCP)}$), the Laplacian of electron density ($\nabla^2\rho_{(BCP)}$), and the total energy density at the BCP ($H_{(BCP)}$). All structures were optimized and refined at the B3LYP-D3(BJ)/6-311++G(3df,2p) level of theory as reported in the methods section. All calculations take into account implicit solvent effects according to the IEFPCM formalism.
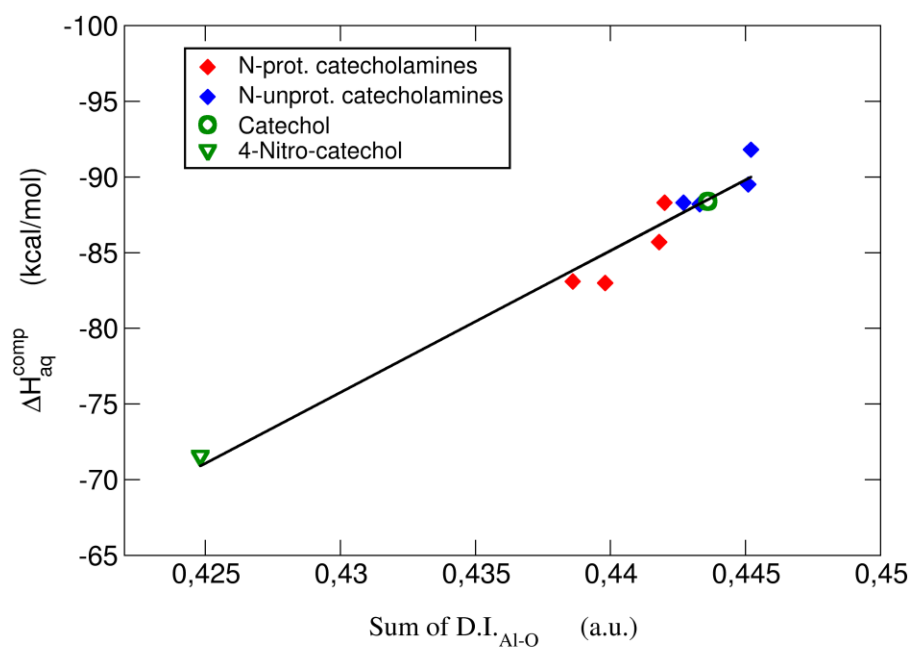
Figure S2. Sum of the delocalization indices of the two Al-O bonds in 1:1 Aluminum-Catechol/Catecholamine complexes versus their values of ΔH_{aq}^{comp}.

Structure	ΔE_{elstat}	(%)	ΔE_{oi}	(%)	ΔE_{Pauli}	ΔE_{disp}	ΔE_{int}
Catecholamines with Protonated Amines							
L-DOPA	-573.5	(62.3)	-346.5	(37.7)	146.6	-6.6	-779.8
Dopamine	-434.5	(57.3)	-323.7	(42.7)	142.0	-6.5	-622.7
Noradrenaline	-442.4	(58.5)	-313.3	(41.5)	141.8	-6.5	-620.4
Adrenaline	-451.6	(58.9)	-314.5	(41.1)	143.0	-6.5	-629.7
Catecholamines with Unprotonated Amines							
L-DOPA	-691.3	(64.5)	-380.3	(35.5)	150.2	-6.6	-927.9
Dopamine	-587.4	(63.1)	-343.4	(36.9)	148.8	-6.5	-788.6
Noradrenaline	-585.1	(63.0)	-343.6	(37.0)	147.9	-6.5	-787.2
Adrenaline	-578.7	(62.4)	-348.0	(37.6)	147.6	-6.5	-785.7
Catecholate	-610.4	(64.9)	-329.7	(35.1)	149.9	-6.5	-796.7
4-nitro catechol	-647.1	(72.4)	-247.1	(27.6)	147.2	-6.5	-753.5

Table S5. Energy Decomposition Analysis, values obtained at the full electron (no frozen core) B3LYP-D3(BJ)/ET-QZ3P-1DIFFUSE level of theory in gas phase, using the ADF2017 modeling suite of programs.

Bibliography

(1)   Exley, C. "Darwin, natural selection and the biological essentiality of aluminium and silicon." *Trends Biochem. Sci.* **2009,** *34* (12), 589-593.

(2)   Exley, C. "Human exposure to aluminium." *Env. Sci.. Processes & impacts* **2013,** *15* (10), 1807-1816.

(3)   Exley, C. "Why industry propaganda and political interference cannot disguise the inevitable role played by human exposure to aluminium in neurodegenerative diseases, including alzheimer's disease." *Front. Neurol.* **2014,** *5*, 1-6.

(4)   Exley, C. "Aluminum should now be considered a primary etiological factor in alzheimer's disease." *J. Alzheimer's Dis. Rep.* **2017,** *1* (1), 23-25.

(5)   Kawahara, M.; Kato-Negishi, M. "Link between aluminum and the pathogenesis of alzheimer's disease: The integration of the aluminum and amyloid cascade hypotheses." *Int. J. Alzheimers Dis.* **2011,** *2011*, 276393-276393.

(6)   Crisponi, G.; Nurchi, V. M.; Bertolasi, V.; Remelli, M.; Faa, G. "Chelating agents for human diseases related to aluminium overload." *Coord. Chem. Rev.* **2012,** *256* (1-2), 89-104.

(7)   Martin, R. B. "Aluminum: A neurotoxic product of acid rain." *Acc. Chem. Res.* **1994,** *27* (7), 204-210.

(8)   Beardmore, J.; Lopez, X.; Mujika, J. I.; Exley, C. "What is the mechanism of formation of hydroxyaluminosilicates?" *Sci. Rep.* **2016,** *6*, 30913.

(9)   Doucet, F. J.; Schneider, C.; Bones, S. J.; Kretchmer, A.; Moss, I.; Tekely, P.; Exley, C. "The formation of hydroxyaluminosilicates of geochemical and biological significance." *Geochim. Cosmochim. Acta* **2001,** *65* (15), 2461-2467.

(10)   Shaw, C. A.; Tomljenovic, L. "Aluminum in the central nervous system (cns): Toxicity in humans and animals, vaccine adjuvants, and autoimmunity." *Immunol. Res.* **2013,** *56* (2-3), 304-316.

(11)   Exley, C.; "Why industry propaganda and political interference cannot disguise the inevitable role played by human exposure to aluminum in neurodegenerative diseases, including alzheimer's disease." *Front. Neurol.* **2014,** *5,* 1-6.

(12)   Tomljenovic, L.; Shaw, C. A. "Do aluminum vaccine adjuvants contribute to the rising prevalence of autism?" *J. Inorg. Biochem.* **2011,** *105* (11), 1489-1499.

(13)   Mold, M.; Umar, D.; King, A.; Exley, C. "Aluminium in brain tissue in autism." *J. Trace Elem. Med. Biol.* **2018,** *46*, 76-82.

(14)   Willhite, C. C.; Karyakina, N. A.; Yokel, R. A.; Yenugadhati, N.; Wisniewski, T. M.; Arnold, I. M.; Momoli, F.; Krewski, D. "Systematic review of potential health risks posed by pharmaceutical, occupational and consumer exposures to metallic and nanoscale aluminum, aluminum oxides, aluminum hydroxide and its soluble salts." *Crit. Rev. Toxicol.* **2014,** *4*, 1-80.

(15)   Yokel, R. A. "The toxicology of aluminum in the brain: A review." *Neurotoxicology* **2000,** *21* (5), 813-828.

(16)   Yokel, R. A. "Aluminum chelation principles and recent ad v ances." *Coord. Chem. Rev.* **2002,** *228*, 97-113.

(17)   Pearson, R. G. "Hard and soft acids and bases." *J. Am. Chem. Soc.* **1963,** *85* (22), 3533-3539.

(18)   Toso, L. "Design, synthesis and characterization of new iron and aluminium chelating agents". PhD dissertation, Università degli studi di Cagliari, 2013.

(19)   Mayr, H.; Breugst, M.; Ofial, A. R. "Farewell to the HSAB treatment of ambient reactivity." *Angew. Chem. Int. Ed. Engl.* **2011,** *50* (29), 6470-6505.

(20)   Martell, A. E.; Hancock, R. D.; Smith, R. M.; Motekaitis, R. J. "Coordination of Al(III) in the environment and in biological systems." *Coord. Chem. Rev.* **1996,** *149*, 311-328.

(21)   Dalla Torre, G.; Mujika, J. I.; Formoso, E.; Matito, E.; Ramos, M. J.; Lopez, X. "Tuning the affinity of catechols and salicylic acids towards Al(III): Characterization of Al–chelator interactions." *Dalton Transactions* **2018,** *47* (29), 9592-9607.

(22)   Kiss, T. "From coordination chemistry to biological chemistry of aluminium." *J. Inorg. Biochem.* **2013,** *128* (SI), 156-163.

(23)   Mujika, J. I.; Dalla Torre, G.; Lopez, X. "Aluminum and fenton reaction: How can the reaction be modulated by speciation? A computational study using citrate as a test case." *Phys. Chem. Chem. Phys.* **2018,** *20* (23), 16256-16265.

(24)   Mujika, J. I.; Dalla Torre, G.; Formoso, E.; Grande-Aztatzi, R.; Grabowski, S. J.; Exley, C.; Lopez, X. "Aluminum's preferential binding site in proteins: Sidechain of amino acids versus backbone interactions." *J. Inorg. Biochem.* **2018,** *181* (October 2017), 111-116.

(25)   Crisponi, G.; Dean, A.; Di Marco, V.; Lachowicz, J. I.; Nurchi, V. M.; Remelli, M.; Tapparo, A. "Different approaches to the study of chelating agents for iron and aluminium overload pathologies." *Anal. Bioanal.Chem.* **2013,** *405* (2-3), 585-601.

(26)   Hay, M. B.; Myneni, S. C. B. "Geometric and electronic structure of the aqueous $Al(H_2O)_6^{(3+)}$ complex." *J. phys. chem. A* **2008,** *112* (42), 10595-10603.

(27)   Hider, R. "Recent developments centered on orally active iron chelators." *Thalassemia Reports* **2014,** *4* (2).

(28)   Crisponi, G.; Remelli, M. "Iron chelating agents for the treatment of iron overload." *Coord. Chem. Rev.* **2008,** *252* (10-11), 1225-1240.

(29)   Martin, R. B. "Fe^{3+} and Al^{3+} hydrolysis equilibria. Cooperativity in Al^{3+} hydrolysis reactions." *J. Inorg. Biochem.* **1991,** *44* (2), 141-147.

(30)   Jensen, J. H. "Predicting accurate absolute binding energies in aqueous solution: Thermodynamic considerations for electronic structure methods." *Phys. Chem. Chem. Phys.* **2015,** *17* (19), 12441-12451.

(31)   Song, B.; Sun, Q.; Li, H.; Ge, B.; Pan, J. S.; Wee, A. T. S.; Zhang, Y.; Huang, S.; Zhou, R.; Gao, X.et al. "Irreversible denaturation of proteins through aluminum-induced formation of backbone ring structures." *Angew. Chem. Int. Ed.* **2014,** *53* (25), 6358-6363.

(32)   Winget, P.; Clark, T. "AM1* parameters for aluminum, silicon, titanium and zirconium." *J. Mol. Model.* **2005,** *11* (6), 439-456.

(33)   Faro, T. M. C.; Thim, G. P.; Skaf, M. S. "A lennard-jones plus coulomb potential for Al^{3+} ions in aqueous solutions." *J. Chem. Phys.* **2010,** *132* (11), 114509-114509.

(34)   Lakatos, A.; Evanics, F. "Speciation of Al(III) in blood serum− the Al(III)− citrate− phosphate ternary system." *Eur. J. of Inorg. Chem.* **2001**, 3079-3086.

(35)   Murko, S.; Milacic, R.; Scancar, J. "Speciation of al in human serum by convective-interaction media fast-monolithic chromatography with inductively coupled plasma mass spectrometric detection." *J. Inorg. Biochem.* **2007,** *101* (9), 1234-1241.

(36)   Milačič, R.; Murko, S.; Ščančar, J.; "Problems and progresses in speciation of al in human serum: An overview." *J. Inorg. Biochem.* **2009,** *103* (11), 1504-1513.

(37)   Ma, J. F.; "Aluminium tolerance in plants and the complexing role of organic acids." *Trends in Plant Science* **2001,** *6* (6), 273-278.

(38)   Klotz, K.; Weistenhofer, W.; Neff, F.; Hartwig, A.; van Thriel, C.; Drexler, H. "The health effects of aluminum exposure." *Deutsches Arzteblatt international* **2017,** *114* (39), 653-659.

(39)   Mujika, J. I.; Ugalde, J. M.; Lopez, X. "Aluminum speciation in biological environments. The deprotonation of free and aluminum bound citrate in aqueous solution." *Phys. Chem. Chem. Phys.* **2012,** *14* (36), 12465-12475.

(40)   Luque, N.; Mujika, J. I.; Formoso, E.; Lopez, X. "Aluminum interaction with 2,3-diphosphoglyceric acid. A computational studyle." *RSC Adv.* **2015,** *5* (78), 63874-63881.

(41)   Formoso, E.; Lopez, X. "A computational study on interaction of aluminum with D-glucose 6-phosphate for various stoichiometries." *RSC Adv.* **2017,** *7* (10).

(42)   Formoso, E.; Mujika, J. I.; Grabowski, S. J.; Lopez, X. "Aluminum and its effect in the equilibrium between folded/unfolded conformation of NADH." *J. Inorg. Biochem.* **2015,** *152*, 139-146.

(43)   Kong, S.; Liochev, S.; Fridovich, I. "Aluminum(III) facilitates the oxidation of NADH by the superoxide anion." *Free Radic. Biol. Med.* **1992,** *13*, 79-81.

(44)   Kiss, T.; Sovago, I.; Martin, R. B. " Al^{3+} binding to catecholamines and tiron." *J. Inorg. Biochem.* **1989,** *36* (3-4), 348-348.

(45)   Luque, N. B.; Mujika, J. I.; Rezabal, E.; Ugalde, J. M.; Lopez, X. "Mapping the affinity of aluminum(III) for biophosphates: Interaction mode and binding affinity in 1 : 1 complexes." *Phys. Chem. Chem. Phys.* **2014,** *16* (37), 20107-20119.

(46)   Mujika, J. I.; Lopez, X.; Rezabal, E.; Castillo, R.; Marti, S.; Moliner, V.; Ugalde, J. M. "A QM/MM study of the complexes formed by aluminum and iron with serum transferrin at neutral and acidic pH." *J. Inorg. Biochem.* **2011,** *105* (11), 1446-1456.

(47)   Mujika, J. I.; Escribano, B.; Akhmatskaya, E.; Ugalde, J. M.; Lopez, X. "Molecular dynamics simulations of iron- and aluminum-loaded serum transferrin: Protonation of tyr188 is necessary to prompt metal release." *Biochemistry* **2012,** *51* (35), 7017-7027.

(48)   Drago, D.; Bettella, M.; Bolognin, S.; Cendron, L.; Scancar, J.; Milacic, R.; Ricchelli, F.; Casini, A.; Messori, L.; Tognon, G.et al. "Potential pathogenic role of beta-amyloid(1-42)-aluminum complex in Alzheimer's Disease." *Int. J. Biochem. Cell Biol.* **2008,** *40* (4), 731-746.

(49)   Exley, C. "The coordination chemistry of aluminium in neurodegenerative disease." *Coord. Chem. Rev.* **2012,** *256* (19-20), 2142-2146.

(50)   Mujika, J. I.; Pedregal, J. R.-G.; Lopez, X.; Ugalde, J. M.; Rodríguez-Santiago, L.; Sodupe, M.; Maréchal, J.-D. "Elucidating the 3D structures of Al(III)–aβ complexes: A template free strategy based on the pre-organization hypothesis." *Chem. Sci.* **2017,** *8* (7), 5041-5049.

(51)   Mujika, J. I.; Ruipérez, F.; Infante, I.; Ugalde, J. M.; Exley, C.; Lopez, X. "Pro-oxidant activity of aluminum: Stabilization of the aluminum superoxide radical ion." *TJ. Phys. Chem. A* **2011,** *115* (24), 6717-6723.

(52)   Exley, C. "The pro-oxidant activity of aluminum." *Free Radic. Biol. Med.* **2004,** *36* (3), 380-387.

(53)   Han, S.; Lemire, J.; Appanna, V. D. V. P. V. D.; Auger, C.; Castonguay, Z.; Appanna, V. D. "How aluminum, an intracellular ros generator promotes hepatic and neurological diseases: The metabolic tale." *Cell Biol. Toxicol.* **2013,** *29* (2), 75-84.

(54)   Prousek, J. "Fenton chemistry in biology and medicine." *Pure Appl. Chem.* **2007,** *79* (12), 2325-2338.

(55)   Mujika, J. I.; Dalla Torre, G.; Lopez, X. "Aluminum and Fenton reaction : How can the reaction be modulated by speciation ? A computational study using citrate as a test case." *Phys. Chem, Chem. Phys.* **2018**, *20*, 16256-16265.

(56)   Ruipérez, F.; Mujika, J. I.; Ugalde, J. M.; Exley, C.; Lopez, X. "Pro-oxidant activity of aluminum: Promoting the fenton reaction by reducing Fe(III) to Fe(II)." *J. Inorg. Biochem.* **2012,** *117*, 118-123.

(57)   Touam, M.; Martinez, F.; Lacour, B.; Bourdon, R.; Zingraff, J.; Dicuilio, S.; Drueke, T. "Aluminum-induced, reversible microcytic anemia in chronic renal failure: Clinical and experimental studies." *Clin. Nephrol.* **1983,** *19*, 295-298.

(58)   Wills, M.; Savory, J. "Aluminium poisoning: Dialysis encephalopathy, osteomalacia, and anaemia." *The Lancet* **1983,** *322* (8340), 29-34.

(59)   Gupta, V. B.; Anitha, S.; Hegde, M. L.; Zecca, L.; Garruto, R. M.; Ravid, R.; Shankar, S. K.; Stein, R.; Shanmugavelu, P.; Jagannatha Rao, K. S. "Aluminium in alzheimer's disease: Are we still at a crossroad?" *Cell. Mol. Life Sci.* **2005,** *62* (2), 143-158.

(60)   Zatta, P.; Drago, D.; Bolognin, S.; Sensi, S. L. "Alzheimer's disease, metal ions and metal homeostatic therapy." *Trends Pharmacol. Sci.* **2009,** *30* (June), 346-355.

(61)   Tomljenovic, L. "Aluminum and alzheimer's disease: After a century of controversy, is there a plausible link?" *J. Alzheimer's Dis.* **2011,** *23* (4), 567-598.

(62)   Altschuler, E. "Aluminum-containing antacids as a cause of idiopathic parkinson's disease." *Med. Hypotheses* **1999,** *53* (1), 22-23.

(63)   Yokel, R. a. "Blood-brain barrier flux of aluminum, manganese, iron and other metals suspected to contribute to metal-induced neurodegeneration." *J. Alzheimer's Dis.* **2006,** *10* (2-3), 223-253.

(64)   Milanese, M.; Lkhayat, M. I.; Zatta, P. "Inhibitory effect of aluminum on dopamine β-hydroxylase from bovine adrenal gland." *J. Trace Elem. Med. Biol.* **2001,** *15* (2-3), 139-141.

(65)   Hollender, D.; Károly-Lakatos, A.; Forgó, P.; Körtvélyesi, T.; Dombi, G.; Majer, Z.; Hollósi, M.; Kiss, T.; Odani, A. "Al(III)-binding ability of an octapeptide and its phosphorylated derivative." *J. Inorg. Biochem.* **2006,** *100* (3), 351-361.

(66)   Grande-Aztatzi, R.; Formoso, E.; Mujika, J. I.; Ugalde, J. M.; Lopez, X. "Phosphorylation promotes al(III) binding to proteins: GEGEGSGG as a case study." *Phys. Chem. Chem. Phys.* **2016,** *18* (10), 7197-7207.

(67)   Selkoe, D. J. "The molecular pathology of alzheimer's disease." *Neuron* **1991,** *6* (4), 487-498.

(68)   Exley, C.; Price, N. C.; Kelly, S. M.; Birchall, J. D. "An interaction of beta-amyloid with aluminium in vitro." *FEBS Lett.* **1993,** *324* (3), 293-295.

(69)   Mirza, A.; King, A.; Troakes, C.; Exley, C. "The identification of aluminum in human brain tissue using lumogallion and fluorescence microscopy." *J. Alzheimers Dis.* **2016,** *54*, 1-6.

(70)   Mirza, A.; King, A.; Troakes, C.; Exley, C. "Aluminium in brain tissue in familial alzheimer's disease." *J. Trace Elem. Med. Biol.* **2017,** *40*, 30-36.

(71)   Khan, A.; Ashcroft, A. E.; Higenell, V.; Korchazhkina, O. V.; Exley, C. "Metals accelerate the formation and direct the structure of amyloid fibrils of NAC." *J. Inorg. Biochem.* **2005,** *99* (9), 1920-1927.

(72)   Khan, A.; Dobson, J. P.; Exley, C. "Redox cycling of iron by Abeta42." *Free Radic. Biol. Med.* **2006,** *40* (4), 557-569.

(73)   Hegde, M. L.; Bharathi, P.; Suram, A.; Venugopal, C.; Jagannathan, R.; Poddar, P.; Srinivas, P.; Sambamurti, K.; Rao, K. J.; Scancar, J.et al. "Challenges associated with metal chelation therapy in alzheimer's disease." *J. Alzheimers Dis.* **2009,** *17* (3), 457-468.

(74)   Mujika, J. I.; Rodríguez-Guerra, J.; Lopez, X.; Ugalde, J. M.; Rodríguez-Santiago, L.; Sodupe, M.; Maréchal, J.-D. "Elucidating the 3D structures of Al(III)-aβ complexes: A template free strategy based on the pre-organization hypothesis." *Chem. Sci.* **2017,***8*(7) , 5041-5049.

(75)   Ferreira, C. R.; Gahl, W. A. "Disorders of metal metabolism." *Trans. Sci. rare dis.* **2017,** *2* (3-4), 101-139.

(76)   Cross, A. J.; Crow, T. J.; Perry, E. K.; Perry, R. H.; Blessed, G.; Tomlinson, B. E. "Reduced dopamine-beta-hydroxylase activity in Alzheimer's Disease." *Br. Med. J. (Clin. Res. Ed.)* **1981,** *282* (6258), 93-94.

(77)   Vendelboe, T. V.; Harris, P.; Zhao, Y.; Walter, T. S.; Harlos, K.; El Omari, K.; Christensen, H. E. M. "The crystal structure of human dopamine beta-hydroxylase at 2.9 a resolution." *Sci. Adv.* **2016,** *2* (4), e1500980.

(78)   Bazzicalupi, C.; Bianchi, A.; Giorgi, C.; Clares, M. P.; García-España, E. "Addressing selectivity criteria in binding equilibria." *Coord. Chem. Rev.* **2012,** *256* (1-2), 13-27.

(79)   Crisponi, G.; Nurchi, V. M. "Thermodynamic remarks on chelating ligands for aluminium related diseases." *J. Inorg. Biochem.* **2011,** *105* (11), 1518-1522.

(80)   Nurchi, V. M.; Alonso, M. C.; Toso, L.; Lachowicz, J. I.; Crisponi, G. "Chelation therapy for metal intoxication: Comments from a thermodynamic viewpoint." *Mini Rev. Med. Chem.* **2013,** *13* (11), 1541-1549.

(81)   Dalla Torre, G.; Mujika, J. I.; Formoso, E.; Matito, E.; João Ramos, M.; Lopez, X. "Tuning the affinity of catechols and salicylic acids towards Al(III): Characterization of al-chelator interactions." *Dalton Trans* **2018**, *47* (49), 9592-9607.

(82)   Beardmore, J.; Rugg, G.; Exley, C. "A systems biology approach to the blood-aluminium problem: The application and testing of a computational model." *J. Inorg. Biochem.* **2007,** *101* (9), 1187-1191.

(83)   Beardmore, J.; Exley, C. "Towards a model of non-equilibrium binding of metal ions in biological systems." *J. Inorg. Biochem.* **2009,** *103* (2), 205-209.

(84)   Bone, I.; Thomas, M. "Dialysis dementia, aluminium, and tetrahydrobiopterin metabolism." *Lancet* **1979,** *1* (8119), 782.

(85)   Yokel, R. a.; Rhineheimer, S. S.; Sharma, P.; Elmore, D.; McNamara, P. J. "Entry, half-life, and desferrioxamine-accelerated clearance of brain aluminum after a single (26)Al exposure." *Toxicol. Sci.* **2001,** *64*, 77-82.

(86)   Nurchi, V. M.; Crisponi, G.; Pivetta, T.; Donatoni, M.; Remelli, M. "Potentiometric, spectrophotometric and calorimetric study on iron(III) and copper(II) complexes with 1,2-dimethyl-3-hydroxy-4-pyridinone." *J. Inorg. Biochem.* **2008,** *102* (4), 684-692.

(87)   Cappellini, M. D.; Pattoneri, P. "Oral iron chelators." *Annu. Rev. Med.* **2009,** *60*, 25-38.

(88)   Kiss, T.; Farkas, E. "Metal-binding ability of desferrioxamine b." *J. Incl. Phenom. Macrocycl. Chem.* **1998,** *32* (Iii), 385-403.

(89)   Biaso, F.; Baret, P.; Pierre, J. L.; Serratrice, G. "Comparative studies on the iron chelators o-trensox and trencams: Selectivity of the complexation towards other biologically relevant metal ions and Al^{3+}." *J. Inorg. Biochem.* **2002,** *89* (1-2), 123-130.

(90)   Chaves, S.; Marques, S. M.; Matos, A. M. F. F.; Nunes, A.; Gano, L.; Tuccinardi, T.; Martinelli, A.; Amélia Santos, M. "New tris(hydroxypyridinones) as iron and aluminium sequestering agents: Synthesis, complexation and in vivo studies." *Chem. Eur. J.* **2010,** *16* (34), 10535-10545.

(91)   Chaves, S.; Capelo, A.; Areias, L.; Marques, S. M.; Gano, L.; Esteves, M. A.; Santos, M. A. "A novel tripodal tris-hydroxypyrimidinone sequestering agent for trivalent hard metal ions: Synthesis, complexation and *in vivo* studies." *Dalton Trans.* **2013,** *42* (17), 6033-6045.

(92)   Di Marco, V. B.; Dean, A.; Ferlin, M. G.; Yokel, R. A.; Li, H.; Venzo, A.; Bombi, G. G. "Methyl-hydroxypyridinecarboxylic acids as possible bidentate chelating agents for aluminium(III): Synthesis and metal-ligand solution chemistry." *Eur. J. Inorg. Chem.* **2006**, (6), 1284-1293.

(93)   Lachowicz, J. I.; Nurchi, V. M.; Crisponi, G.; Jaraquemada-Pelaez, M. G.; Arca, M.; Pintus, A.; Santos, M. A.; Quintanova, C.; Gano, L.; Szewczuk, Z.et al. "Hydroxypyridinones with enhanced iron chelating properties. Synthesis, characterization and *in vivo* tests of 5-hydroxy-2-(hydroxymethyl)pyridine-4(1H)-one." *Dalton Trans.* **2016,** *45* (15), 6517-6528.

(94)   Nurchi, V. M.; Pivetta, T.; Lachowicz, J. I.; Crisponi, G. "Effect of substituents on complex stability aimed at designing new iron(III) and aluminum(III) chelators." *J. Inorg. Biochem.* **2009,** *103* (2), 227-236.

(95)   Shanzer, a.; Libman, J.; Lifson, S.; Felder, C. E. "Origin of the iron(III) binding and conformational properties of enterobactin." *J. Am. Chem. Soc.* **1986,** *108* (6), 7609-7619.

(96)   Santos, M. A.; Marques, S. M.; Chaves, S. "Hydroxypyridinones as " privileged" chelating structures for the design of medicinal drugs." *Coord. Chem. Rev.* **2012,** *256* (1-2), 240-259.

(97)   Gama, S.; Gil, M.; Gano, L.; Farkas, E.; Amélia Santos, M. "Combined chelation of bi-functional bis-hydroxypiridinone and mono-hydroxypiridinone: Synthesis, solution and *in vivo* evaluation." *J. Inorg. Biochem.* **2009,** *103* (2), 288-298.

(98)   Gama, S.; Dron, P.; Chaves, S.; Farkas, E.; Santos, M. A. "A bis(3-hydroxy-4-pyridinone)-EDTA derivative as a strong chelator for m3+ hard metal ions: Complexation ability and selectivity." *Dalton Trans.* **2009**, (31), 6141-6150.

(99)   Chaves, S.; Dron, P. I.; Danalache, F. A.; Sacoto, D.; Gano, L.; Santos, M. A. "Combined chelation based on glycosyl-mono- and bis-hydroxypyridinones for aluminium mobilization: Solution and biodistribution studies." *J. Inorg. Biochem.* **2009,** *103* (11), 1521-1529.

(100)   Toso, L.; Crisponi, G.; Nurchi, V. M.; Crespo-Alonso, M.; Lachowicz, J. I.; Mansoori, D.; Arca, M.; Santos, M. A.; Marques, S. M.; Gano, L.et al. "Searching for new aluminium chelating agents: A family of hydroxypyrone ligands." *J. Inorg. Biochem.* **2014,** *130*, 112-121.

(101)   Nurchi, V. M.; Lachowicz, J. I.; Crisponi, G.; Murgia, S.; Arca, M.; Pintus, A.; Gans, P.; Niclos-Gutierrez, J.; Domínguez-Martín, A.; Castineiras, A. "Kojic acid derivatives as powerful chelators for iron(III) and aluminium(III)." *Dalton Trans.* **2011,** *40* (22), 5984-5998.

(102)   Nurchi, V. M.; Crisponi, G.; Lachowicz, J. I.; Murgia, S.; Pivetta, T.; Remelli, M.; Rescigno, A.; Niclós-Gutíerrez, J.; González-Pérez, J. M.; Domínguez-Martín, A. "Iron(III) and aluminum(III) complexes with hydroxypyrone ligands aimed to design kojic acid derivatives with new perspectives." *J. Inorg. Biochem.* **2010,** *104* (5), 560-569.

(103)   Shanzer, A.; Libman, J.; Lifson, S. In *Pure Appl. Chem.*, 1992; Vol. 64.

(104)   Garrett, T. M.; Cass, M. E.; Raymond, K. N. "Hydrogen bonding in catechoylamides." *J. Coord. Chem.* **1992,** *25* (3), 241-253.

(105)   Serratrice, G.; Boukhalfa, H.; Be, C.; Baret, P.; Caris, C.; Pierre, J.-l. "O-trensox , a new tripodal iron chelator based on 8-hydroxyquinoline subunits : Thermodynamic and kinetic studies." *Inorg. Chem.* **1997,** *36* (18), 3898-3910.

(106)   Baret, P.; Beguin, C. G.; Boukhalfa, H.; Caris, C.; Laulhtre, J.-p.; Pierre, J.-l. "0-trensox: A promising water-soluble iron chelator (both feli1 and fe") potentially suitable for plant nutrition and iron chelation therapy." *J. Am. Chem. Soc.* **1995,** *117* (38), 9760-9761.

(107)   Skoog, D. A. *Fundamentals of analytical chemistry*; Saunders College Pub: New York, **1988**.

(108)   Gutten, O.; Rulisek, L. "Predicting the stability constants of metal-ion complexes from first principles." *Inorg. Chem.* **2013,** *52* (18), 10347-10355.

(109)   Harris, W. R.; Raymond, K. N.; Weitl, F. L. "Ferric ion sequestering agents. 6. The spectrophotometric and potentiometric evaluation of sulfonated tricatecholate ligands." *J. Am. Chem. Soc.* **1981,** *103* (10), 2667-2675.

(110)   Lachowicz, J. I.; Nurchi, V. M.; Crisponi, G.; Pelaez Mde, G.; Rescigno, A.; Stefanowicz, P.; Cal, M.; Szewczuk, Z. "Metal coordination and tyrosinase inhibition studies with kojic-betaala-kojic." *J. Inorg. Biochem.* **2015,** *151*, 36-43.

(111)   Clevette, D. J.; Nelson, W. O.; Nordin, A.; Orvig, C.; Sjoeberg, S. "The complexation of aluminum with n-substituted 3-hydroxy-4-pyridinones." *Inorg. Chem.* **1989,** *28* (11), 2079-2081.

(112)   Crisponi, G.; Nurchi, V. M.; Lachowicz, J. I.; Crespo-Alonso, M.; Zoroddu, M. a.; Peana, M. "Kill or cure: Misuse of chelation therapy for human diseases." *Coord. Chem. Rev.* **2014,** *284*, 278-285.

(113) Sigel, A.; Sigel, H. "Metal ions in biological systems, volume 35: Iron transport and storage microorganisms, plants, and animals." *Metal-based drugs* **1998**.

(114) Fulgenzi, A.; Vietti, D.; Ferrero, M. E. "Aluminium involvement in neurotoxicity." *BioMed. Res. Int.* **2014,** 758323-758323.

(115) Mujika, J. I.; Rezabal, E.; Mercero, J. M.; Ruipérez, F.; Costa, D.; Ugalde, J. M.; Lopez, X. "Aluminium in biological environments: A computational approach." *Comput. and Struct. Biotech. J.* **2014,** *9* (15), e201403002.

(116) Neves, R. P. P.; Fernandes, P. A.; Varandas, J. C.; Ramos, M. J. "Benchmarking of density functionals for the accurate description of thiol − disulfïide exchange." *J. Chem. Theory Comput.* **2014,** *10* (11), 4842-4856.

(117) Pereira, A. T.; Ribeiro, A. J. M.; Fernandes, P. A.; Ramos, M. J. "Benchmarking of density functionals for the kinetics and thermodynamics of the hydrolysis of glycosidic bonds catalyzed by glycosidases." *Int. J. Quantum Chem.* **2017,** *117* (18), 1-12.

(118) Ribeiro, A. J. M.; Ramos, M. J.; Fernandes, P. A. "Benchmarking of dft functionals for the hydrolysis of phosphodiester bonds." *J. Chem. Theory Comput.* **2010,** *6* (8), 2281-2292.

(119) Cramer, C. J. *Essentials of computational chemistry, theories and models, second edition*; John Wiley and Sons: West Sussex, England, **2004**.

(120) Born, M.; Oppenheimer, R. "Zur quantentheorie der molekeln." *Annalen der Physik* **1927,** *389* (20), 457-484.

(121) Novoa, E. M.; Pouplana, L. R. D.; Orozco, M. "Computational modeling of biological systems." Springer, **2012,**.

(122) Orozco, M. "A theoretical view of protein dynamics." *Chem. Soc. Rev.* **2014,** *43* (14), 5051-5051.

(123) Brunk, E.; Rothlisberger, U. "Mixed quantum mechanical/molecular mechanical molecular dynamics simulations of biological systems in ground and electronically excited states." *Chem. Rev.* **2015,** *115* (12), 6217-6263.

(124) Jensen, F. *Introduction to computational chemistry*; John Wiley & Sons, Inc., **2006**.

(125) Hohenberg, P.; Kohn, W. "Inhomogeneous electron gas." *Phys. Rev.* **1964,** *136* (3B), B864---B871.

(126) Mardirossian, N.; Head-Gordon, M. "Thirty years of density functional theory in computational chemistry: An overview and extensive assessment of 200 density functionals." *Mol. Phys.* **2017,** *115* (19), 2315-2372.

(127) Thomas, L. H. *Math. Proc. Cambridge Philos. Soc.* **1927,** *23*, 542.

(128) Kohn, W.; Sham, L. J. "Self-consistent equations including exachange and correlation effects." *Phys. Rev.* **1965,** *140*, A1133.

(129) Peverati, R.; Truhlar, D. G. "Quest for a universal density functional: The accuracy of density functionals across a broad spectrum of databases in chemistry and physics." *Philos. Trans.. Series A* **2013,** *372*, 20120476.

(130) Perdew, J. P. "Jacob's ladder of density functional approximations for the exchange-correlation energy." *AIP Conference Proceedings* **2001,** *577* (2001), 1-20.

(131) Mardirossian, N.; Head-Gordon, M. "wb97X-V: A 10-parameter, range-separated hybrid, generalized gradient approximation density functional with nonlocal correlation, designed by a survival-of-the-fittest strategy." *Phys. Chem. Chem. Phys.* **2014,** *16* (21), 9904-9924.

(132) Becke, A. D. "Density-functional thermochemistry. Iii. The role of exact exchange." *J. Chem. Phys.* **1993,** *98* (7), 5648-5648.

(133) Becke, A. D. " Density-functional thermochemistry. III. The role of exact exchange" *J. Chem. Phys.* **1993,** *98*, 1372.

(134) Harris, J.; Jones, R. O " The surface energy of a bounded electron gas". *J. Phys. F: Metal Phys.* **1974,** *4*, 1170.

(135) Gunnarsson, O.; Lundqvist, B. I. Exchange and correlation in atoms, molecules, and solids by the spin-density-functional formalism" *Phys. Rev. B* **1976,** *13*, 4274.

(136) Langreth, D. C.; Perdew, J. P. " Exchange-correlation energy of a metallic surface: Wave-vector analysis" *Phys. Rev. B* **1977,** *15*, 2884.

(137) Harris, J. " Adiabatic-connection approach to Kohn-Sham theory" *Phys. Rev. A* **1984,** *29*, 1648.

(138) Vosko, S. H.; Wilk, L.; Nusair, M. " Accurate spin-dependent electron liquid correlation energies for local spin density calculations: a critical analysis" *Can. J. Phys.* **1980,** *58*, 1200.

(139) Becke, A. D. " Density-functional exchange-energy approximation with correct asymptotic behavior" *Phys. Rev. A* **1988,** *38*, 3098.

(140) Lee, C.; Yang, W.; Parr, R. G. " Development of the Colle-Salvetti correlation-energy formula into a functional of the electron density" *Phys. Rev. B* **1988,** *37*, 785.

(141) Hujo, W.; Grimme, S. "Performance of non-local and atom-pairwise dispersion corrections to DFT for structural parameters of molecules with noncovalent interactions." *J. Chem. Theory Comput.* **2013,** *9* (1), 308-315.

(142) Iikura, H.; Tsuneda, T.; Yanai, T.; Hirao, K. "A long-range correction scheme for generalized-gradient-approximation exchange functionals." *J. Chem. Phys.* **2001,** *115* (8), 3540-3544.

(143) Yanai, T.; Tew, D. P.; Handy, N. C. "A new hybrid exchange–correlation functional using the Coulomb-attenuating method (CAM-B3LYP)." *Chem. Phys. Lett.* **2004,** *393* (1), 51-57.

(144) Heyd, J.; Scuseria, G. E.; Ernzerhof, M. "Hybrid functionals based on a screened coulomb potential." *J. Chem. Phys.* **2003,** *118* (18), 8207-8215.

(145) Krukau, A. V.; Vydrov, O. A.; Izmaylov, A. F.; Scuseria, G. E. "Influence of the exchange screening parameter on the performance of screened hybrid functionals." *J. Chem. Phys.* **2006,** *125* (22), 224106.

(146) Peverati, R.; Truhlar, D. G. "Screened-exchange density functionals with broad accuracy for chemistry and solid-state physics." *Phys. Chem. Chem. Phys.* **2012,** *14* (47), 16187-16191.

(147) Grimme, S.; Hansen, A.; Brandenburg, J. G.; Bannwarth, C. "Dispersion-corrected mean-field electronic structure methods." *Chem. Rev.* **2016,** *116* (9), 5105-5154.

(148) Eisenschitz, R.; London, F. "Über das verhältnis der van der Waalsschen kräfte zu den homöopolaren bindungskräften | springerlink." *Eur. Phys. J.* **1930,** *60* (7-8), 491-527.

(149) Mackie, I. D.; Dilabio, G. A. "Accurate dispersion interactions from standard density-functional theory methods with small basis sets." *Phys. Chem. Chem. Phys.* **2010,** *12* (23), 6092-6098.

(150) Torres, E.; DiLabio, G. A. "A (nearly) universally applicable method for modeling noncovalent interactions using B3LYP." *J. Phys. Chem. Lett.* **2012,** *3* (13), 1738-1744.

(151) DiLabio, G. A.; Koleini, M.; Torres, E. "Extension of the B3LYP - dispersion-correcting potential approach to the accurate treatment of both inter- and intramolecular interactions." *Theor. Chem. Acc.* **2013,** *132*, 1389.

(152) Vydrov, O. a.; Van Voorhis, T. "Nonlocal van der Waals density functional: The simpler the better." *J. Chem. Phys.* **2010,** *133* (24), 244103-244103.

(153) Grimme, S.; Antony, J.; Ehrlich, S.; Krieg, H. "A consistent and accurate ab initio parametrization of density functional dispersion correction (DFT-D) for the 94 elements H-Pu." *J. Chem. Phys.* **2010,** *132* (15).

(154) Grimme, S; Steinmetz, M. "Effects of London dispersion correction in density functional theory on the structures of organic molecules in the gas phase." *Phys. Chem. Chem. Phys.* **2013**. *15*, 16031-16042.

(155) Sedlak, R.; Janowski, T.; Pitoňák, M.; Rezáč, J.; Pulay, P.; Hobza, P.; Pitoňák, M.; Řezáč, J.; Pulay, P.; Hobza, P. "Accuracy of quantum chemical methods for large noncovalent complexes." *J. Chem. Theory Comput.* **2013,** *9* (8), 3364-3374.

(156) Goerigk, L.; Kruse, H.; Grimme, S. "Benchmarking density functional methods against the s66 and s66x8 datasets for non-covalent interactions." *Chemphyschem* **2011,** *12* (17), 3421-3433.

(157) Goerigk, L.; Grimme, S. "A thorough benchmark of density functional methods for general main group thermochemistry, kinetics, and noncovalent interactions." *Phys. Chem. Chem. Phys.* **2011,** *13* (14), 6670-6670.

(158) Goerigk, L. "How do DFT-DCO, DFT-NL, and DFT-D3 compare for the description of London-dispersion effects in conformers and general thermochemistry?" *J. Chem. Theory Comput.* **2014,** *10* (3), 968-980.

(159)   Grimme, S. "Density functional theory with london dispersion corrections." *WIREs* **2011,** *1* (2), 211-228.

(160)   Becke, A. D.; Johnson, E. R. "Exchange-hole dipole moment and the dispersion interaction." *J. Chem. Phys.* **2005,** *122* (15), 154104-154104.

(161)   Hostaš, J.; Řezáč, J.; Hobza, P. "On the performance of the semiempirical Quantum mechanical PM6 and PM7 methods for noncovalent interactions." *Chem. Phys. Lett.* **2013,** *568*, 161-166.

(162)   Řezáč, J.; Hobza, P. "Advanced corrections of hydrogen bonding and dispersion for semiempirical Quantum mechanical methods." *J. Chem. Theory Comput.* **2012,** *8* (1), 141-151.

(163)   Vorontsov, A. V.; Smirniotis, P. G. "Benchmarking semiempirical and dft methods for the interaction of thiophene and diethyl sulfide molecules with a ti(OH)4(H$_2$O) cluster." *J. Mol. Model.* **2017,** *23* (8).

(164)   Christensen, A. S.; Elstner, M.; Cui, Q. "Improving intermolecular interactions in DFTB3 using extended polarization from chemical-potential equalization." *J. Chem. Phys.* **2015,** *143* (8), 1-11.

(165)   Schrödinger, E. "An undulatory theory of the mechanics of atoms and molecules." *Phys. Rev.* **1926,** *28* (6), 1049-1070.

(166)   Lennard-Jones, J. E. "The electronic structure of some diatomic molecules." *Trans. Faraday Soc.* **1929,** *25*, 668-686.

(167)   Slater, J. C. "Atomic shielding constants." *Phys. Rev.* **1930,** *36* (1), 57-64.

(168)   "Electronic wave functions - I. A general method of calculation for the stationary states of any molecular system." *Proceedings of the Royal Society of London. Series A.* **1950,** *200* (1063), 542.

(169)   Liu, B.; McLean, A. D. "Accurate calculation of the attractive interaction of two ground state helium atoms." *J. Chem. Phys.* **1973,** *59* (8), 4557-4558.

(170)   Kestner, N. R. "He–He interaction in the SCF–MO approximation." *J. Chem. Phys.* **1968,** *48* (1), 252-257.

(171)   Bowen, J. P. P.; Sorensen, J. B. B.; Kirschner, K. N. N. "Calculating interaction energies using first principle theories: Consideration of BSSE and fragment relaxation." *J. Chem. Educ.* **2007,** *84* (7), 1225-1229.

(172)   Boys, S. F.; Bernardi, F. "The calculation of small molecular interactions by the differences of separate total energies. Some procedures with reduced errors." *Mol. Phys.* **1970,** *19* (4), 553-566.

(173)   Simon, S.; Duran, M.; Dannenberg, J. J. "How does basis set superposition error change the potential surfaces for hydrogen-bonded dimers?" *J. Chem. Phys.* **1996,** *105* (24), 11024-11031.

(174) Alvarez-Idaboy, J. R.; Galano, A. "Counterpoise corrected interaction energies are not systematically better than uncorrected ones: Comparison with CCSD(T) CBS extrapolated values." *Theor. Chem. Acc.* **2010,** *126* (1), 75-85.

(175) Ditchfield, R.; Hehre, W. J.; Pople, J. A. "Self-consistent molecular-orbital methods. Ix. An extended gaussian-type basis for molecular-orbital studies of organic molecules." *J.Chem. Phys.* **1971,** *54* (2), 724-728.

(176) Raffenetti, R. C. "Even-tempered atomic orbitals. II. Atomic scf wavefunctions in terms of even-tempered exponential bases." *J.Chem. Phys.* **1973,** *59* (11), 5936-5936.

(177) Tomasi, J.; Mennucci, B.; Cammi, R. "Quantum mechanical continuum solvation models." *Chem. Rev.* **2005**, *105* (8), 2999-3094

(178) Miertuš, S.; Scrocco, E.; Tomasi, J. "Electrostatic interaction of a solute with a continuum. A direct utilizaion of ab initio molecular potentials for the prevision of solvent effects." *Chem. Phys.* **1981,** *55* (1), 117-129.

(179) Miertuš̃, S.; Tomasi, J. "Approximate evaluations of the electrostatic free energy and internal energy changes in solution processes." *Chem. Phys.* **1982,** *65* (2), 239-245.

(180) Exley, C. "A biogeochemical cycle for aluminium?" *J. Inorg. Biochem.* **2003,** *97* (1), 1-7.

(181) Yokel, R. A.; McNamara, P. J. "Aluminium toxicokinetics: An updated minireview." *Pharmacol. Toxicol.* **2001,** *88* (4), 159-167.

(182) Willhite, C. C.; Karyakina, N. A.; Yokel, R. A.; Yenugadhati, N.; Wisniewski, T. M.; Arnold, I. M. F.; Momoli, F.; Krewski, D. "Systematic review of potential health risks posed by pharmaceutical, occupational and consumer exposures to metallic and nanoscale aluminum, aluminum oxides, aluminum hydroxide and its soluble salts." *Crit. Rev. Toxicol.* **2014,** *44*, 1-80.

(183) Mujika, J. I.; Ruiperez, F.; Infante, I.; Ugalde, J. M.; Exley, C.; Lopez, X. "Pro-oxidant activity of aluminum: Stabilization of the aluminum superoxide radical ion." *J. Phys. Chem. A* **2011,** *115* (24), 6717-6723.

(184) Exley, C.; Price, N. C.; Birchall, J. D. "Aluminum inhibition of hexokinase-activity in-vitro - a study in biological availability." *J. Inorg. Biochem.* **1994,** *54* (1994), 297-304.

(185) Yang, S. J.; Huh, J. W.; Lee, J. E.; Choi, S. Y.; Kim, T. U.; Cho, S. W. "Inactivation of human glutamate dehydrogenase by aluminum." *Cell. Mol. Life Sci.* **2003,** *60* (11), 2538-2546.

(186) Mujika, J. I.; Ugalde, J. M.; Lopez, X. "Aluminum interaction with glutamate and α-ketoglutarate: A computational study." *J. Phys. Chem. B* **2014,** *118* (24), 6680-6686.

(187) Zatta, P.; Lain, E.; Cagnolini, C."Effects of aluminum on activity of Krebs cycle enzymes and glutamate dehydrogenase in rat brain homogenate." *Eur. J. Biochem.* **2000,** *267* (10), 7-7.

(188) Lemire, J.; Mailloux, R.; Puiseux-Dao, S.; Appanna, V. D. "Aluminum-induced defective mitochondrial metabolism perturbs cytoskeletal dynamics in human astrocytoma cells." *J. Neurosci. Res.* **2009,** *87* (6), 1474-1483.

(189) Lemire, J.; Auger, C.; Mailloux, R.; Appanna, V. D. "Mitochondrial lactate metabolism is involved in antioxidative defense in human astrocytoma cells." *J. Neurosci. Res.* **2014,** *92* (4), 464-475.

(190) Mailloux, R. J.; Hamel, R.; Appanna, V. D. "Aluminum toxicity elicits a dysfunctional tca cycle and succinate accumulation in hepatocytes." *J. Biochem. Mol. Toxicol.* **2006,** *20* (4), 198-208.

(191) Kumar, V.; Gill, K. D. "Aluminium neurotoxicity: Neurobehavioural and oxidative aspects." *Arch. Toxicol.* **2009,** *83* (11), 965-978.

(192) Klatzo, I.; Wisniewski, H. M.; Streicher, E."Experimental production of neurofibrillary degeneration." *J. Neuropath. Exp. Neur.* **1965,** *24*, 139-139.

(193) Kiss, T.; Gajda-Schrantz, K.; Zatta, P. "The role of aluminum in neurotoxic and neurodegenerative processes." *Metal Ions in Life Sciences* **2006**.

(194) Abdel-Ghany, M.; Khalek, A.; Shalloway, D. "Aluminum-induced nonenzymatic phospho-incorporation into human tau and other proteins." *J. Biol. Chem.* **1993,** *268* (16), 11976-11981.

(195) Kaur, T.; Bijarnia, R. K.; Nehru, B. "Effect of concurrent chronic exposure of fluoride and aluminum on rat brain." *Drug Chem. Toxicol.* **2009,** *32* (3), 215-221.

(196) Kiss, T.; Sovago, I.; Martin, R. B. "Complexes of 3,4-dihydroxyphenyl derivatives. 9. Aluminum(3+) binding to catecholamines and tiron." *J. Am. Chem. Soc.* **1989,** *111* (10), 3611-3614.

(197) Kiss, T. "Interaction of aluminum with biomolecules--any relevance to Alzheimer's disease ?" *Arch. Gerontol. Geriatr.* **1995,** *21*, 99-112.

(198) Miu, A. C.; Benga, O. "Aluminum and Alzheimer's disease: A new look." *J. Alzheimers Dis.* **2006,** *10*, 179-201.

(199) Nurchi, V. M.; Crespo-Alonso, M.; Toso, L.; Lachowicz, J. I.; Crisponi, G.; Alberti, G.; Biesuz, R.; Dominguez-Martin, A.; Niclos-Gutierrez, J.; Gonzalez-Perez, J. M. "Iron(III) and aluminium(III) complexes with substituted salicyl-aldehydes and salicylic acids." *J. Inorg. Biochem.* **2013,** *128*, 174-182.

(200) Dean, A.; Sija, É.; Zsigó, É.; Ferlin, M. G.; Marton, D.; Gandin, V.; Marzano, C.; Badocco, D.; Pastore, P.; Venzo, A. "Possible chelating agents for iron and aluminium : 4-hydroxy-5-methyl- and 4-hydroxy-1,5-dimethyl-3-pyridinecarboxylic acid." *Eur. J. Inorg. Chem.* **2013,** *2013* (8), 1310-1319.

(201) Dean, A.; Ferlin, M. G.; Brun, P.; Castagliuolo, I.; Yokel, R. A.; Venzo, A.; Giorgio Bombi, G.; Di Marco, V. B. "Evaluation of 4-hydroxy-6-methyl-3-pyridinecarboxylic acid and 2,6-dimethyl-4-hydroxy-3-pyridinecarboxylic acid as chelating agents for iron and aluminium." *Inorg. Chim. Acta* **2011,** *373* (1), 179-186.

(202) Wu, Q.-Y.; Song, Y.-T.; Ji, L.; Wang, C.-Z.; Chai, Z.-F.; Shi, W.-Q. "Theoretically unraveling the separation of AmIII/EuIII: Insights from mixed n,o-donor ligands with variations of central heterocyclic moieties." *Phys. Chem. Chem. Phys.* **2017,** *19* (39), 26969-26979.

(203) Lan, J. H.; Shi, W. Q.; Yuan, L. Y.; Li, J.; Zhao, Y. L.; Chai, Z. F. "Recent advances in computational modeling and simulations on the An(III)/Ln(III) separation process." *Coord. Chem. Rev.* **2012,** *256* (13-14), 1406-1417.

(204) Pliego, J. R.; Riveros, J. M. "The cluster–continuum model for the calculation of the solvation free energy of ionic species." *J. Phys. Chem. A* **2001,** *105* (30), 7241-7247.

(205) Riccardi, D.; Guo, H. B.; Parks, J. M.; Gu, B.; Liang, L.; Smith, J. C. "Cluster-continuum calculations of hydration free energies of anions and group 12 divalent cations." *J. Chem. Theory Comput.* **2013,** *9* (1), 555-569.

(206) Lonsdale, R.; Harvey, J. N.; Mulholland, A. J. "Effects of dispersion in density functional based Quantum mechanical/molecular mechanical calculations on cytochrome P450 catalyzed reactions." *J. Chem. Theory Comput.* **2012,** *8* (11), 4637-4645.

(207) Alí-Torres, J.; Rodríguez-Santiago, L.; Sodupe, M. "Computational calculations of pKa values of imidazole in cu(ii) complexes of biological relevance." *Phys. Chem. Chem. Phys.* **2011,** *13* (17), 7852-7861.

(208) Bader, R. F. W. *Atoms in molecules: A quantum theory*; Oxford Univ. Press: Oxford, **1990**.

(209) Kitaura, K.; Morokuma, K. "A new energy decomposition scheme for molecular interactions within the Hartree-Fock approximation." *Int. J. Quantum Chem.* **1976,** *10* (2), 325-340.

(210) Ziegler, T.; Rauk, A. "On the calculation of bonding energies by the hartree fock slater method." *Theoret. Chim. Acta* **1977,** *46* (1), 1-10.

(211) Giambiagi, M.; de Giambiagi, M. S.; dos Santos Silva, C. D.; de Figuereido, A. P. "Multicenter bond indices as a measure of aromaticity." *Phys. Chem. Chem. Phys.* **2000,** *2*, 3381-3392.

(212) Bultinck, P.; Ponec, R.; Van Damme, S. "Multicenter bond indices as a new measure of aromaticity in polycyclic aromatic hydrocarbons." *J. Phys. Org. Chem.* **2005,** *18*, 706-718.

(213) Kiss, T.; Atkári, K.; Jezowska-bojczuk, M.; Decock, P. "Complexes of Al (III) with hydroxyaromatic ligands." *J. Coord. Chem.* **1993,** *29* (1), 81-96.

(214) Gervasio, G.; Bianchi, R.; Marabello, D. "About the topological classification of the metal-metal bond." *Chem. Phys. Lett.* **2004,** *387* (4-6), 481-484.

(215) Koritsanszky, T. S.; Coppens, P. "Chemical applications of X-ray charge-density analysis." *Chem. Rev.* **2001,** *101* (6), 1583-1627.

(216) Silvi, B.; Gatti, C. "Direct space representation of the metallic bond." *J. Phys. Chem. A* **2000,** *104* (5), 947-953.

(217) Matito, E.; Sola, M.; Salvador, P.; Duran, M. "Electron sharing indexes at the correlated level. Application to aromaticity calculations." *Faraday Discuss.* **2007,** *135*, 325-345.

(218) Feixas, F.; Matito, E.; Poater, J.; Solà, M. "Quantifying aromaticity with electron delocalisation measures." *Chem. Soc. Rev.* **2015,** *44* (18), 6434-6451.

(219) Rubini, P.; Lakatos, A.; Champmartin, D.; Kiss, T. "Speciation and structural aspects of interactions of Al (III) with small biomolecules." *Coord. Chem. Rev.* **2002,** *228*, 137-152.

(220) Richards, J. W. *Aluminium; its history, occurrence, properties, metallurgy and applications, including its alloys*; H.C. Baird & Co.: Philadelphia, **1896**.

(221) Kopacek, J.; Hejzlar, J.; Kana, J.; Norton, S. A.; Porcal, P.; Turek, J. "Trends in aluminium export from a mountainous area to surface waters, from deglaciation to the recent: Effects of vegetation and soil development, atmospheric acidification, and nitrogen-saturation." *J. Inorg. Biochem.* **2009,** *103* (11), 1439-1448.

(222) Crisponi, G.; Fanni, D.; Gerosa, C.; Nemolato, S.; Nurchi, V. M.; Crespo-Alonso, M.; Lachowicz, J. I.; Faa, G. "The meaning of aluminium exposure on human health and aluminium-related diseases." *Biomol. Concepts* **2013,** *4* (1), 77-87.

(223) Alfrey, A. C.; LeGendre, G. R.; Kaehny, W. D. "The dialysis encephalopathy syndrome. Possible aluminum intoxication." *N. Engl. J. Med.* **1976,** *294* (4), 184-188.

(224) Bushinsky, D. A.; Sprague, S. M.; Hallegot, P.; Girod, C.; Chabala, J. M.; Levi-Setti, R. "Effects of aluminum on bone surface ion composition." *J. Bone Miner. Res.* **1995,** *10* (12), 1988-1997.

(225) Campbell, A.; Bondy, S. C. "Aluminum induced oxidative events and its relation to inflammation: A role for the metal in alzheimer's disease." *Cell. Mol. Biol. (Noisy-le-grand)* **2000,** *46* (4), 721-730.

(226) Aaseth, J.; Gerhardsson, L.; Skaug, M. A.; Alexander, J. In *Chelation therapy in the treatment of metal intoxication*; Aaseth, J.;Crisponi, G.;Andersen, O., Eds.; Academic Press: Boston, **2016**.

(227) Canteros-Piccotto, M. A.; Fernandez-Martin, J. L.; Cannata-Ortiz, M. J.; Cannata-Andia, J. B. "Effectiveness of Deferiprone (II) releasing the aluminum bound to plasma proteins in chronic renal failure." *Nephrol. Dial. Transplant.* **1996,** *11* (7), 1488-1489.

(228) Kan, W. C.; Chien, C. C.; Wu, C. C.; Su, S. B.; Hwang, J. C.; Wang, H. Y. "Comparison of low-dose deferoxamine versus standard-dose deferoxamine for treatment of aluminium overload among haemodialysis patients." *Nephrol. Dial. Transplant.* **2010,** *25* (5), 1604-1608.

(229) Nguyen, B. C. Q.; Tawata, S. "The chemistry and biological activities of mimosine: A review." *Phytother. Res.* **2016**, 1230-1242.

(230) Lalande, M. "A reversible arrest point in the late G1 phase of the mammalian cell cycle." *Exp. Cell Res.* **1990,** *186* (2), 332-339.

(231) Upadhyay, A.; Chompoo, J.; Taira, N.; Fukuta, M.; Gima, S.; Tawata, S. "Solid-phase synthesis of mimosine tetrapeptides and their inhibitory activities on neuraminidase and tyrosinase." *J. Agric. Food Chem.* **2011,** *59* (24), 12858-12863.

(232) Nguyen, B. C.; Tawata, S. "Mimosine dipeptide enantiomsers: Improved inhibitors against melanogenesis and cyclooxygenase." *Molecules* **2015,** *20* (8), 14334-14347.

(233) Mascaliovas, B. Z.; Bergamini, F. R. G.; Cuin, A.; Corbi, P. P. "Synthesis and crystal structure of a palladium(II) complex with the amino acid L-citrulline." *Powder Diffraction* **2015,** *30* (4), 357-361.

(234) Chruscinska, E.; Garribba, E.; Micera, G.; Panzanelli, A. "L-mimosine, an amino acid with maltol-type binding properties toward copper(II), oxovanadium(IV) and other metal ions." *J. Inorg. Biochem.* **1999,** *75* (3), 225-232.

(235) Scarrow, R. C.; Riley, P. E.; Abu-Dari, K.; White, D. L.; Raymond, K. N. "Ferric ion sequestering agents. 13. Synthesis, structures, and thermodynamics of complexation of cobalt(III) and iron(III) tris complexes of several chelating hydroxypyridinones." *Inorg. Chem.* **1985,** *24* (6), 954-967.

(236) Telpoukhovskaia, M. a.; Rodríguez-Rodríguez, C.; Scott, L. E.; Page, B. D. G.; Patrick, B. O.; Orvig, C. "Synthesis, characterization, and cytotoxicity studies of cu(ii), zn(ii), and fe(iii) complexes of n-derivatized 3-hydroxy-4-pyridiones." *J. Inorg. Biochem.* **2014,** *132*, 59-66.

(237) Case, D. A.; Babin, V.; Berryman, J. T.; Betz, R. M.; Cai, Q.; Cerutti, D. S.; Cheatham, T. E.; Darden, T. A.; Duke, R. E.; Gohlke, H *AMBER 14*, **2014**.

(238) Stewart, J. J. P. In *J. Mol. Model.*, **2007**; Vol. 13.

(239) Maier, J. A.; Martinez, C.; Kasavajhala, K.; Wickstrom, L.; Hauser, K. E.; Simmerling, C. "FF14SB: Improving the accuracy of protein side chain and backbone parameters from FF99SB." *J. Chem. Theory Comput.* **2015,** *11* (8), 3696-3713.

(240) Jorgensen, W. L.; Chandrasekhar, J.; Madura, J. D.; Impey, R. W.; Klein, M. L. "Comparison of simple potential functions for simulating liquid water." *J. Chem. Phys.* **1983,** *79* (2), 926-935.

(241) Ryckaert, J.-P.; Ciccotti, G.; Berendsen, H. J. C. "Numerical integration of the cartesian equations of motion of a system with constraints: Molecular dynamics of n-alkanes." *J. Comput. Phys.* **1977,** *23* (3), 327-341.

(242) Darden, T.; York, D.; Pedersen, L. "Particle mesh Ewald: An n·log(n) method for Ewald sums in large systems." *J.Chem. Phys.* **1993,** *98* (12), 10089-10092.

(243) Essmann, U.; Perera, L.; Berkowitz, M. L.; Darden, T.; Lee, H.; Pedersen, L. G. "A smooth particle mesh Ewald method." *J. Chem. Phys.* **1995,** *103* (19), 8577-8593.

(244) Roe, D. R.; Cheatham, T. E., 3rd. "Ptraj and cpptraj: Software for processing and analysis of molecular dynamics trajectory data." *J. Chem. Theory Comput.* **2013,** *9* (7), 3084-3095.

(245) Bashford, D.; Case, D. A. "Generalized born models of macromolecular solvation effects." *Annu. Rev. Phys. Chem.* **2000,** *51*, 129-152.

(246) Yadegari, H.; Jabbari, A.; Heli, H.; Majdi, S. "Electrochemistry of Deferiprone as an orally active iron chelator and HIV-1 replication inhibitor and its determination." *J. Braz. Chem. Soc.* **2008,** *19* (5), 1017-1022.

(247) Mujika, J. I.; Ugalde, J. M.; Lopez, X. "Computational evaluation of pKa for oxygenated side chain containing amino acids interacting with aluminum." *Theor. Chem. Acc.* **2010,** *128* (4-6), 477-484.

(248) Fradera, X.; Austen, M. A.; Bader, R. F. W. "The lewis model and beyond." *J. Phys. Chem. A* **1999,** *103*, 304-314.

(249) Bader, R. F. W.; Stephens, M. E. "Spatial localization of the electronic pair and number distributions in molecules." *J. Am. Chem. Soc.* **1975,** *97*, 7391-7399.

(250) Keith, T. A. AIMAll (Version 19.02.13), TK Gristmill Software, Overland Park KS, USA, 20 **2014**.

(251) Nelson, W. O.; Karpishin, T. B.; Rettig, S. J.; Orvig, C. "Aluminum and gallium compounds of 3-hydroxy-4-pyridinones: Synthesis, characterization, and crystallography of biologically active complexes with unusual hydrogen bonding." *Inorg. Chem.* **1988,** *27*, 1045-1051.

(252) Macdonald, T. L.; Bruce Martin, R. "Aluminum ion in biological systems." *Trends Biochem. Sci.* **1988,** *13* (1), 15-19.

(253) Lai, J. C.; Blass, J. P. "Inhibition of brain glycolysis by aluminum." *J. Neurochem.* **1984,** *42* (2), 438-446.

(254) Socorro, J. M.; Olmo, R.; Teijon, C.; Blanco, M. D.; Teijon, J. M. "Analysis of aluminum-yeast hexokinase interaction: Modifications on protein structure and functionality." *J. Protein Chem.* **2000,** *19* (3), 199-208.

(255) Bhattacharjee, S.; Zhao, Y.; Hill, J. M.; Percy, M. E.; Lukiw, W. J. "Aluminum and its potential contribution to Alzheimer's disease (AD)." *Front. Aging Neurosci.* **2014,** *6*, 62.

(256) Mujika, J. I.; Rodríguez-Guerra Pedregal, J.; Lopez, X.; Ugalde, J. M.; Rodríguez-Santiago, L.; Sodupe, M.; Maréchal, J.-D. "Elucidating the 3d structures of al(<scp>iii</scp>)–aβ complexes: A template free strategy based on the pre-organization hypothesis." *Chem. Sci.* **2017,** *8* (7), 5041-5049.

(257) Yang, W.; Qian, Z.; Miao, Q.; Wang, Y.; Bi, S. "Density functional theory study of the aluminium(III) hydrolysis in aqueous solution." *Phys. Chem. Chem. Phys.* **2009,** *11* (14), 2396-2401.

(258) Frisch, M. J.; Trucks, G. W.; Schlegel, H. B.; Scuseria, G. E.; Robb, M. A.; Cheeseman, J. R.; Scalmani, G.; Barone, V.; Mennucci, B.; Petersson, G. A. Gaussian16.

(259) Stephens, P. J.; Devlin, F. J.; Chabalowski, C. F.; Frisch, M. J. "Ab initio calculation of vibrational absorption and circular dichroism spectra using density functional force fields." *J.Phys. Chem.* **1994,** *98* (45), 11623-11627.

(260) Johansson, G. In *Adv. Inorg. Chem.*; Sykes, A. G., Ed.; Academic Press, **1992**.

(261) Persson, I. In *Pure Appl. Chem.*, **2010**.

(262) Szefczyk, B.; Sokalski, W. A.; Leszczynski, J. "Optimal methods for calculation of the amount of intermolecular electron transfer." *J. Chem. Phys.* **2002,** *117* (15), 6952-6958.

(263) Martin, R. B. "The chemistry of aluminum as related to biology and medicine." *Clin. Chem.* **1986,** *32* (10), 1797-1806.

(264) Beardmore, J.; Lopez, X.; Mujika, J. I.; Exley, C. "What is the mechanism of formation of hydroxyaluminosilicates?" *Sci. Rep.* **2016,** *6*, 30913-30913.

(265) Rengel, Z. "Aluminium cycling in the soil-plant-animal-human continuum." *Biometals* **2004,** *17* (6), 669-689.

(266) A. Yokel, R. "The pharmacokinetics and toxicology of aluminum in the brain." *Curr. Inorg. Chem.* **2012,** *2* (1), 54-63.

(267) Arieff, A. I. "Aluminum and the pathogenesis of dialysis encephalopathy." *Am. J. Kidney Dis.* **1985,** *6* (5), 317-321.

(268) Zatta, P.; Kiss, T.; Suwalsky, M.; Berthon, G. "Aluminium(iii) as a promoter of cellular oxidation." *Coord. Chem. Rev.* **2002,** *228* (2), 271-284.

(269) Fukuzumi, S.; Ohkubo, K. "Quantitative evaluation of lewis acidity of metal ions derived from the G values of ESR spectra of superoxide: Metal ion complexes in relation to the promoting effects in electron transfer reactions." *Chem. Eur. J.* **2000,** *6* (24), 4532-4535.

(270) Fukuzumi, S. "Catalysis in electron transfer reactions: Facts and mechanistic insights." *J. Phys. Org. Chem.* **2002,** *15* (8), 448-460.

(271) Fukuzumi, S.; Ohtsu, H.; Ohkubo, K.; Itoh, S.; Imahori, H. "Formation of superoxide-metal ion complexes and the electron transfer catalysis." *Coord. Chem. Rev.* **2002,** *226* (1-2), 71-80.

(272) Van Landeghem, G. F.; De Broe, M. E.; D'Haese, P. C. "Al and Si: Their speciation, distribution, and toxicity." *Clin. Biochem.* **1998,** *31* (5), 385-397.

(273) Berthon, G. "Aluminium speciation in relation to aluminium bioavailability, metabolism and toxicity." *Coord. Chem. Rev.* **2002,** *228* (2), 319-341.

(274) Johnson, E. R.; Becke, A. D. "A post-Hartree-Fock model of intermolecular interactions." *J. Chem. Phys.* **2005,** *123* (2), 174104-174104.

(275) Chai, J.-D.; Head-Gordon, M. "Long-range corrected hybrid density functionals with damped atom-atom dispersion corrections." *Phys. Chem. Chem. Phys.* **2008,** *10* (44), 6615-6615.

(276) Frisch, M. J.; Trucks, G. W.; Schlegel, H. B.; Scuseria, G. E.; Robb, M. A.; Cheeseman, J. R.; Scalmani, G.; Barone, V.; Petersson, G. A.; Nakatsuji, H. Gaussian09..

(277) Ruedenberg, K. "The physical nature of the chemical bond." *Rev Mod. Phys.* **1962,** *34* (2), 326-376.

(278) Matito, E.; Solà, M.; Salvador, P.; Duran, M. "Electron sharing indexes at the correlated level. Application to aromaticity calculations." *Faraday Discuss.* **2006,** *135* (0), 325-345.

(279) Bogatko, S.; Moens, J.; Geerlings, P. "Cooperativity in al3+ hydrolysis reactions from density functional theory calculations." *J. Phys. Chem. A* **2010,** *114* (29), 7791-7799.

(280) Rubini, P.; Lakatos, A.; Champmartin, D.; Kiss, T. "Speciation and structural aspects of interactions of al(iii) with small biomolecules." *Coord. Chem. Rev.* **2002,** *228* (2), 137-152.

(281) Grimme, S.; Hansen, A.; Brandenburg, J. G.; Bannwarth, C. "Dispersion-corrected mean-field electronic structure methods." *Chem. Rev.* **2016,** *116* (9), 5105-5154.

(282) Palascak, M. W.; Shields, G. C. "Accurate experimental values for the free energies of hydration of H^+, OH^-, and H_3O^+." *J.Phys. Chem. A* **2004,** *108* (16), 3692-3694.

(283) Alderighi, L.; Gans, P.; Ienco, A.; Peters, D.; Sabatini, A.; Vacca, A. "Hyperquad simulation and speciation (hyss): A utility program for the investigation of equilibria involving soluble and partially soluble species." *Coord. Chem. Rev.* **1999,** *184* (1), 311-318.

(284) Grabowski, S. J. "What is the covalency of hydrogen bonding?" *Chem. Rev.* **2011,** *111* (4), 2597-2625.

(285) Zhao, L.; von Hopffgarten, M.; Andrada, D. M.; Frenking, G. "Energy decomposition analysis." *WIREs* **2017,** *8* (3), e1345.

(286) Chong, D. P.; Van Lenthe, E.; Van Gisbergen, S.; Baerends, E. J. "Even-tempered slater-type orbitals revisited: From hydrogen to krypton." *J. Comput. Chem.* **2004,** *25* (8), 1030-1036.

(287) te Velde, G.; Bickelhaupt, F. M.; Baerends, E. J.; Fonseca Guerra, C.; van Gisbergen, S. J. A.; Snijders, J. G.; Ziegler, T. "Chemistry with {adf}." *J. Comput. Chem.* **2001,** *22* (9), 931-967.

(288) Fonseca Guerra, C.; Snijders, J. G.; Te Velde, G.; Baerends, E. J. "Towards an order- n DFT method." *Theoret. Chem. Acc.* **1998,** *99* (6), 391-403.

(289) Baerends, E. J.; Ziegler, T.; Atkins, A. J.; Autschbach, J.; Bashford, D.; Bérces, A.; Bickelhaupt, F. M.; Bo, C.; Boerritger, P. M.; Cavallo, L.et al. ADF Modelling Suite 2017

(290) Zhao, Y.; Truhlar, D. G. "The M06 suite of density functionals for main group thermochemistry, thermochemical kinetics, noncovalent interactions, excited states, and transition elements: Two new functionals and systematic testing of four M06-class functionals and 12 other function." *Theor. Chem. Acc.* **2008,** *120* (1-3), 215-241.

(291) Head-Gordon, M.; Pople, J. A.; Frisch, M. J. "MP2 energy evaluation by direct methods." *Chem. Phys. Lett.* **1988,** *153* (6), 503-506.

(292) Møller, C.; Plesset, M. S. "Note on an approximation treatment for many-electron systems." *Phys. Rev.* **1934,** *46* (7), 618-622.

(293) Flatmark, T. "Catecholamine biosynthesis and physiological regulation in neuroendocrine cells." *Acta Physiol. Scand.* **2000,** *168* (1), 1-17.

(294) Kurian, M. A.; Gissen, P.; Smith, M.; Heales, S. J. R. R.; Clayton, P. T. "The monoamine neurotransmitter disorders: An expanding range of neurological syndromes." *Lancet Neurol.* **2011,** *10* (8), 721-733.

(295) Eisenhofer, G.; Kopin, I. J.; Goldstein, D. S. "Catecholamine metabolism: A contemporary view with implications for physiology and medicine." *Pharmacol. Rev.* **2004,** *56* (3), 331-349.

(296) Purves, D. *Neuroscience*; Sinauer Associates: Sunderland, Mass., **2012**.

(297) Hofstetter, J. R.; Vincent, I.; Bugiani, O.; Ghetti, B.; Richter, J. A. "Aluminum-induced decreases in choline acetyltransferase, tyrosine hydroxylase, and glutamate decarboxylase in selected regions of rabbit brain." *Neurochem. Pathol.* **1987,** *6* (3), 177-193.

(298) Erazi, H.; Ahboucha, S.; Gamrani, H. "Chronic exposure to aluminum reduces tyrosine hydroxylase expression in the substantia nigra and locomotor performance in rats." *Neurosci. Lett.* **2011,** *487* (1), 8-11.

(299) Wenk, G. L.; Stemmer, K. L. "The influence of ingested aluminum upon norepinephrine and dopamine levels in the rat brain." *Neurotoxicology* **1981,** *2* (2), 347-353.

(300) Moshtaghie, A. A.; Malekpouri, P.; Moshtaghie, M.; Mohammadi-nejad, M.; Ani, M. "Protective effects of copper against aluminum toxicity on acetylcholinesterase and catecholamine contents of different regions of rat's brain." *Neurol. Sci.* **2013,** *34* (9), 1639-1650.

(301) Zatta, P. "*Aluminium toxicity in infants' health and disease*; World Scientific, **1998**.

(302) Mason, L.; Weinkove, C. "Radioenzymic assay of catecholamines: Reversal of aluminum inhibition of enzymic O-methylation by desferrioxamine." *Ann. Clin. Biochem.* **1983,** *20* (2), 105-111.

(303) Harris, W. R.; Messori, L. "A comparative study of aluminum(III), gallium(III), indium(III), and thallium(III) binding to human serum transferrin." *Coord. Chem. Rev.* **2002,** *228* (2), 237-262.

(304) Sparta, M.; Alexandrova, A. N. "How metal substitution affects the enzymatic activity of catechol-O-methyltransferase." *PLoS One* **2012,** *7* (10).

(305) Georgieva, P.; Wu, Q.; McLeish, M. J.; Himo, F. "The reaction mechanism of phenylethanolamine N-methyltransferase: A density functional theory study." *Biochim. Biophys. Acta* **2009,** *1794* (12), 1831-1837.

(306) Gaweska, H.; Fitzpatrick, P. F. "Structures and mechanism of the monoamine oxidase family." *Biomol. Concepts* **2011,** *2* (5), 365-377.

(307) Huh, J.-W.; Choi, M.-M.; Lee, J. H.; Yang, S.-J.; Kim, M. J.; Choi, J.; Lee, K. H.; Lee, J. E.; Cho, S.-W. "Activation of monoamine oxidase isotypes by prolonged intake of aluminum in rat brain." *J. Inorg. Biochem.* **2005,** *99* (10), 2088-2091.

(308) Zatta, P.; Zambenedetti, P.; Milanese, M. "Activation of monoamine oxidase type-B by aluminum in rat brain homogenate." *Neuroreport* **1999,** *10* (17), 3645-3648.

(309) Schedin-Weiss, S.; Inoue, M.; Hromadkova, L.; Teranishi, Y.; Yamamoto, N. G.; Wiehager, B.; Bogdanovic, N.; Winblad, B.; Sandebring-Matton, A.; Frykman, S.. "Monoamine oxidase b is elevated in alzheimer disease neurons, is associated with gamma-secretase and regulates neuronal amyloid beta-peptide levels." *Alzheimers Res. Ther.* **2017,** *9* (1), 57.

(310) Riederer, P.; Laux, G. "Mao-inhibitors in Parkinson's disease." *Exp. Neurobiol.* **2011,** *20* (1), 1-17.

(311) Cowburn, J. D.; Blair, J. A. "Effect of aluminium on *in-vitro* tetrahydrobiopterin synthesis in brain preparations." *Lancet* **1987,** *2* (8550), 105-105.

(312) Leeming, R. J.; Blair, J. A. "Dialysis dementia, aluminium, and tetrahydrobiopterin metabolism." *The Lancet* **1979,** *313* (8115), 556.

(313) Kocot, J.; Luchowska-Kocot, D.; Kielczykowska, M.; Musik, I.; Kurzepa, J. "Does vitamin C influence neurodegenerative diseases and psychiatric disorders?" *Nutrients* **2017,** *9* (7).

(314) Kruck, T. P.; Cui, J. G.; Percy, M. E.; Lukiw, W. J. "Molecular shuttle chelation: The use of ascorbate, desferrioxamine and feralex-G in combination to remove nuclear bound aluminum." *Cell. Mol. Neurobiol.* **2004,** *24* (3), 443-459.

(315) Domingo, J.; Gomez, M.; Llobet, J.; Richart, C. "Effect of ascorbic acid on gastrointestinal aluminium absorption." *The Lancet* **1991,** *338* (8780), 1467.

(316) Martell, A. E. In *Ascorbic acid: Chemistry, metabolism, and uses*;ACS, **1982**.

(317) Cesario, D.; Furia, E.; Mazzone, G.; Beneduci, A.; De Luca, G.; Sicilia, E. "Complexation of $Al^{(3+)}$ and $Ni^{(2+)}$ by l-ascorbic acid: An experimental and theoretical investigation." *J. Phys. Chem. A* **2017,** *121* (51), 9773-9781.